PB98-118391

NTIS®
Information is our business.

CENTRIFUGE MODELING OF LATERALLY LOADED BATTERED PILE GROUPS IN SAND

NOV 97

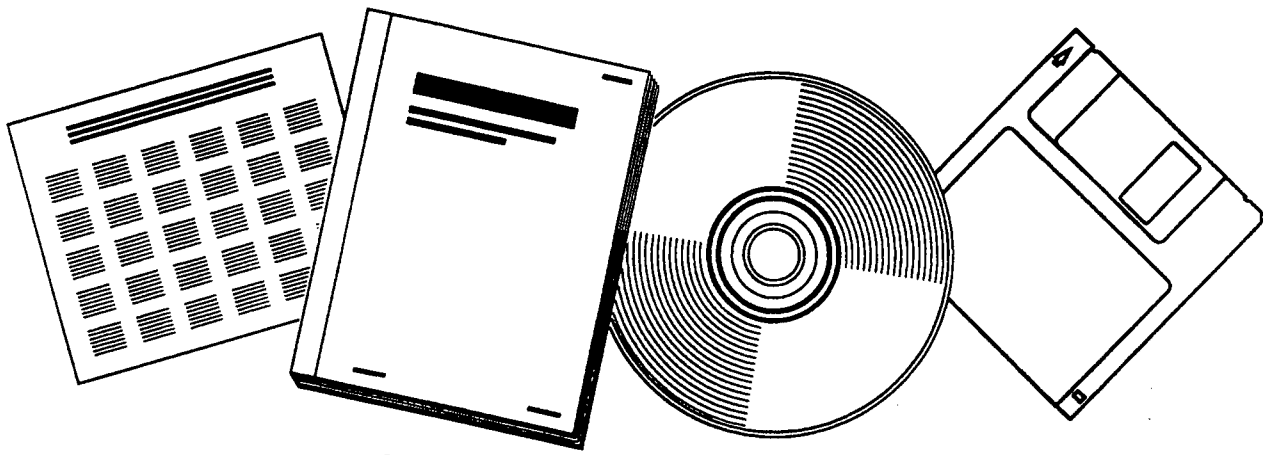

U.S. DEPARTMENT OF COMMERCE
National Technical Information Service

Final Report

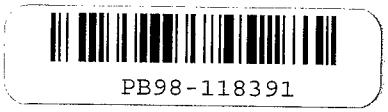

CENTRIFUGE MODELING OF LATERALLY LOADED BATTERED PILE GROUPS IN SAND

FDOT No.: 99700-7564-010
UF Report No.: 49104504505-12
WPI No.: 0510627
Contract No.: B-9210

Principal Investigator: Michael C. McVay

Researchers: Robert Gardner
Liman Zhang

November 1997

SI* (MODERN METRIC) CONVERSION FACTORS

APPROXIMATE CONVERSIONS TO SI UNITS

Symbol	When You Know	Multiply By	To Find	Symbol
		LENGTH		
in	inches	25.4	millimeters	mm
ft	feet	0.305	meters	m
yd	yards	0.914	meters	m
mi	miles	1.61	kilometers	km
		AREA		
in^2	square inches	645.2	square millimeters	mm^2
ft^2	square feet	0.093	square meters	m^2
yd^2	square yards	0.836	square meters	m^2
ac	acres	0.405	hectares	ha
mi^2	square miles	2.59	square kilometres	km^2
		VOLUME		
fl oz	fluid ounces	29.57	milliliters	ml
gal	gallons	3.785	liters	l
ft^3	cubic feet	0.028	cubic meters	m^3
yd^3	cubic yards	0.765	cubic meters	m^3
NOTE: Volumes greater than 1000 l shall be shown in m^3.				
		MASS		
oz	ounces	28.35	grams	g
lb	pounds	0.454	kilograms	kg
T	short tons (2000 lb)	0.907	megagrams	Mg
		Temperature (exact)		
°F	Fahrenheit temperature	5(F-32)/9 or (F-32)/1.8	Celcius temperature	°C
		ILLUMINATION		
fc	foot-candles	10.76	lux	lx
fl	foot-Lamberts	3.426	candela/m^2	cd/m^2
		FORCE and PRESSURE or STRESS		
lbf	poundforce	4.45	newtons	N
psi	poundforce per square inch	6.89	kilopascals	kPa

APPROXIMATE CONVERSIONS FROM SI UNITS

Symbol	When You Know	Multiply By	To Find	Symbol
		LENGTH		
mm	millimeters	0.039	inches	in
m	meters	3.28	feet	ft
m	meters	1.09	yards	yd
km	kilometers	0.621	miles	mi
		AREA		
mm^2	square millimeters	0.0016	square inches	in^2
m^2	square meters	10.764	square feet	ft^2
m^2	square meters	1.195	square yards	yd^2
ha	hectares	2.47	acres	ac
km^2	square kilometers	0.386	square miles	mi^2
		VOLUME		
ml	milliliters	0.034	fluid ounces	fl oz
l	liters	0.264	gallons	gal
m^3	cubic meters	35.71	cubic feet	ft^3
m^3	cubic meters	1.307	cubic yards	yd^3
		MASS		
g	grams	0.035	ounces	oz
kg	kilograms	2.202	pounds	lb
Mg	megagrams	1.103	short tons (2000 lb)	T
		Temperature (exact)		
°C	Celcius temperature	1.8C + 32	Fahrenheit temperature	°F
		ILLUMINATION		
lx	lux	0.0929	foot-candles	fc
cd/m^2	candela/m^2	0.2919	foot-Lamberts	fl
		FORCE and PRESSURE or STRESS		
N	newtons	0.225	poundforce	lbf
kPa	kilopascals	0.145	poundforce per square inch	psi

* SI is the symbol for the International System of Units. Appropriate rounding should be made to comply with Section 4 of ASTM E380.

(Revised August 1992)

DISCLAIMER

"The opinions, findings and conclusions expressed in this publication are those of the authors and not necessarily those of the Florida Department of Transportation or the U.S. Department of Transportation.

Prepared in cooperation with the State of Florida department of Transportation and the U.S. Department of Transportation."

ACKNOWLEDGEMENTS

The investigators would like to thank Mr. Peter Lai, project officer, from the FDOT Structures Office in Tallahassee for a number of good suggestions in regards to the experimental work, as well as carefully reviewing the final manuscript. Most of the experimental results reported herein were conducted on equipment that Mr. Michael Johnson designed and fabricated. Finally, the investigators would like to thank the Florida Department of Transportation for making this research possible through the following State Job #997000-7564-010, contract #B-9210 and WPI #0510627.

TABLE OF CONTENTS

LIST OF TABLES

LIST OF FIGURES

CHAPTER 1
INTRODUCTION

1.1 BACKGROUND

Pile foundations are often required to resist lateral loading. Lateral loads come from a variety of sources including wind, earthquakes, waves, and ship impacts. The lateral capacity of a pile is usually much smaller than the axial capacity and as a result groups of piles are often installed to increase the lateral capacity of the entire foundation system. When vertical or plumb pile groups do not provide sufficient lateral resistance the piles can be battered in order to mobilize some of the higher axial capacity to resist the lateral load.

The behavior of piles under lateral loading is complicated. This complexity is due to the fact that the pile's deflection depends on the soil response and that the soil response is dependant upon the pile's deflection. A method of modeling lateral behavior for a single pile is the use of non linear curves that relate soil resistance (p) to pile deflection (y) at all points along the pile, which itself is modeled as a beam-column. Typically, the p-y curve for a single pile is then multiplied by a p-y multiplier to account for the loss of resistance due to the presence of other piles within a group, the so called shadowing effect. This loss of resistance is caused by the disruption of adjacent shear zones between piles in a group.

Past research in this area has centered around full scale lateral load testing and centrifugal lateral load testing. Full scale lateral load tests are very expensive and as a result there have been few conducted. In the absence of full scale tests, centrifuge tests have proven to be an inexpensive and good substitute. In such tests a scaled down model of the prototype pile is placed in the centrifuge and subjected to an artificially high acceleration field. This acceleration field reproduces the insitu

stresses due to gravity that the prototype pile would experience. A lateral load test can then be run in flight and the results scaled up to the prototype.

1.2 OBJECTIVE

This research is sponsored by the Florida Department of Transportation and is part of an on going study of the effects of ship impact loads on waterway structures underlain by pile foundations. The objectives of this research are:

1. To modify the existing pile driver and make it capable of driving 3 by 3 and 4 by 4 battered pile groups in flight onto a base plate and achieve fixed head conditions at the pile cap.
2. To instrument each of the piles in both groups to measure shear and axial force and bending moment.
3. To conduct the lateral load tests in samples with relative densities of 36% and 55% and also to test with dead loads equivalent to 20%, 50%, and 80% of the vertical capacity of the model pile group.
4. Analyze the effect of dead load on the lateral capacity at different relative densities.
5. To gather data about the internal force distribution of the pile groups and to investigate the pattern of pile group rotation.
6. Finally, to use measured test data to validate a coupled bridge superstructure-foundation-finite-element-code (FLORIDA- PIER).

1.3 SCOPE OF TESTING

Eighteen tests were conducted throughout this project. The following table presents the testing schedule that was followed.

In the 3 by 3 tests the 3F6R and 6F3R designations state the ratio of piles battered in tension and compression. The number before the F stands for the number of piles battered in the forward direction, the direction of the applied load.

Table 1-1 Testing Schedule

Density	3 by 3		4 by 4
	3F6R	6F3R	8F8R
36%	3	3	3
55%	3	3	3

Similarly the number before the R represents number of piles battered in the reverse direction, the direction opposite to the applied load. The 4 by 4 tests have no such distinction as the even number of rows ensures that the number of piles battered in either direction will be equal. The outer two rows for the four by four group were battered reverse and the inner two rows were battered forward. The three tests in each category are for the three dead loads, nominally equal to 20%, 50%, and 80% of the vertical bearing capacity, on the pile group.

1.4 THEORY OF SIMILITUDE

In centrifuge research, modeling is used to reproduce the behavior of some larger prototype structure in the relatively small confines of a centrifuge. This represents major savings when compared to the cost of conducting a full scale test. In the scaling down from, model to prototype it is assumed that the same soil response will be observed. The most important soil response in geotechnical engineering is the stress-strain behavior of a soil. When a soil sample is in flight it is sub-

jected to a radial acceleration acting outward from the center of rotation and a gravitational acceleration acting downward and perpendicular to the radial component. The model experiences centrifugal force acting on it as it spins. The magnitude of this force depends upon the radial distance from the center of rotation to the model and on the number of RPM's. The force due to gravitational acceleration acts perpendicular to this and is much smaller than the radial force when the centrifuge spins fast enough. Under that condition it can be assumed that the model is only influenced by the centrifugal force and radial acceleration at high enough RPM's.

The centrifugal acceleration acts on the model as gravitational acceleration would act on the prototype. The general equation for stress due to an acceleration is,

$$\sigma = \gamma \cdot z \cdot (a/g)$$

where σ = stress in soil

γ = unit weight of soil

a = centrifugal acceleration

g = gravitational acceleration

The stresses in the model must be equivalent to the prototype stresses. As a consequence of this the stress (σ), unit weight (γ), and gravitational acceleration (g) remain constant between model and prototype. The depth of soil (z) is much smaller, requiring an increased acceleration (a) to maintain equivalency. The ratio of centrifuge to gravitational acceleration is defined as N and is called the scaling factor. Once the tests are complete the tests can be scaled up using the N. Table 1-2 gives the scaling relationships for some important soil properties.

Table 1-2 Centrifuge Scaling Properties

Property	Prototype	Model
Acceleration [L/T^2]	1	N
Area [L^2]	1	1/N
Density [M/L^2]	1	$1/N^2$
Force [ML/T^2]	1	$1/N^3$
Linear Dimension [L]	1	$1/N^2$
Mass [M]	1	$1/N^2$
Moment [ML^2]	1	N
Strain [L/L]	1	1
Stress [F/L^2]	1	1
Unit Weight [F/L^3]	1	1
Volume [L^3]	1	1

CHAPTER 2
LITERATURE REVIEW

The following literature review will focus on a discussion of previous full scale and centrifugal lateral load tests.

2.1 FULL SCALE LATERAL LOAD TESTS

One of the first recorded lateral load tests was conducted by Feagin (1953) at Lock No. 25 on the Mississippi river in 1936. The purpose of the testing was to determine the resistance of battered, plumb, and groups of battered and plumb piles together to lateral loading. Some of the pile groups tested included: a 2 by 4 group with the two lead row piles battered in tension, and the rest plumb, a 3 by 3 group with the middle row battered in compression and the outer row piles plumb, a 2 by 4 group with all the piles battered in compression, and a 2 by 4 group with the lead and second rows battered in tension and the third and trail rows battered in compression. The test also called for the application of vertical loads on the pile caps. The piles themselves were 32 foot steel pipe piles with a wall thickness of 0.218 inches and an EI of 1.518×10^6 ton-in^2. The piles were driven 30 feet into the ground and the tops were encased in a 2 foot thick concrete pile cap. All of the battered piles were inclined at 20 degrees to the vertical. The soil at the site was a fine to coarse sand with some gravel as determined from the boring logs. The data reported the deflections for 5^T, 10^T and maximum lateral load per pile, as well as the load required for 0.25 inches of deflection.

The following conclusions were made from the test data:

1. Groups with battered piles were always more resistant than groups with the same number of plumb piles, regardless of the batter direction. Groups with a combination of battered and plumb piles had a higher lateral capacity than all plumb pile groups.

2. The resistance of a pile battered in compression increases with the application of a vertical load whereas the resistance of a pile battered in tension does not increase significantly in the presence of a vertical load.
3. Pile groups with piles battered in both the tension and compression directions showed higher resistance to lateral loading than groups with piles battered in a single direction.
4. Piles battered in compression showed a higher lateral resistance than piles battered in tension for similar pile group configurations, with or without vertical load.

Another important test was conducted by Tschebotariof (1953) in which the capacity of a single pile battered 15 degrees in tension and compression and plumb was measured. The results showed that the lateral capacity of a pile battered in compression was much smaller than the capacity of a pile battered in tension. The tension pile had a capacity that is 50% to 70% higher than the capacity of the compression pile. The tension battered pile was also higher than the plumb pile which itself was higher than the compression pile. He attributed the capacity difference between the two battered piles to the tension pile's larger passive shear block.

Another test was done at the Foundation Test Facility at the University of Houston, (Brown et al., 1988). In this test a single plumb pile and group of steel plumb pipe piles were driven into a dense sand that was artificially saturated using underground pipes. The piles in the group were arranged into a 3 by 3 configuration with a 3 diameter spacing and were 40.5 feet long, 10.75 inches in diameter and had wall thicknesses equal to 0.375 inch.

All the piles were instrumented to measure the distribution of bending moments along each pile, the distribution of load to each pile, and the slope at the top of each pile. These measurements would help determine the soil resistance as a function of depth for each pile. Inside each of the piles

in the group a smaller 6.625 inch diameter pipe was grouted and strain gages were attached. The single pile was instrumented by putting strain gages on the outer surface of the pile.

The soil at the site was a medium dense sand with a stiff clay layer above it. The site had been excavated and the sand placed in 6 inch lifts with a relative density approximately equal to 50%. It was assumed that the sand response was more significant than the clay because the sand layer extended to a depth of more than 10 pile diameters. The piles were loaded cyclically using a double acting hydraulic cylinder attached to a moment free loading frame. From the test results it was determined that 45% of the applied load is taken by the lead row, 32% is taken by the middle row and 23% by the trail row. It was also noted that the deflection of the pile group was more than of the single pile. This is due to the movement of the leading rows which makes the soil ahead of them flow around it, thereby reducing the lateral load bearing capacity behind them. This shadowing effect tends to reduce the loads taken up by the trailing rows. From a comparison of the single pile to pile group data the efficiency of each pile in the group was determined. The p-y multipliers were back calculated as 0.8 for the lead row, 0.4 for the middle row, and 0.3 for the trail row.

2.2 CENTRIFUGE LATERAL LOAD TESTS

At the University of Florida centrifuge lateral load tests began in 1992 with Vander Linde's development of a model pile group and pile driving equipment. It continued with Clausen's (1992) experiments with 5D pile groups in loose sand (D_r = 36%). McAdams (1993) conducted 3D tests in both loose and medium dense sands. McVay et al. (1994b) conducted further 5D tests in medium dense sands and analyzed all previous data. The prototype response and the p-y multipliers were predicted using COM624P. The following conclusions were reached from this research.

1. For a group with 3D pile spacing the distribution of load varies from 41%, 32%, and 27% for medium dense sands and from 37%, 33%, and 30% for loose sands. Clearly, the load distribution depends upon soil density.
2. The load distribution for a 5D configuration does not significantly change with a changes in soil density. For medium dense sands the distribution was 36%, 33%, and 31% and 35%, 33%, and 31% for loose sands.
3. The p-y multipliers determined using COM624P were 0.8, 0.4, and 0.3 for medium dense sands and 0.65, 0.45, and 0.35 for loose sands in a 3D configuration. This implied that the efficiency of a 3D group is about constant and is not dependant upon the soil density.
4. From a comparison of the 3D and 5D tests it was concluded that the shadowing effect , the decrease of lateral load taken up by the trailing rows, was less significant in the 5D tests. The 5D test results showed less variation in load percentage between the lead and trailing rows than did the 3D tests. Also in the 3D tests the load distribution was more skewed toward the leading row for the groups founded in medium dense soil.
5. Because of an improperly functioning locking mechanism on the pile cap all the test data are for free head piles.

TE-I Shang (1994) Performed lateral load tests on 3 by 3 batter pile groups in medium dense ($D_r = 55\%$) and loose ($D_r = 33\%$) sand. A series of plumb pile tests were conducted for comparison. The pile spacings used were 3D and 5D. The results were as follows:

1. The groups in the higher density sample had significantly higher lateral resistance than did the looser samples. At 3 inches lateral deflection the 3D pile group has a 57% higher lateral capacity in a 55% than in a 33% relative density sample. Also at 5D spacing the pile groups

in the 55% relative density samples had a 48% higher lateral capacity than the ones in the 33% relative density sample.

2. In both dense and loose samples, the pile groups arranged in 5D spacing had a higher lateral load capacity than the ones arranged in 3D spacing. In particular, the `capacity was 28% higher in the 55% relative density sample and 36% higher in the 33% relative density sample. This was attributed to the reduction of overlapping passive shear zones between piles with increasing distance. At 5D spacing there is less overlapping and disruption of adjacent passive shear zones than at the closer 3D spacing.

3. The pile groups with 6 piles battered in tension always provided higher lateral resistance, for the same pile spacing and relative density, than their counterparts with only three piles battered in tension. This disparity was especially noticeable for the 3D pile group at 55% relative density and for the 5D pile group at 33% relative density. Two possible explanations for this phenomenon were offered. The first stated that if it is assumed that each pile battered in tension can provide the same skin friction then the difference in lateral capacity is merely due to the difference in the number of piles. The second one is based on the assumption that the passive earth pressure of the soil zone in front of a pile battered in tension is greater than the one in front of a pile battered in compression. It follows then that this would lead to a group with six piles in tension having a higher lateral capacity.

4. A series of plumb pile tests was conducted to compare results with the batter pile groups. For all cases except the 3D at $D_r = 33\%$ the slope of the load deflection curve for the battered pile group was steeper than the plumb pile group from 0 to 1 inch lateral deflection. This stiffer response eventually softened and the curves became parallel. The initially steeper slope represents the battered pile group's greater efficiency of lateral resistance and its flattening out is

a reduction in efficiency. The reason that the 3D group at 33% relative density showed no significant increase over the plumb pile response was that the loose sand condition and the proximity of the piles in the group effectively negated any increase in resistance that the battering could furnish.

5. During these tests a dead load was added to the pile group with 3D spacing and three piles in tension in a 55% relative density sample. As was expected the lateral resistance increased. In particular it increased 31% over the battered pile group with no dead load and 54% over the plumb pile group at 1 inch of lateral deflection. At 3 inches of deflection the lateral resistance was 17% higher than the battered group with no dead load and 24% greater than the plumb pile group.

Molnit (1995) made new centrifuge equipment for lateral load tests on plumb piles but was unable to get it working properly. Eventually, the tests were finished and the results were analyzed. The tests were on 3 by 3, 3 by 4, 3 by 5, 3 by 6, and 3 by 7 pile groups in loose (D_r = 33%) and medium dense sand (D_r = 55%) sands. This was done in order to determine the p-y multipliers because it was not known if they were a function of the group's ultimate load and deformation or if they were constant. The p-y multipliers were back calculated using FLORIDA-PIER. The following conclusions were reached:

1. The lateral resistance of an individual row is independent of the group size, it is function of row position and the soil density.
2. For the medium dense sands (D_r = 55%) the p-y multipliers used in FLORIDA-PIER were 0.8, 0.4, 0.3, 0.2 for the lead to trailing rows and they were 1.0, 0.4, 0.3, 0.2 and 0.2 for the loose sand (D_r=33%). Because of the similarity in all the multipliers it was suggested that

values of 0.8 for the lead row, 0.4 for the second row, 0.3 for the third row, and 0.2 be used for the trailing rows be used in all cases.

CHAPTER 3
CENTRIFUGE EQUIPMENT AND MODIFICATIONS

3.1 INTRODUCTION

The existing equipment for driving and testing battered piles was not sufficient for this new research and modifications were necessary. The equipment used in this experiment was a modification of the pile driver used in Shang's (1994) experiments and the bucket used in Molnit's (1995) experiments. This chapter focuses on the current equipment and the modifications done to it. The centrifuge itself was designed and constructed by John Gill in 1988. It has since been modified so that the distance from the center of rotation to the platform is 63.375 inches and it now has an allowable payload of 12.5 g-tons. The electrical access to the centrifuge is provided by two 40 channel electrical slip-rings while the pneumatic access is provided by a two port hydraulic rotary union.

3.2 CHANGES TO BUCKET

The existing bucket is made of aluminum alloy 6061 and uses bolts for all of its connecting joints. It is rectangular in shape with an inside length, width, and height of 18, 10, and 12 inches respectively. A picture of the driver and bucket is shown in Figure 3-1. The base plate that the bucket is attached to is 5 inches wider on the short sides of the rectangular box.

In past experiments, four hydraulic cylinders were mounted on the bucket and used for pile driving. In these experiments the cylinders were removed because the piles were to be driven by air pressure. A pair of aluminum channels bolted to the bottom of the plate provide reinforcement. Additionally, four 1/4 inch holes were drilled into the top side walls of the bucket. These holes are aligned with four steel pins on the driver and are used to ensure proper alignment between the bucket and driver.

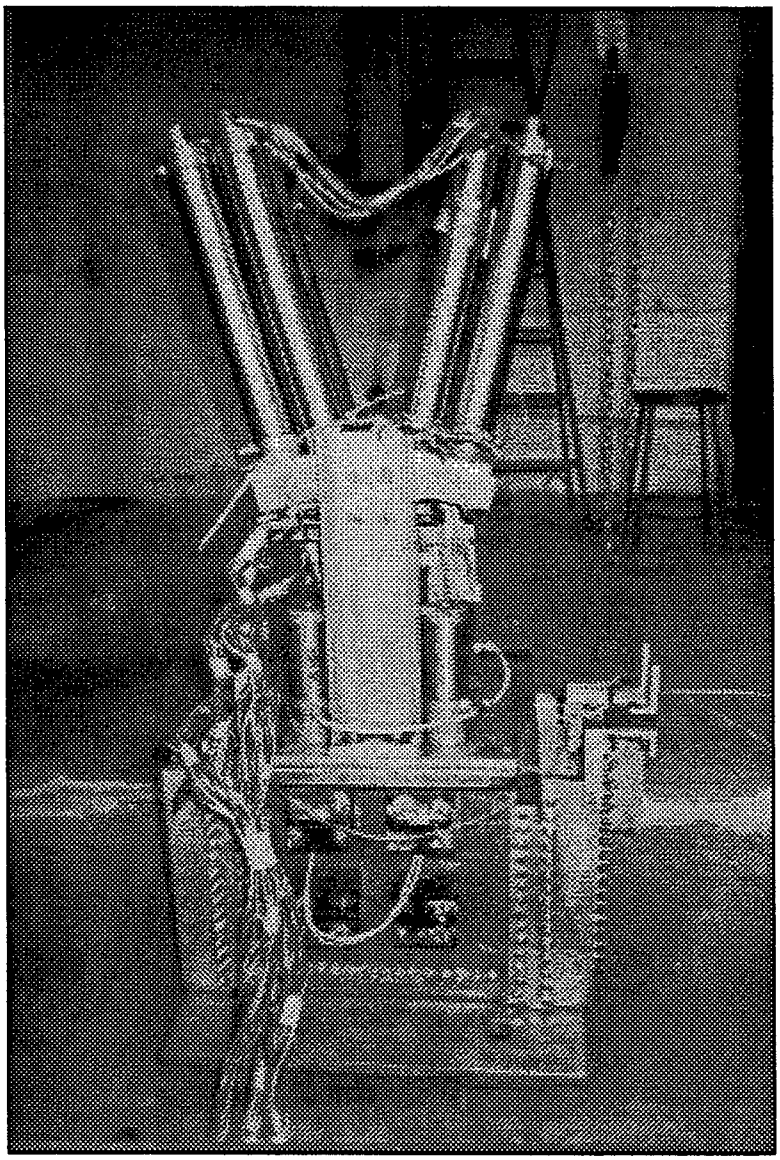

Figure 3-1 Pile Driver and Bucket

3.3 TRAP DOOR

The trap door was used to hold the base plate while the driving pistons pushed the piles down. Once the piles were on the base plate, the pressure in the pistons was adjusted to a setting pressure for three hours to allow the epoxy to hardened. The trap door had to hold the pile cap in place during both driving and epoxy setting otherwise the pile and base plate would be pushed down into the soil sample and the centrifuge would have to be stopped and the test started over.

The trap door itself was a rectangular piece of aluminum with a 5.9 inches by 4.5 inches cut and a 0.5 inch hole at each of the four corners. Through each of these holes the threaded shaft of an air piston was linked to the trap door by a nut. Bimba air pistons with a 1-1/16 inch diameter were used to lift the trap door up during the 3 by 3 pile group tests. They were inadequate for the 4 by 4 tests with its higher dead loads and higher setting pressures. They were subsequently replaced by air pistons with a 2 inch inner diameter.

3.4 STEEL FRAME

The driving mechanism was attached to the bucket using a rectangular steel frame with a hole in each of the corners. These holes approximately lined up with the holes that formerly held the hydraulic pistons onto the bucket. Threaded steel rods were inserted through the frame and through both sets of holes. At the bottom of the bucket a nut with several washers was screwed onto the rod thereby securing the driver onto the bucket. The frame itself served as a mechanism for firmly securing the driver to the bucket.

3.5 DEFLECTION AND LOAD MEASURING DEVICES

3.5.1 Deflection Measuring Devices

A Linear Variable Differential Transducer (LVDT) was used to measure the deflection of the pile group in the horizontal and vertical directions. The horizontal LVDT was mounted to one end of the bucket by a threaded connection. The shaft of the LVDT was allowed to touch a steel bar that was connected to the loading piston. The movement of the steel bar during loading, which equaled the deflection of the pile group, was recorded by the LVDT. The vertical LVDT was mounted on the pile driver at the opposite side of the bucket. A small rectangular piece of aluminum was attached to each pile base plate and served as the contact point for the vertical LVDT. The range of the LVDTs was + 0.3 in. to - 0.3 in. They required 30 DC volts which was provided by a +15 volt to -15 volt DC power supply.

3.5.2 Load Measuring Device

A 4 inch air piston mounted on a aluminum plate attached to the bucket was used to apply the lateral load for these tests. A shaft guided by a pillow block ball bearing, which helped to reduce friction as the shaft moved, was used to transfer the load from air piston to the pile group. At the tip of the shaft a 1000 pound load cell was mounted to measure the applied load. The amount of air pressure applied to the loading piston was regulated by the pneumatic manually operated control panel that is described in Chapter 5.

3.6 DATA ACQUISITION DEVICES

3.6.1 HRES Card

The system used for data acquisition was a 486, 33MHz Personal Computer with a 16 bit HRES card for the voltage readings and three EXP-20 multiplexers with 16 channels each (i.e., 48

channels total). In this experiment the data acquisition card was programmed to handle bipolar voltage readings due to the possibility of negative readings. The card sampled readings on eight analog channels and then translated them into a digital signal using the HRES card. The 16 bit card used in this experiment had a precision of 2^{16} bytes or 65,536 bytes per 10 volt (uni polar) when the gain setting was set to 1. This allowed voltage readings between -10 V and +10 V with a factor of translation equal to 0.305 mV/byte using a HRES gain setting equal to 1. The HRES card can transmit a four bit digital signal through the 50 pin ribbon cable that was linked to a connector box placed outside the centrifuge. This connector box accepted data on all eight input channels and was used for sampling the LVDT (channel 4), weighing the sample container, and sampling the load cell (channel 5).

3.6.2 EXP-20 Multiplexer

The three multiplexers used in this experiment were placed on the centrifuge arm. They were housed in a data acquisition box and were used to sample strain gage and load cell readings. The gain setting was set at 3 which amplified the output signals from the load cells and strain gages 300 times. When taking bipolar voltage readings with the HRES the gain was set to 1, the voltage output from the signal source was translated to digital signal by a factor of 1.017 micro volts per byte. On this setting the maximum and minimum source outputs that can be read through the multiplexers were ± 32,767 bytes or 33,333 micro volts. A picture of the multiplexer mounted on the centrifuge arm with the pile plugs inserted is shown in Figure 3-2.

3.7 AIR PRESSURE SYSTEM

The pressure needed to drive the piles and hold the trap door stationary was provided by the Laboratory air compressor. It was supplied to the centrifuge through a pneumatic rotary union to

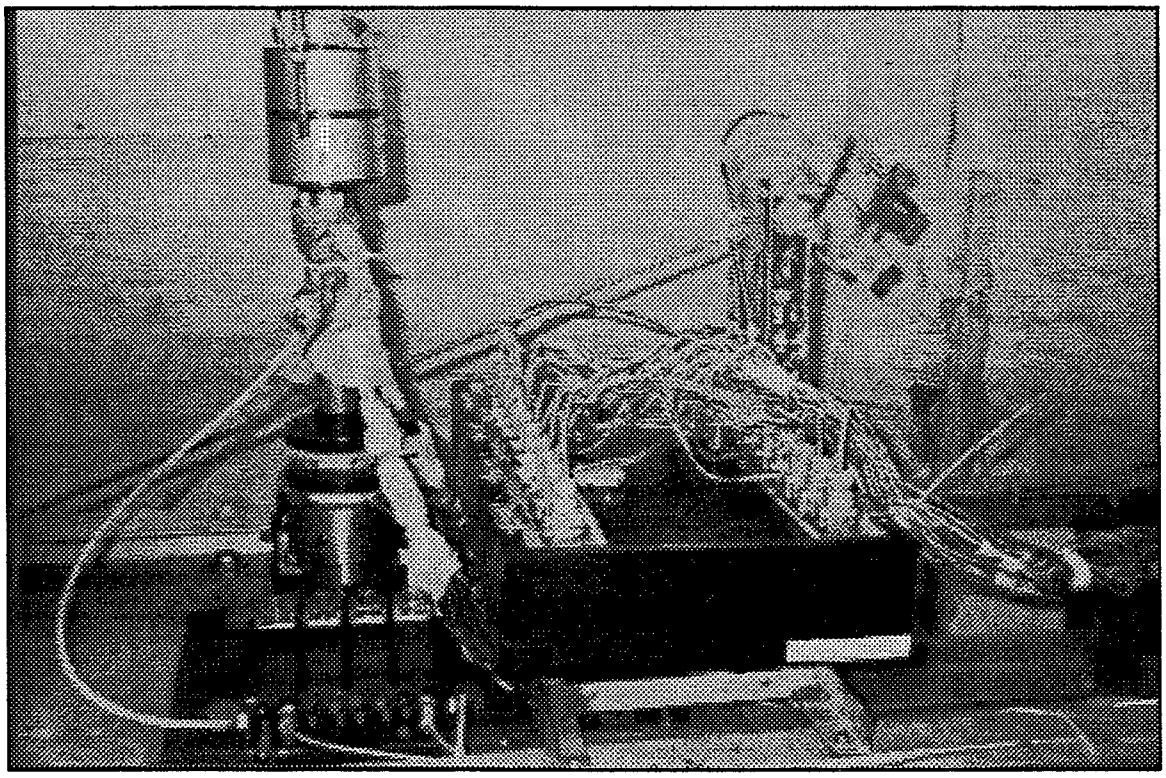

Figure 3-2 Multiplexer Mounted on Centrifuge Arm

a pair of solenoid air valve manifolds, which were mounted on the centrifuge arm. From there the air was sent to the Bimba air pistons. Both manifolds had four valves with two ports each. One of these four sets of valves are shown in the bottom left corner of Figure 3-2. In this experiment three of the valves were used for driving the piston rods on each Bimba piston and three more were used for the following functions: retracting the piston rods, controlling the trap door, and loading the group. Each valve has a pair of output ports marked as A and B and a pair of corresponding vents marked as EA and EB. Only ports A and vents EA were used in this experiment to apply and release air pressure. The ports B and vents EB were not used and were sealed. When an individual port was activated during testing the A port was opened and vent EA was closed and the reverse was done during deactivation. The link from the air valve on the solenoid to the various pistons on the swing out platform was made using plastic tubing. Three such tubes linked three of the air valves on the

solenoid air valve manifold with the top ports of the driving pistons. A fourth tube linked all three bottom ports of the same driving pistons to the air supply. A fifth tube connected an air valve to the top port of the trap door piston and a sixth one connected an air valve to the loading piston mounted on the bucket.

An air pressure regulator was used to regulate the 100 psi air input from the laboratory air compressor and an air pressure control panel to distribute the pressure through this network to the pistons. The control panel consisted of a three and a four way air valve and six electrical toggle switches that were linked to a 24 volt DC power supply. A picture of this is shown in Figure 5-4 in Chapter 5. Each switch controlled an air valve on the manifold and sent 24 volts to energize the solenoid and open port A, delivering air pressure to the loading piston.

The air from the compressor went through a T fitting where it was separated into two streams. One stream went to a three way valve and eventually to the trap door air pistons. The other went to the air regulator and was divided by another T fitting. One part of this air went directly through the pneumatic rotary union and to the air manifold where it controlled the pile driving and piston rod retraction during testing. The other went to the three way air valve.

3.8 VIDEO MONITORING SYSTEM

During pile driving and lateral load testing a PANASONIC black and white camera was used to monitor the activity. It was mounted on the centrifuge arm on an aluminum C channel, which rose vertically, and was focused on the pile driver and pile group. The camera was visible in the upper right hand corner of Figure 3-1. The image was transferred onto a monitor in the control room and was observed throughout the duration of the test.

CHAPTER 4
MODEL PILES AND TEST SAND PROPERTIES

4.1 PILES

The piles used in both sets of tests were solid aluminum (alloy 6061) and were 12 inches long and 0.375 inch square. Each pile had twelve strain gages on it that were attached to the piles in three sets of four strain gages. The first two sets were affixed to the tension and compression sides of the pile, using a two part adhesive, to measure the shear force. These strain gages were from Omega and were type SG-3/1000-DY43 with a gage factor of 2.05 and an electrical resistance of 1000 ohms. Wires were soldered to the gages' solder pads and were then connected to the terminal pads on the side of the pile. From these terminal pads the gages were connected to a full wheatstone bridge configuration. The third set of strain gages was placed in pairs below the first two sets of gages and was used to measure the axial force applied on each of the piles. They were also linked from their solder pads to the terminal pads on the side of the piles and then to a full wheatstone bridge. The strain gages were from Micro-Measurements and were type N2A-06-S053P-350 with a gage factor of 2.08 and an electrical resistance of 350 ohms.

In all cases the strain gages were brushed with a protective coating, covered with silicon, and then wrapped in masking tape for protection.

4.2 PILE GROUP CONFIGURATION

A picture of the pile group configuration is given below in Figure 4-1. A desciption of each part of the pile groups is given in the following sections.

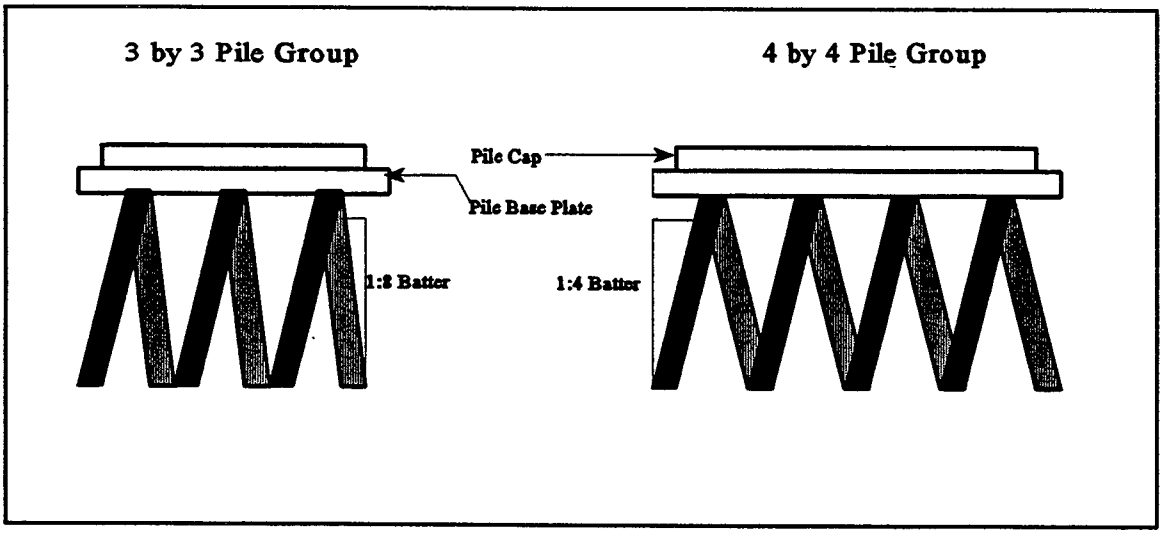

Figure 4-1 Pile Group Configuration

4.2.1 Pile Cap

The pile group for each experiment consisted of two parts. The first part was the top of the pile rows or the pile cap. A picture of the piles attached to the cap is shown in Figure 4-2. Each row of piles in both sets of experiments were connected to an aluminium pile cap that was made of two parts, held together by four allen bolts for the 3 by 3 tests and by five allen bolts in the 4 by 4 tests. At either end of the pile cap there was a hole to allow the pile cap to travel down along the guide rods during driving. The guide rods will be discussed in the section describing the pile base plate.

In the 4 by 4 tests the middle pile cap actually contained the inner two pile rows where in the 3 by 3 tests the pile cap contained just the middle row. Also in the 4 by 4 tests the dead load needed for 80% of the vertical bearing capacity of the pile was epoxied to the middle pile cap.

4.2.2 Pile Base Plate

The second part of the pile group was the base plate. The pile base plate was 5.25 inches long, 5.5 inches wide, and 0.375 inch thick. The holes for the piles themselves were 0.875 inch in diameter.

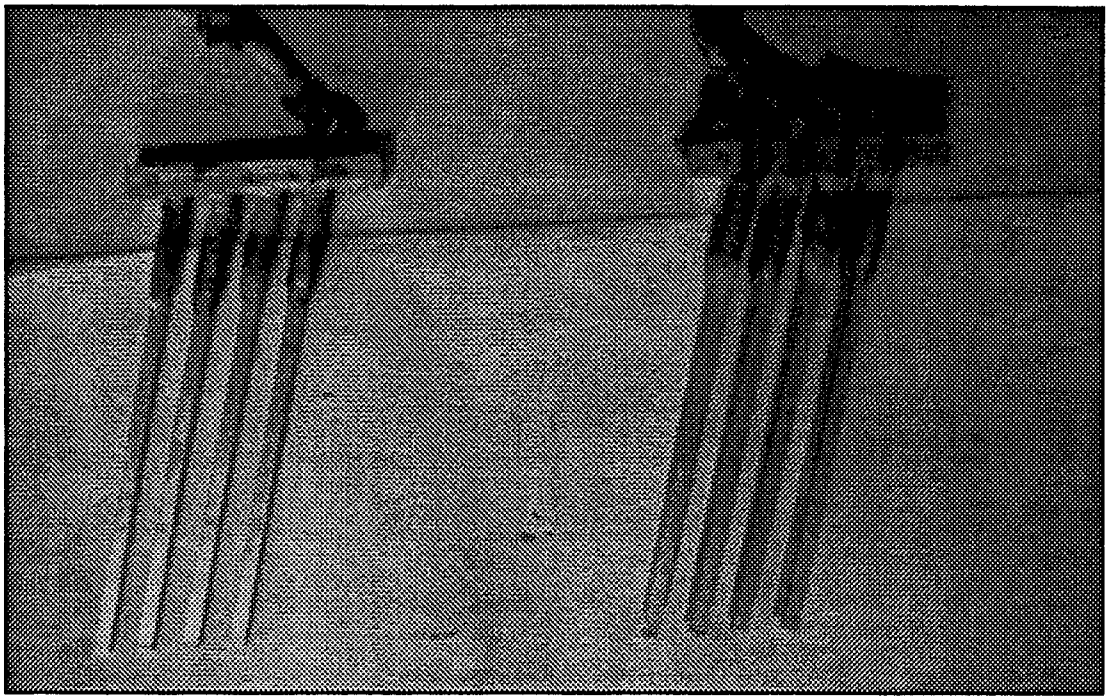

Figure 4-2 Pile Cap and Piles

The 3 by 3 pile base plate was 5.25 inches square and 0.375 inch thick. On the end where the lateral load was to be applied, a 2 inch by 1 inch aluminum plate was screwed on, perpendicular to the pile base plate to provide a normal contact area for the loading rod. On the opposite end a 2 inch square aluminum plate, with the outside corners chamfered, was screwed on, parallel to the pile base plate to provide a horizontal contact area for the vertical LVDT. Dead load was attached to the bottom of the pile base plate in the form of rectangular lead bars. Figure 4-3 is a photograph of the base plates used. When the piles were driven in flight, the pile cap would be pushed down onto the pile base plate. After this, three hours was allowed as a setting time for the epoxy so that the two parts would act as a singular pile cap during loading. Pile driving and lateral load testing will be discussed in detail in Chapter 5.

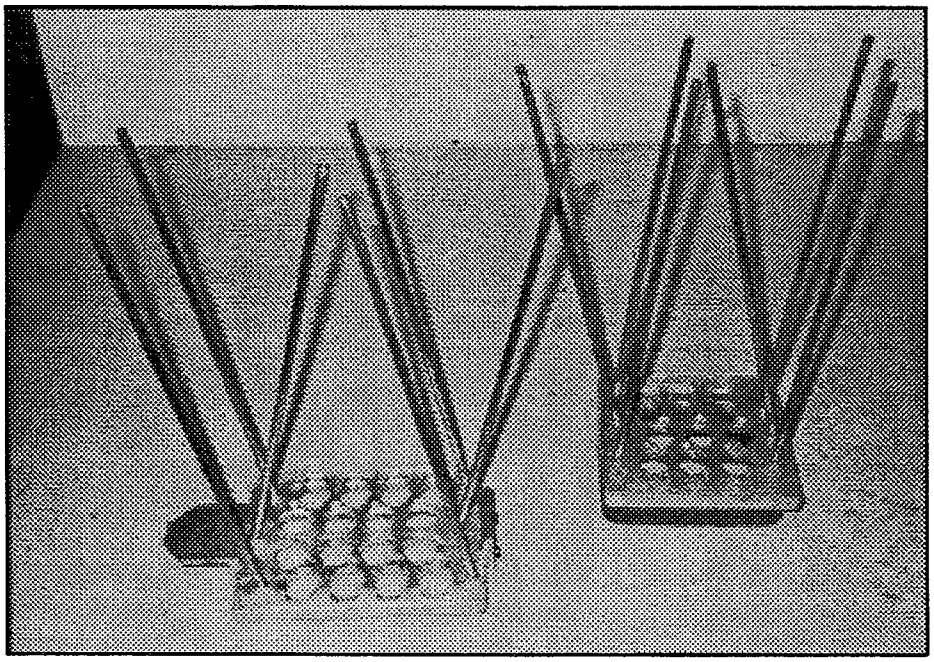

Figure 4-3 Pile Base Plates and Guiding Rods

4.2.3 Pile Dead Load

The testing outline for these experiments called for a dead load on the pile groups during lateral loading. In particular, dead loads of 20%, 50%, and 80% of the vertical bearing capacity of each pile group were applied. The vertical bearing capacity was determined by conducting axial loading tests on 3 by 3 and 4 by 4 pile groups at 36% and 55% relative density. The results of these tests are shown in Figure 4-4 and the results of this capacity determination method are listed in Table 4-1. Once these capacities were determined it was discovered that the dead weight due to the guiding rods, pile caps, and base plate was approximately equal to 20% of the bearing capacity of each group. The weight need for the 50% and 80% dead loads were fashioned out of lead and they were all attached to the pile group at either the bottom of the pile base plate or on top of the individual pile row caps. In the 3 by 3 tests a ring of lead was attached to the bottom of the pile base plate to supply the dead load for 50% of the axial group capacity. For the 80% dead load a lead bar was placed on

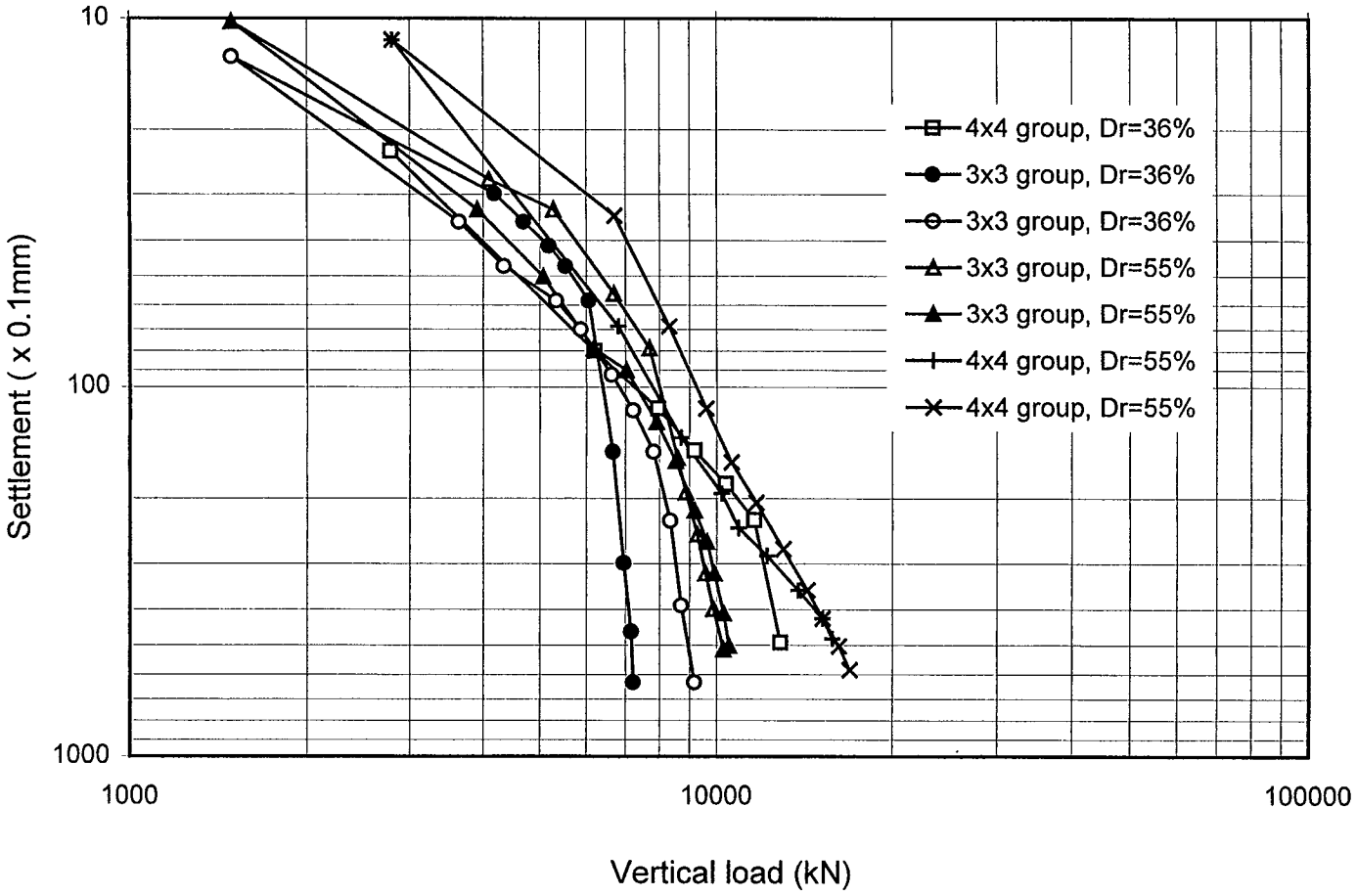

Figure 4-4 Vertical bearing capacities in logarithmic scales

Table 4-1 Pile Group Bearing Capacities

Density (%)	3 by 3 (kN)	(Kip)	4 by 4 (kN)	(Kip)
36	8400	1876	6063	1363
55	6900	1540	7410	1666

each pile row cap. In the 4 by 4 tests a lead ring attached to the pile group base plate provided the dead weight equal to 50 % of the capacity. An additional lead weight was placed on top of the middle two rows to provide the weight for 80% of the bearing capacity.

4.3 TEST SAND

In previous tests Reid-Bedford sand was used for centrifuge testing at the University of Florida. Due to a short supply and the difficulty to obtain more, it was decided to make a soil mixture with similar properties as a substitute.

4.3.1 Test Sand Properties

The new soil mixture, hereafter referred to as mixed sand, is composed of two different types of sand from nearby sand mines. After analyzing several trial mixtures by grain size distribution analysis a final mixture and sieve analysis were conducted in accordance with ASTM D-42. The results of this are given in Tables 4-2 through 4-4. A series of triaxial tests were also run and the results are reproduced in Table 4-3.

Table 4-2 Sieve Analysis on Mixed Sand

Sieve Number	20	30	40	50	60	100	200
Opening size (mm)	0.85	0.60	0.43	0.30	0.25	0.15	0.08
Percent Passing	99.97	99.30	94.84	77.46	59.35	8.31	0.10

Table 4-3 Triaxial Test Results

Unit weight [KN/m^3]	13.76	14.37	14.71	14.81	15.16
Relative Density	23.8%	51.7%	66.2%	70.4%	84.8%
Phi angle [degrees]	32.6	36.9	38.2	39.2	41.0

Additional laboratory testing included a determination of the maximum and minimum void ratio and a specific gravity test in accordance with ASTM D-422 specifications. The results are shown in Table 4-4.

Table 4-4 Additional Laboratory Testing

Specific Gravity	2.645
Maximum Void Ratio	0.957
Minimum Void Ratio	0.671
Minimum Unit Weight [kN/m^3]	13.28
Maximum Unit Weight [kN/m^3]	15.56
Uniformity Coefficient	1.7
50% passing size [mm]	0.23

CHAPTER 5
SAMPLE PREPARATION AND TEST PROCEDURE

5.1 SAMPLE PREPARATION

Two relative densities were used for each of the tests (loose and medium dense) and they were 36% and 55%. The samples were prepared by pouring the sand through three rectangular screens stretched tightly across and encased in a wooden box which prevents the sand from falling out of the sample container. The screen size opening is roughly equivalent to a number 14 sieve. When preparing the 36% relative density sample, the sand was rained down through this wooden box on top of another resulting in a drop height of 22 inches to the soil sample bucket. For the 55% relative density sample, the sand was rained down through two additional boxes for a drop height of 31 inches to the bucket. A picture of the boxes is shown in Figure 5-1.

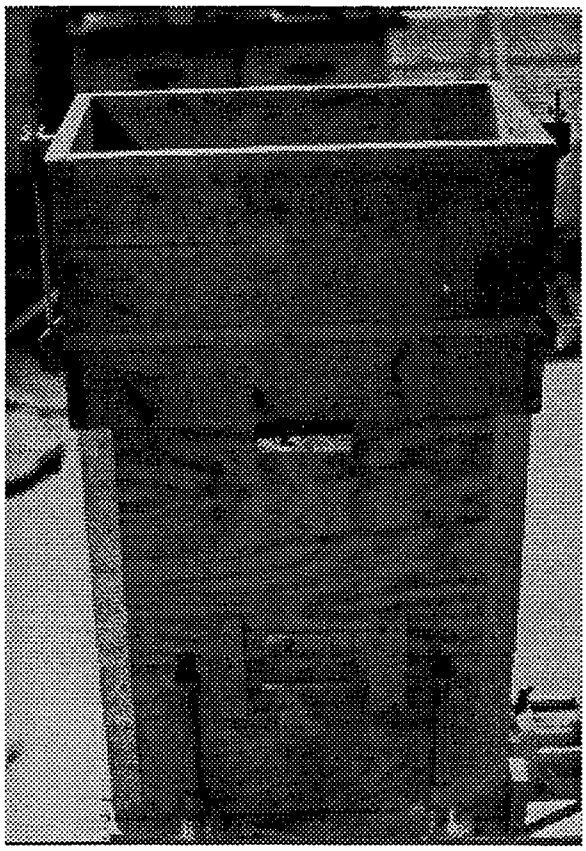

Figure 5-1 Sand Raining Boxes

The volume of the bucket is 1.116 cubic feet. Once the sand was in the bucket it needed to be scraped flush with the top of the bucket and then weighed. Repeat this process until the correct weight to yield the prescribed sample density. Samples were weighed using a transducer and the WEIGH program on the centrifuge PC. For the 36% loose sample the weight had to be 101.95 ± .05 lbs before scraping and for the 55% relative density dense sample the weight before scraping had to be 105.25 ± .05 lbs. During the weighing, sand usually had to be added to increase the weight. Once the weight was obtained the actual sample density was calculated and recorded. Then a 1 inch layer was scraped from the top of the sample to ensure that the strain gages would not be in the sand during loading.

5.2 TEST PREPARATION

5.2.1 Centrifuge Balance Calculations

Before testing could begin, the additional weights of the equipment on the swing out platform side of the centrifuge arm due to the samples had to be balanced by an appropriate counterweight on the opposite side. The weights were calculated at 1g and the distances were from the axis of rotation to the centroid of the object when the swing out platform was up. The centrifuge arm length was 63.375 inches measured from the center of rotation to the bottom of the swing out platform when it was fully extended. From past data it was assumed that the moment due to the permanent centrifuge equipment was equal to 17,934 inch lbs and that the out of balance moment caused by the camera weight was within acceptable tolerances. The distance from the bottom of the platform to the center of the bucket was equal to 6.5 inches, and the distance from the top of the bucket to the center of the pile driver was 14.5 inches.

The maximum and minimum moments on the equipment side of the centrifuge arm are given in the bottom of Table 5-1. These extremes were the result of weights differences among the samples due to dead loads (20%, 50%, 80%) and soil densities (loose versus medium dense). In particular, the maximum moment was calculated for a medium dense sample with 80% dead load and the minimum was for a loose sample with 20% dead load. The average of these, 17,146 inch lbs, when compared to the moment produced by the permanent centrifuge equipment, 17,934 inch lbs, was found to be out of balance by 788 inch lbs which was not acceptable.

After a review of the material immediately available at the centrifuge, it was decided to place two plates totaling 16.5 lbs on the counterweight side and to place a 25 lb plate on swing out platform to balance these. The additional calculations are given in Table 5-2 below. The new permanent moment on the centrifuge with the addition of these plates was 18,644 inch lbs and the average of the testing side was 18,730 inch lbs. This led to an out of balance moment of 86 inch lbs which was within the acceptable tolerances of the centrifuge.

Table 5-1 Centrifuge Balance Calculations

Equipment	Wt_{max} (lbs)	Wt_{min} (lbs)	R_{max} (inches)	R_{min} (inches)	M_{min} (inch lbs)	M_{max} (inch lbs)
Sand Sample	105.27	101.95	55.875	55.875	5696.46	5881.96
Bucket	149.46	149.46	56.375	56.375	8425.81	8425.81
Pile Driver	49.75	49.75	35.375	34.495	1716.13	1759.91
Dead Load	16.07	6.3	43.775 41.885	50.775 48.885	275.8	785.581
Multiplexer box	21.0	21.0	11.5	11.5	241.5	241.5
Bucket connecting cable	5.6	5.6	52.875	52.875	296.1	296.1
2 LVDT, clamps, loading rods	2.5	2.5	49.875	49.875	124.7	124.7
				Sum =	16776.5	17515.6

Table 5-2 Additional Centrifuge Calculations

Location of Weight	Additional Weight (lbs)	Distance from COR (inches)	Additional Moment (inch-lbs)	New Moment (inch-lbs)
Counter Weight Side	16.5	43	709.5	18,644
Swing out Platform side	25	63.375	1584	18,730
			Difference =	86

5.2.2 Preparing and Securing the Pile Driver Onto the Bucket

The piston rods in the pile driving pistons were fully retracted and the pile base plate and pile caps were put up into the pile driving superstructure. The pile caps were then attached to the piston rods using duct tape. This was done in order to prevent the pile tips from disturbing the sample as the pile driver superstructure was lowered onto the bucket. The trap door was then attached to the threaded ends of the trap door piston rods. After this the trap door was lifted up. The pile driver was then lowered onto the bucket, making sure the steel pins on the driver fit securely into the corresponding holes on the bucket. Once the driver was onto the bucket the steel frame was put onto the pile driving base plate. Four 0.375 inch steel threaded rods were then inserted through the steel frame and into the holes in the base plate of the bucket and secured using a series of washers.

5.2.3 Securing Bucket Into the Centrifuge

Once a sample was prepared and the driver attached to the bucket, the testing apparatus was lowered into the centrifuge and placed onto the swing out platform. As it was lowered the holes on the bucket were lined up with the corresponding ones on the swing out platform of the centrifuge. The bucket and driver were then secured to each other using four 0.4375 inch bolts. A picture of the bucket and driver mounted on the centrifuge arm is shown in Figure 5-2.

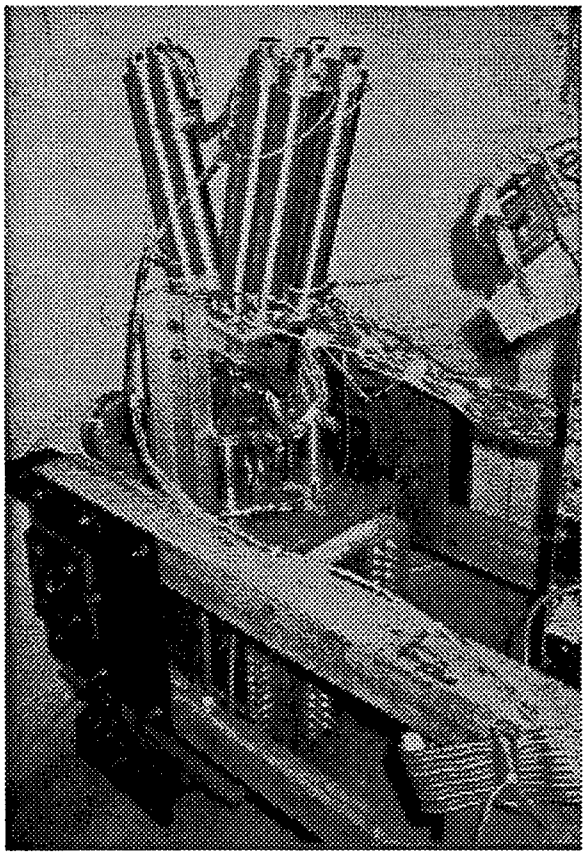

Figure 5-2 Bucket and Driver Mounted on the Centrifuge Arm

5.2.4 Instrumentation Assembly and Testing

Once the driver was secured onto the bucket in this manner the plugs from the piles were inserted into the appropriate outlets on the multiplexer. This connected the strain gage output to the centrifuge PC. Next the loading rod with the 1000 pound load cell at the tip was inserted into the 4 inch diameter air piston.

After this the horizontal LVDT was then screwed into a bar projecting upwards from the bucket so that it touched the cross bar that moved in tandem with the loading piston. Next the tubes from the air valves on the manifold for the loading piston, three driving pistons, retraction, and trap door were screwed in the appropriate ports. The vertical LVDT was screwed into its bar on the pile driver base so that it was touching the pile base plate so it could record vertical deflection during

loading. At this point a zero reading was taken in LPG-TOM to see if the load cell was reading correctly. Another reason was to see that the LVDT output was within the correct range, +15 Volts to -15 Volts, and to check the strain gage output to see if any wires had been inadvertently severed. A picture of the LVDT, loading piston, and air piston as they are set up down inside the centrifuge is given in Figure 5-3.

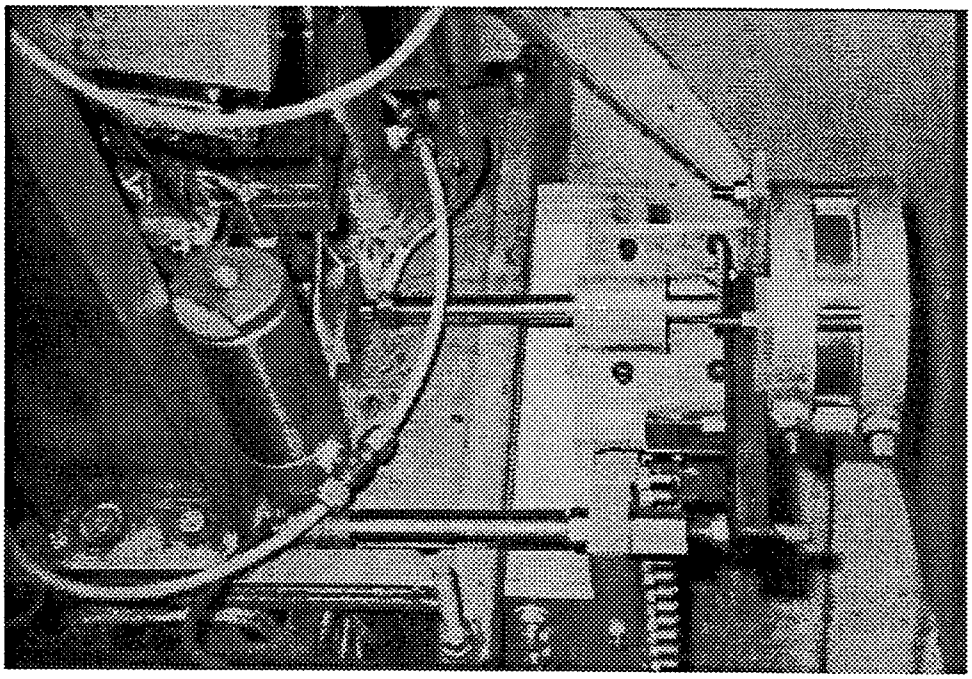

Figure 5-3 Horizontal LVDT, Loading Rod and Piston

5.2.5 Pile Pre-embedment and Epoxy Application

Once the readings were determined to be satisfactory the tape holding the pile rows to the retracted driving pistons was removed and the pile rows were carefully pre-embedded into the soil a distance of approximately 3 inches. This was done making sure to minimize sample disturbance. The primary reason for pre-embedding the pile group was to provide stability during driving. After

the piles were pre-embedded, DEVCON 2 ton epoxy and it's hardener were mixed together and stirred for three minutes before being applied to the pile base plate. No epoxy was applied to the bottom of the pile cap and care was taken not to get any epoxy on the guiding rods as this would interfere with driving.

5.3 TEST PROCEDURE

At this point the door to the centrifuge was closed and the speed control driver was programmed to output a frequency of 30.17 Hz. A picture of the speed control driver is given in Figure 5-4. This brought the centrifuge's speed of rotation to 178 rpm which resulted in an acceleration 45 times normal gravitational acceleration at the surface of the sample.

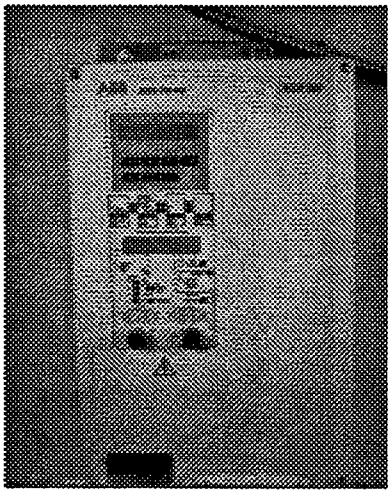

Figure 5-4 Speed Control Driver

5.3.1 Pile Driving

Pile driving was controlled with the control panel which was mounted on the air pressure regulator as shown in Figure 5-5. Six switches are visible above the pressure regulator. These switches

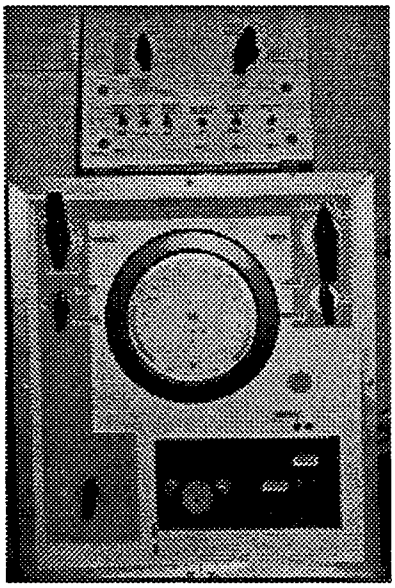

Figure 5-5 Air Pressure Regulator and Control Panel

are numbered 1 through 6 from left to right and they control the flow of air pressure to the various pistons on the bucket and the driving superstructure.

The two valves above these switches are the three and four way valves which govern the usage of regulated and unregulated air pressure. The regulator knob directly below the large pressure gage controls the magnitude of the applied lateral load. To start driving, switches 1 to 3 were toggled on, allowing regulated air through the rotary union to the top ports of the driving pistons. Subsequently, pressure was controlled with the regulator and the rows were driven individually. In the case of the 3 × 3, the middle was driven and then the 2 outer rows. For the case of the 4 × 4, the two inner rows were driven first and then the 2 outer rows.

Once all the piles were driven, switches 1 to 3 were toggled off, and switch number four was toggled on, allowing regulated pressure into the bottom ports of the driving pistons and allowing the driving pressure to vent from the top ports. The pressure regulator was set to an appropriate seating pressure, usually 30 psi. Sometimes the seating pressure was set higher if it was felt that there was

insufficient contact between the pile caps and the base plate. This seating pressure was maintained for at least three hours in all tests to allow the epoxy to adequately harden before lateral load testing began. If the epoxy was not hard enough during testing the pile caps for each row could separate from the base plate and jeopardize all of the test results.

5.3.2 Lateral Load Testing

After the three hours had passed the lateral load test began. This was conducted using the pressure regulator and the computer program LPG-TOM. A picture of the apparatus during testing is given in Figure 5-6. The first step was setting the three way valve and the four way valves such that the regulated pressure passed through the E/P transducer and was under the control of the LPG-TOM computer program. The next step was to turn off switches 1 through 3 and turn on switch 4.

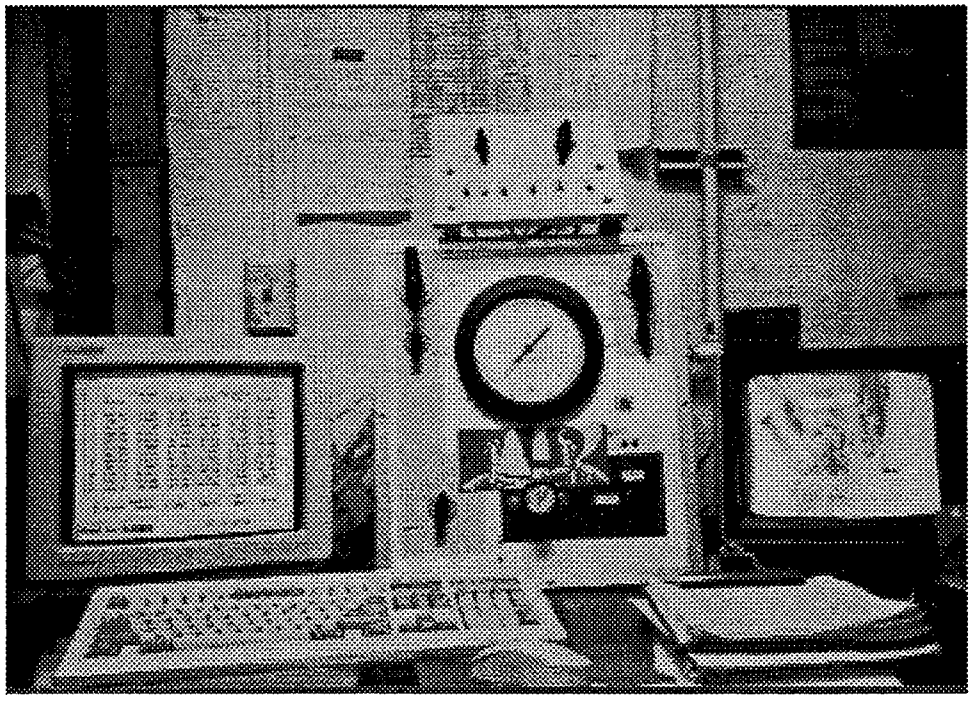

Figure 5-6 Testing Apparatus

Once this was done the driving pistons were fully retracted into the driving superstructure. After this, switch 4 was switched to the off position. Next the switch controlling the trap door, switch 5, was

set to the down position, dropping the trap door below the pile base plate. At this point the pile group was supported by the soil only. After the trap door was dropped, switch 6 was turned on, allowing regulated pressure down into the loading piston. A zero reading was taken for all the equipment as a final check on instrumentation. Next the three way and four way valves were set so that they allowed regulated pressure to travel through the PC controlled E/P transducer to the loading piston. This transducer was controlled by PC in order to produce the correct air pressure in the loading piston.

The lateral load was then applied. The load applied, as measured by the load cell at the tip of the piston, and the lateral movement, as measured by the LVDT, was sent to LPG-TOM through the data acquisition unit at each load step. The computer stored these voltage signals in a text file and displayed them on the screen in model and prototype units. The computer would sample data 5000 times and report the average every two minutes for a period of 6 minutes. This continued until the pile group reached failure at a lateral deflection of 3 inches.

5.3.3 End of Testing

After the pile group failed the centrifuge was stopped and all the air pressure was turned off as were the power supplies. The pile group was then examined to see if there were any problems with contact pile cap and pile base plate contact. Another possible problem was the one of excessive pile cap rotation. This was a problem because it could cause the top of the guiding rods to touch the bottom of the retracted driving pitons during testing. It could also cause the pile base plate to come in contact with the trap door during testing. Any one or a combination of these occurrences could adversely affect the results and necessitate repeating the entire testing procedure. After the driver, bucket, and pile group was lifted out of the centrifuge, the epoxy on the pile base plate was scraped off and the area cleaned to ensure a clean contact area for future tests.

CHAPTER 6
RESULTS AND DISCUSSION

6.1 3 BY 3 LOAD DEFLECTION RESULTS

The load deflection data for the 3 by 3 groups are given in Table 6-1 below. The loads given are the average of two different days' tests. The repeatability was good for the majority of the tests. The Dead loads are a percentage of the bearing capacity of the pile group as determined by centrifuge tests. Appendix B contains the original data from which this table was made.

Table 6-1 3 by 3 Load Deflection Results

3 by 3	R_d (%)	Dead Load (% of capacity)	Batter Configuration	Average Load at 1 in. deflection (ton)	Average Load at 2 in. deflection (ton)	Average Load at 3 in. deflection (ton)
	36	21.8	3F6R	110	145	170
	36	21.8	6F3R	115	145	175
	36	48.4	3F6R	120	155	190
	36	48.4	6F3R	115	165	195
	36	78.5	3F6R	110	140	175
	36	78.5	6F3R	125	165	190
	55	17.9	3F6R	140	182	210
	55	17.9	6F3R	95	145	180
	55	48.1	3F6R	155	205	235
	55	48.1	6F3R	130	185	225
	55	82	3F6R	135	185	230
	55	82	6F3R	145	195	225

6.1.1 Effect of Batter Direction in 36% R_d Soil

In 36% R_d soil and at 21.8% of vertical dead load it can be seen that there is no great difference in lateral capacity with respect to the batter direction; the 6F3R group is only 2.94% higher at

3 inches. The At 48.4% vertical dead load on the pile cap there is also no significant change in lateral capacity with a change in batter configuration; the 6F3R group has a 2.6% higher capacity at 3 inches. At 78.5% dead load the greatest capacity increase with increasing number of forward battered piles was observed. The increase was 14%, 18% and 9% at 1, 2 and 3 inches respectively.

6.1.2 Effect of Batter Direction in 55% R_d Soil

At 55% relative density the difference in capacity with batter direction was more discernible for every load case. At 17.9 % dead load the group with the greater number of piles battered in the reverse direction has a higher capacity. In particular the increases were 47%, 26%, and 17% at 1, 2, and 3 inches respectively. The same was true for the groups with 48.4% dead load though the increases were smaller. They were 19%, 11%, and 4% at 1, 2, and 3 inches respectively. At 82% the smallest capacity increase with increasing number of tension piles was observed. The increases were 7%, 5%, and 2% at 1, 2, and 3 inches respectively.

6.1.3 Effect of Dead Load in 36% R_d Soil

There was a significant increase, 11.8% at 3 inches, in lateral resistance for the groups with 3F6R configuration as the dead load increased from 21.8% and 48.4%. Increases of 9% and 7% were observed at 1 and 2 inches. As the dead load increased to 78.5%, the resistance at 3 inches was observed to decrease by 8.6%, load at 2 inches decreased by 10.7% and at 1 inch by 9%. This data suggests that the lateral capacity of groups in 36% soil increases with dead load up to a point, most likely because of increased pull out resistance of the tension piles, and then decreases. The decrease probably occurs because of the bearing failure capacity of the compression piles.

The capacity of 6F3R groups increased as the dead load amount went from 21.8% to 48.4% of the bearing capacity. The magnitude of this increase was 11.4% at 3 inches of deflection. The load at one inch remained the same and the 2 inch load increased by 14%. As the dead load increased

to 78.5% the resistance of the group at 2 and 3 inches of deflection remained essentially constant while at 1 inch it increased by 9%.

6.1.4 Effect of Dead Load in 55% R_d Soil

For the groups battered 3F6R there was an increase in lateral resistance between the pile groups with 17.9% and 48.1% dead load. The magnitude of this increase was almost equal at all deflections being 12%, 13%, and 11% and 1, 2, and 3 inches respectively. As the dead load increased from 48.1% and the 82% the lateral resistance at 3 inches decreased by 4%. Similarly, the loads at 1 and 2 inches decreased by 15% and 11% respectively.

The groups with 6F3R pile configurations showed a large increase in lateral resistance at all deflections as the dead load changed from 17.8% to 48.1% of the vertical bearing capacity. The increases were 37%, 28%, and 25% at 1, 2 and 3 inches respectively. The 3 inch capacity remained about the same with the increase in dead load from 48.1% to 78.5% dead load. At 1 and 2 inch deflections the load increased slightly by 5.4% and 7.4% respectively.

6.1.5 Effect of Density

There was a large increase in capacity with density for the 3F6R groups at 20% dead load. At 1, 2 and 3 inches of deflection the resistance increased by 27%, 26%, and 18% respectively. An even larger increase was observed for the groups with 50% dead load; 29%, 32% and 24% at 1, 2, and 3 inches of deflection. A similarly large increase was observed at 80% dead load being 31.4%, 32%, and 23% at 1, 2 , and 3 inches of deflection respectively.

For the groups battered 6F3R and with 20% dead load the changes in lateral resistance with increasing density at all deflections were small, less than 5%. In contrast to this the groups with 50% dead load experienced significant resistance increases with increasing density. They were 13%, 12%,

and 13% at 1, 2, and 3 inches of deflection respectively. At 80% dead load the capacity increased by nearly equal percentages, between 16% and 18% at all deflections.

Overall the groups with 3F6R pile configurations experienced a much higher increase in lateral resistance, almost twice as much, with density than the 6F3R groups at all dead loads.

6.2 LATERAL LOAD DISTRIBUTION FOR 3 BY 3 GROUPS

Table 6-2 shows how the lateral load was taken up by the individual rows in each of the pile groups tested. The percentages for each row were in terms of total lateral load and the dead load was in terms of percentage of bearing capacity determined by centrifuge tests. These results of these tests were discussed in Chapter 4.

Table 6-2 Lateral Load Distribution for 3 by 3 Groups

Density (%)	Dead Load (%)	Batter Configuration	Lead Row (%)	Second Row (%)	Trail Row (%)
36	21.8	3F6R	43.50	35.4	21.1
36	21.8	6F3R	49.5	29.4	21.1
36	48.4	3F6R	36.3	35.2	28.5
36	48.4	6F3R	44.3	29.4	26.3
36	78.5	3F6R	32.2	27.4	40.4
36	78.5	6F3R	28	31.2	40.8
55	17.9	3F6R	43.8	34.3	21.9
55	17.9	6F3R	42.5	28.1	29.4
55	48.1	3F6R	32.5	33.1	34.4
55	48.1	6F3R	35.5	34.7	29.8
55	82	3F6R	30.6	29.3	40.1
55	82	6F3R	30.2	35.5	34.3

6.2.1 Effect of Batter Direction

At 36% density, 3F6R and 21.8% dead load, the highest percentage of the load was taken by the lead row and for the group battered 6F3R the highest percentage was also in the lead row. With the increasing number of piles battered forward the lead row's percentage of the lateral load increased while the middle row decreased and the trail row remained constant. The same was true for groups with 48.4% dead load for both configurations although the trail row showed a slight decrease in load percentage. At 78.5% dead load, 3F6R, the load percentage in the lead row decreases and was taken mostly by the middle row, with only a small increase in the trail row percentage.

At 55% density, 3F6R and 17.9% dead load, the lateral load taken by the lead row decreased slightly with a larger reduction in the second row as the configuration changed to 6F3R. This load was taken by the trail row. With 48.1% dead load, the lateral load was fairly evenly distributed among the rows at the 3F6R configuration. When the configuration was reversed, increasing the number of forward battered piles, the distribution became skew toward the leading rows and middle rows. At 82% dead load, the data suggest for the 3F6R configuration that the trail row took the most load while the lead and second rows took about equal portions of the lateral load. As the number of piles battered forward increased, at 82% dead load, the load became more evenly distributed among the rows. The percentages for the 6F3R case at 82% dead load were 30.2%, 35.5%, 34.3% for the lead, second, and trail row respectively. The load percentages should be increasing from the lead to the trail row.

6.2.2 Effect of Dead Load in 36% R_d Soil

From the results it was observed that a greater portion of the lateral load was being carried by the trailing rows for the 3F6R groups with increasing dead loads. The lead row showed the largest reduction in load percentage and the middle row showed a smaller reduction. For the groups battered

6F3R, the greater portion of the load shifted from the lead row to the trail row. Also in these groups the percentage taken by the middle row remained almost constant (i.e., 29.4% vs. 31.2%) as the dead load changed from 21.8% to 78.5% of the bearing capacity of the group. In both configurations the load percentage of the trail row almost doubled as the dead went from 20% to 80%.

6.2.3 Effect of Dead Load in 55% R_d Soil

It was observed for the 55% density samples with 3F6R configurations that the amount of increase in the lateral load was taken mostly by the trail row as the dead load increased. The percentage in both the lead and middle rows decreased. The load percentage in the lead row experienced a larger reduction than the middle row. As the dead load changed from 17.9% to 82% the percentage of lateral load carried by the trail row nearly doubled, from 21.9% to 40.1%. For the groups battered 6F3R, a larger portion of the lateral load was taken by the second and trail rows with increasing dead load. The overall effect was that the lateral load was distributed more evenly among the rows. This was evident after comparing the load percentages for 17.9% and 82% dead load (42.5%, 28.1%, 29.4% to 30.6%, 34.3%, 35.5%). The load percentages for 17.9% dead load were unusual since the load percentages were expected to decrease from the lead row to the trail row.

6.2.4 Effect of Density

Groups with 3F6R configuration for 20% dead load experienced no significant change in load distribution with a change in density. In contrast, the groups with 6F3R and 20% dead load, the percentage of load taken by the lead and second row decreased and the trail row load percentage increased with increasing densities. The decrease in the middle row was smaller than in the lead row suggesting that the load basically shifted from the lead to the trail row.

For the 50% dead load in 3F6R, the lateral load percentages changed significantly with change in densities, from 36.3%, 35.2%, 28.5% to 32.5%, 33.1%, 34.4%% for the lead, middle and trail

rows, respectively. It was clear that the load shifted from the lead and second rows to the trail row. This also occurred for the 6F3R cases; however the trend was not as significant as observed in the 3F6R groups.

For the 80% dead load case there was no major redistribution in load for any rows in the 3F6R groups. For the groups with 6F3R, the effect of the density increase was that the lateral load shifted from the trail row to the lead and middle rows. The load distribution percentages for the 6F3R groups at 55% density were 30.2%, 35.5%, and 34.3% for the lead, middle and trail rows, respectively. These distribution percentages were unusual, normally they would decrease from the lead to trail row.

6.3 PILE GROUP ROTATION FOR 3 BY 3 GROUPS

Table 6-3 below gives a summary of the vertical displacements, as measured by the vertical LVDT, for the 3 by 3 pile groups at 150 tons of lateral load. The values listed in the table represent the averages of two days' tests.

6.3.1 Effect of Batter Configuration

In the tests performed in the 36% relative density soil, the data implied that the pile group rotation decreased as the number of piles battered in the forward direction increased. For 21.8 and 78.5% dead load, the vertical deflection for the 6F3R was significantly lower than the 3F6R. At 48.4% dead load the vertical deflections for the 3F6R and the 6F3R were similar in value, 0.55 and 0.6. For both group configurations with 48.4% dead load, it appeared that the dead load tended to minimize rotation. The results in the tests conducted in the 55% relative density soil were nearly the opposite of the 36% relative density tests in which the rotation of the pile group increased with an increase in the number of piles battered forward. The sole exception was at 80% dead load where

Table 6-3 Pile Group Rotation for 3 by 3 Groups

Density (%)	Dead Load (%)	Batter Configuration	Vertical Deflection at 150 tons (inches)
36	21.8	3F6R	1.02
36	48.4	3F6R	0.5
36	78.5	3F6R	1.1
55	17.9	3F6R	0.35
55	48.1	3F6R	0.24
55	82	3F6R	0.48
36	21.8	6F3R	0.6
36	48.4	6F3R	0.55
36	78.5	6F3R	0.8
55	17.9	6F3R	0.58
55	48.1	6F3R	0.55
55	82	6F3R	0.36

the vertical deflection was higher for the 3F6R than the 6F3R configuration. The smallest rotation was found at the 48.1% dead load case.

6.3.2 Effect of Dead Load

The data suggested that at 50% dead load the least amount of rotation occurred regardless of soil density or batter direction. The only exception was in the 6F3R group in the 55% density soil. In this case the smallest rotation occurred at the 82% dead load. For the 6F3R groups in the 36% and 55% soil densities the pile cap rotations for the 20% and 50% dead load cases were very similar. The amount of rotation for the 50% dead load case was 10% (36% soil density) and 5% (55% soil density) smaller than the 20% dead load case even though the dead load was more than doubled. This result suggests that the pile cap rotation will not change significantly until the dead load reaches some value beyond 50% for a 6F3R group.

6.3.3 Effect of Density

The result of the tests showed that the rotations of the pile groups decreased as the soil density increased. This effect was more pronounced in the 3F6R groups where the rotations decreased by at least one half for all dead loads. In the 6F3R groups, the rotations were similar at the 20% dead load as that of the 50% dead load case. It suggests that the group rotations might be independent of soil density at dead loads less than 50% for 6F3R groups. For the 80% dead load, the rotation decreased by more than one half as the soil density increased from 35% to 55%.

6.4 4 BY 4 LOAD DEFLECTION RESULTS

Table 6-4 gives the lateral load deflection results for the 4 by 4 pile group tests. The loads in this table represent the average of two days' tests. The repeatability was generally good for all the tests. The dead loads are percentages of the bearing capacity of the pile group as determined by centrifuge tests. Appendix B contains the original data from which this table was made.

Table 6-4 4 by 4 Lateral Load Deflection Results

4 by 4	R_d (%)	Dead Load (%)	Average Load at 1" deflection	Average Load at 2" deflection	Average Load at 3" deflection
	36	22.9	170	240	300
	55	18.7	230	290	370
	36	48.6	220	320	390
	55	51.6	220	340	430
	36	82.6	220	340	400
	55	79.6	260	400	500

6.4.1 Effect of Dead Load

The lateral resistance of the group increased with increasing dead load for 36% and 55% soil densities. For 36% relative density, the largest increase occurred between the 22.9% and 48.6% dead load cases. These were 18%, 25%, and 38% at 1, 2, and 3 inches deflection, respectively. The resistance increase between the 48.6% and 82.6% dead load cases was almost negligible being, i.e., 0%, 6%, and 3% for all deflections. For 55% relative density, the lateral resistance increases with the increase of dead load. The increases between the 18.7% and 51.6% dead loads were 17% and 16% at 2 and 3 inches deflection, respectively, with the exception of the 1" deflection at which the load decreased slightly. The percentage increase of the 51.6% and the 79.6% dead load cases was similar ranging from 16% to 18% for each deflection.

6.4.2 Effect of Density

As expected the lateral capacity of the group increased with increasing soil density. The largest increase occurred at 20% dead load. The increases were 35%, 20%, and 23% at 1, 2, and 3 inches of deflection, respectively. The smallest rise (0%, 6%, and 10%) was observed at 50% dead load. For 80% dead load, the increase was 18%, 18%, and 25% for all deflections.

6.5 LATERAL LOAD DISTRIBUTION FOR 4 BY 4 PILE GROUPS

A description of how the lateral load was distributed among the rows is given in Table 6-5. The lateral loads given for each row are the percentages of the total applied lateral load. The dead loads are the percentages of the vertical ultimate bearing capacity of the group as determined in Chapter 4.

6.5.1 Effect of Dead Load

In 36% relative density soils as the amount of dead load increased from 22.9% to 48.6%, the load taken by the trail row increased significantly, and the lead rows decreased slightly. As the dead load went up from 48.6% to 82.6% the load taken by the lead row increased at the expense of the trailing rows. The load distribution remained practically constant when the dead load increased from 18.7% to 51.6% of the bearing capacity for the 55% soil density case. As the dead load increased

Table 6-5 Lateral Load Distribution for 4 by 4 Groups

Density (%)	Dead Load (%)	Lead Row (%)	Second Row (%)	Third Row (%)	Trail Row (%)
36	22.9	33.3	29.3	26.4	11
36	48.6	31.2	26.1	25.7	17
36	82.6	39	23.8	23.2	14
55	18.7	34.8	27.4	24.6	13.2
55	51.6	34.8	27	24.2	14
55	79.6	28.4	27.2	26.2	18.2

from 51.6% to 79.6%, the percentages of load carried by the middle two rows did not change significantly while the load shifted from the lead to the trail row.

6.5.2 Effect of Density

At approximately 20% dead load, it appeared that lead and trail rows carried slightly more loads at the expense of the middle rows. At approximately 50% dead load, the load percentages of the trailing two rows decreased while the leading rows increased with increasing density. At 80% dead load, the lead row percentage dropped by 10.6%, when density increased from 36% to 55%. The decreased amount was evenly distributed among the trailing rows.

6.6 PILE GROUP ROTATIONS FOR 4 BY 4 GROUPS

Table 6-6 below gives the displacements measured by the vertical LVDT when the pile group was loaded to 200 tons. The graphs of the original data used to generate this table are presented in Appendix B.

Table 6-6 Pile Group Rotations for 4 by 4 Groups

Density (%)	Dead Load (%)	Vertical Deflection at 200 tons (inches)
36	22.9	0.3
36	48.6	0.03
36	82.6	0.1
55	18.7	0.15
55	51.6	0.07
55	79.6	0.07

6.6.1 Effect of Dead Load

In loose sands the smallest rotations occurred in the pile groups with 50% dead load. It also suggests that in medium dense sands the pile group rotation decreased while dead load increased from 18.7% to 51.6% and then remained constant, while dead load increased from 51.6% to 79.6%.

6.6.2 Effect of Density

At 20% dead loads, the cap rotation reduced by one half as the density increased from 36% to 55%. At 50% dead loads the rotation increased from 0.03 to 0.07 inches as the density increased from 36% to 55%. At 80% dead loads the rotation decreased from 0.1 to 0.07 inches with increasing soil density.

CHAPTER 7
FLORIDA PIER COMPARISON

7.1 INTRODUCTION

FLORIDA-PIER is a finite elements program that can be used to predict the behavior of pile groups in sand subjected to both lateral and vertical loads. In these experiments the program was used to model the centrifuge load-deflection, shear, and axial force responses. When using this program the lateral and axial soil-pile interaction model, and the required soil properties used to predict the behavior of piles are chosen by the user. This chapter gives some general background of the FLORIDA-PIER. Some representative test results are also presented to compare with the program's predictions.

7.2 SOIL PROPERTIES

The soil model used in this analysis is based on the p-y model developed by Reese, Cox, and Koop (1974) through their testing of pipe piles. The input soil properties required by this model are the unit weight, angle of internal friction angle, Poisson's ratio, subgrade reaction modulus, shear modulus, and coefficient of skin friction on the pile. The unit weight was obtained by weighing a sample of known volume. The angle of internal friction was obtained from triaxial tests previously performed by Molnit (1995); the results of which are given in Chapter 4. Poisson's ratio was taken as 0.2 as recommended in Appendix B of the FLORIDA-PIER manual. The remaining properties were difficult to measure and estimations were required. A more detailed discussion of their determination is provided in Appendix A. All properties were input into FLORIDA-PIER in kips and inches. Table 7-1 lists the final soil properties used in the program. The asterisk on the shear modulus (G) values indicates that the value is at the pile tip.

Table 7-1 FLORIDA-PIER Input Data

Density	ϕ	k (kci)	γ (ksi)	G (ksi)	τ_f (ksi)
Loose (top)	34.5	0.029	0.0000517	0.0015	0.0015
(bottom)	34.5	0.029	0.0000517	1.05 / 0.95*	0.00806
Dense (top)	37.1	0.06	0.000053	0.0015	0.0019
(bottom)	37.1	0.06	0.000053	1.3 / 1.1*	0.0085

7.3 PROTOTYPE DIMENSIONS

The diagram given in Figure 7-1 is the dimensions of the scaled up pile group configurations. The free length for each pile group was 107.9 inches, the pile length was 517.5 inches as measured from the center of the pile cap, and the soil depth was 517.5 inches. Also when the pile groups were input into FLORIDA-PIER a 1.5 pile diameter overhang was added to the pile cap.

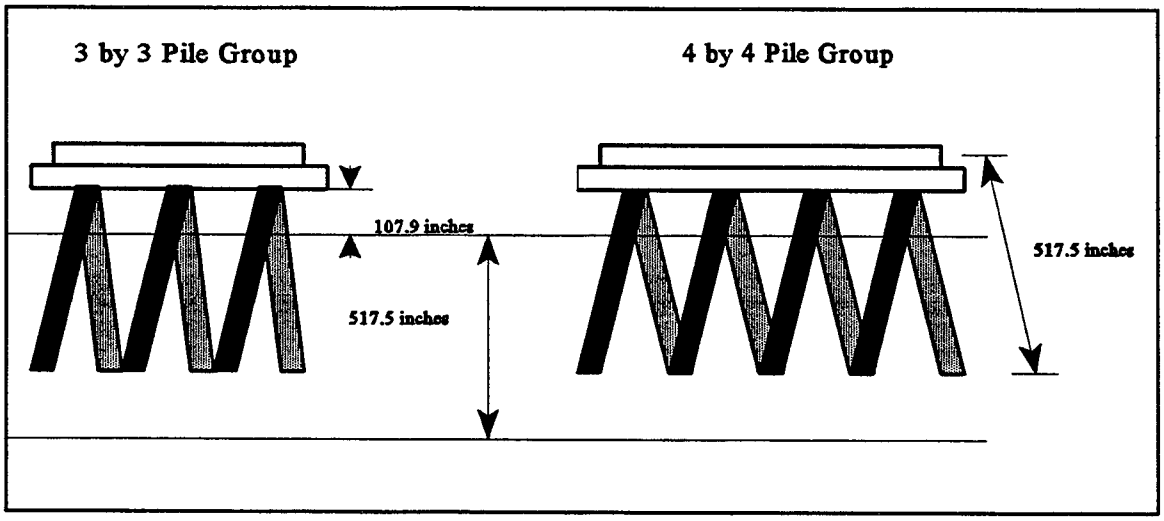

Figure 7-1 Pile Group Dimensions

7.4 py MULTIPLIERS

P-Y curves were based on the ones developed by Reese, Cox, Koop (1974) and the general shape of them are shown in Figure 7-2. P-Y multiplier values used were 0.8 for the lead row, 0.4 for

the second row, 0.3 for the third row, and 0.3 for the trail row in the 4 by 4 groups. These values were used for all of the load cases according to McVay et al. (1994). The p-y multipliers are for pile spacing of 3 pile diameters.

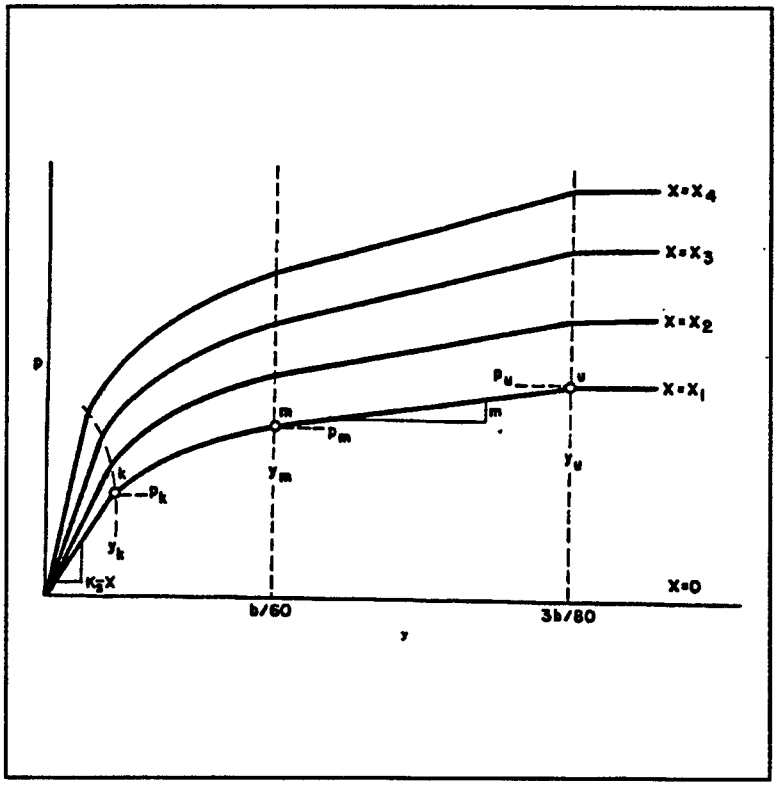

Figure 7-2 P-Y Curves for Static and Cyclic Loading of Sand (after Reese, et al, 1974)

7.5 REPRESENTATIVE PREDICTIONS FROM FLORIDA-PIER

A representative sample of the FLORIDA-PIER predictions and the data collected in these experiments are given below. The figures in this section are for a 3 by 3 pile group founded in medium dense sand with a dead load equal to 17.9% of its ultimate vertical bearing capacity on top of it. Figure 7-3 depicts the lateral load versus the lateral defection measured during testing. The results from the tests of three different days are repeatable and they show the same general shape. The FLORIDA-PIER prediction is the solid line with the FP abbreviation. It is evident that the pre-

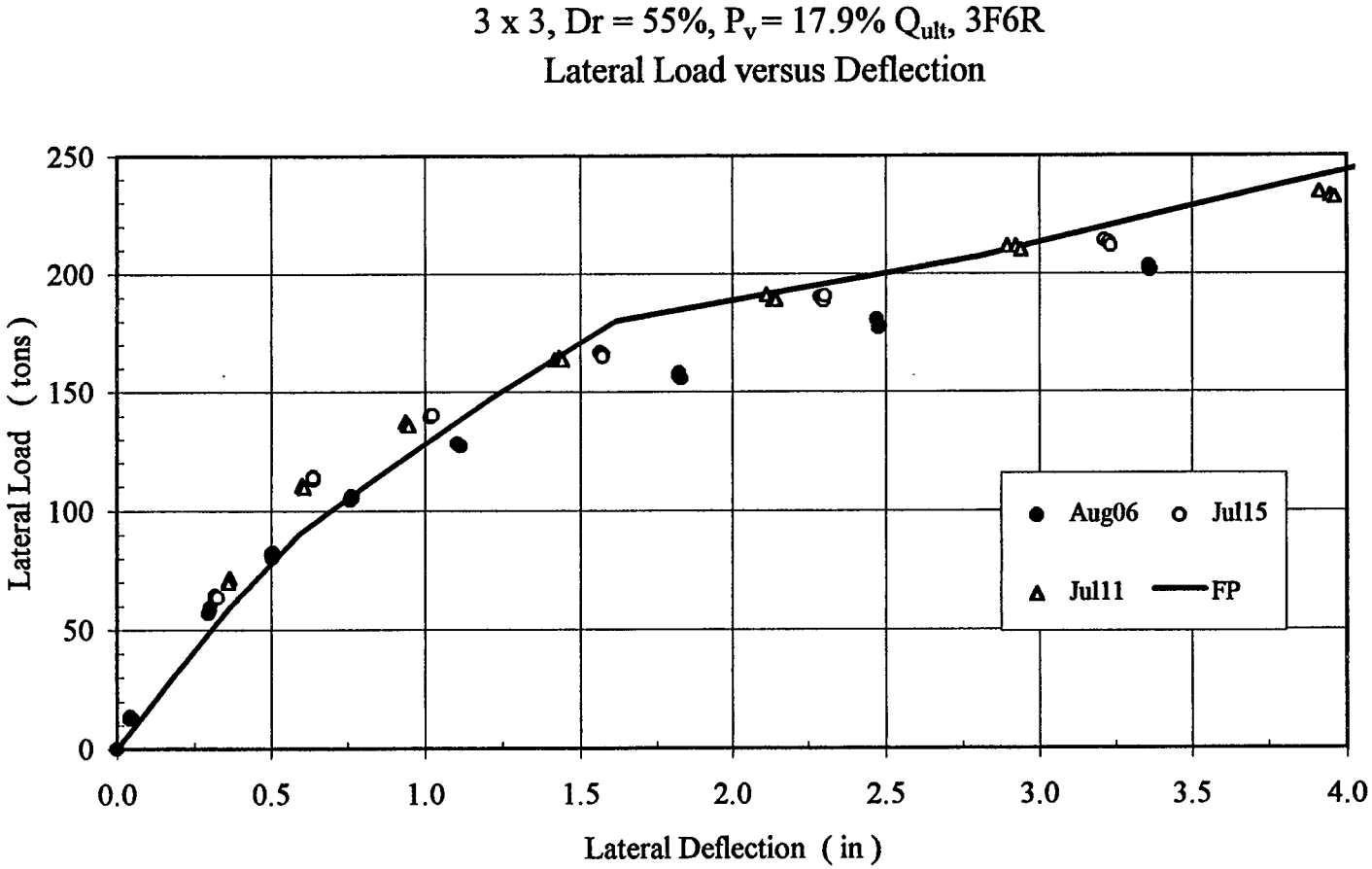

Figure 7-3 Lateral Load versus Deflection

diction follows the same general shape of the measured loading curves. In the beginning portions the predictions show slightly softer behavior than that of measured but after approximately 1.5 inches of deflection it matches almost exactly with the measured data.

Figure 7-4 shows the shear in each of the piles in the lead row versus the measured lateral deflection. The "O" stands for the outer piles of the group and the "I" stands for the inner piles of the group. The dashed line is the prediction for the inner rows and the solid is the prediction for the outer rows. The predictions are close to the measured values at lower deflections and then become significantly higher than the data after approximately 1.5 inches deflections. There are some scattering among the data obtained from tests at different dates but they retain the same general shape. In particular the inner rows whereas the measured data tend to flatten out below the FLORIDA-PIER predictions. The predictions for the outer rows is reasonably close to the measured data.

Figure 7-5 shows the shear force of the piles in the second row versus the lateral deflection. It is evident that the FLORIDA-PIER predictions follow the same general trend of all the test data. However, data obtained from tests performed at various dates were not quite the same.

Figure 7-6 shows the shear force in the trail row versus the lateral deflection. The data shows fairly good repeatability between the tests performed on two different dates. Also the FLORIDA-PIER predictions follow the same trend as the data.

Figure 7-7 depicts the sum of the shear in each pile row versus the lateral deflection of the group. The L, 2, and T in the legend stand for the lead, second, and trail rows respectively. The data shows that the second and trail rows had good repeatability between the two days' tests. The lead row, however, did vary significantly. The FLORIDA-PIER predictions for the second and trail rows begin very close to the data and then become slightly higher. The lead row prediction matches one day's data well while it is significantly higher than the other day's.

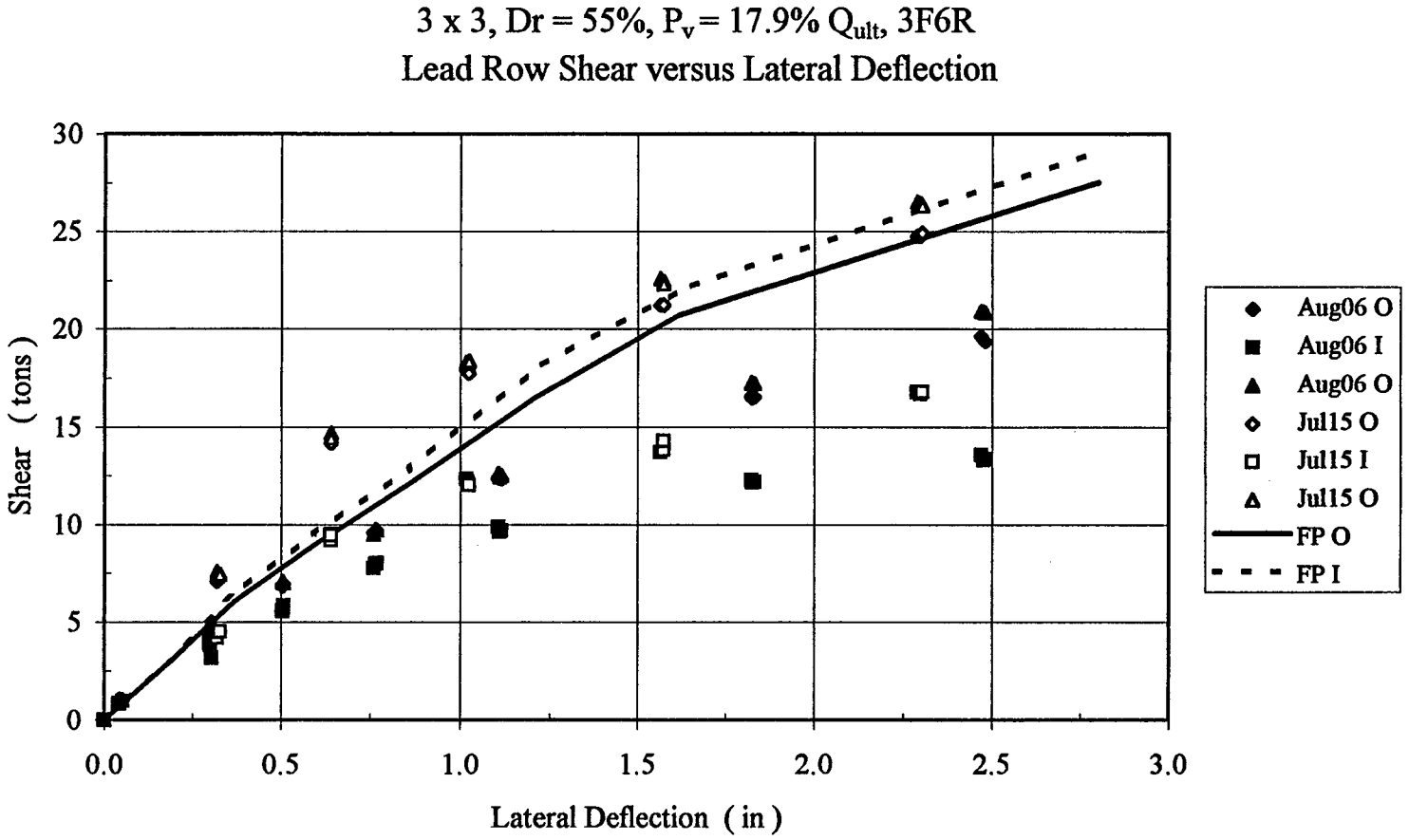

Figure 7-4 Lead Row Shear versus Lateral Deflection

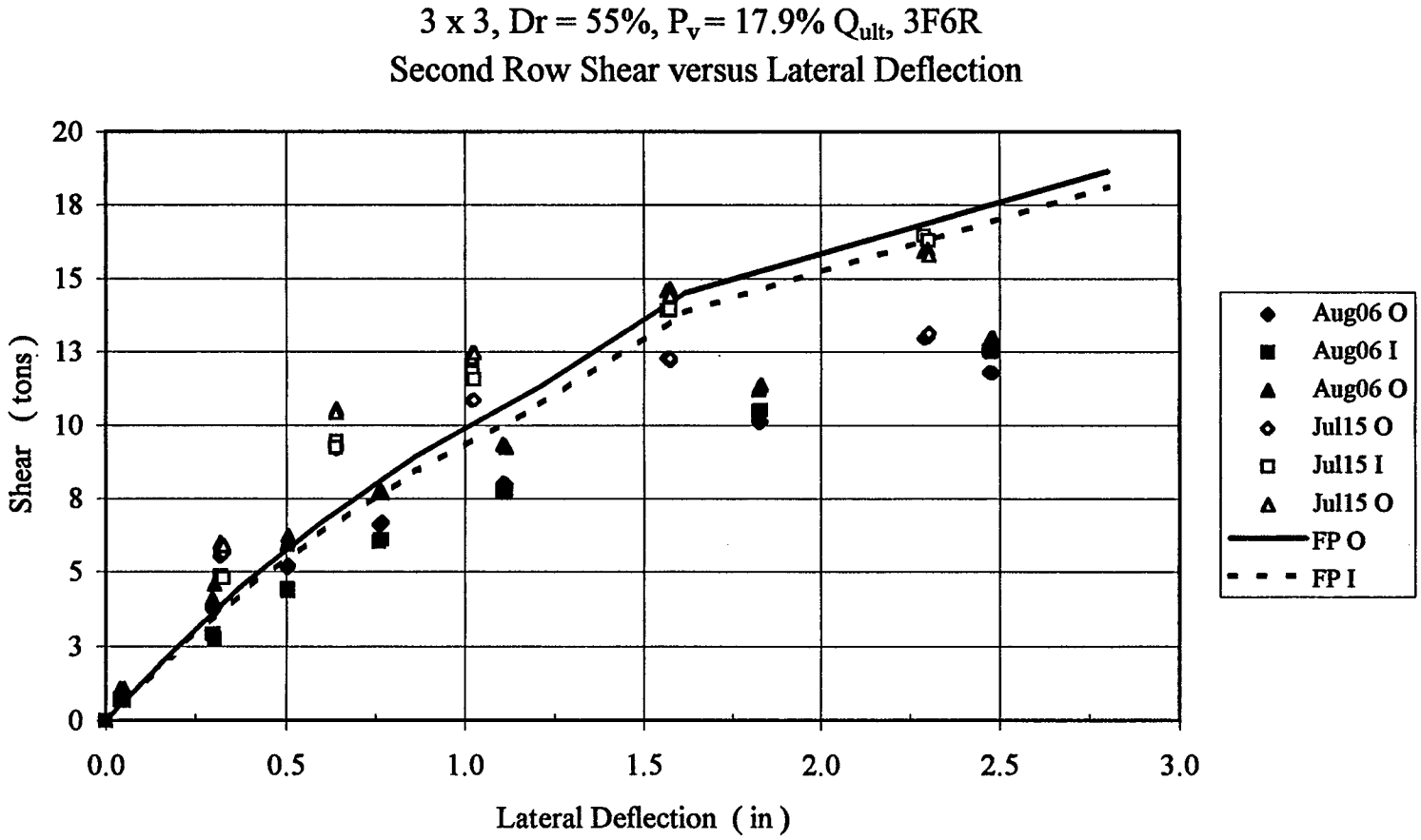

Figure 7-5 Second Row Shear versus Lateral Deflection

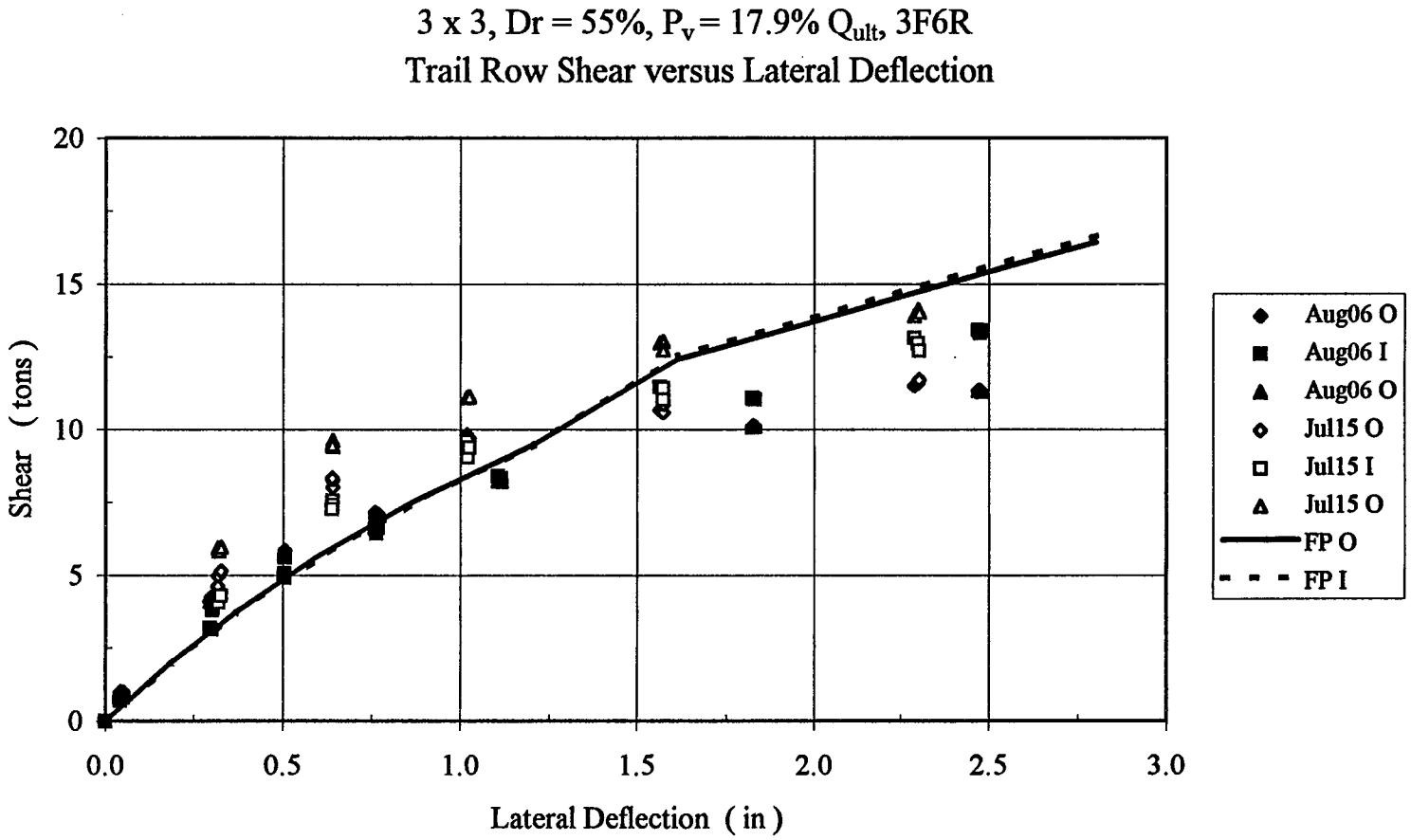

Figure 7-6 Trail Row Shear versus Lateral Deflection

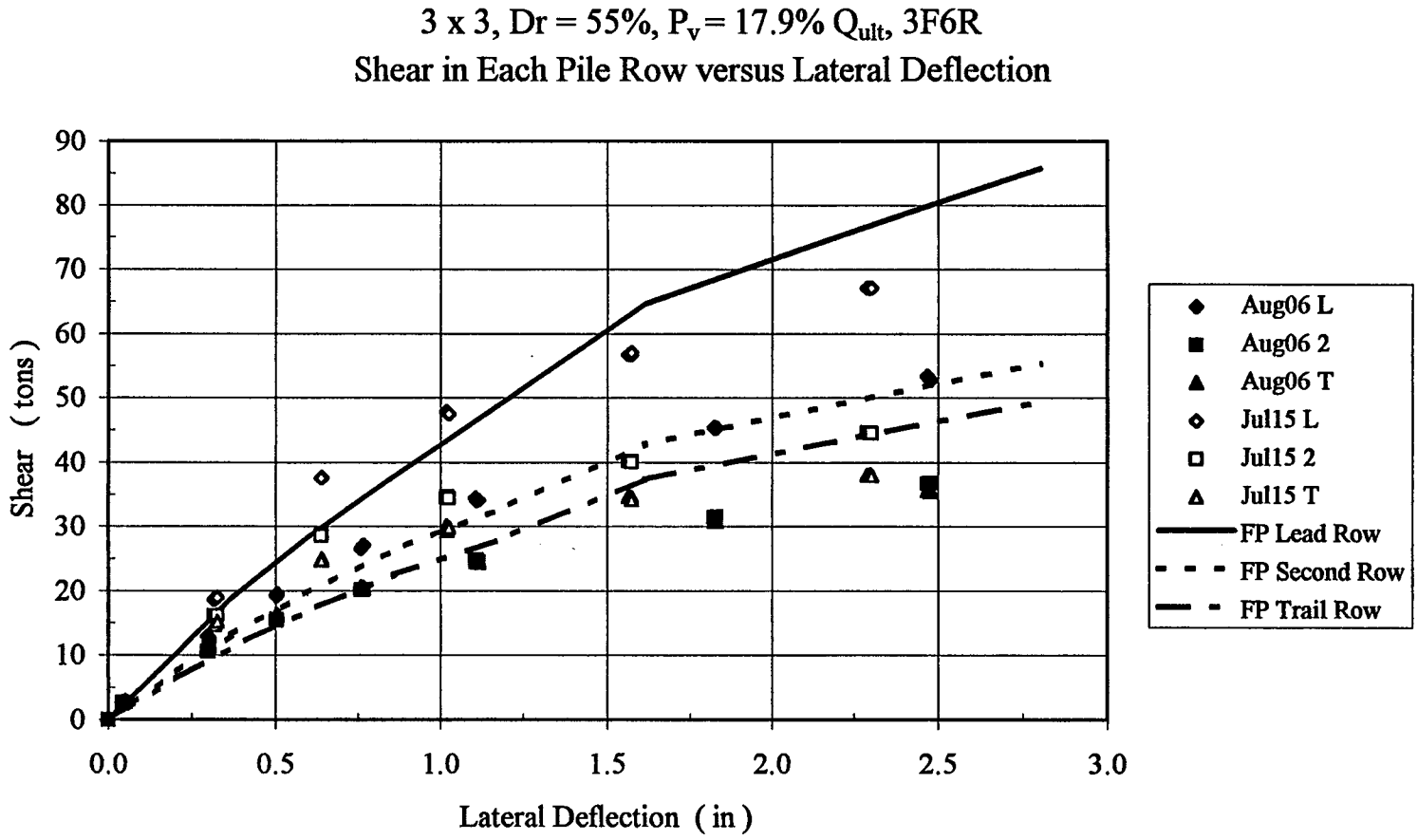

Figure 7-7 Shear in Each Pile Row versus Lateral Deflection

Figure 7-8 shows the axial resistance in the lead row versus the lateral displacement of the group. The data for the inner rows shows excellent repeatability. The data for the outer rows shows fairly good repeatability although the July 15 data for one of the outer rows shows it in compression while the rest are in tension. The FLORIDA-PIER prediction for the inner rows follows the same general trend as the data though it is slightly lower. The prediction for the outer piles follows one day's data well, showing it in compression, but does not predict the other set of outer piles very accurately.

Figure 7-9 shows the axial force of each of the piles in the second row versus the lateral deflection. The repeatability of the outer piles' data is good while the inner piles do vary significantly. The FLORIDA-PIER predictions for the outer rows follow the same general trend and match the data well. The prediction for the inner row follows the same general trend as the data and matches one of the day's data almost exactly.

Figure 7-10 shows the axial force in the trail row versus the lateral deflection. There is some scatter between both day's measured values for the inner piles. The most likely cause is imperfect bonding. There is a much smaller discrepancy between the outer pile measurements on both days. The FLORIDA-PIER prediction for the inner row matches the data in that it starts in compression and later goes into tension. The outer row prediction follows the same general trend as the measured data until about 1.25 inches and then it begins to go into compression.

Figure 7-11 shows the vertical displacement versus the lateral load. The measured data is fairly repeatable. The FLORIDA-PIER prediction begins predicting too high a settlement but as the load increases to 200 tons it begins to match the measured data well.

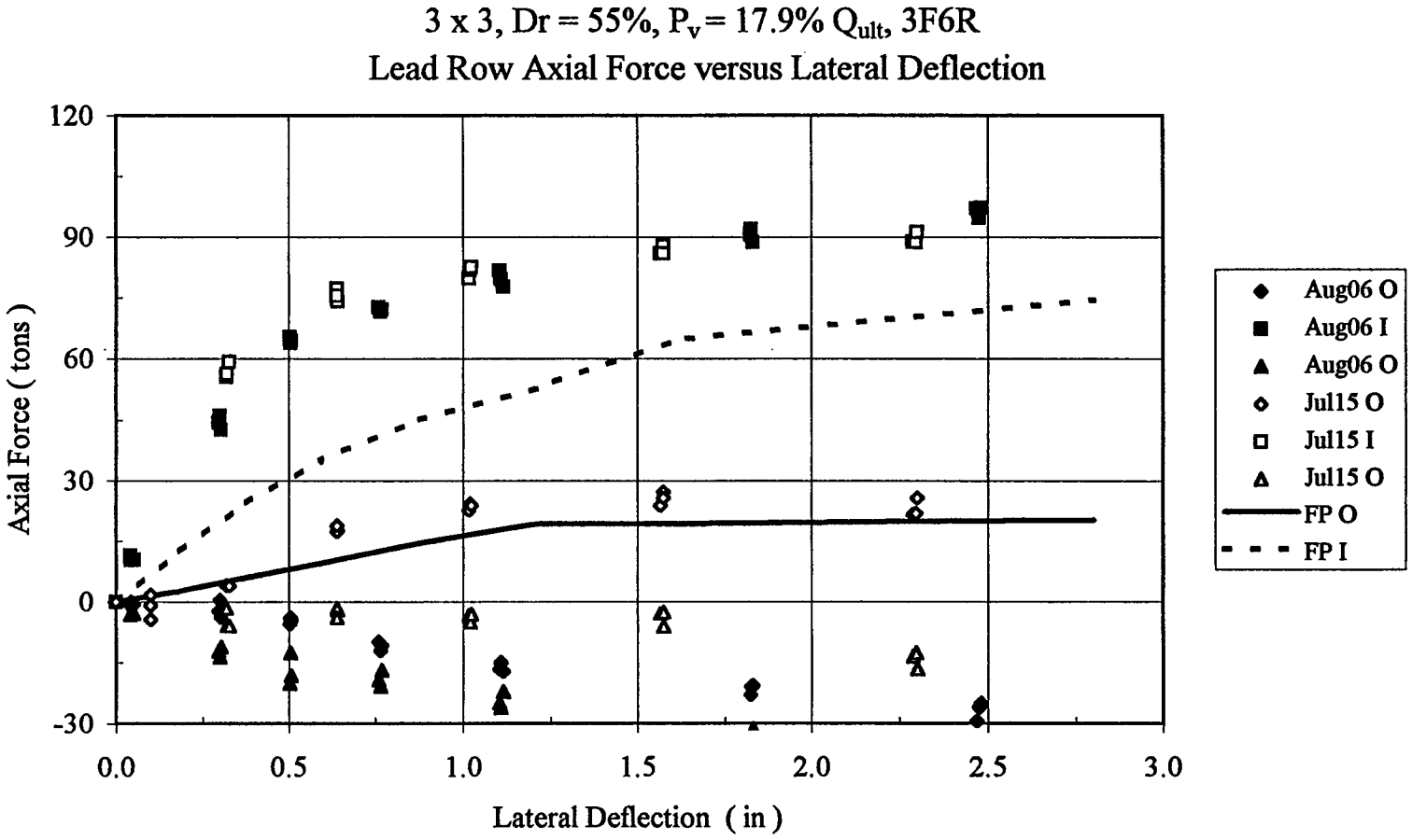

Figure 7-8 Lead Row Axial Force versus Lateral Deflection

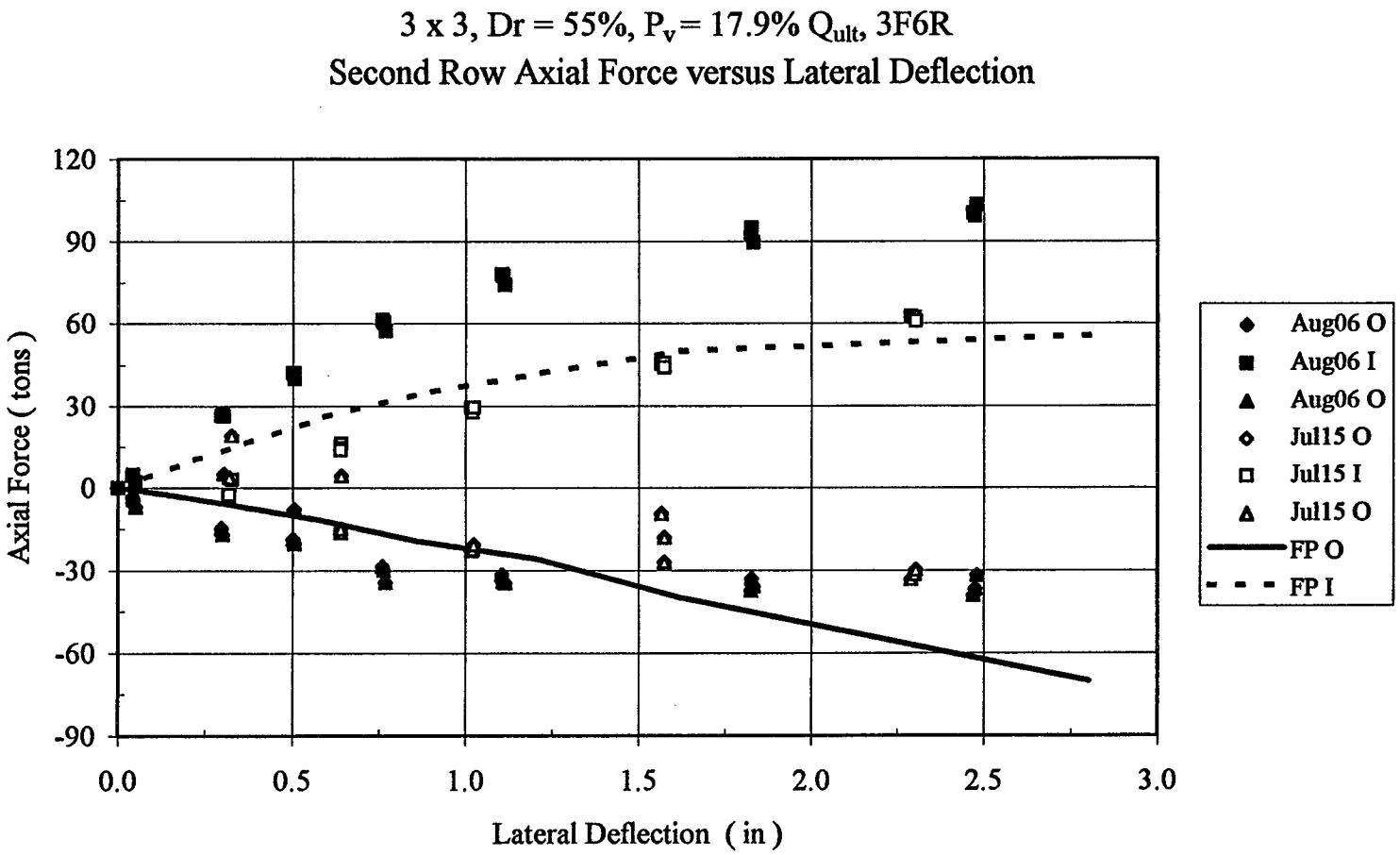

Figure 7-9 Lead Row Axial Force versus Lateral Deflection

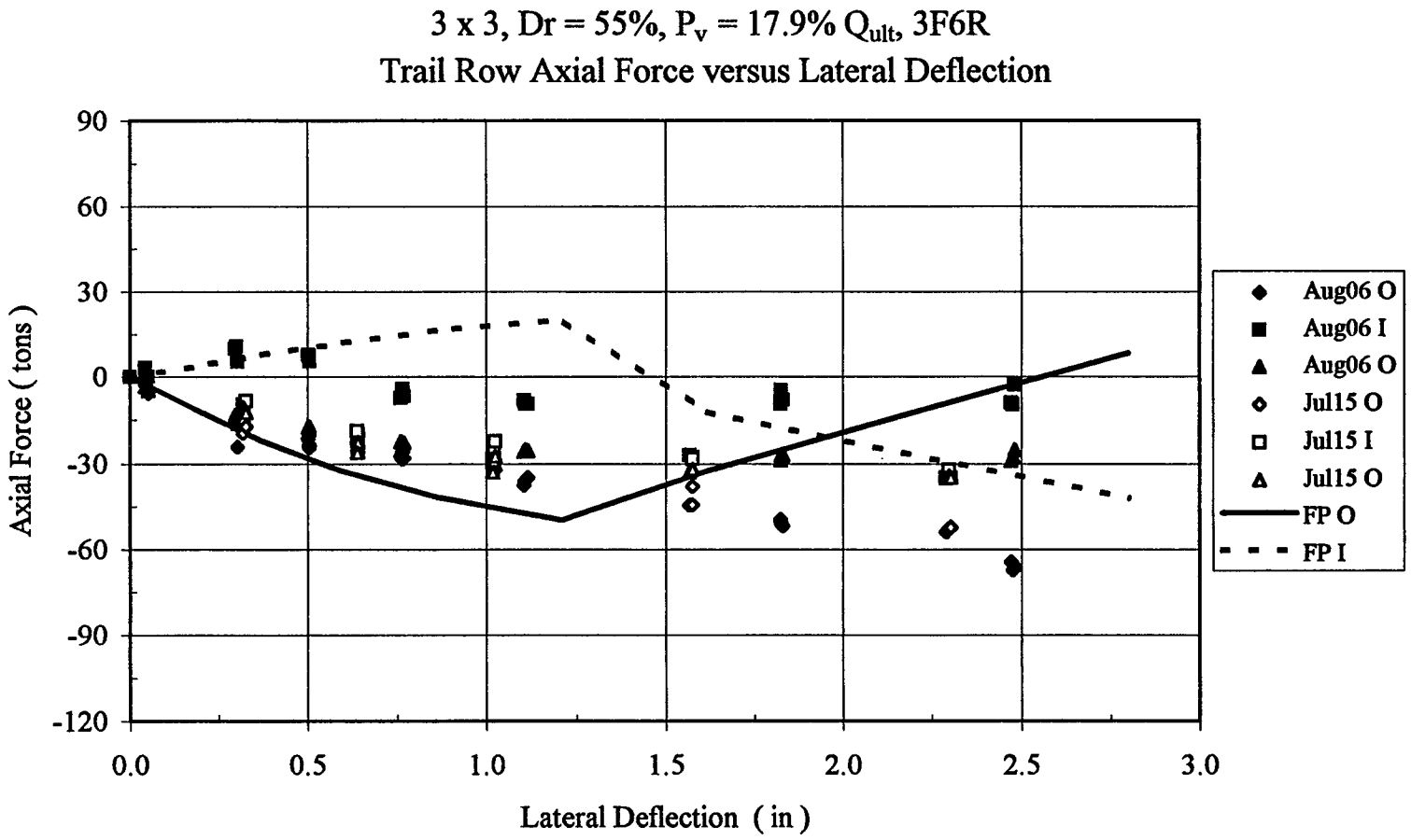

Figure 7-10 Trail Row Axial Force versus Lateral Deflection

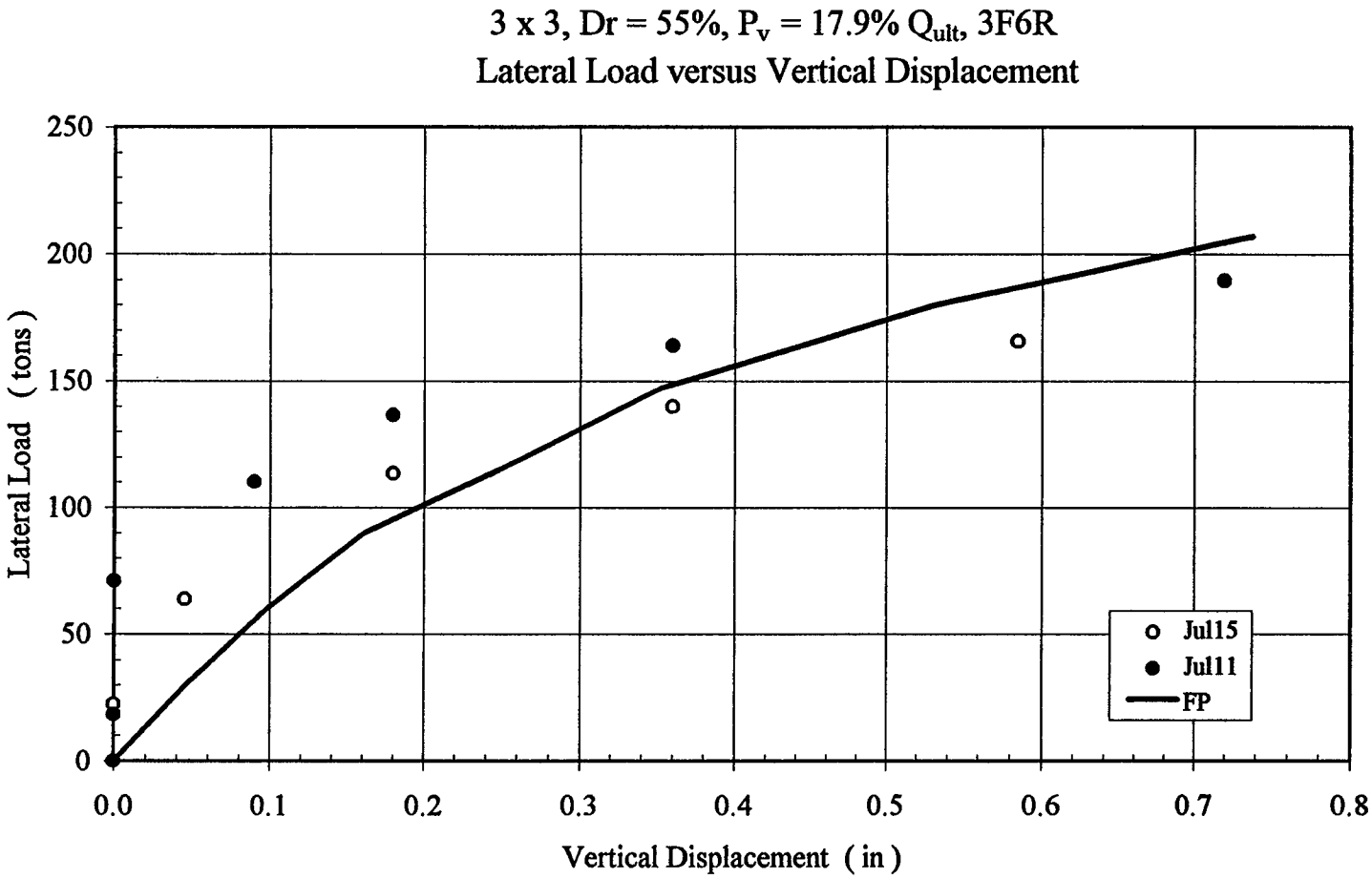

Figure 7-11 Lateral Load versus Vertical Displacement

CHAPTER 8
CONCLUSIONS AND RECOMMENDATIONS

8.1 CONCLUSIONS

The following conclusions were made from this research.

1. An increase in the amount of dead load on the pile group, from 20% to 50% dead load, increased the overall lateral resistance for 3 by 3 groups in both batter configurations and soil densities. In all of the 4 by 4 pile groups an increase in capacity was observed with increasing dead loads for the 20%, 50%, and 80% ultimate dead load cases.
2. In loose soil the change in capacity with a change in dead load from 50% to 80% was dependant on the batter configuration. For the 3F6R groups a softer response was observed with increasing dead load. In contrast, a slightly stronger response was seen in the 6F3R groups at both dead loads.
3. In medium dense sands the lateral resistance at 3 inches did not change significantly with the dead load change from 50% to 80% for both batter configurations. At 3F6R a softer response was observed at 1 and 2 inches of deflection and a stiffer response was observed at 6F3R. This implies that as the dead load nears the bearing capacity of the group the ultimate lateral capacity doesn't change significantly while the initial portion load deflection response depends on the pile batter configuration.
4. In the 3 by 3 tests with 3F6R configuration a greater portion of the lateral load was taken by the trail row at the expense of the lead and second rows as dead load increased for both densities. In the 6F3R groups founded in loose sand the lateral load shifts primarily from the lead to the trail row with only a slight increase in the middle row. In medium dense sand it became

more evenly distributed among the rows, with the lead row force being increasingly taken by the second and trail rows as the increase of dead load.

5 In 3 by 3 piles groups at both densities, 50% dead load seems to represent the amount of dead load needed to minimize pile group rotation. For the 3 by 3 groups founded in loose sand the rotation decreased with the amount of piles battered forward except at 50% dead load where they were nearly equal. In medium dense sand the rotation increased with the number of forward battered piles except at 80%dead load where a decrease was observed. In looser soil the pile group rotation of a 4 by 4 group appeared to be minimized at the 50% dead load case and in denser soil it seemed to decrease with increasing dead load.

6. At the same dead load, the lateral load primarily tended to be shifted from the lead row to the trailing row with increasing density. The only exception to this was the 6F3R group founded in medium dense sand which showed the load in the trail row being transferred to the second row and some to the lead row. The load distribution of 4 by 4 groups founded in loose sand was such that the load in the lead, second and third rows was increasingly taken by the trail row with increasing dead load. The load distribution in 4 by 4 groups founded in medium dense sand tended to shift from the lead row to the trail row, with little change in the middle rows, with increasing dead load. In 3 by 3 groups the lead and trail rows began to take more of the lateral load from the second and third rows as the dead load increased.

7. In general FLORIDA-PIER does a good job of predicting the load deflection response for the test results in this series of experiments. The only exception, for all groups, was the response for the groups with 80% dead load on top; the predictions were consistently too soft at the beginning of the curve but eventually came to match the data well at larger deflections.

8. FLORIDA-PIER does a good job of predicting the general shape of the shear curves for all of the different rows. Its predictions for the trailing rows are generally close to the measured values. Its prediction for the lead rows, however, in the pile groups is usually slightly high especially in some of the 4 by 4 groups.
9. FLORIDA-PIER does a good job of predicting the axial force in general. In the 3 by 3 groups trail row it has some problems predicting the force correctly. For the lead and trail rows the prediction is generally accurate. In the 4 by 4 tests the axial results were good all around with only a few significant discrepancies

REFERENCES

Bowles, J.E., "Foundation Analysis and Design, Fifth Edition," The McGraw-Hill Co., Inc., 1996.

Brown, D.A., Morrison, "Lateral Load Behavior of a Pile Group in Sand," Journal of Geotechnical Engineering, ASCE, Vol. 115, No. 11, pp. 1261-1271, November, 1988.

Clausen, J.B., "Centrifugal Model Tests on Laterally Loaded Pile Groups in Homogeneous Sand," Master's Thesis, University of Florida, Gainesville, Florida, 1992.

Feagin, L.B., "Lateral Load Tests on Groups of Battered and Vertical Piles," Symposium on Lateral Load Tests on Piles, pp. 12-20, American Society for Testing Materials, Philadelphia, Pennsylvania, 1953.

McVay, M.C., Shang Te-I, Casper, Robert, "Centrifuge Testing of Fixed Head Laterally Loaded Battered and Plumb Pile Groups in Sand," Geotechnical Testing Journal, Vol. 19, No. 1, March, 1996, pp. 41-50.

McVay et al., "Development of a Coupled Bridge Superstructure-Foundation Finite Element Code," Florida Department of Transportation report, Gainesville, Florida, 1996.

Molnit, T., "Centrifuge Modeling of Laterally Loaded, Large Pile Plumb Pile Groups in Sand," Master's Thesis, University of Florida, Gainesville, Florida, 1995.

Reese, L.C., Cox, W.R., and Koop, F.D., "Centrifuge Modeling of Laterally Loaded, Three Row Battered and Plumb Pile Groups in Sand," Proceedings, 5th Annual Offshore Technology Conference," Houston, Texas, Paper No. 2080, 1974.

Shang, TE-I, "Analysis of Laterally Loaded Piles in Sand," Master's Thesis, University of Florida, Gainesville, Florida.

Tschebotarioff, G.P., "The Resistance to Lateral Loading of Single Piles and of Pile Groups," Symposium on Lateral Load Tests on Piles, American Society of Testing Materials, No. 154, pp. 38-48, Philadelphia, Pennsylvania, 1953.

Bradley, G.S., Townsend, F.C., Fagundo, F.E., and Davidson, J.L., "Centrifugal Scaling Laws for Ground Laws for Ground Launch Cruise Missile Shelter," ESL-TR-84-07, Air Force Engineering Services Center, Tyndall Air Force Base, Florida, April 1984.

APPENDIX A

FLORIDA-PIER INPUT PROPERTIES

This Appendix describes how three important input soil properties were determined for use in the FLORIDA-PIER program. These properties are the modulus of subgrade reaction R_k, the shear modululs, and the Poisson's ratio.

A.1 Modulus of Subgrade Reaction

The modulus of subgrade reaction is defined as the change in contact pressure to the corresponding change in deflection and has units of force per cubic length. It was particularly important in these analyses because it governed how the piles moved through the soil. In the program the user inputs the value of R_k for the top and the bottom of the layer. In these analyses the values at the top and bottom were set equal to each other because the initial slope of the contact pressure versus deflection plot was linear. Figure B-3 in Appendix B of the FLORIDA-PIER 5.0 manual was used to make the estimate. This figure is a graph of in situ k versus relative density with consideration given to the position of the water table. It is reproduced in Figure A-1. For sand above the water table and at a relative density of 36% and 55% the estimates were 0.04 and 0.11 k/in^3 respectively. These values were used as a starting point in the subsequent analysis.

A.2 Poisson's Ratio

Poisson's ratio was input as 0.2 for sands as recommended in Appendix of FLORIDA-PIER.

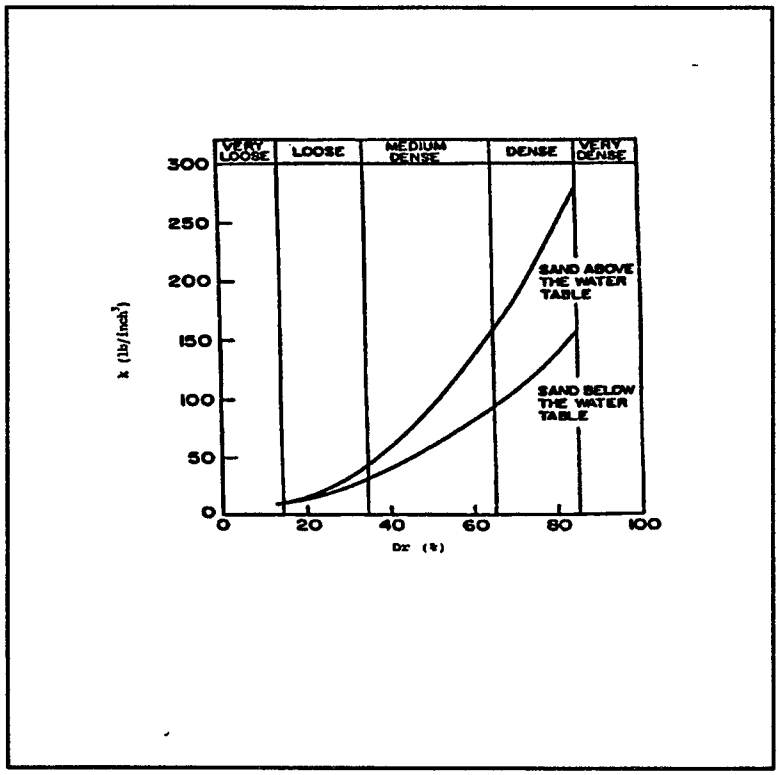

Figure A-1 k versus Relative Density

A.3 Shear Modulus (G)

Another of the soil properties the user needs to input is the initial shear modulus of the soil. This value must be supplied for the top and bottom of each layer in the profile and at the tip of the pile. The shear modulus is a function of the geological and loading history and type of the soil being investigated. Usually these values are obtained through SPT and CPT methods. It was not possible in these tests to obtain any insitu values but an estimate of the SPT blow count was made and a correlation by Kulhways and Mayne (1990) was used to estimate G. The SPT blow count was estimated using Figure B-2 in Appendix B of the FLORIDA-PIER manual which is reproduced in this appendix as Figure A-2. The graph was entered with the internal friction angle of the soil and an SPT.

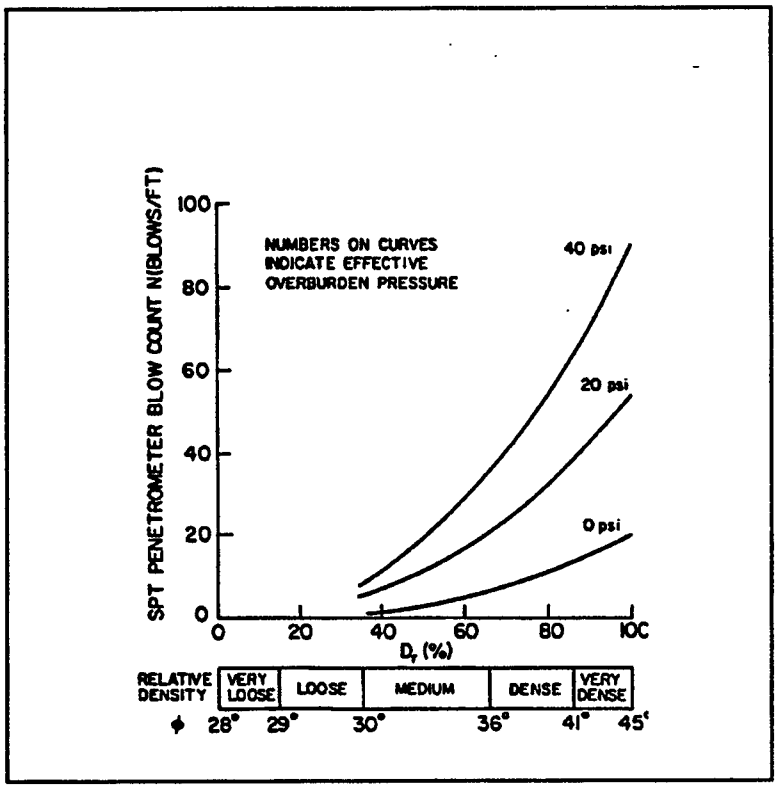

Figure A-3 SPT Blow Count vs Friction Angle and Relative Density (From FLORIDA-PIER 5.0)

number read from the curve corresponding to the correct value of overburden pressure on the soil layer. SPT values at the top and bottom of the layer and at the tip were obtained. Once all of these values were obtained the following equations were used to calculate the shear modulus.

$$E = 20{,}000\ (N_{60})$$

E = Young's Modulus for Normally Consolidated sand (psf)

N_{60} = SPT blow count at 60% hammer efficiency

Once the Young's modulus was determined the following equation from the FLORIDA-PIER manual was used to calculate the shear modulus.

$$G=0.5 \times k \times z/(1+RNU)$$

k = Soil modulus (F/L^3)

z = Depth below ground surface (L)

RNU = Poisson's ratio = 0.2 for sands

APPENDIX B

ORIGINAL DATA AND FLORIDA-PIER COMPARISON

The following paragraphs describe how to read and interpret the graphs presented in this appendix. Each paragraph relates to the particular type of graph mentioned in the heading.

B.1 Lateral Load versus Deflection

The two sets of points in these graphs refer to the different days' tests, the dates of which are listed in the legend. The lines represents the FLORIDA-PIER prediction.

B.2 Axial and Shear Force versus Lateral Deflection

The three symbols of the diamond, square and triangle in the 3 by 3 graphs represent the piles in each row for each day mentioned in the graph's title. The load acts perpendicular to the plane of the symbols. The diamond and triangle represent the outer piles while the square represents the middle pile. In the 4 by 4 groups there is an additional symbol, the circle, and it along with the diamond represent the outer piles. The square and the triangle represent the inner piles. In both sets of graphs the solid and dashed lines represent the FLORIDA-PIER prediction for the outer and inner rows respectively.

B.3 Sum of Shear in Each Pile Row versus Lateral Deflection

In the 3 by 3 groups the diamond, square, and the triangle represent the lead, second, and trail row respectively. The 4 by 4 groups have an additional symbol, a circle, which represents the trail row. The diamond, square, and the triangle now represent the lead, second and third row respectively. The FLORIDA-PIER predictions are as noted in the legend.

B.4 Lateral Load versus Vertical Deflection

The two sets of data points represent the values for the two different days of testing. The line represents the FLORIDA-PIER prediction for the group.

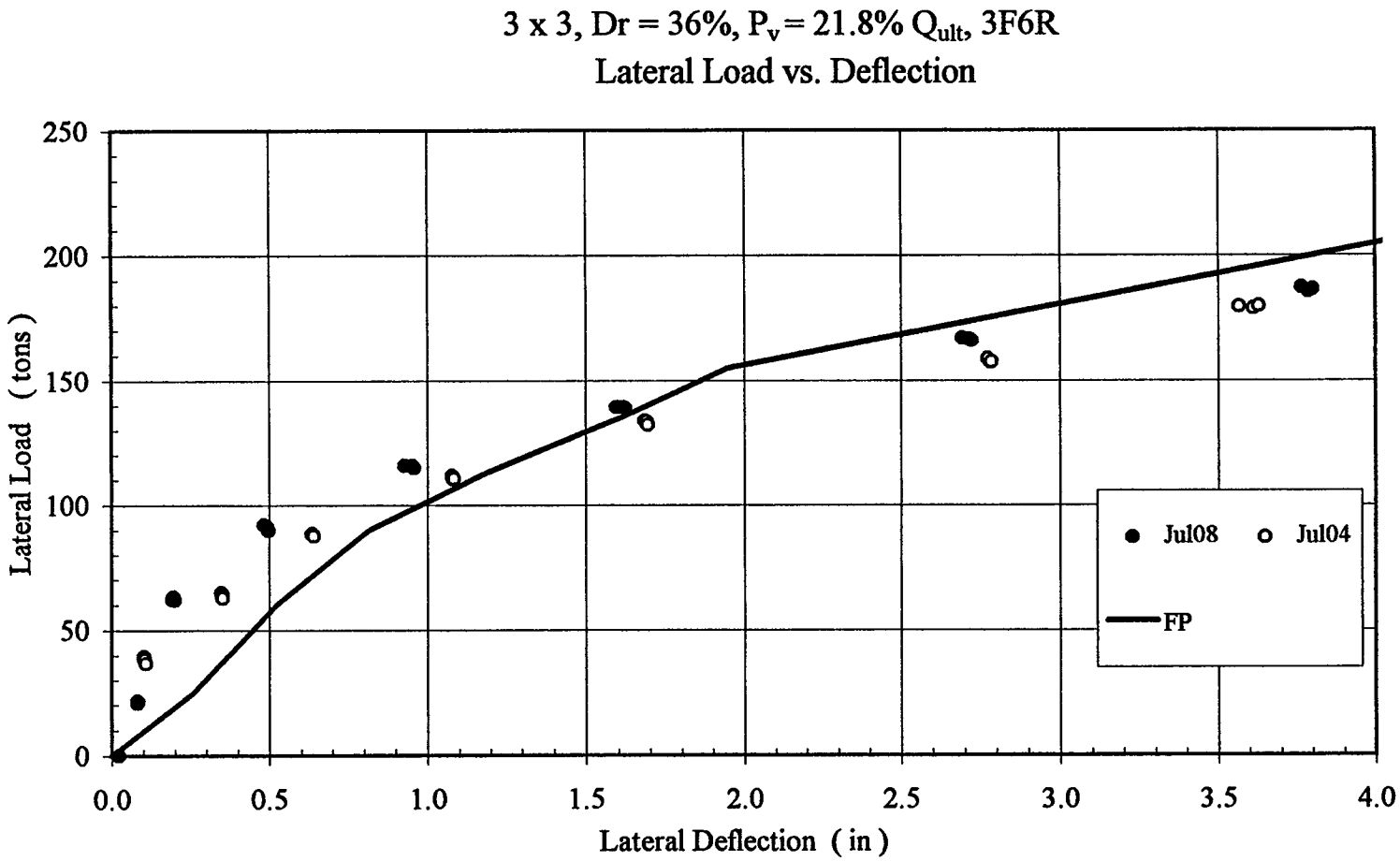

Figure B-1 Lateral Load versus Deflection

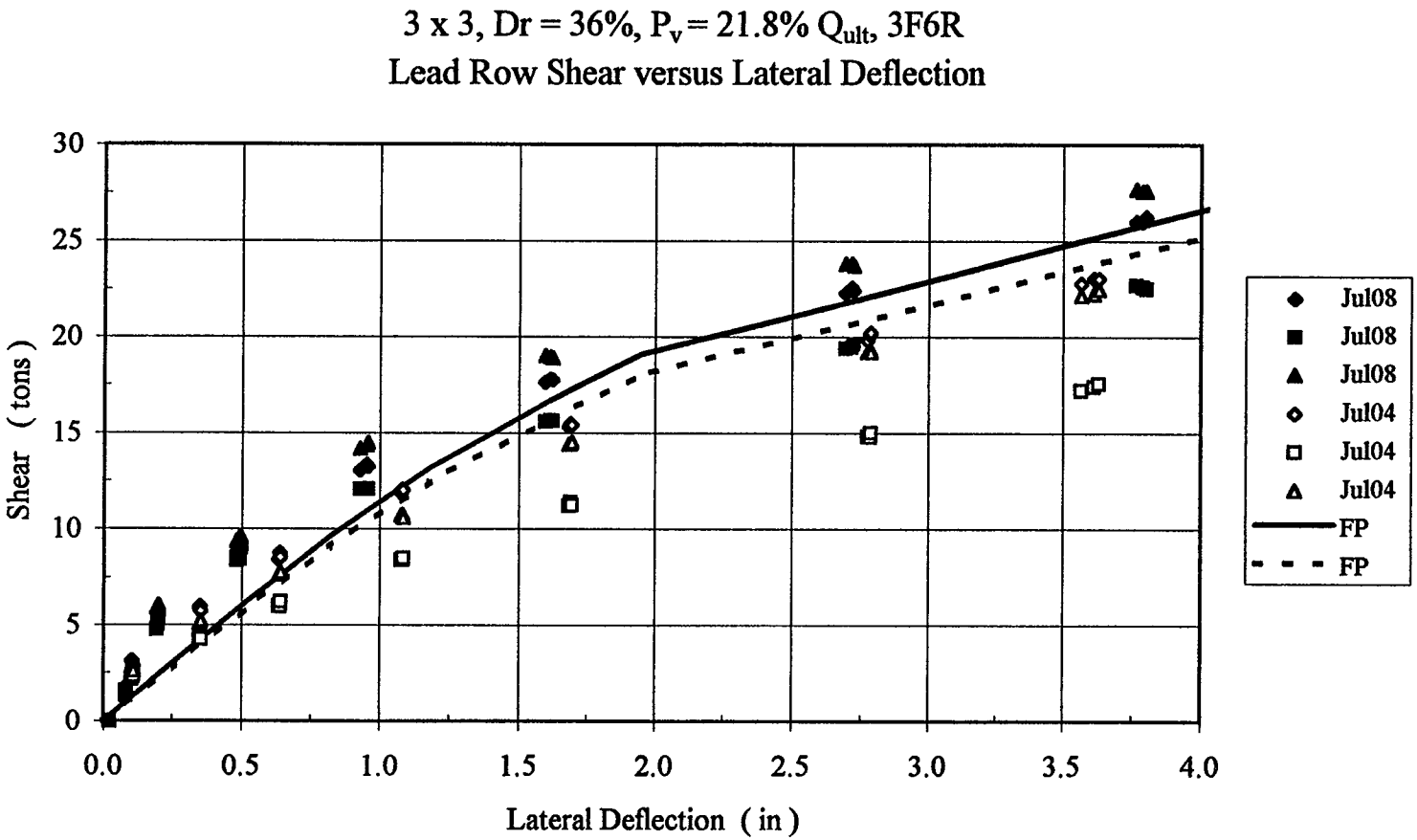

Figure B-2 Lead Row Shear Force versus Lateral Deflection

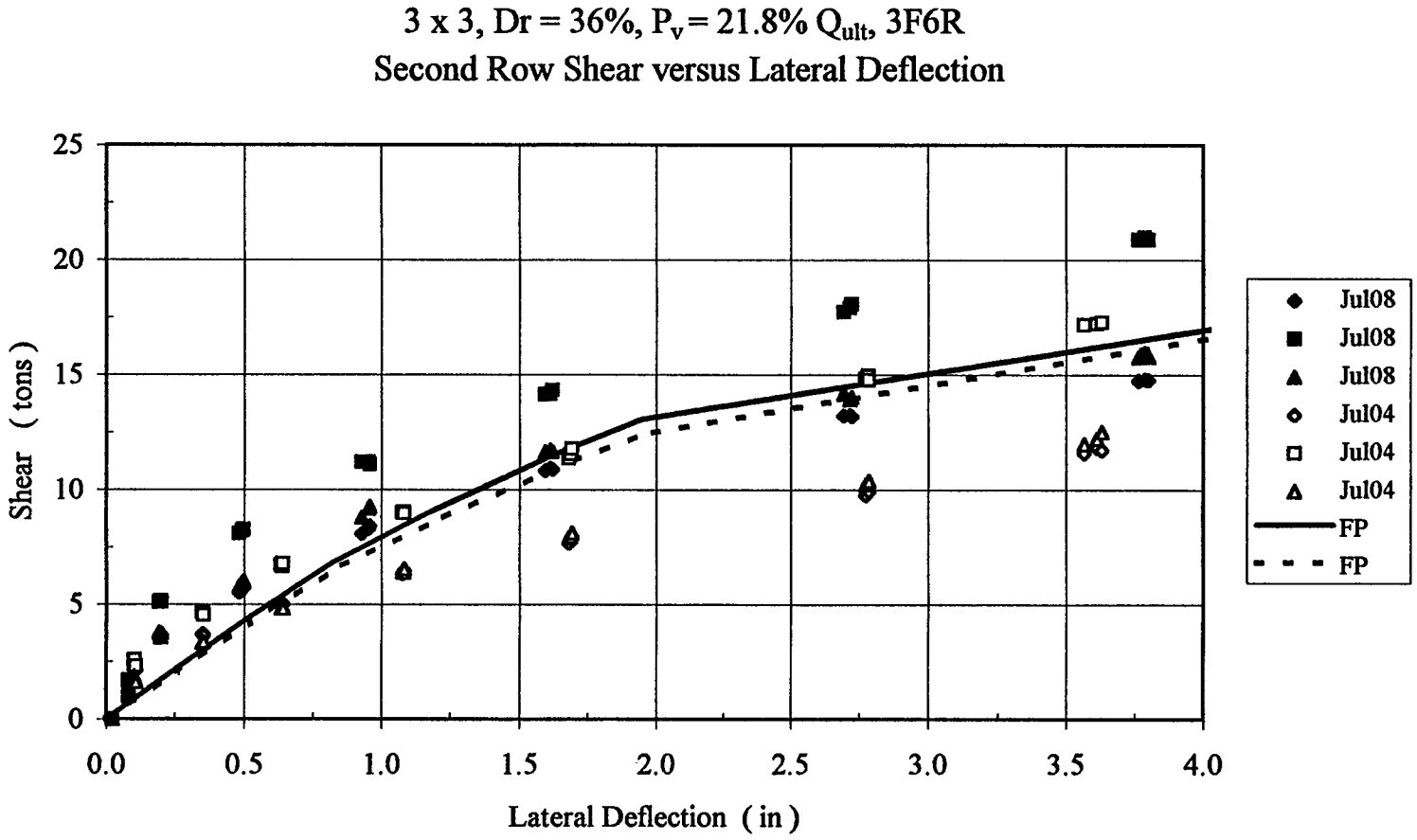

Figure B-3 Second Row Shear versus Lateral Deflection

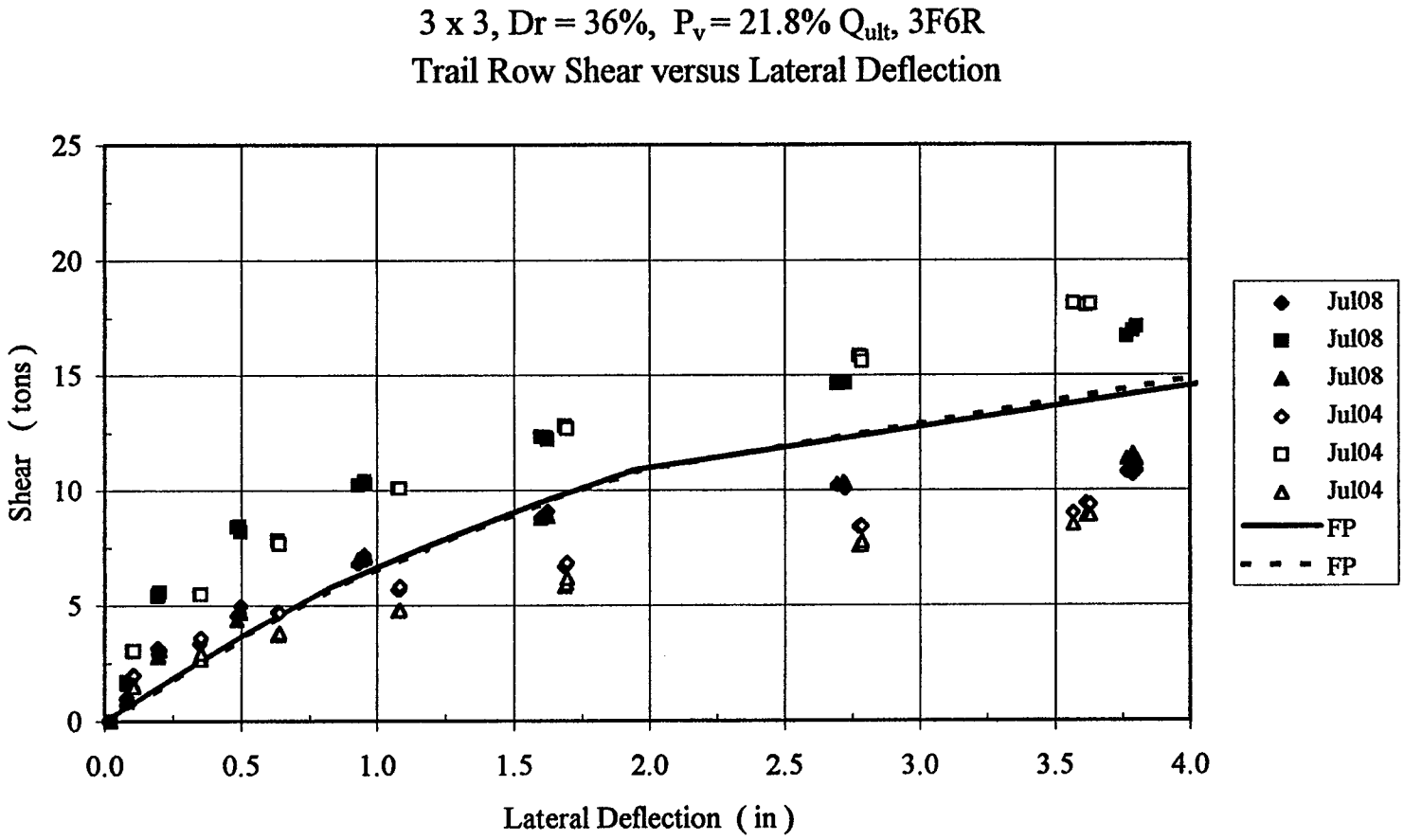

Figure B-4 Shear Force in The Trail Row versus Lateral Deflection

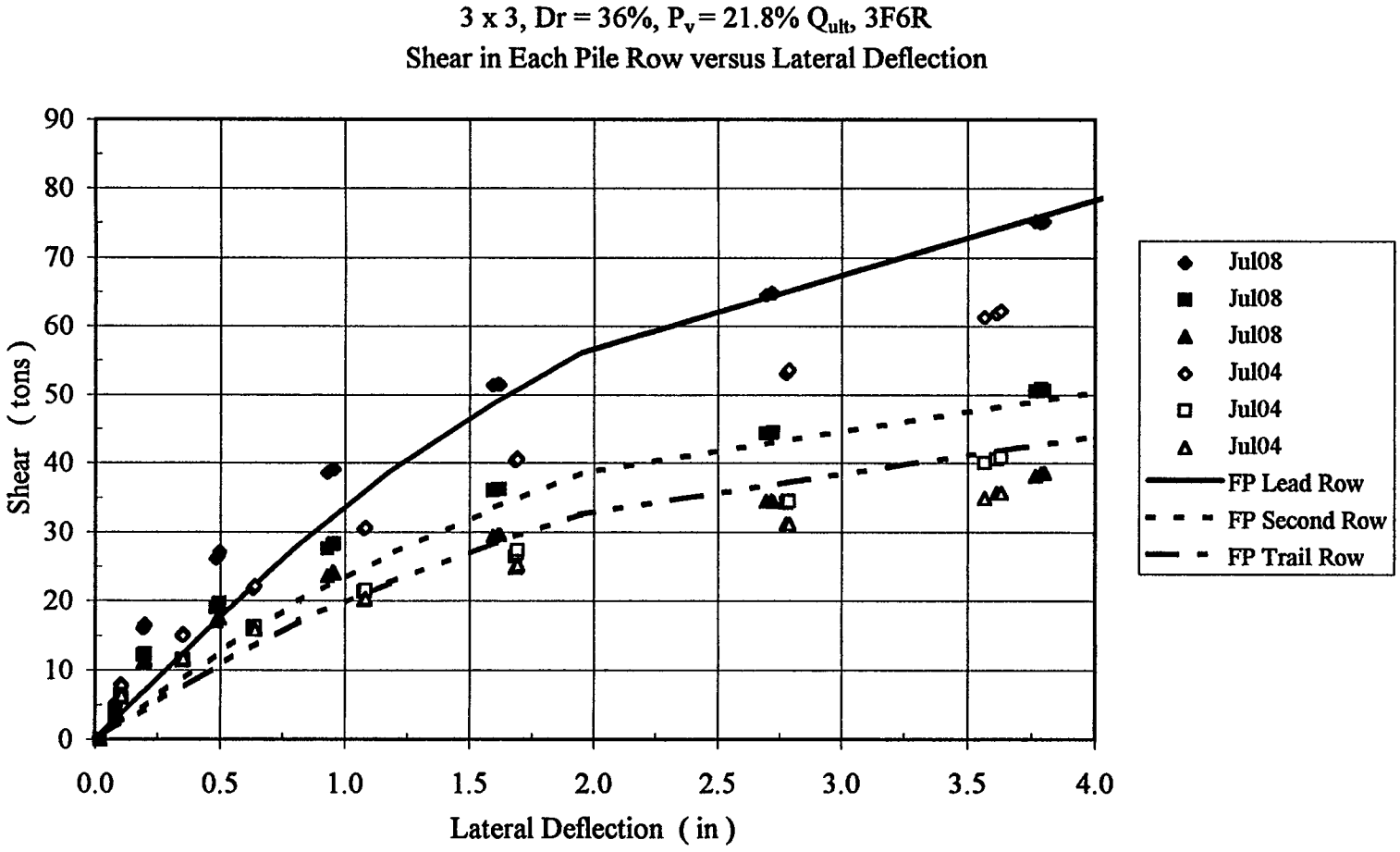

Figure B-5 Shear in Each Pile Row versus Lateral Deflection

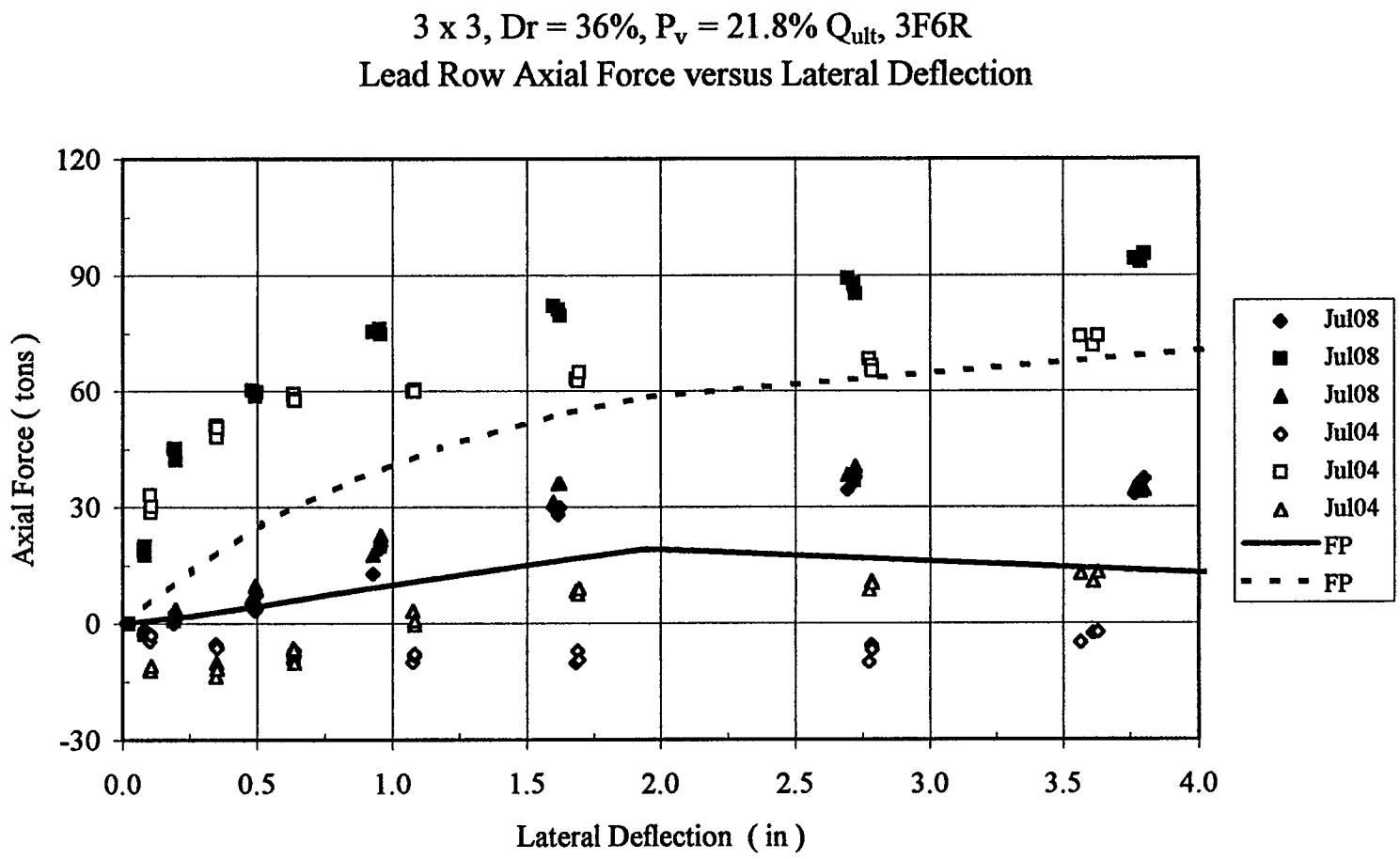

Figure B-6 Lead Row Axial Force versus Lateral Deflection

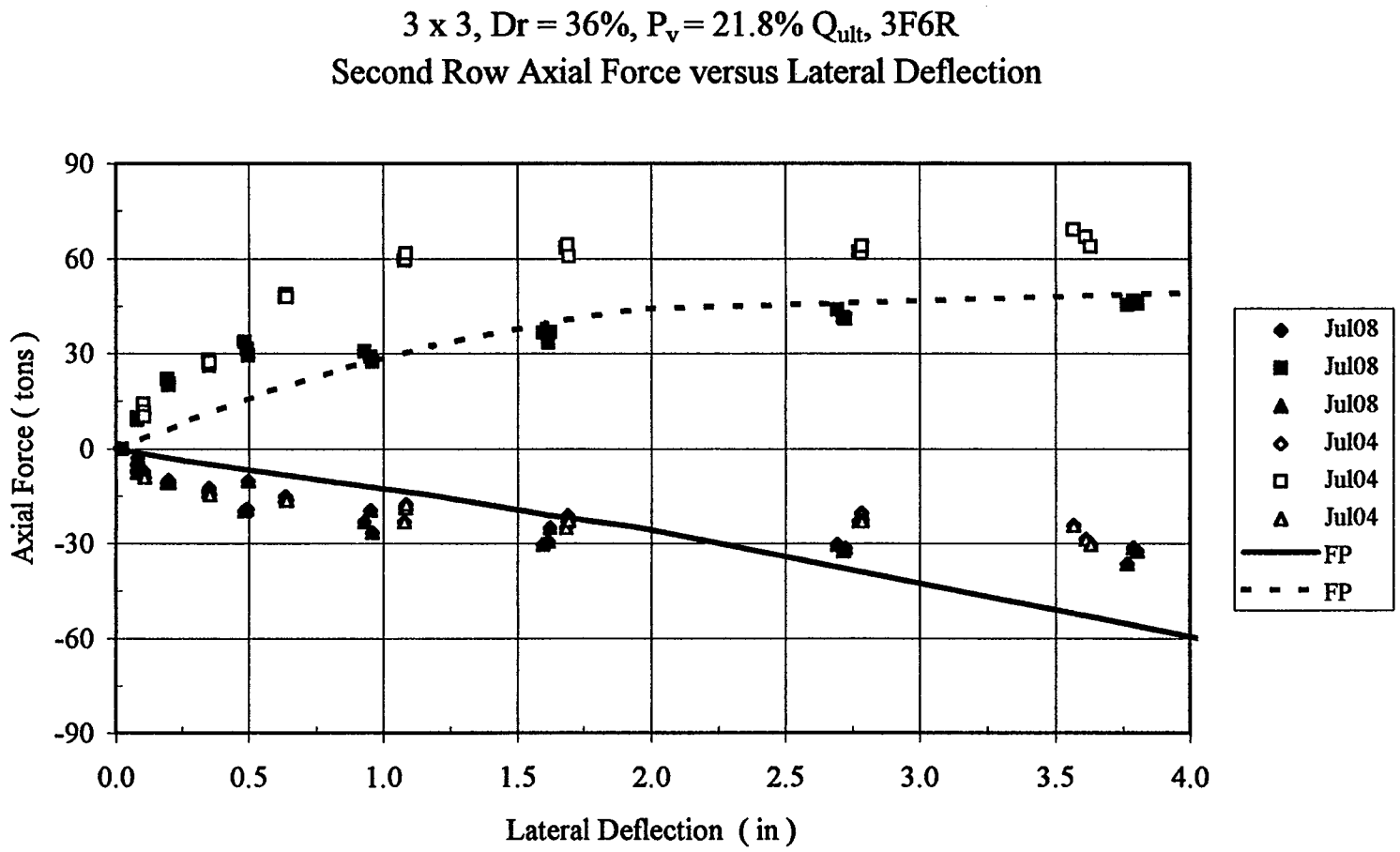

Figure B-7 Second Row Axial Force versus Lateral Deflection

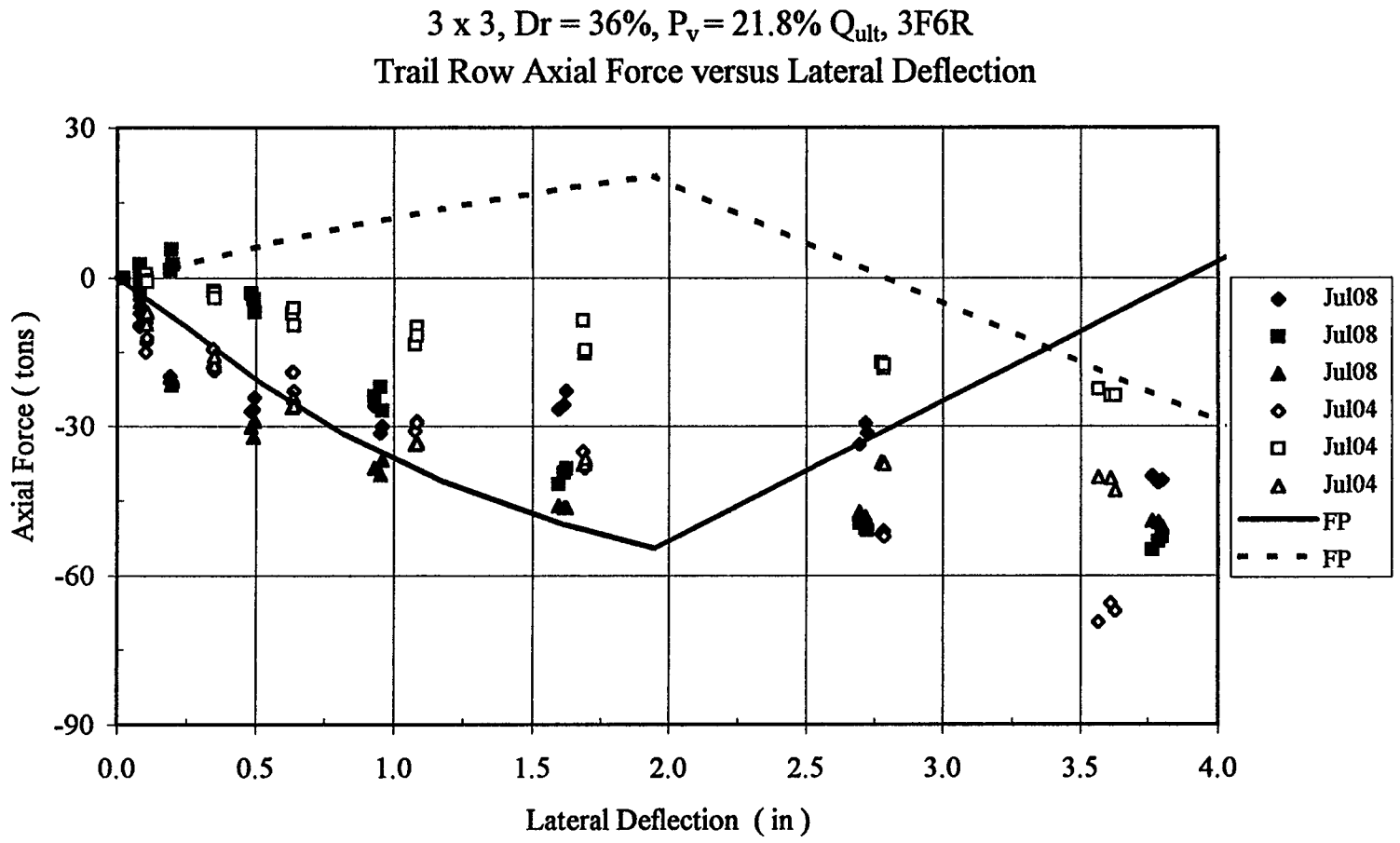

Figure B-8 Trail Row Axial Force versus Lateral Deflection

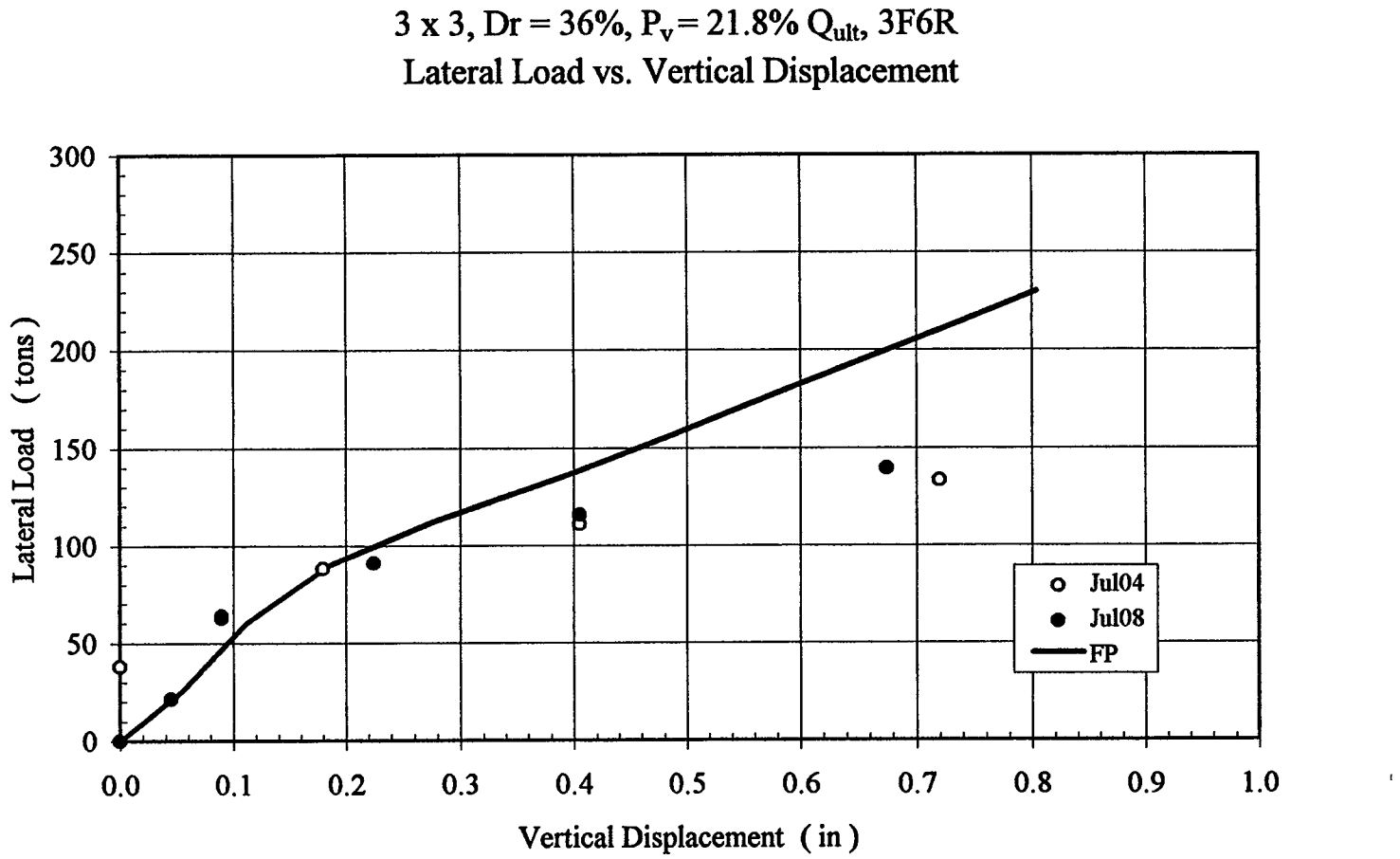

Figure B-9 Lateral Load versus Vertical Displacement

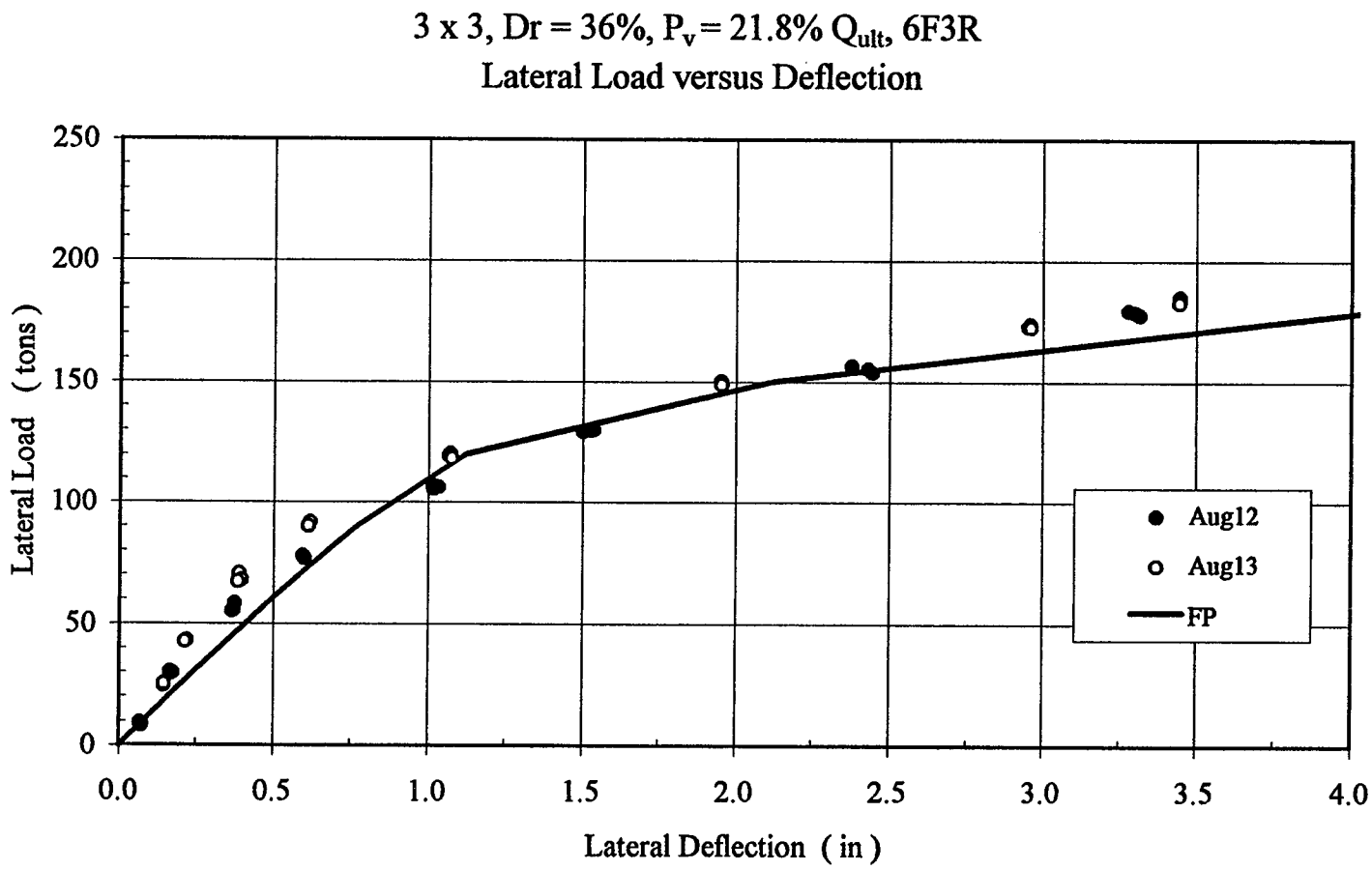

Figure B-10 Lateral Load versus Deflection

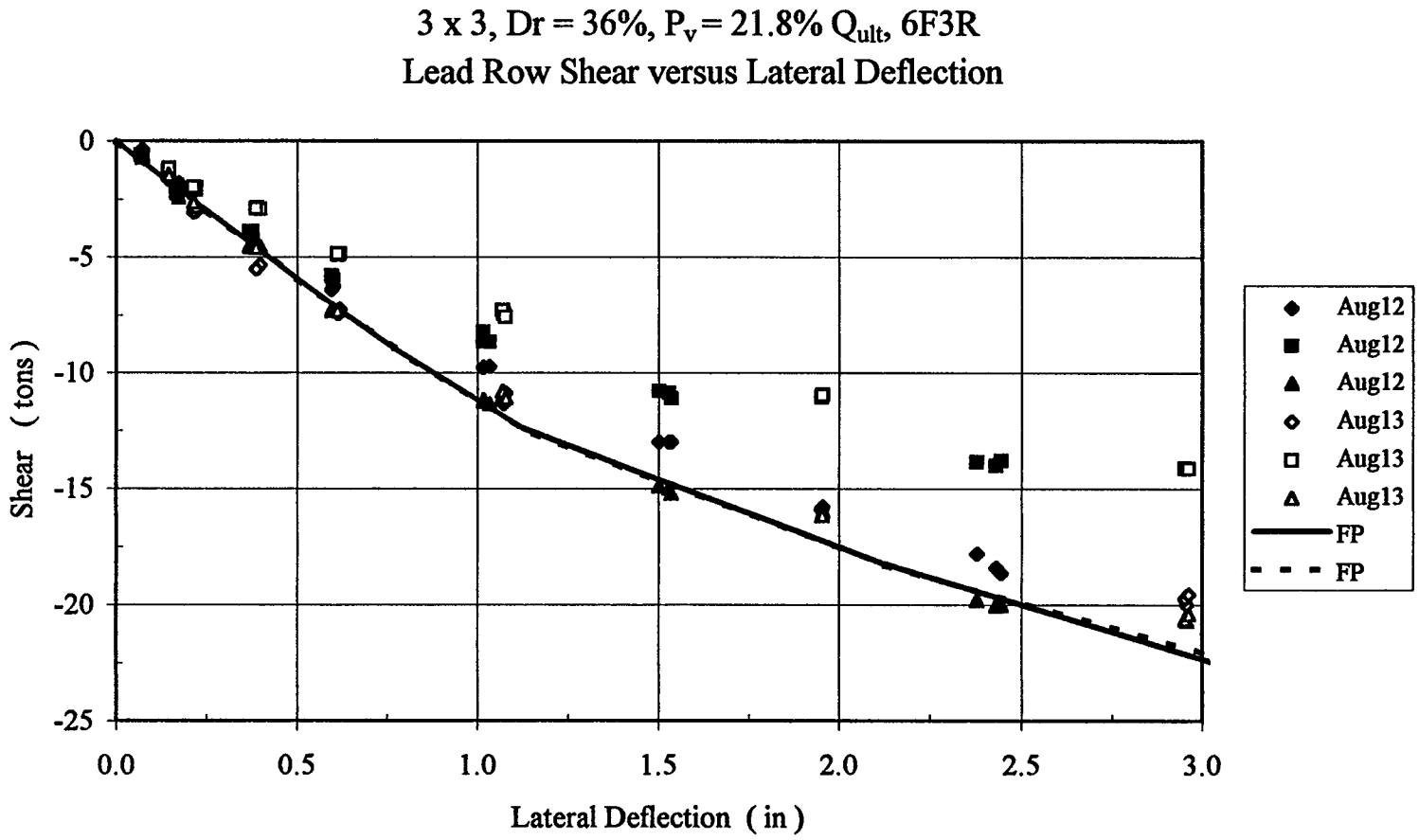

Figure B-11 Lead Row Shear versus Lateral Deflection

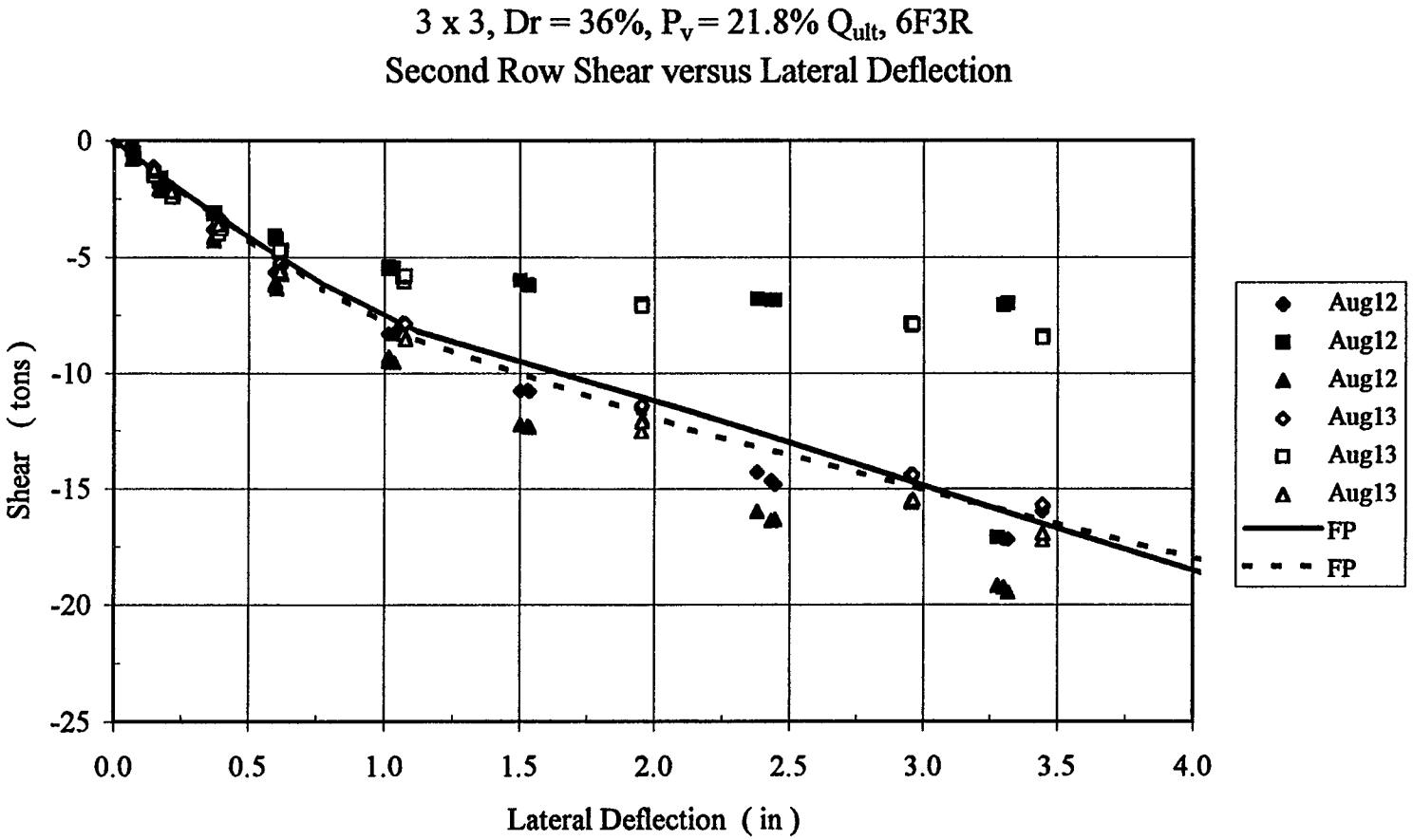

Figure B-12 Second Row Shear versus Lateral Deflection

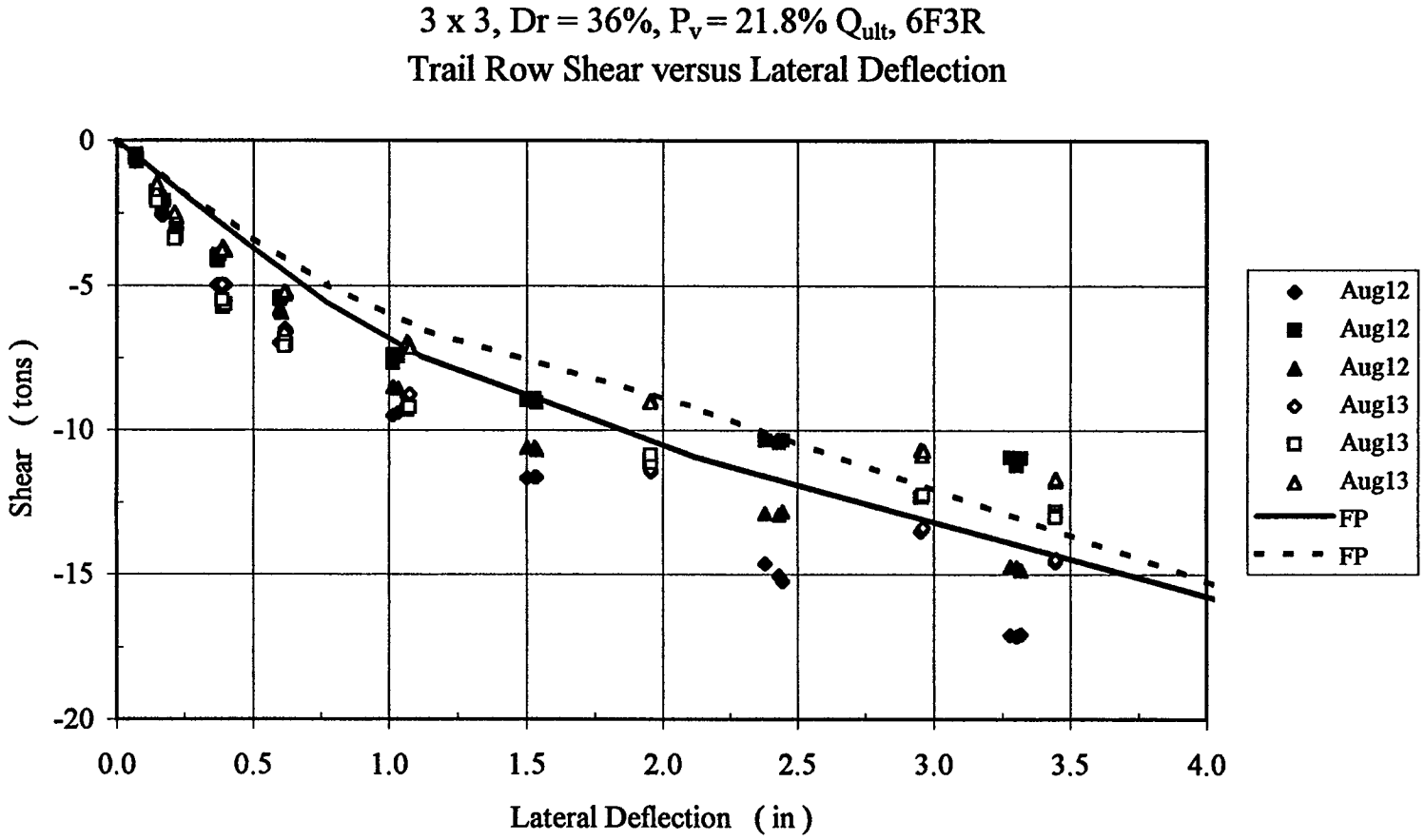

Figure B-13 Trail Row Shear versus Deflection

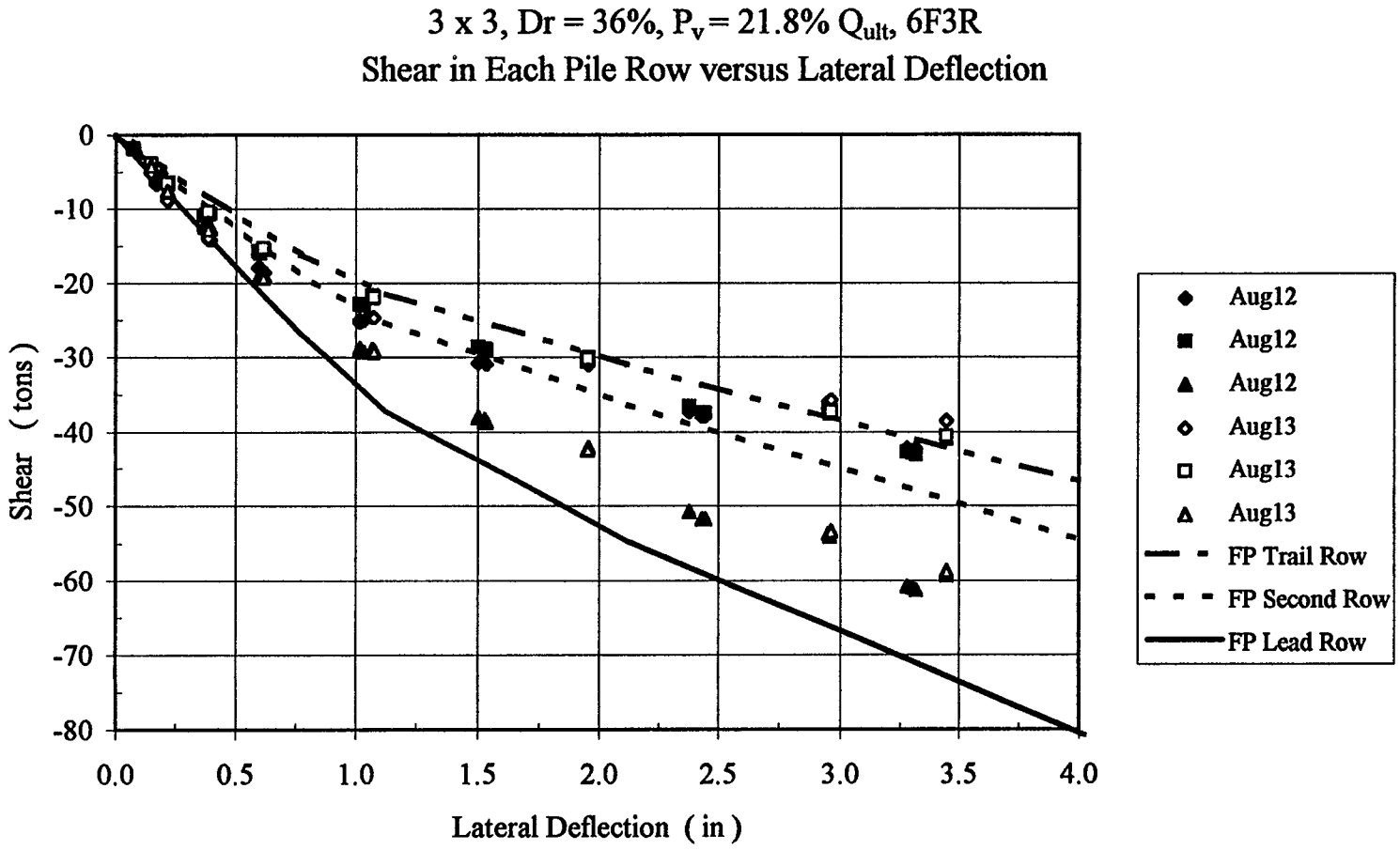

Figure B-14 Shear in Each Pile Row versus Lateral Deflection

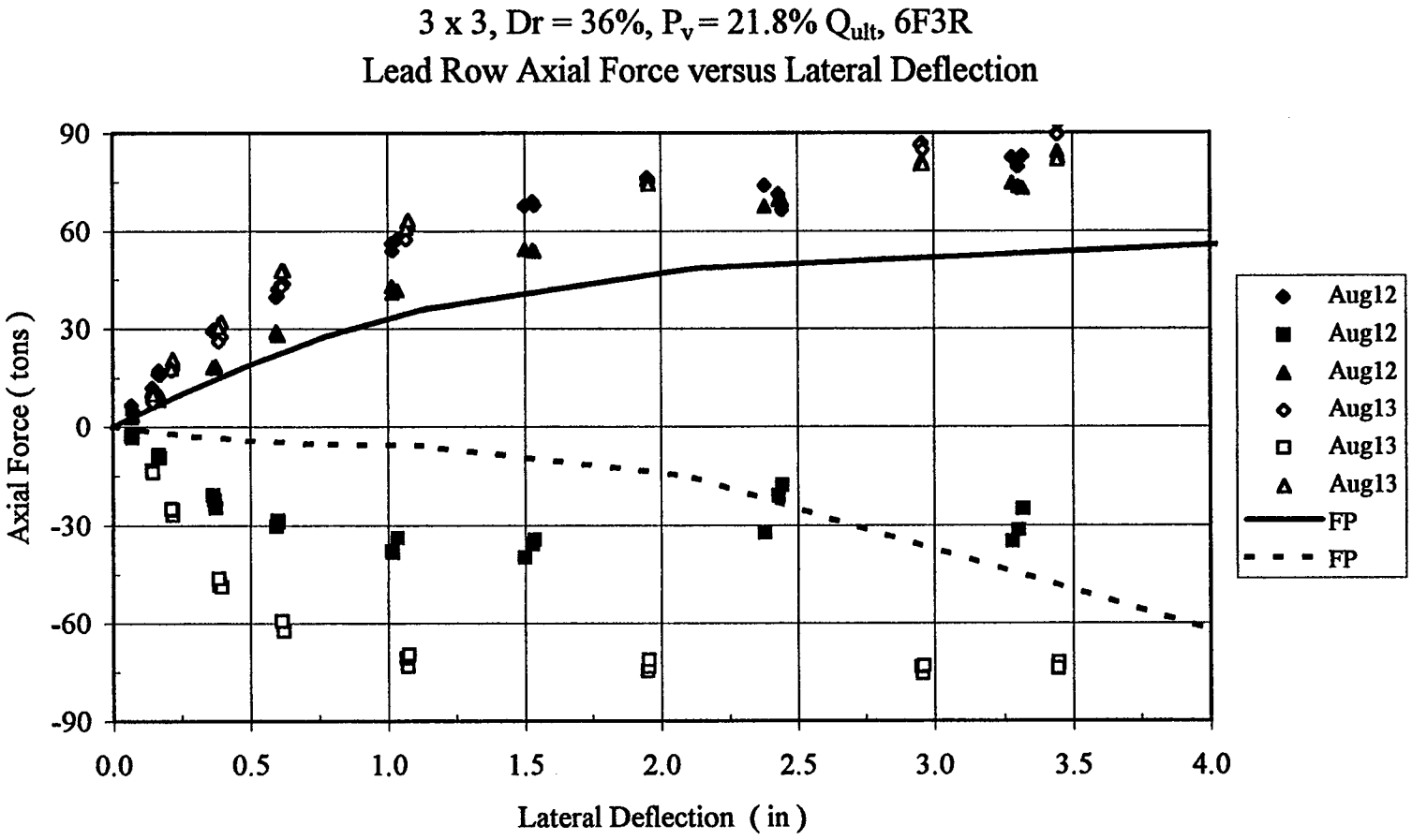

Figure B-15 Lead Row Axial Force versus Lateral Deflection

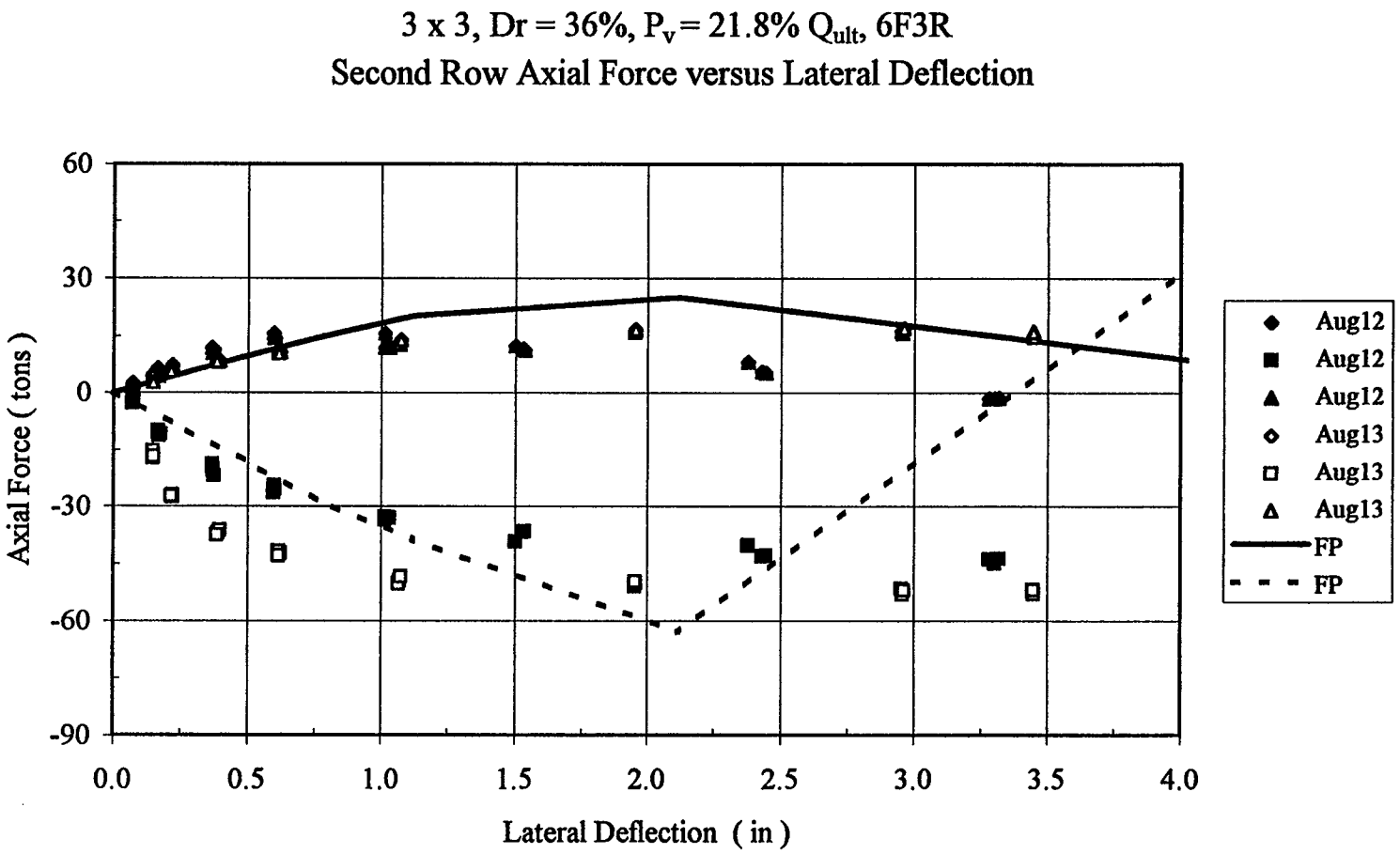

Figure B-16 Second Row Axial Force versus Lateral Deflection

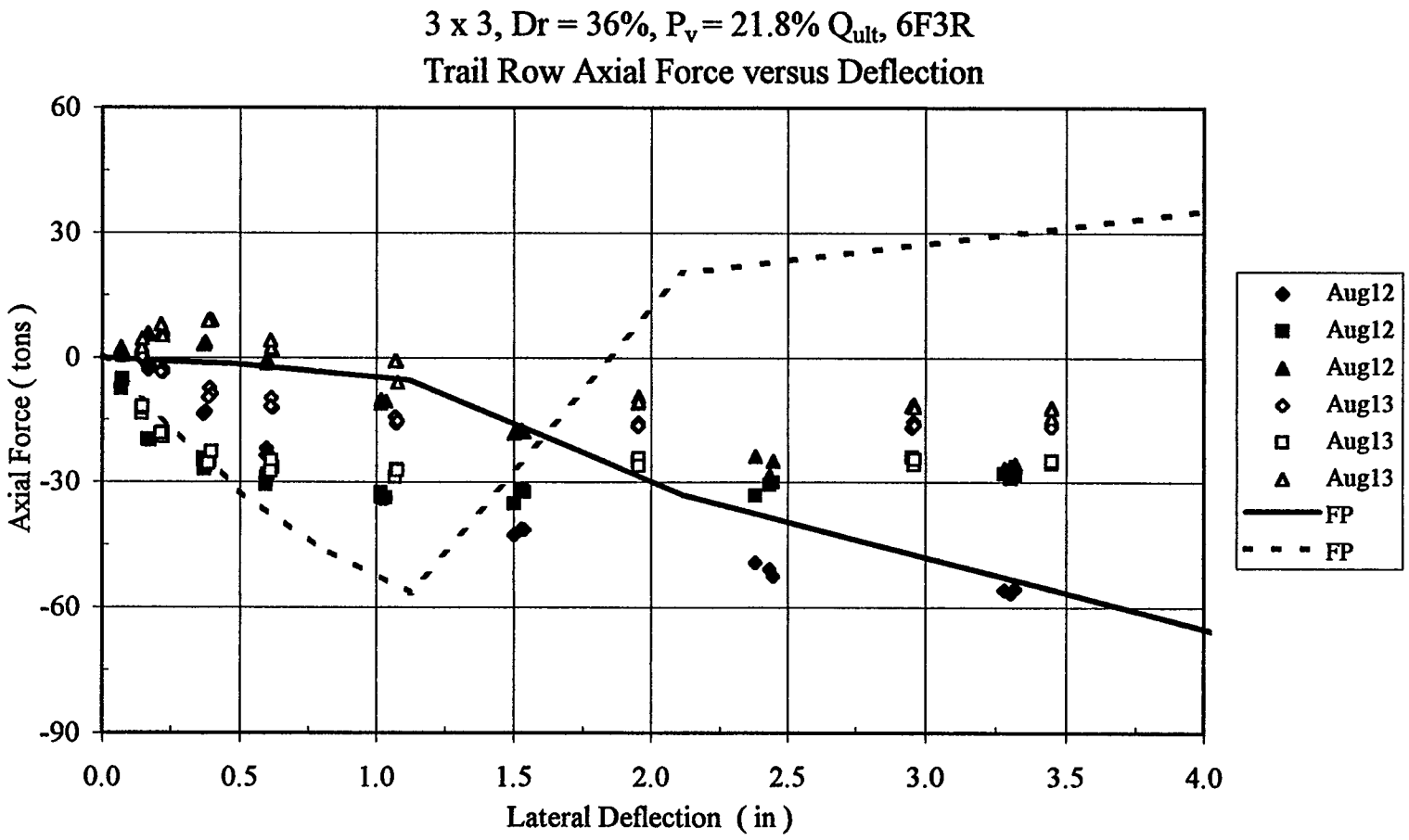

Figure B-17 Trail Row Axial Force versus Lateral Deflection

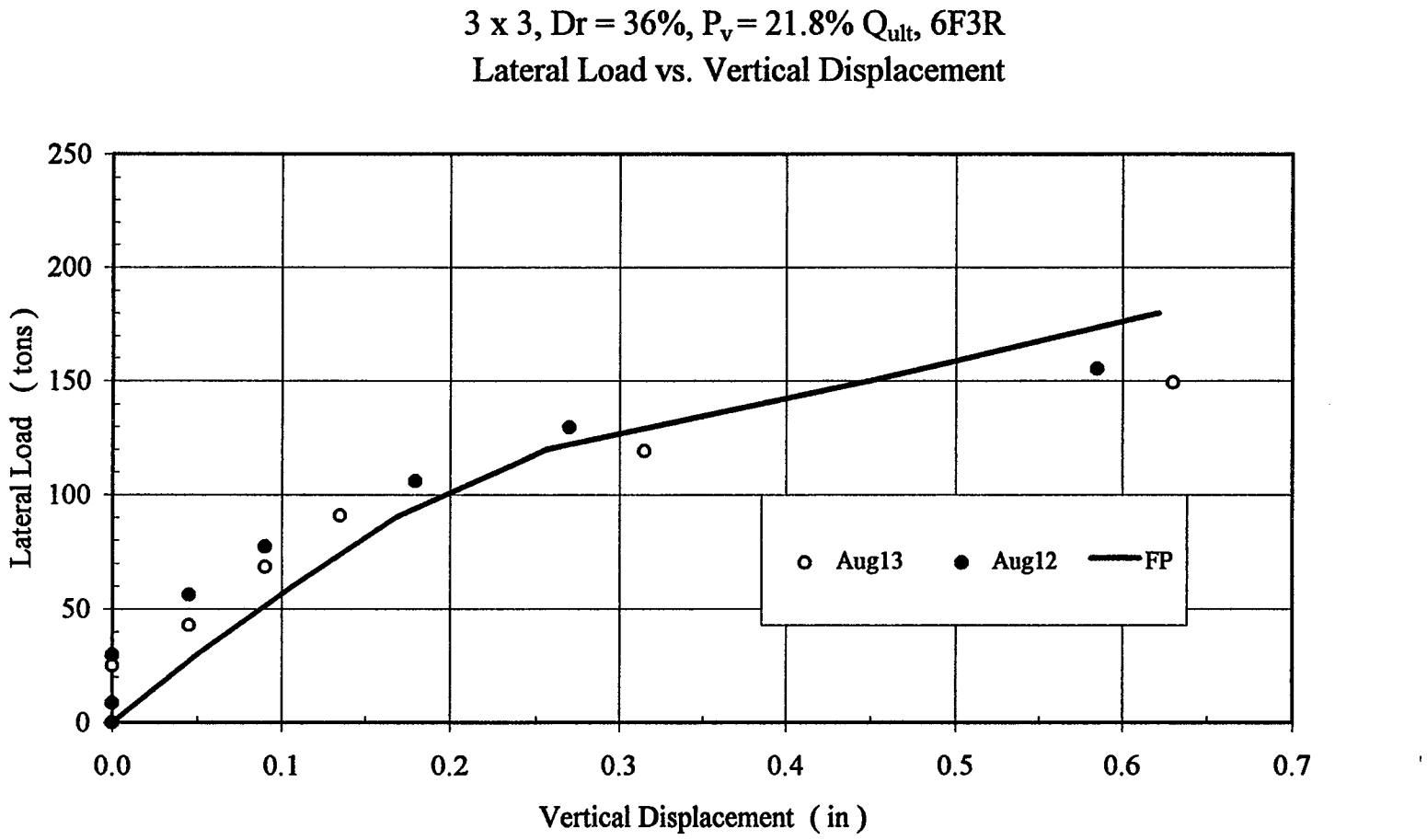

Figure B-18 Load Cell versus Veritcal LVDT

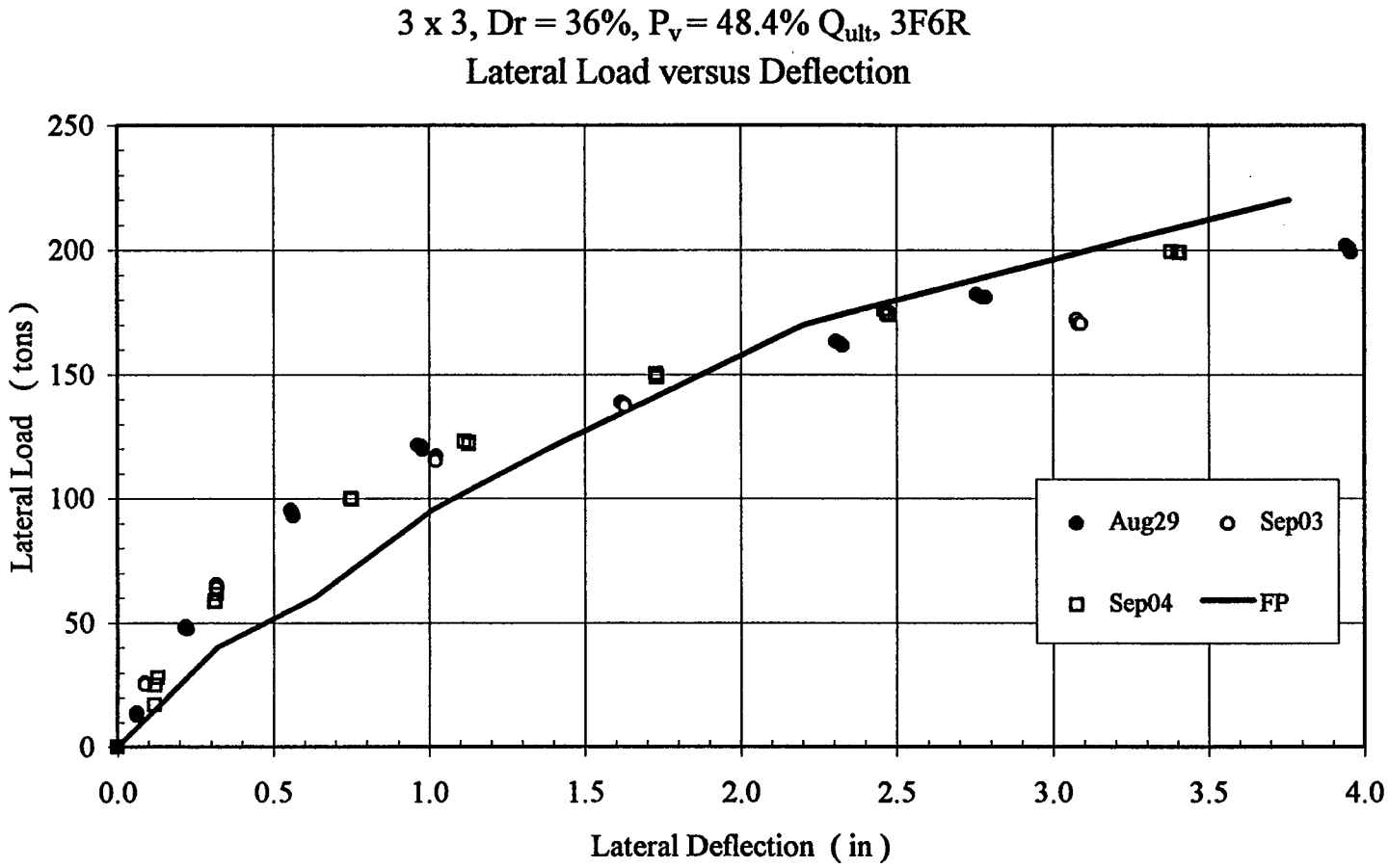

Figure B-19 Lateral Load versus Deflection

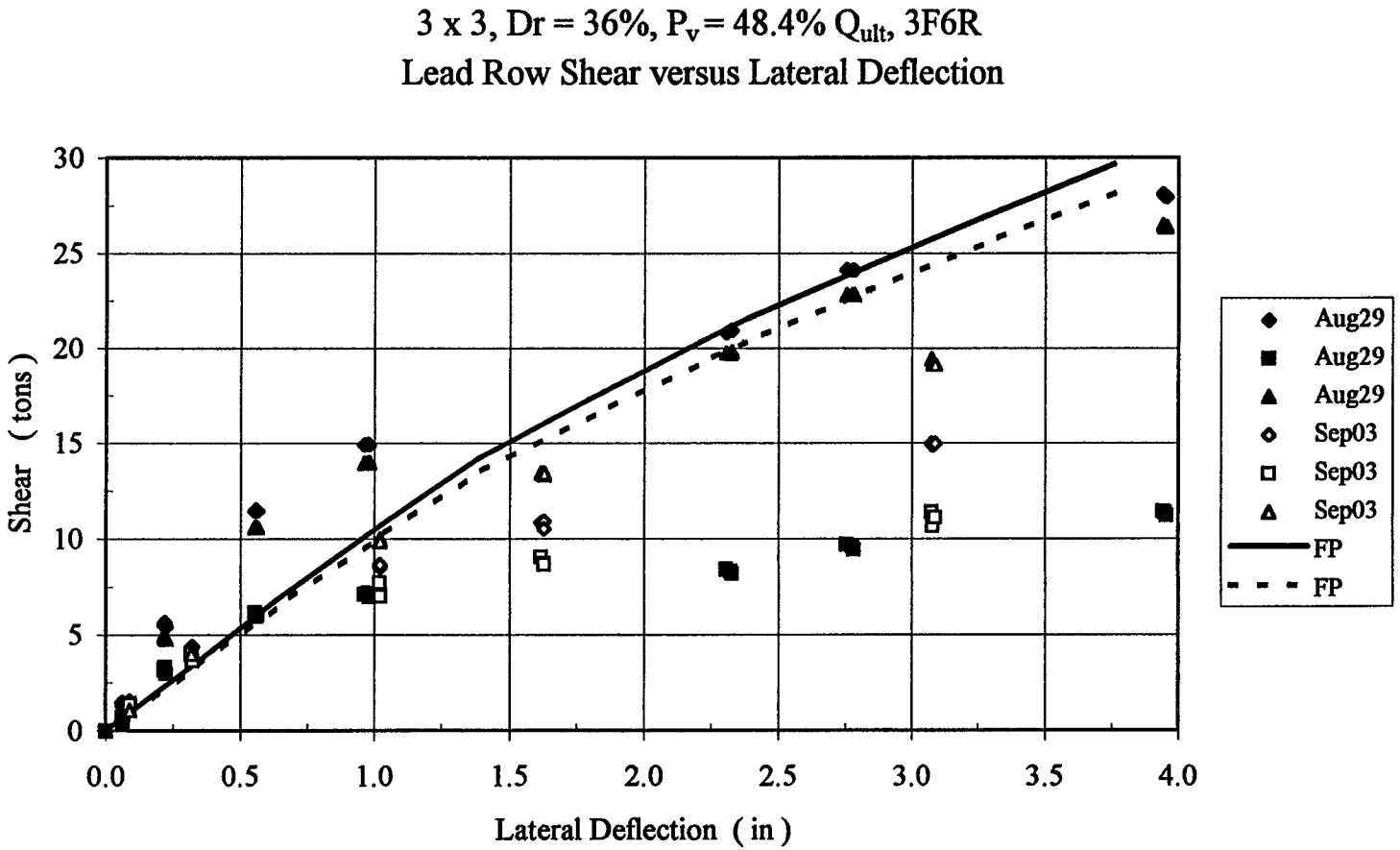

Figure B-20 Lead Row Shear versus Lateral Deflection

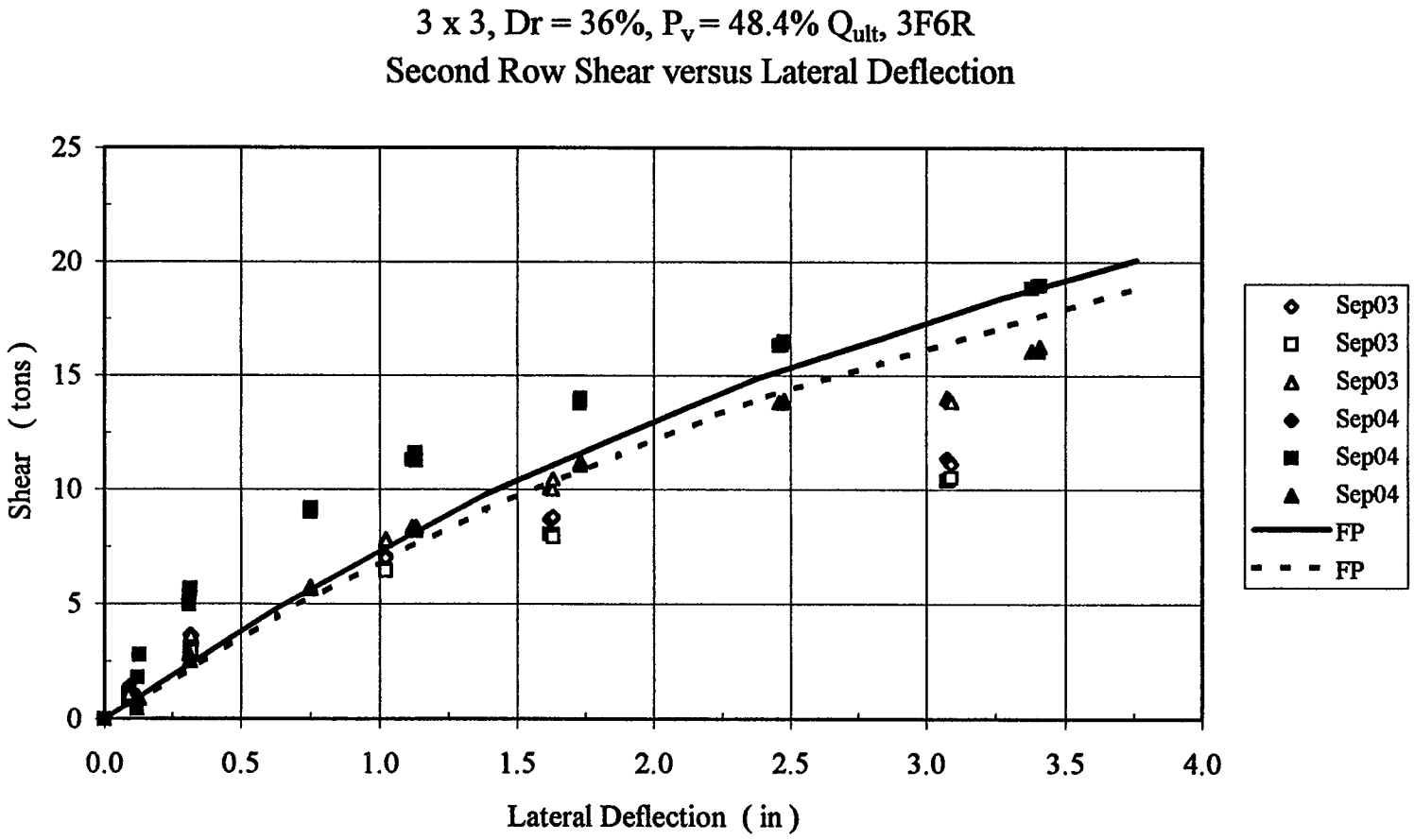

Figure B-21 Second Row Shear versus Lateral Deflection

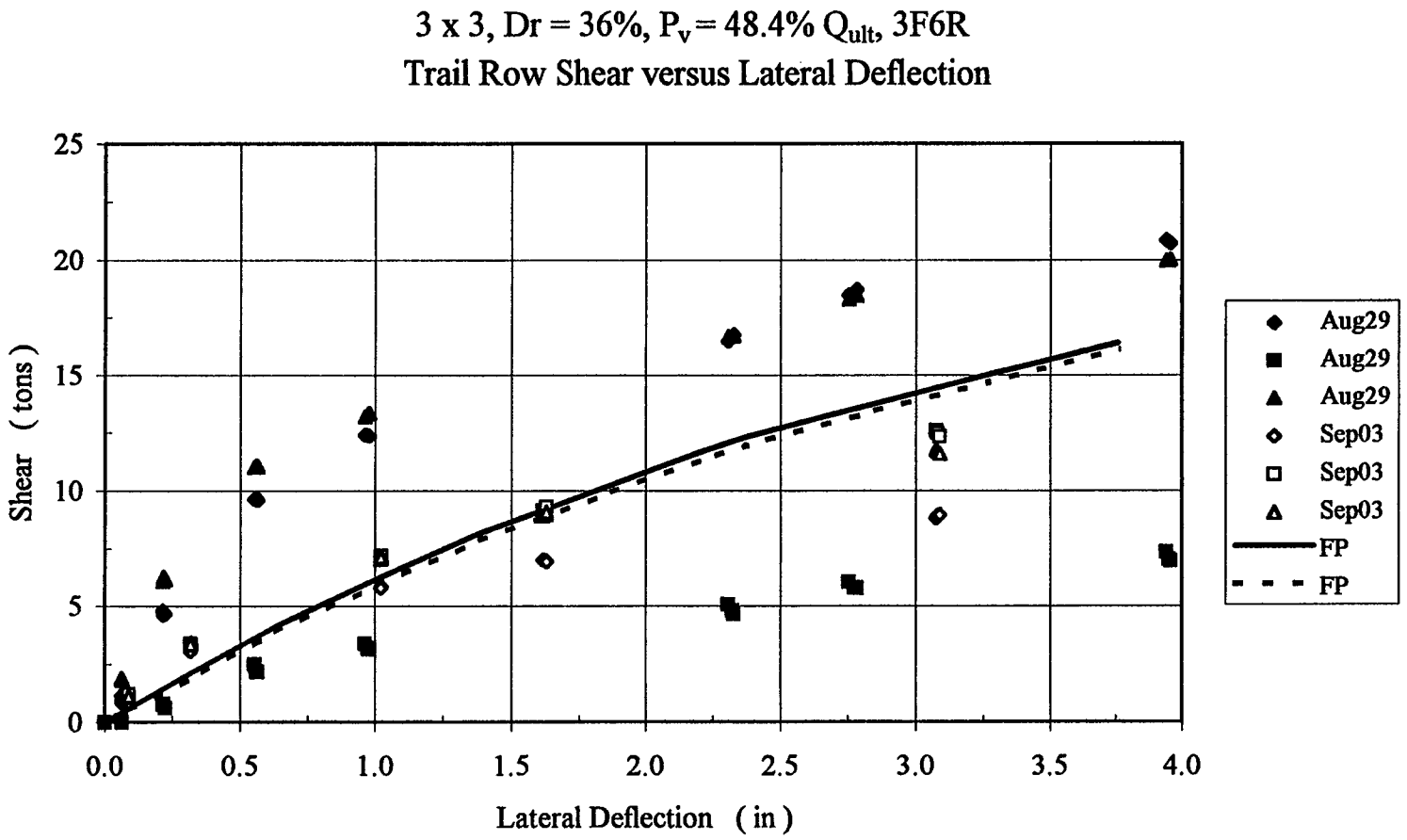

Figure B-22 Trail Row Shear versus Lateral Deflection

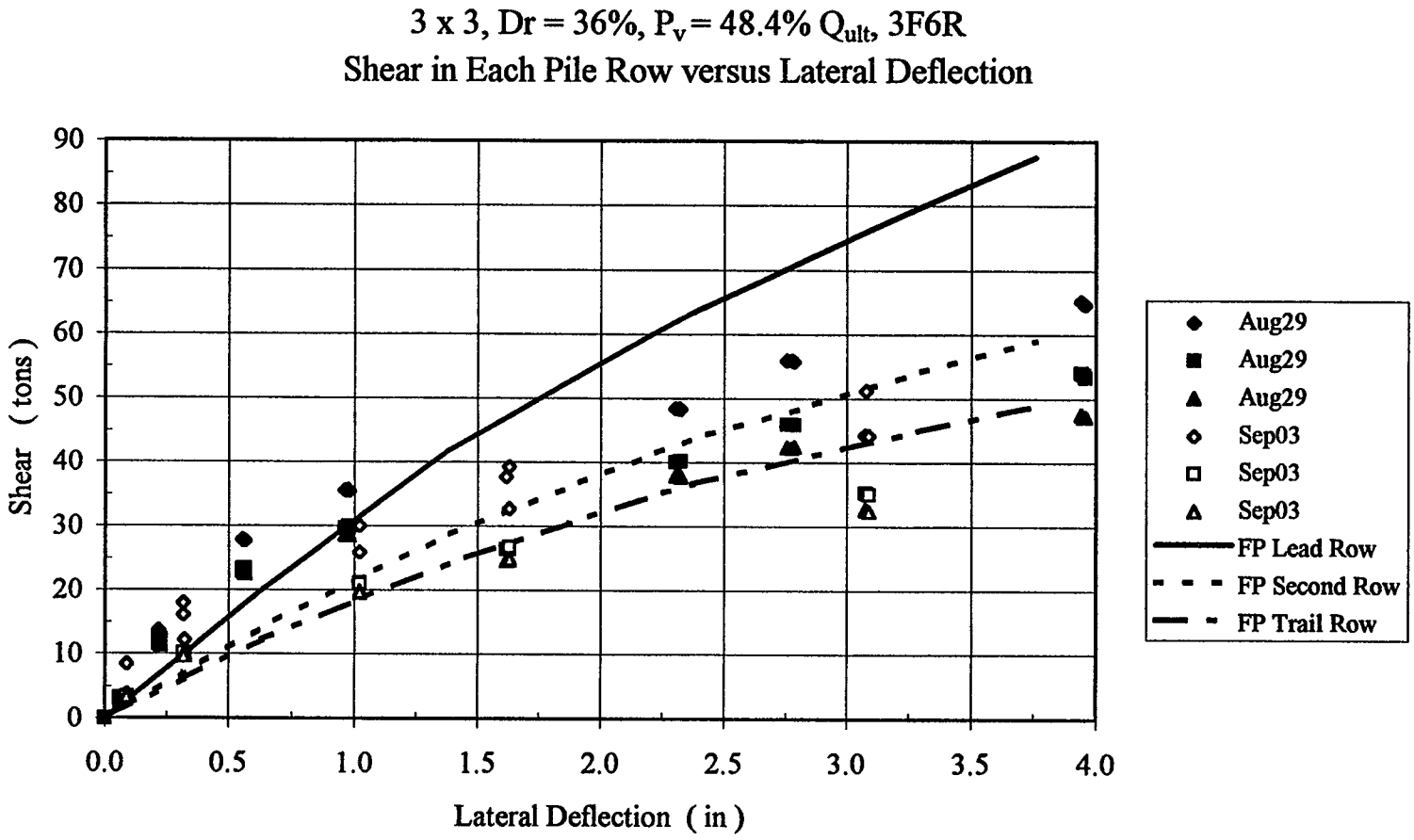

Figure B-23 Shear in Each Pile Row versus Lateral Deflection

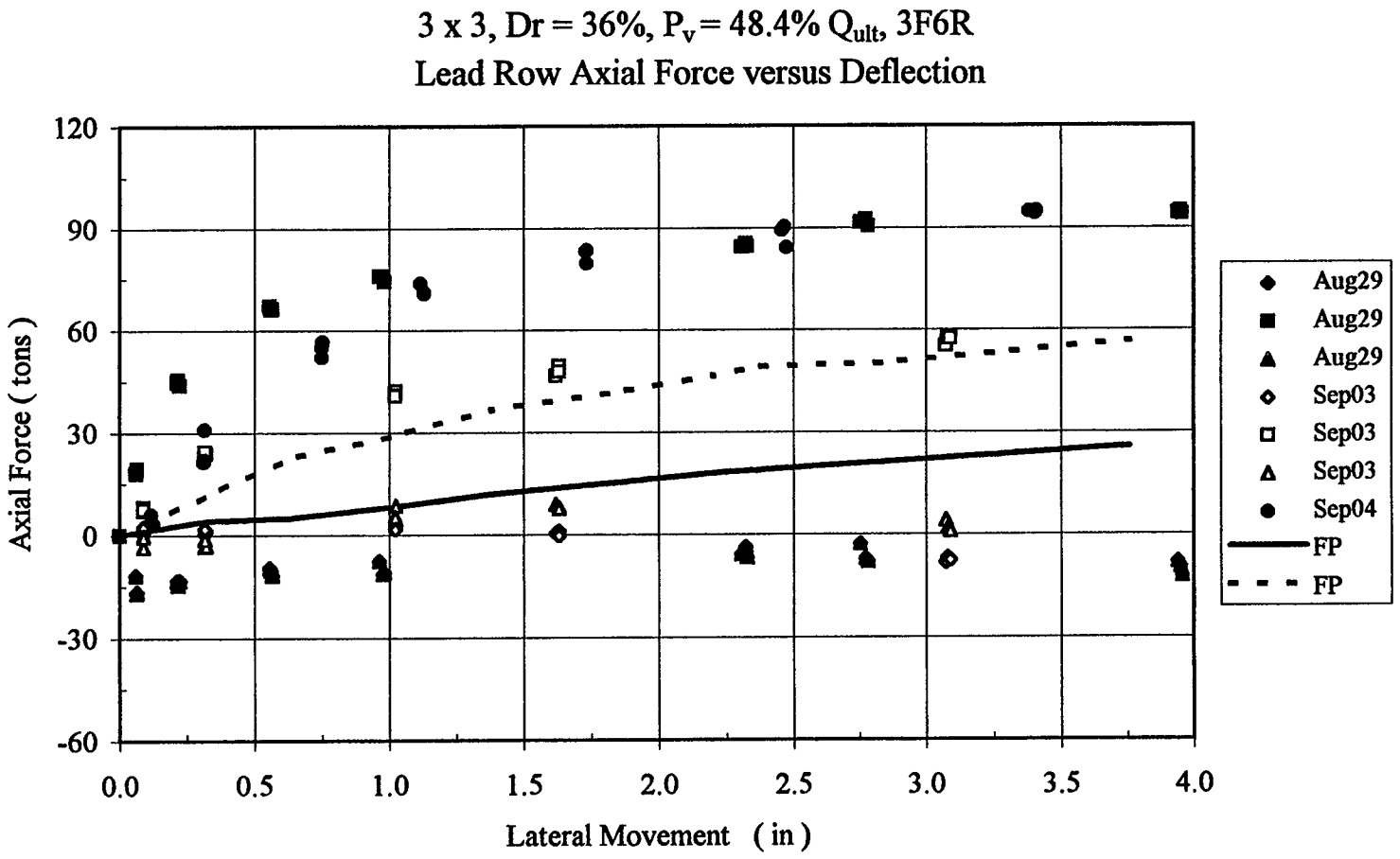

Figure B-24 Lead Row Axial Force versus Lateral Deflection

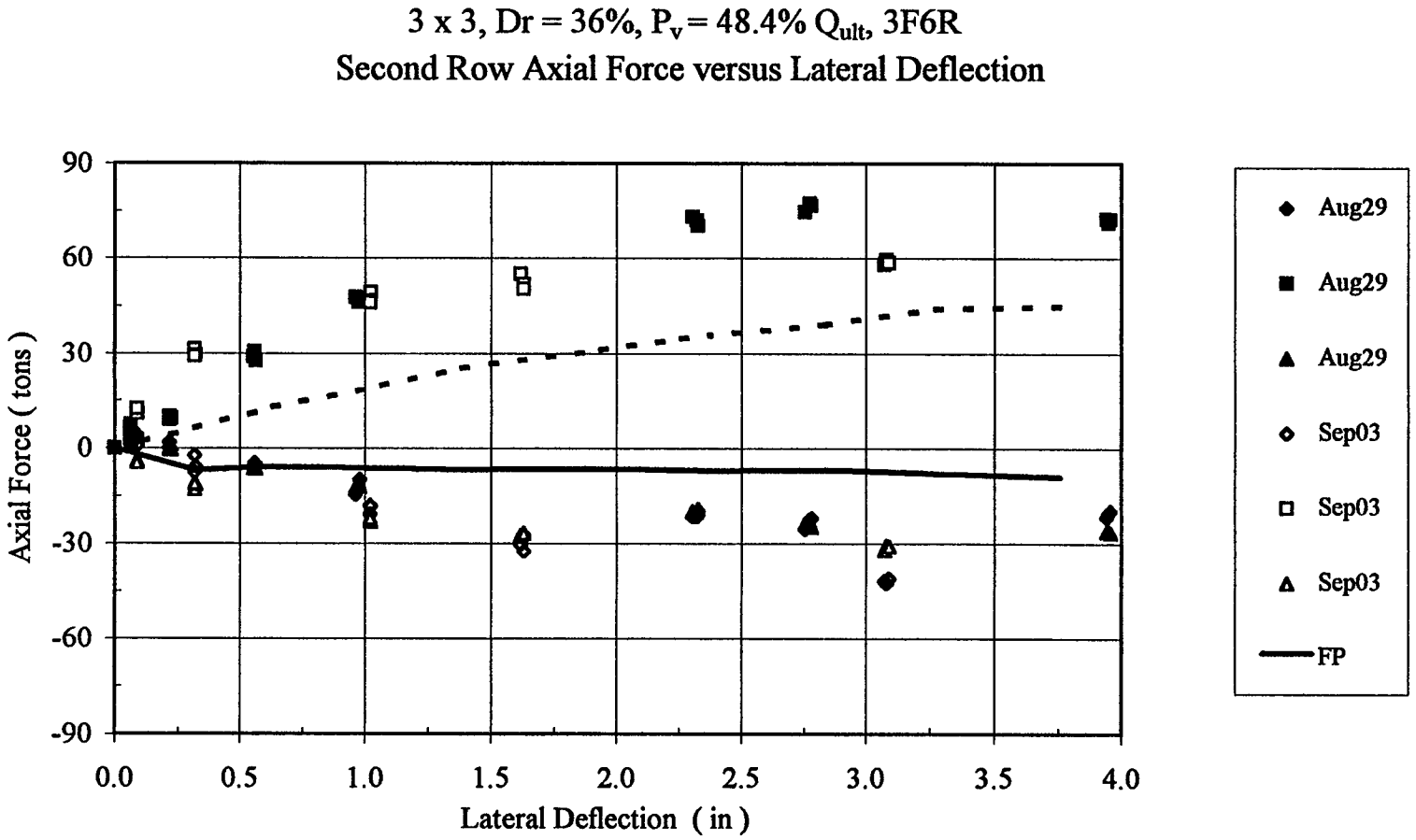

Figure B-25 Second Row Axial Force versus Lateral Deflection

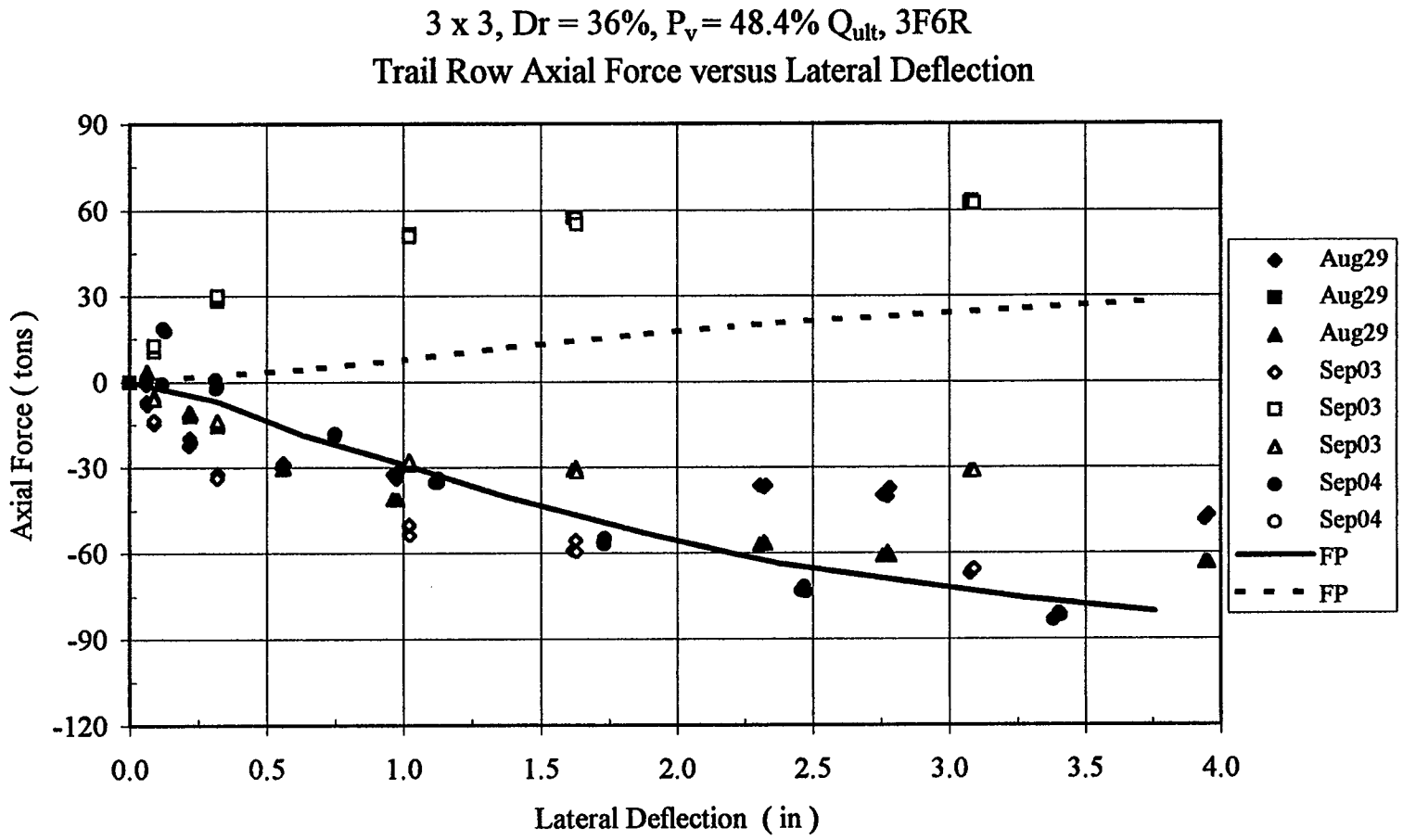

Figure B-26 Trail Row Axial Force versus Lateral Deflection

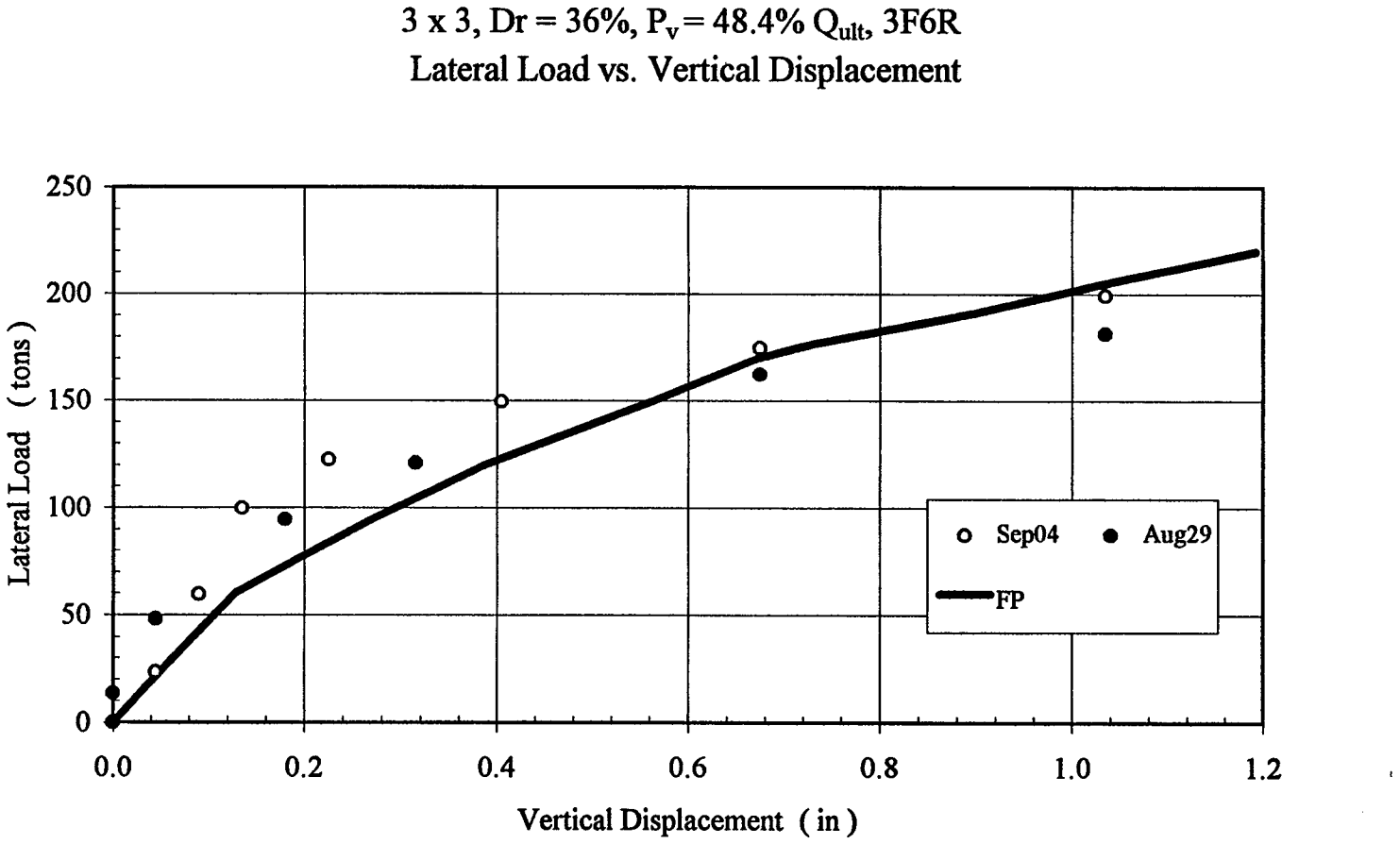

Figure B-27 Lateral Load versus Vertical Displacement

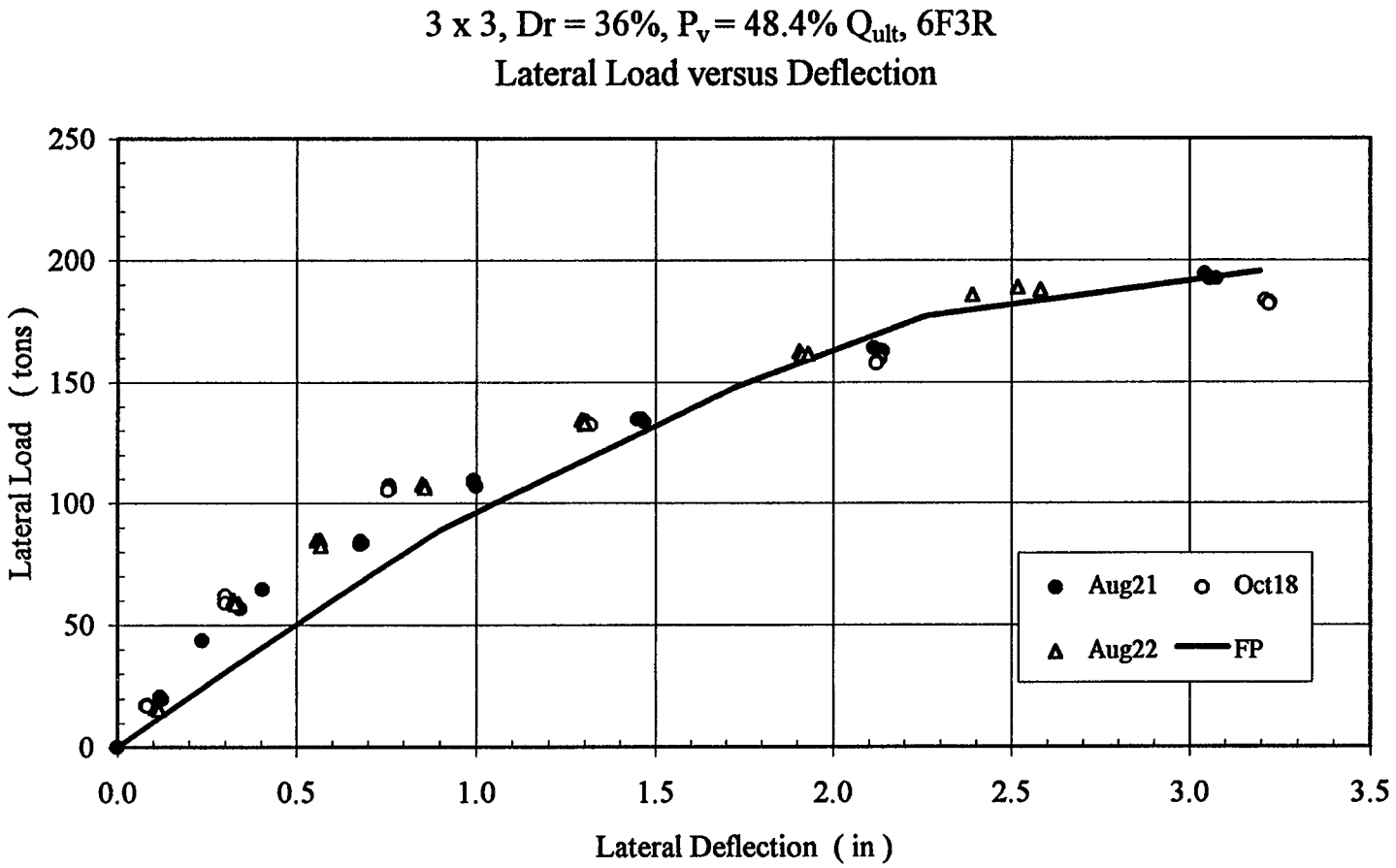

Figure B-28 Lateral Load versus Deflection

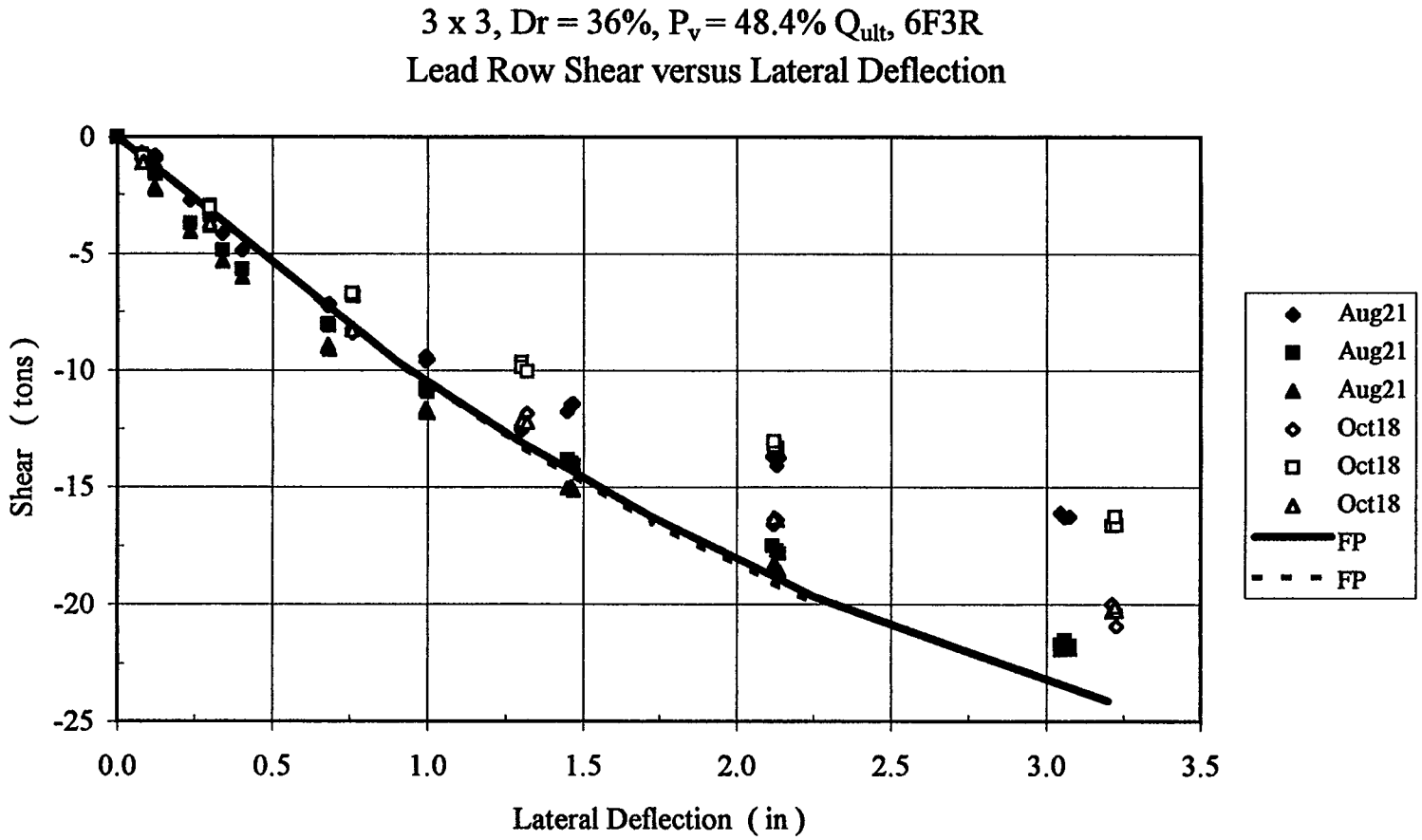

Figure B-29 Lead Row Shear versus Lateral Deflection

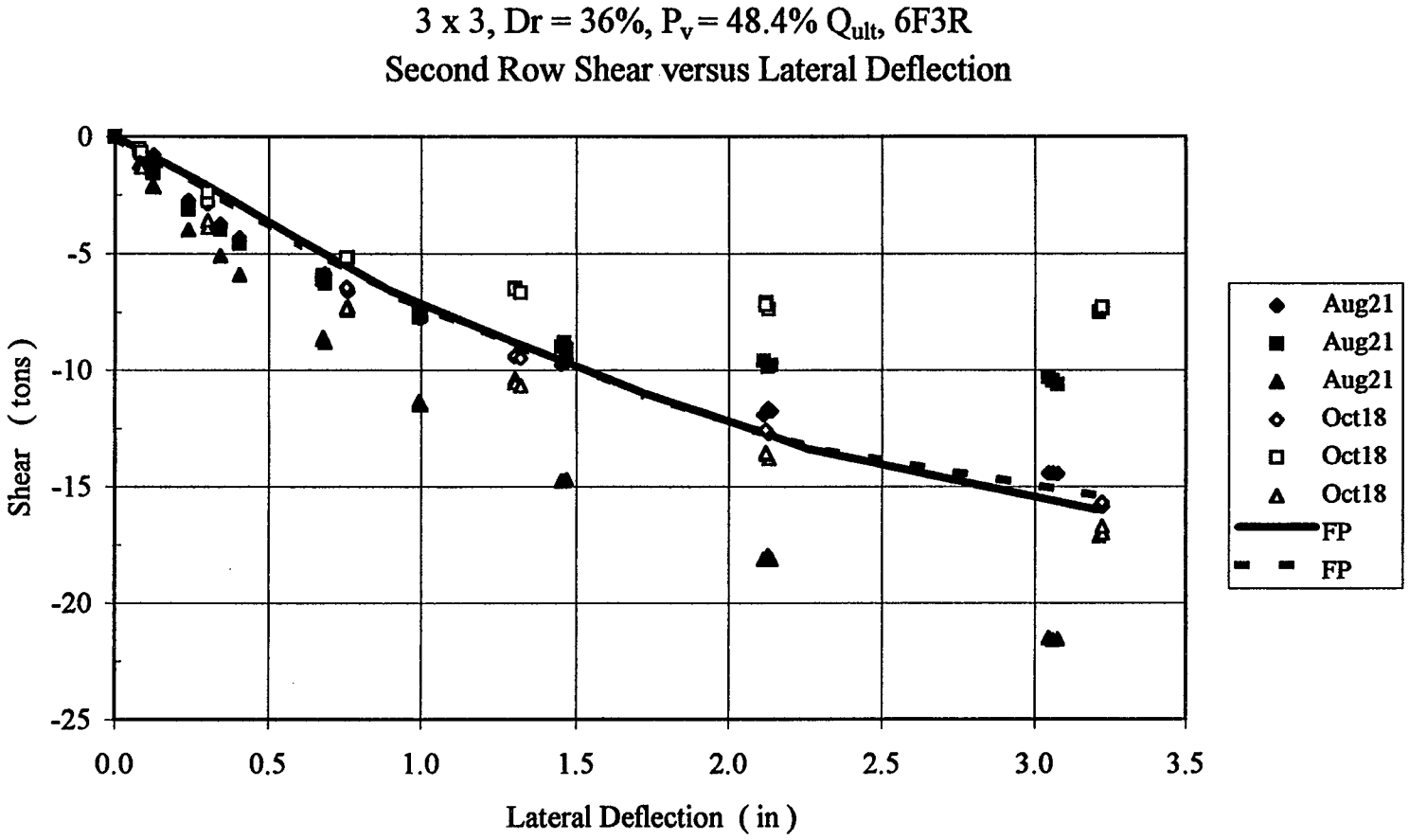

Figure B-30 Second Row Shear versus Lateral Deflection

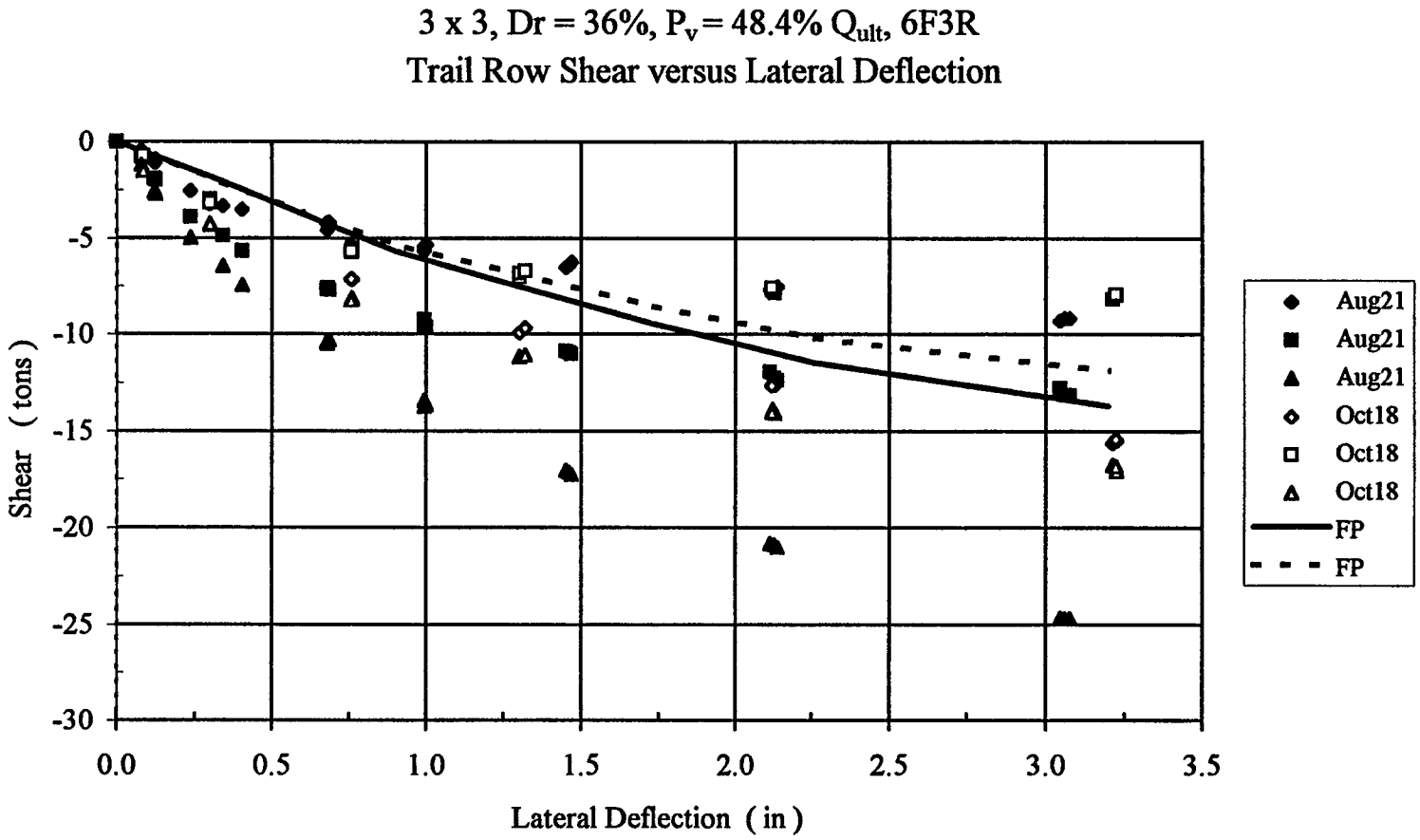

Figure B-31 Trail Row Shear versus Lateral Deflection

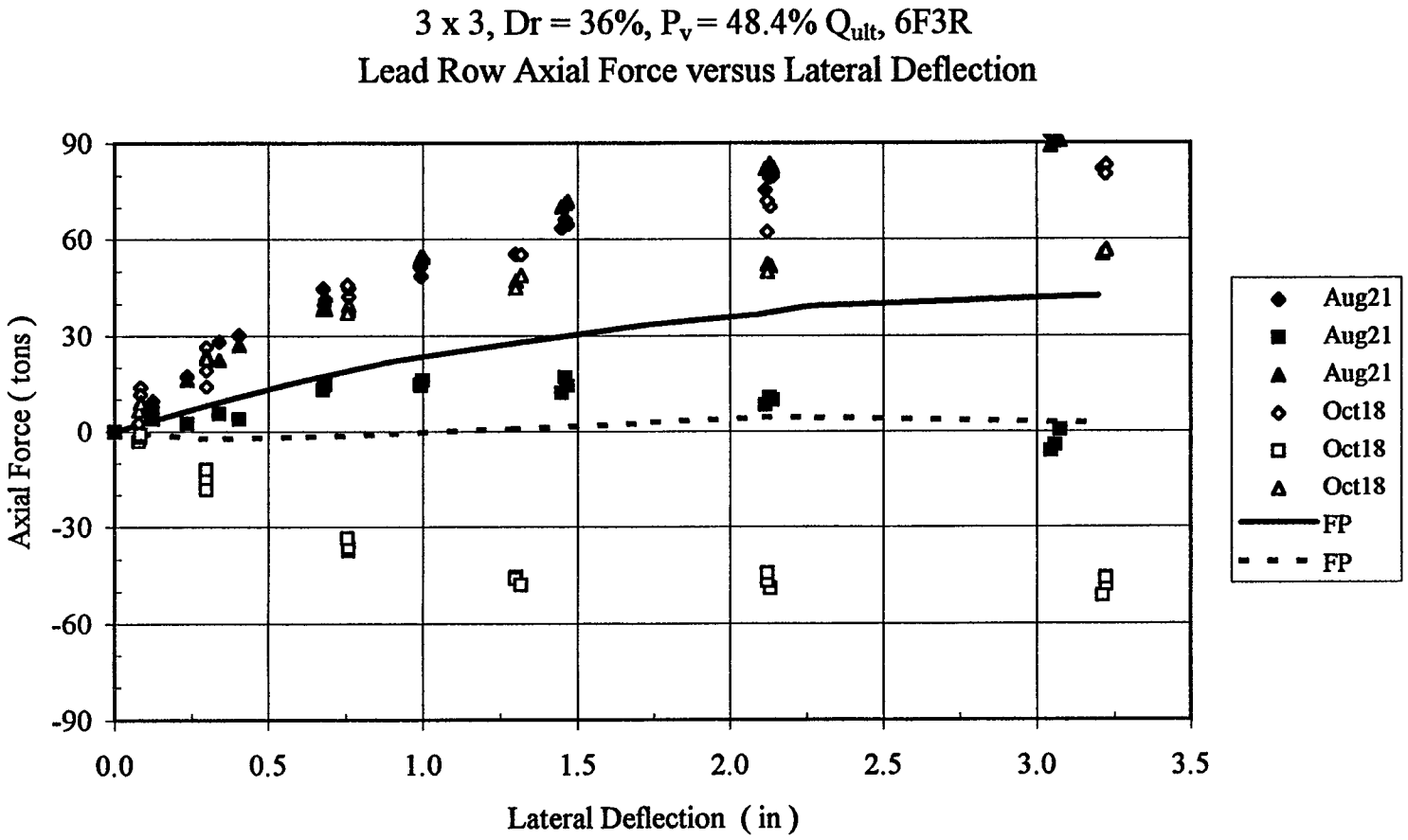

Figure B-32 Lead Row Axial Force versus Lateral Deflection

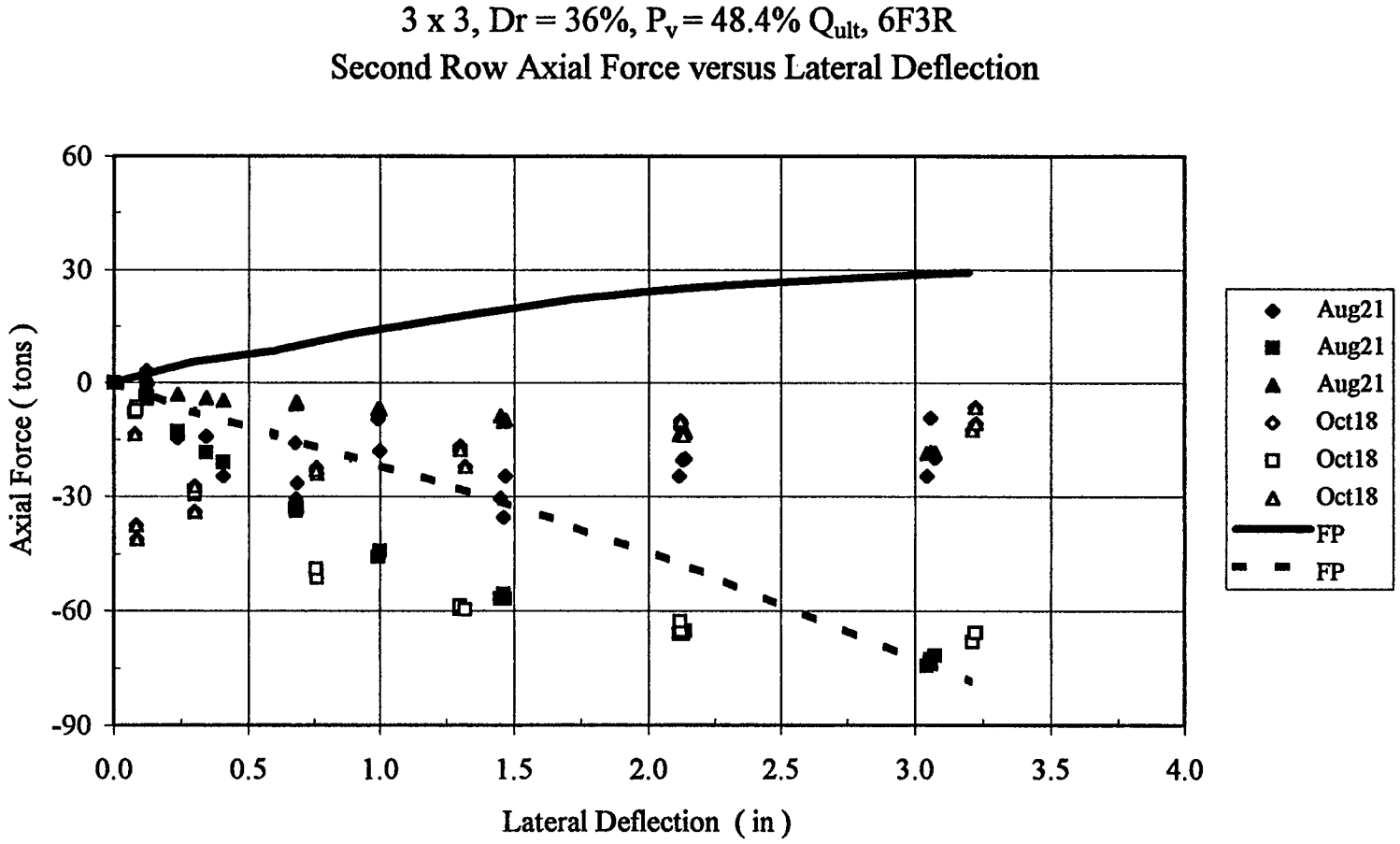

Figure B-33 Second Row Axial Force versus Deflection

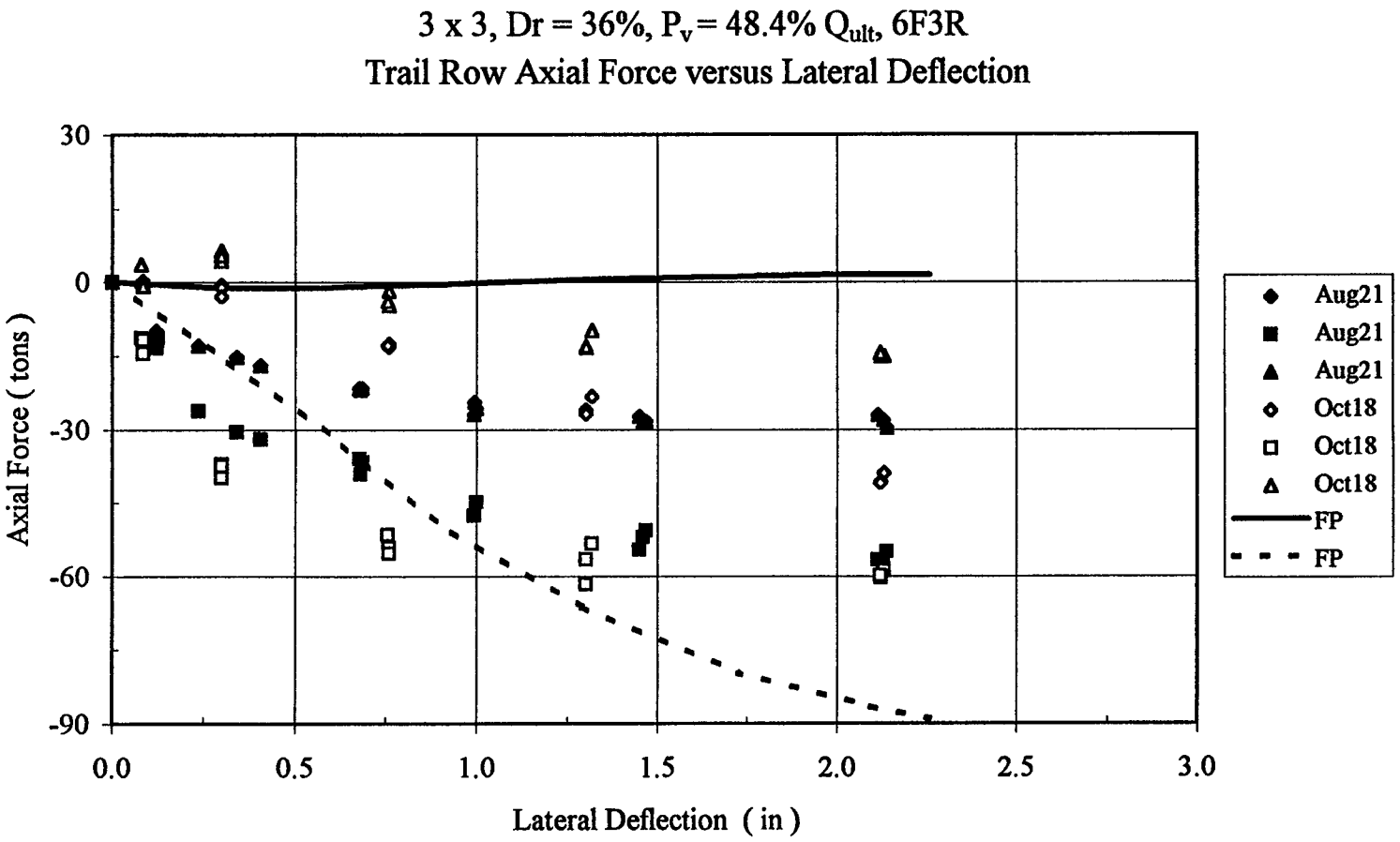

Figure B-34 Trail Row Axial Force versus Lateral Deflection

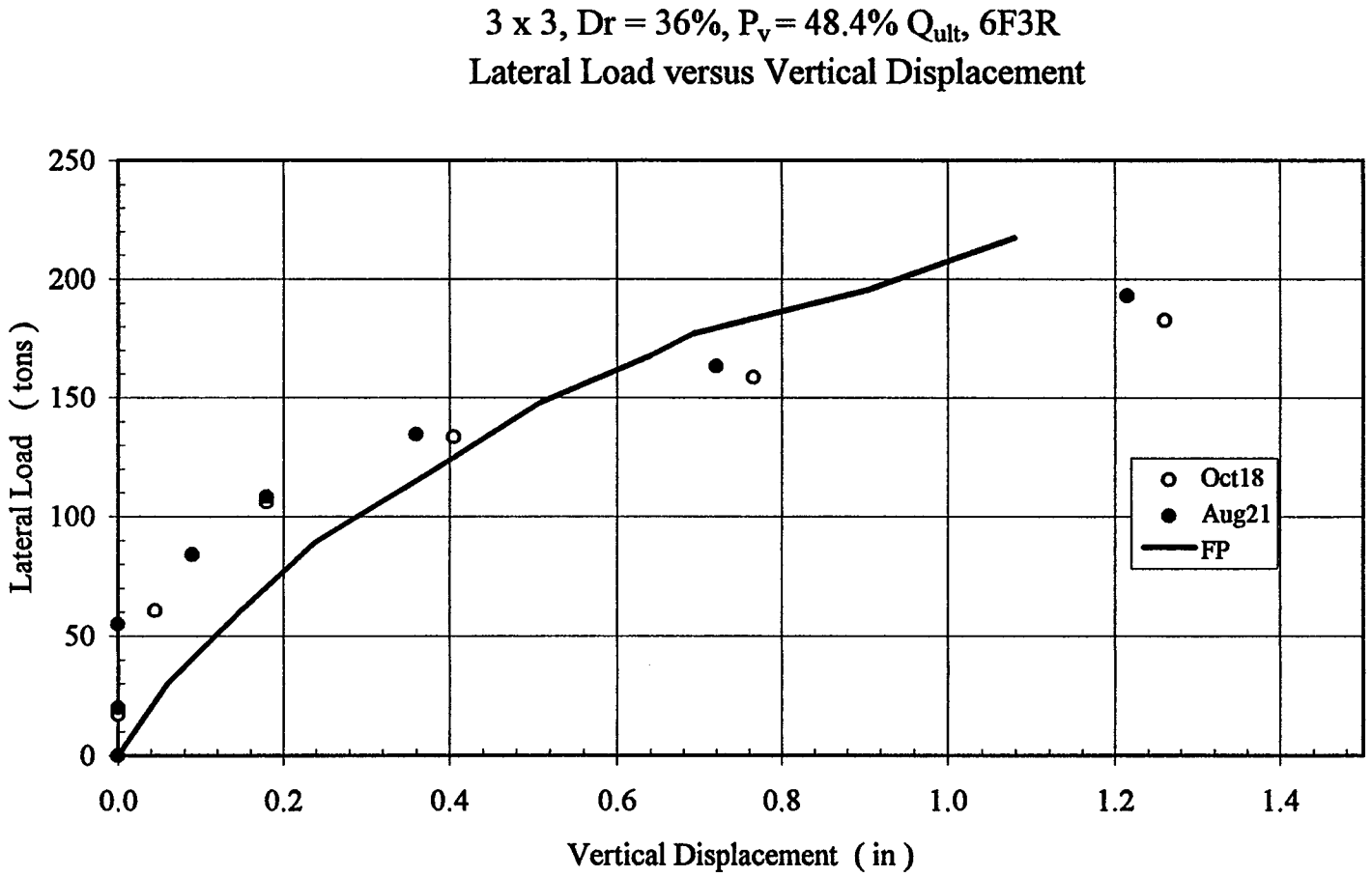

Figure B-35 Lateral Load versus Vertical Displacement

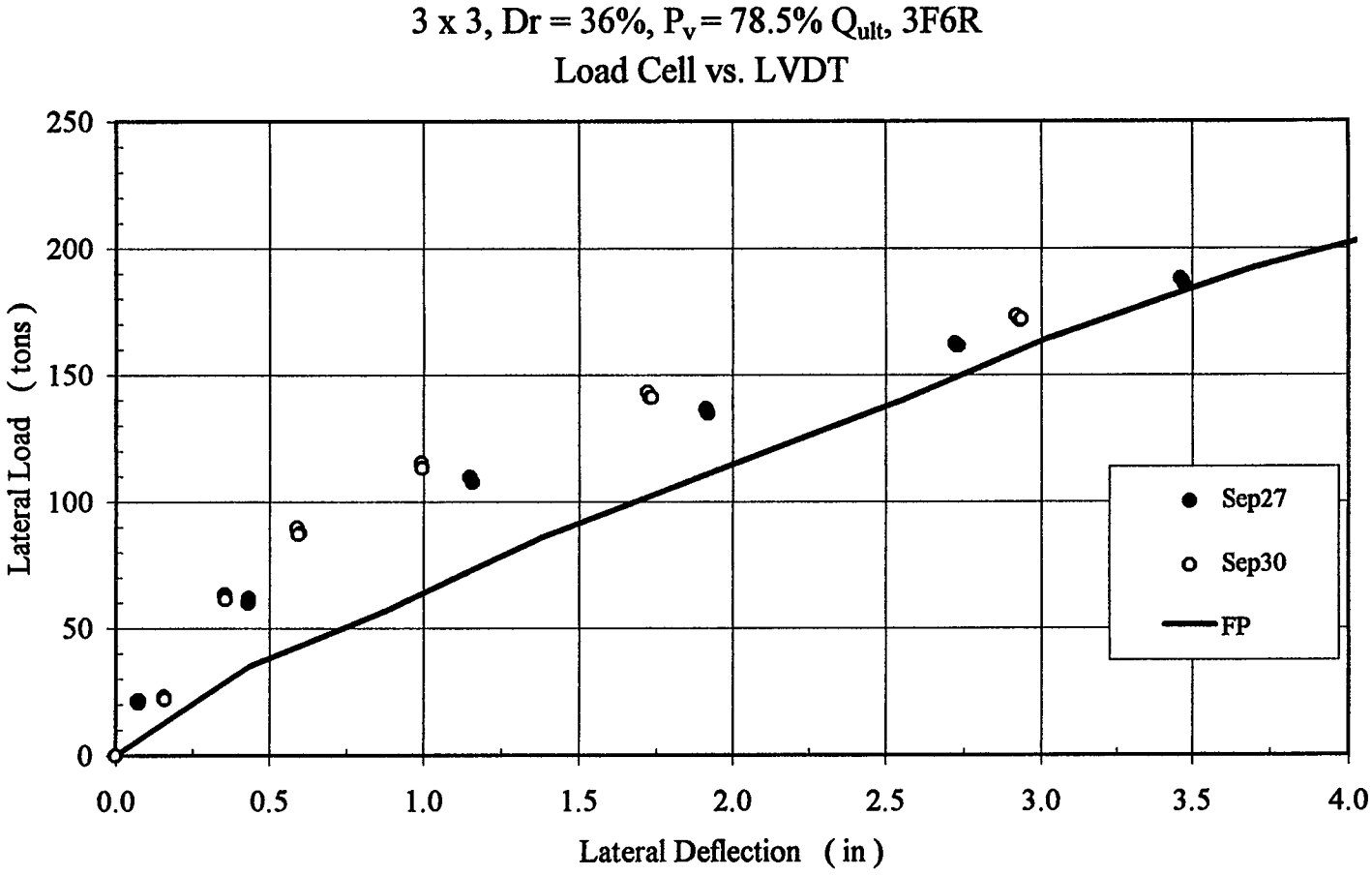

Figure B-36 Lateral Load versus Deflection

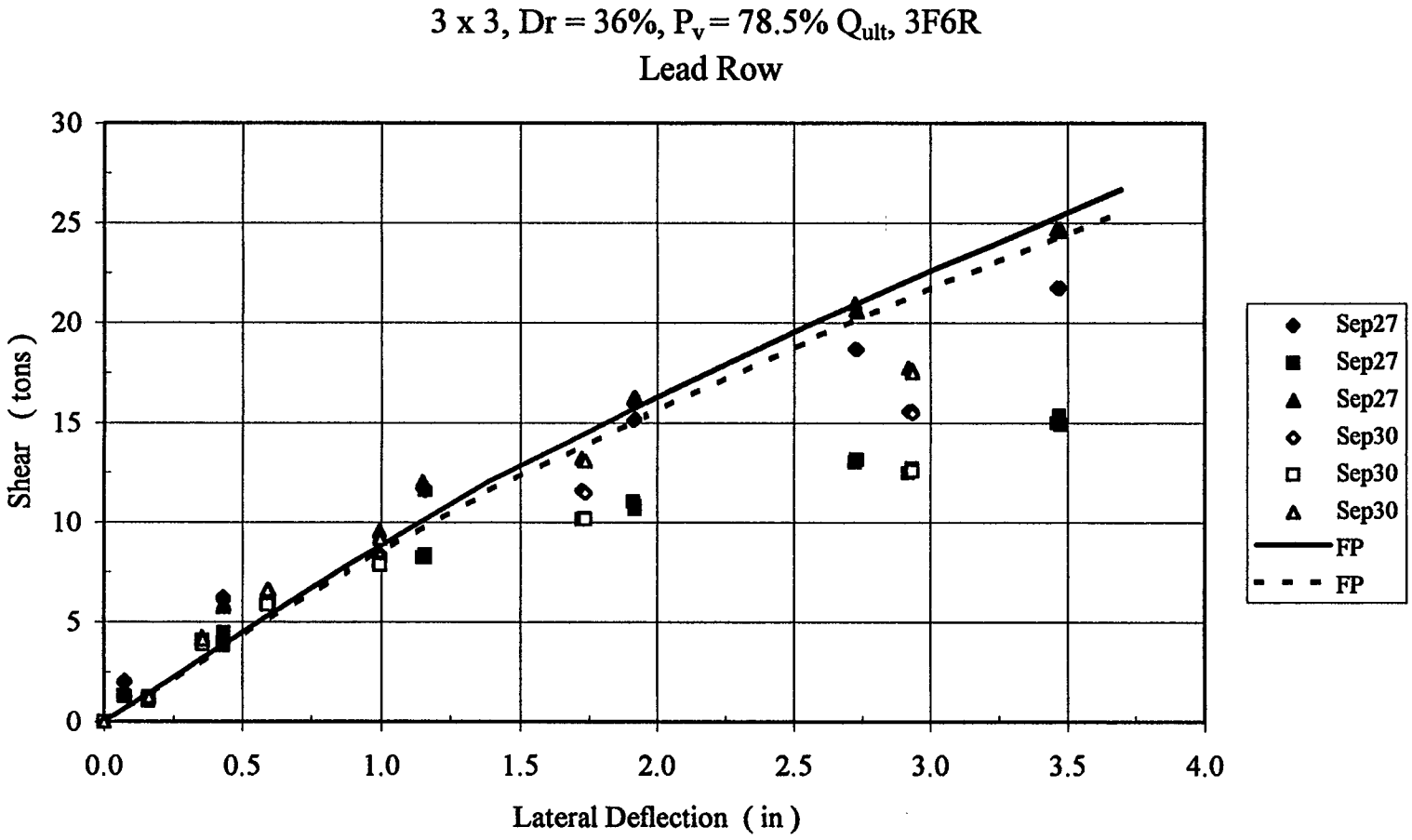

Figure B-37 Lead Row Shear versus Deflection

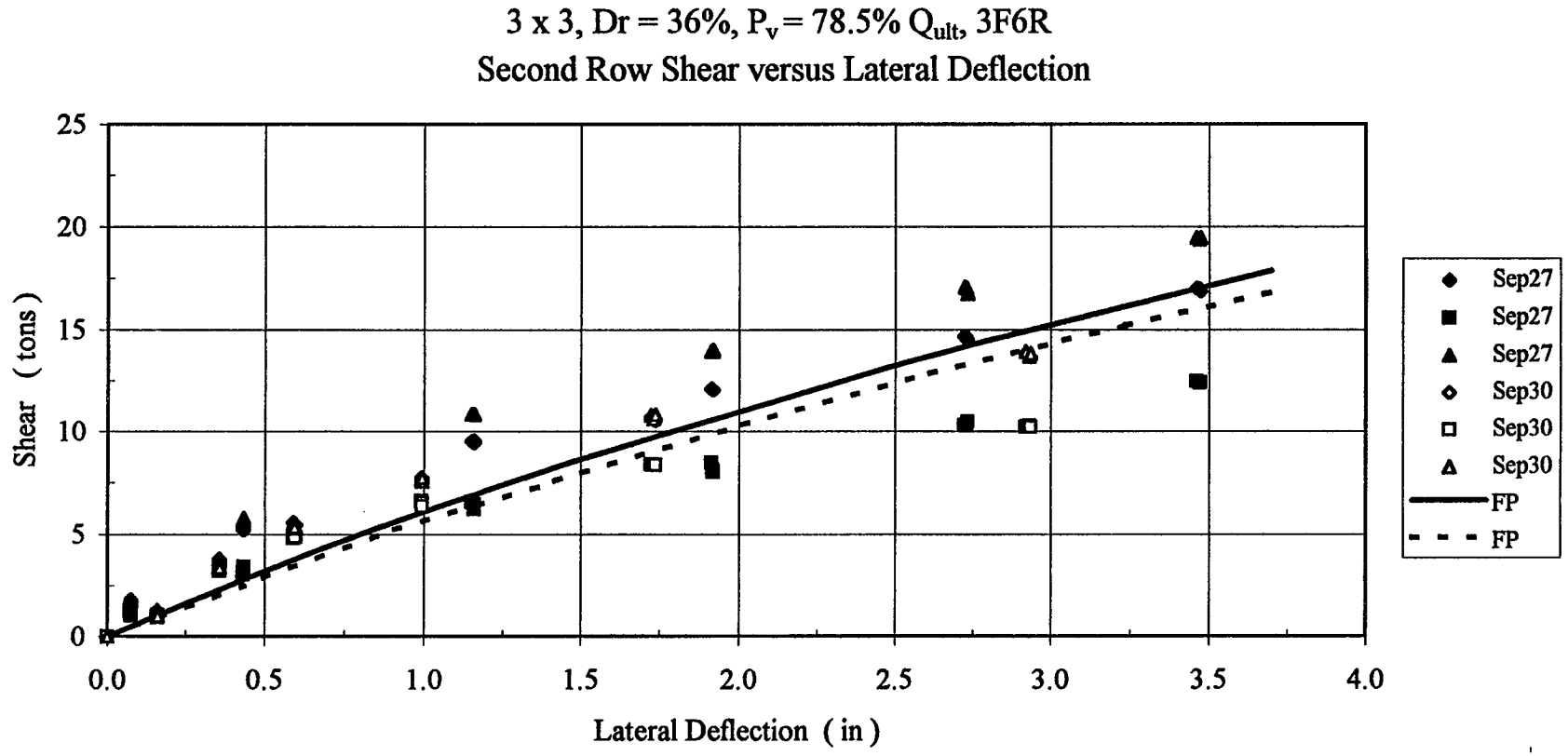

Figure B-38 Second Row Shear versus Deflection

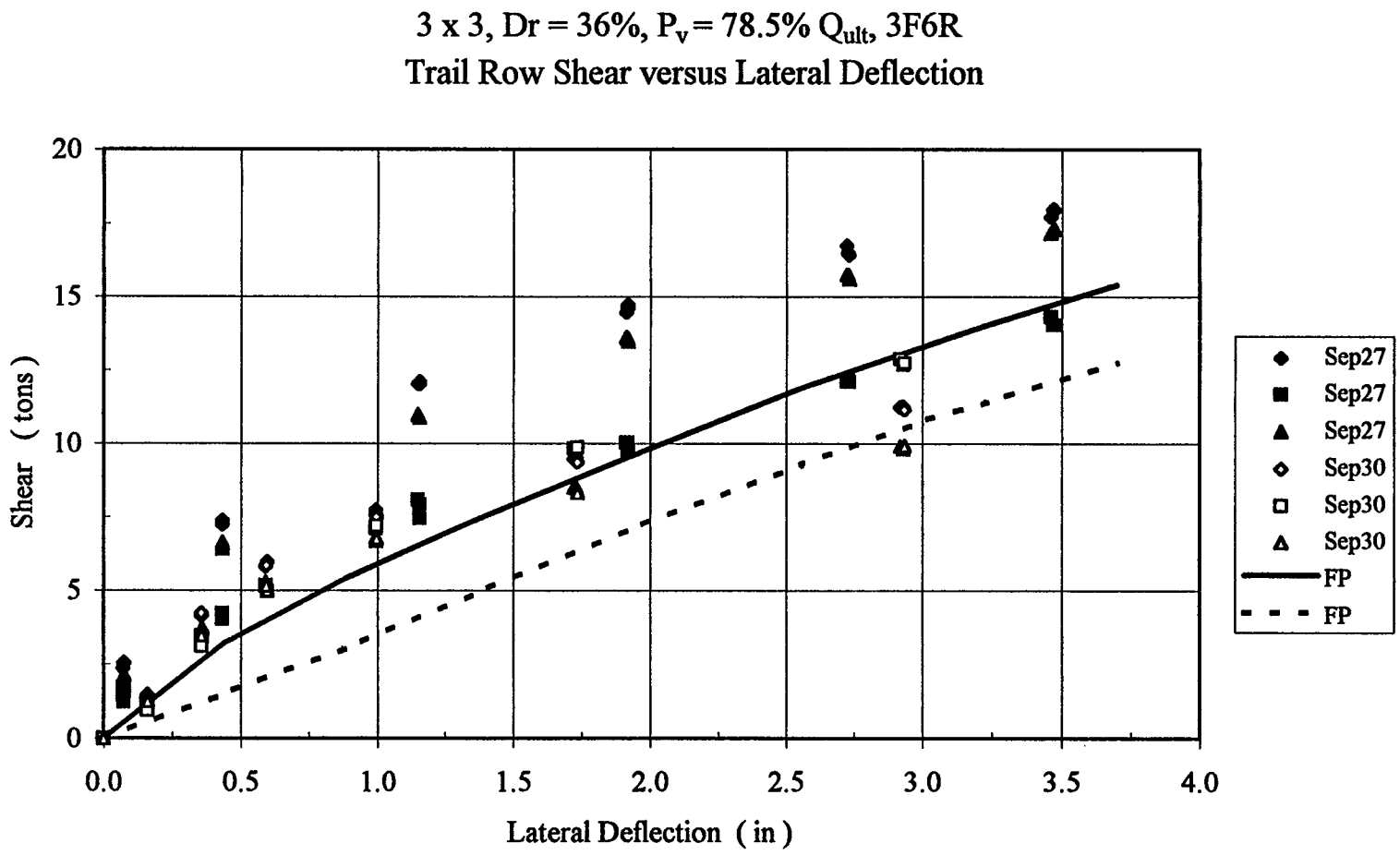

Figure B-39 Trail Row Shear versus Deflection

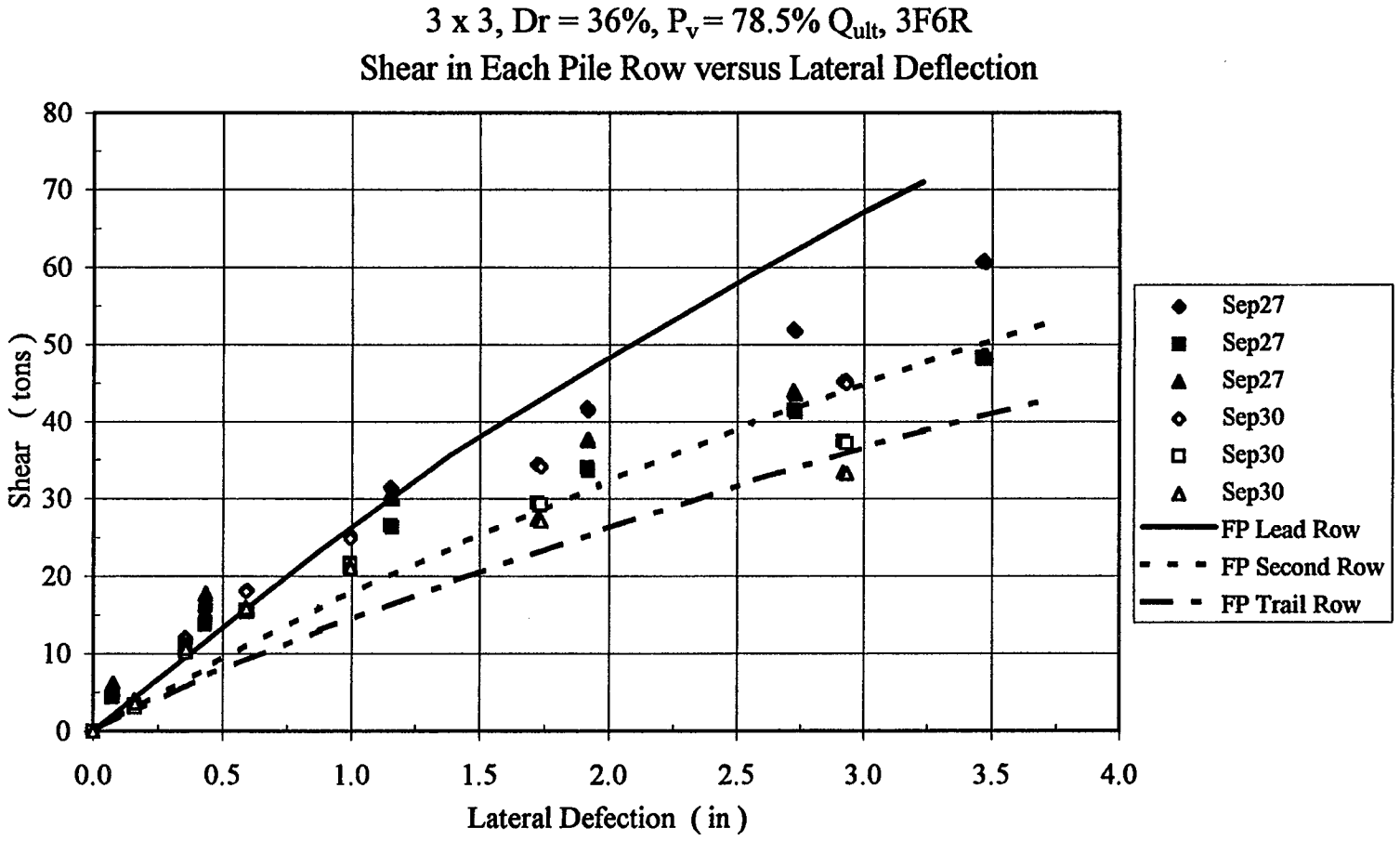

Figure B-40 Shear in Each Pile Row versus Deflection

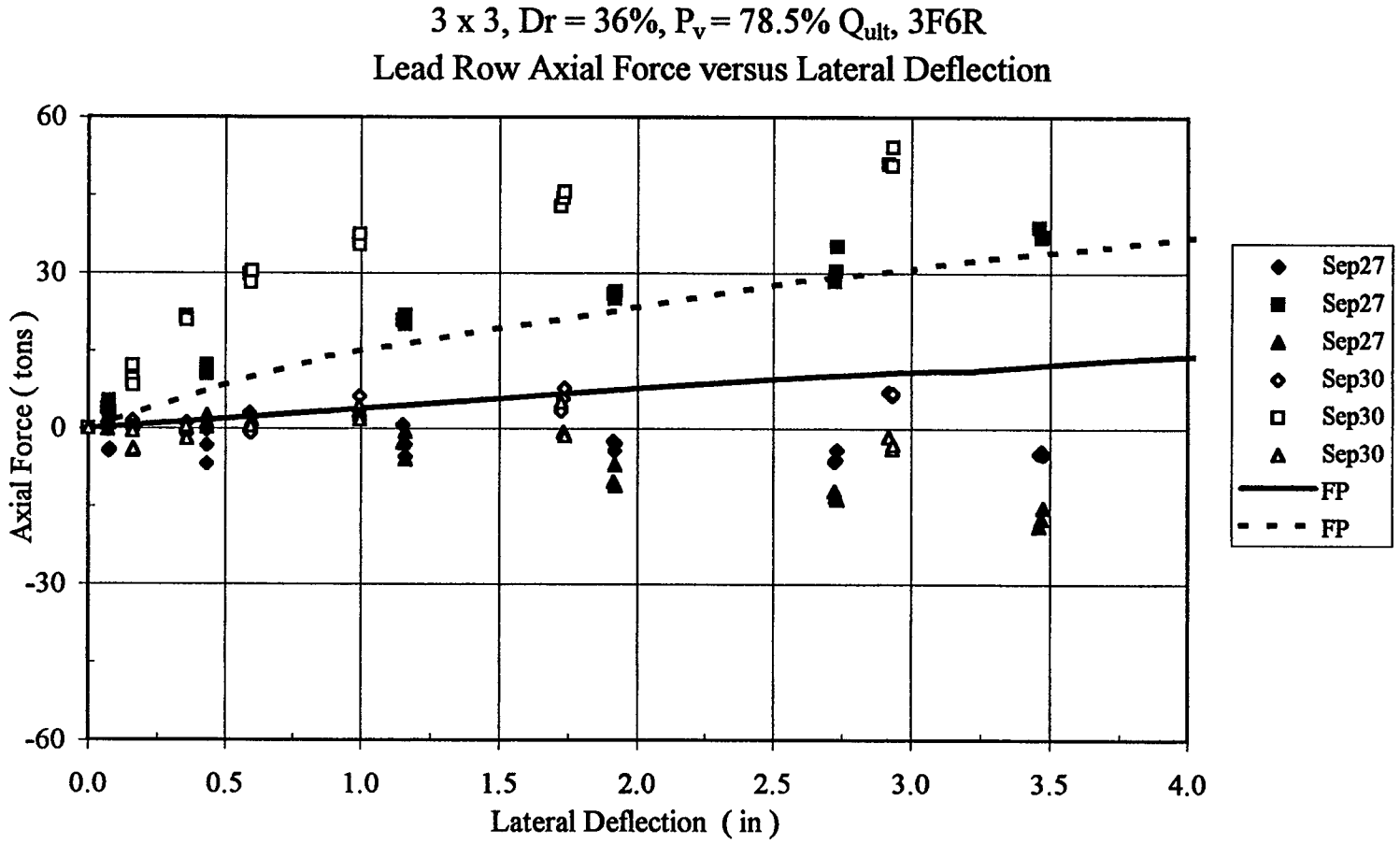

Figure B-41 Lead Row Axial Force versus Deflection

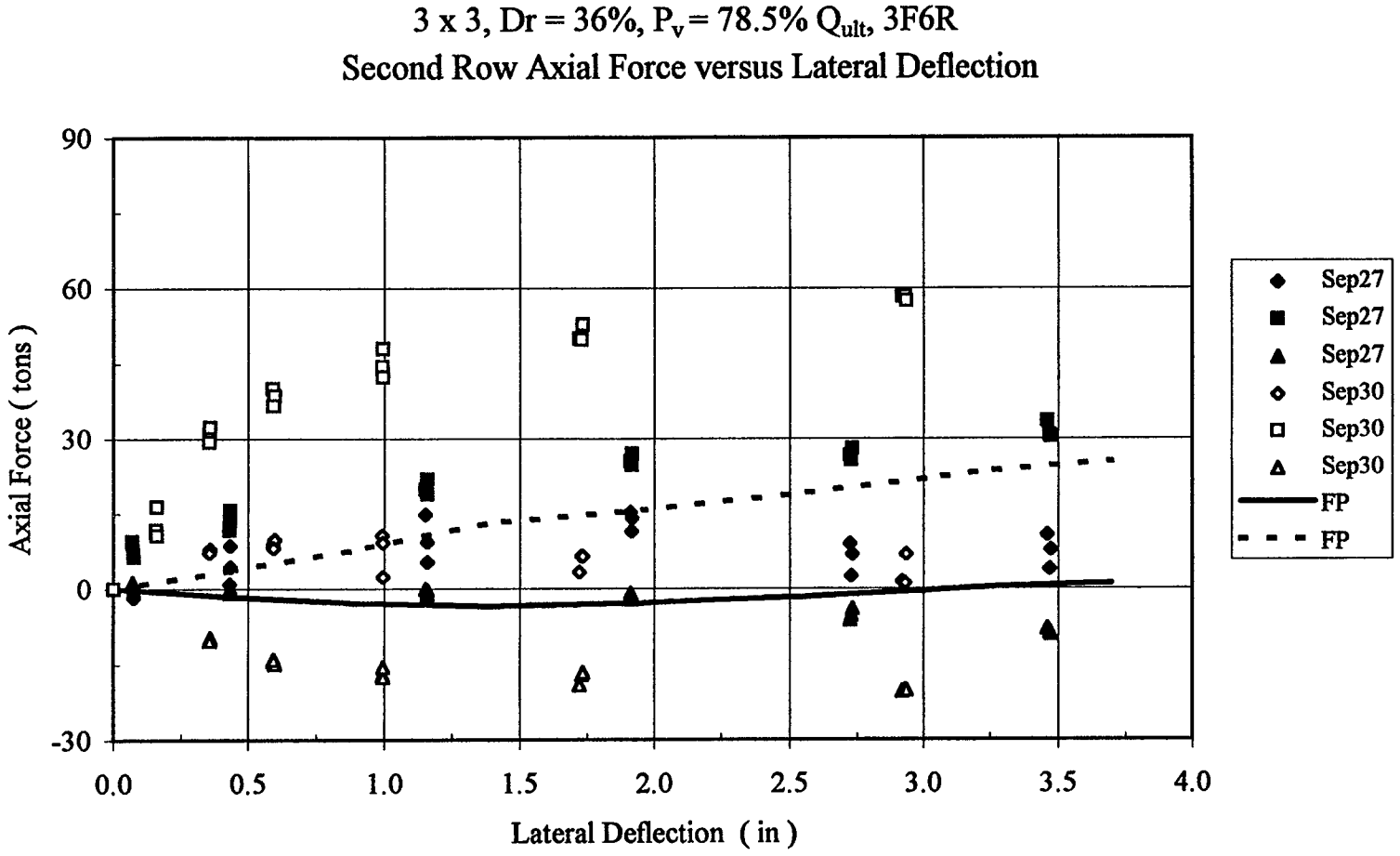

Figure B-42 Second Row Axial Force versus Lateral Deflection

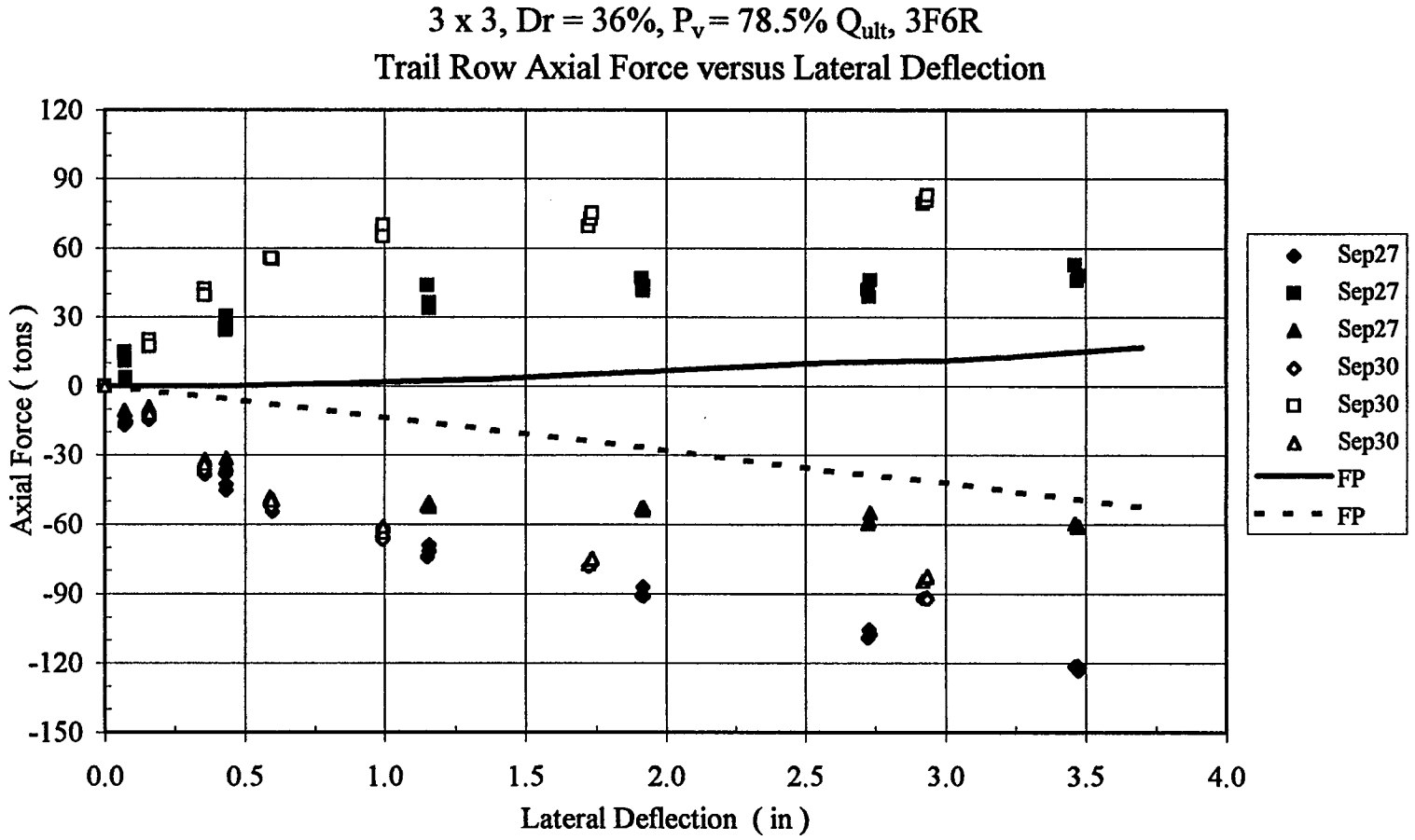

Figure B-43 Trail Row Axial Force versus Deflection

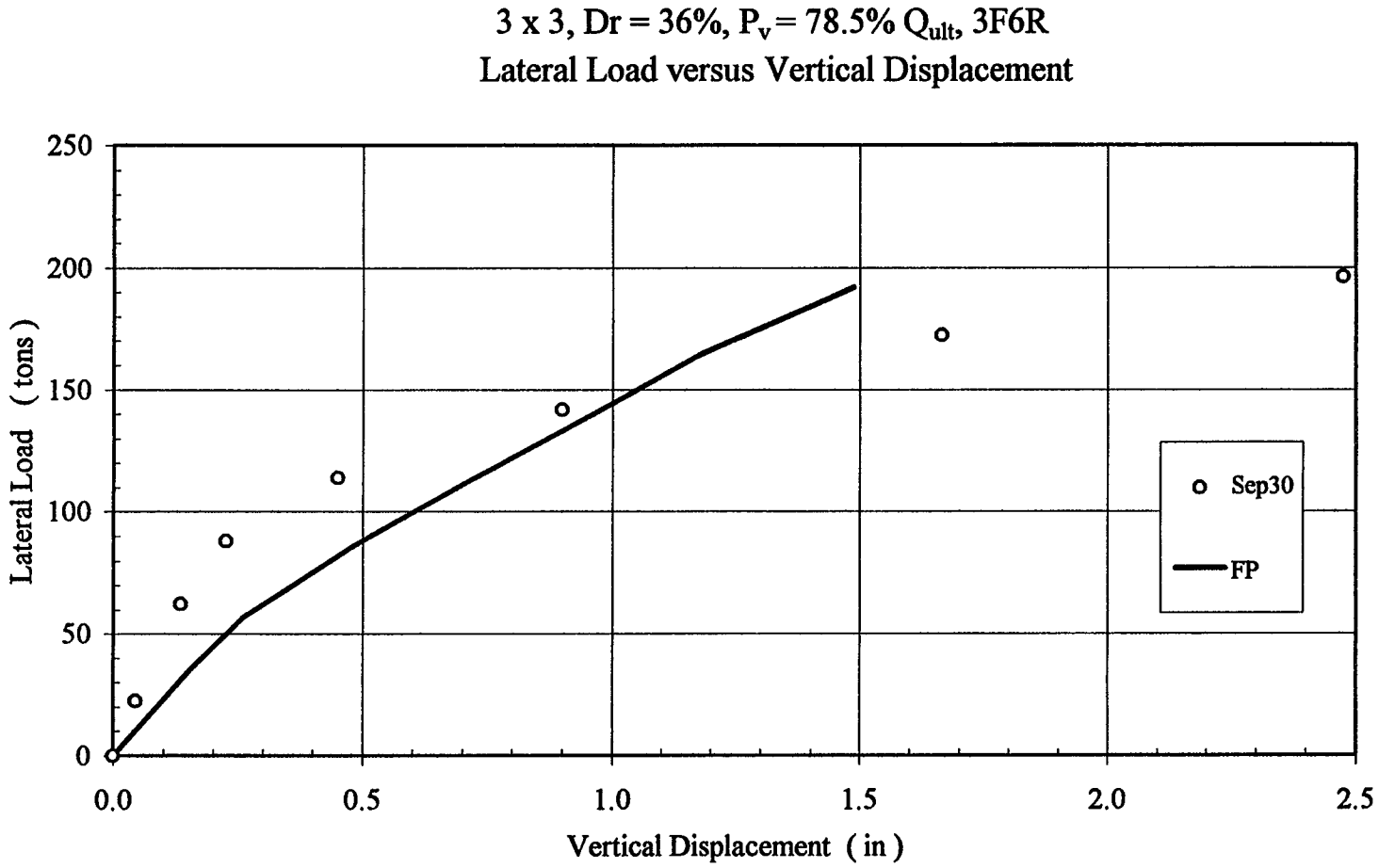

Figure B-44 Lateral Load versus Vertical Displacement

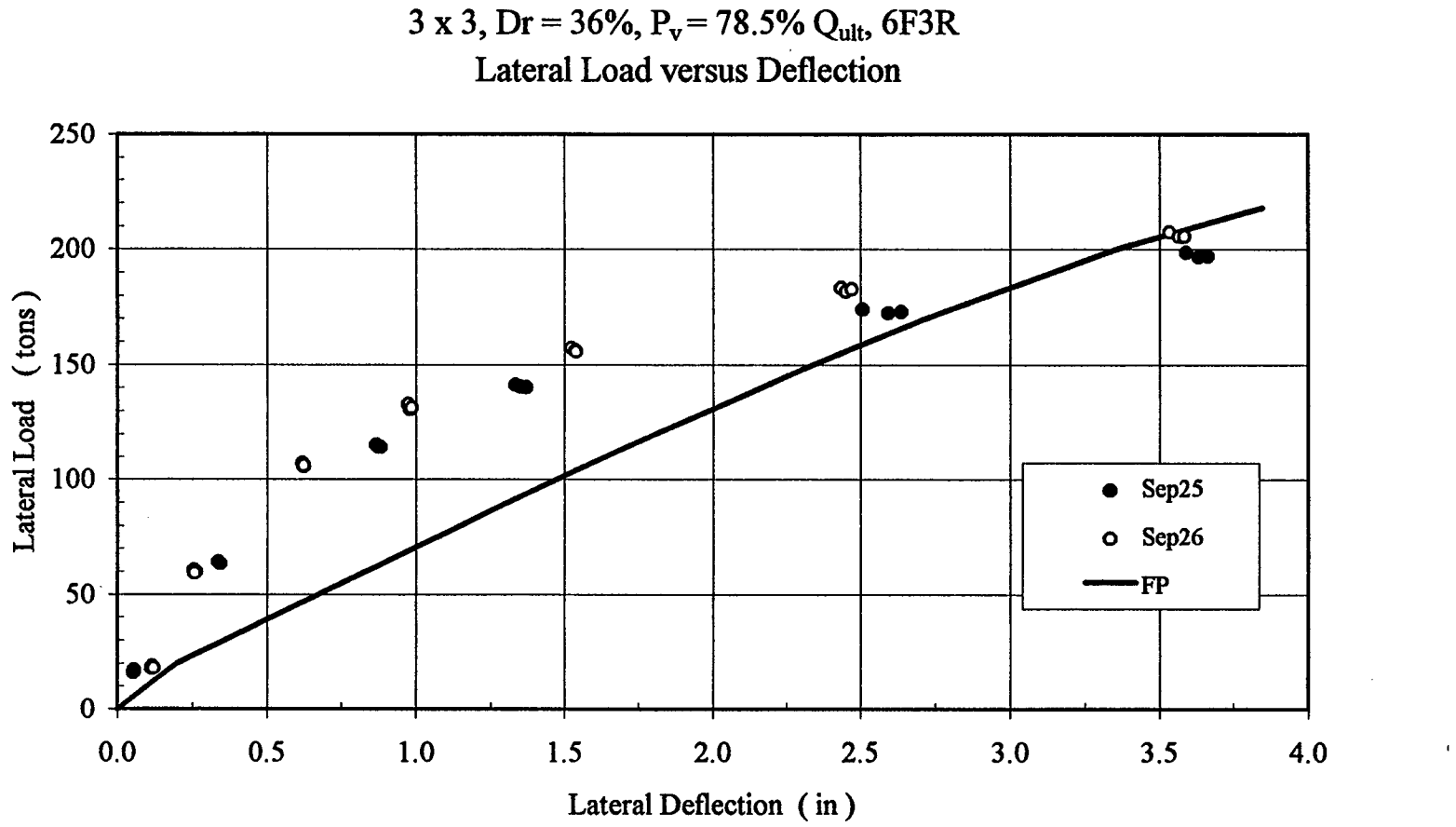

Figure B-45 Lateral Load versus Deflection

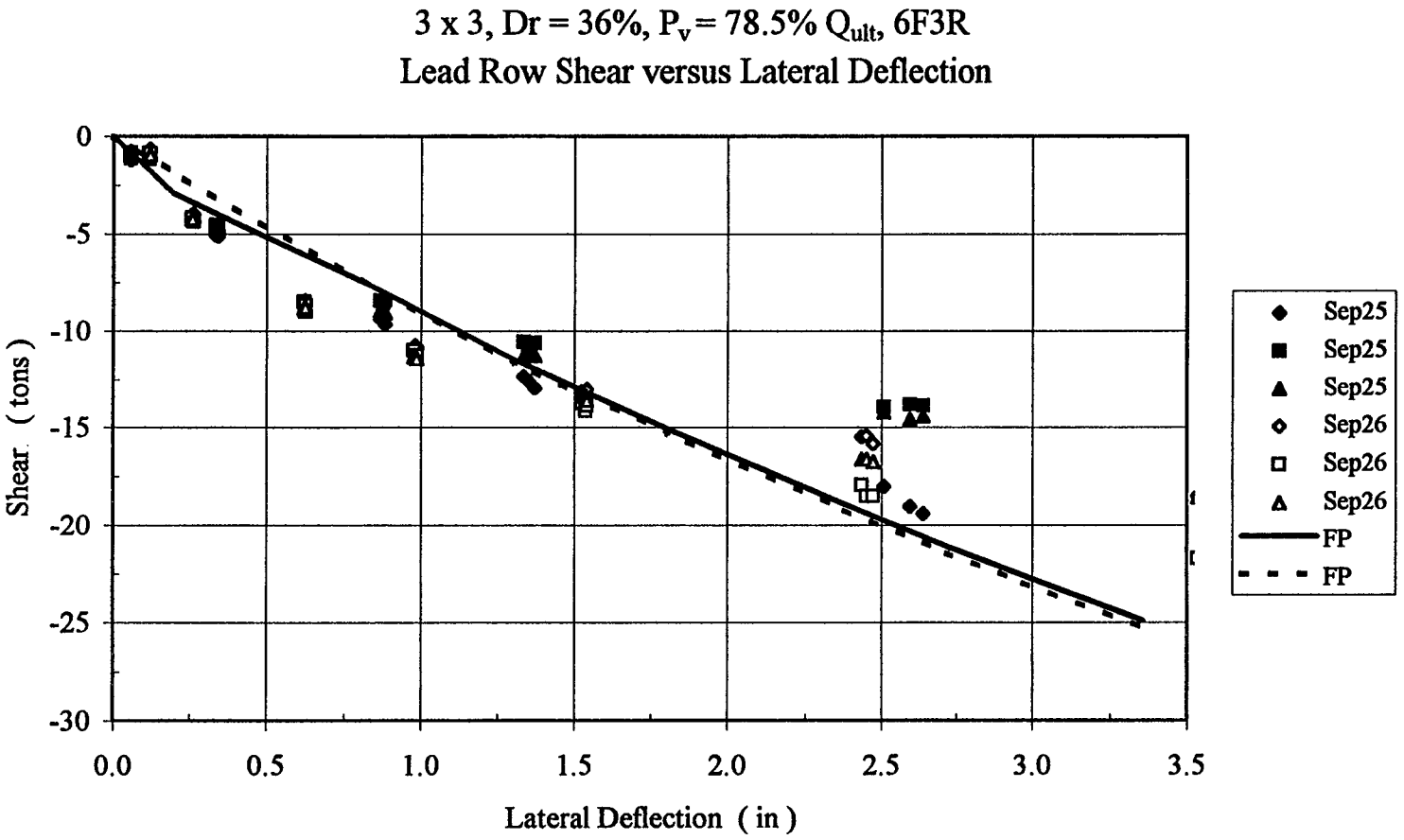

Figure B-46 Lead Row Shear versus Lateral Deflection

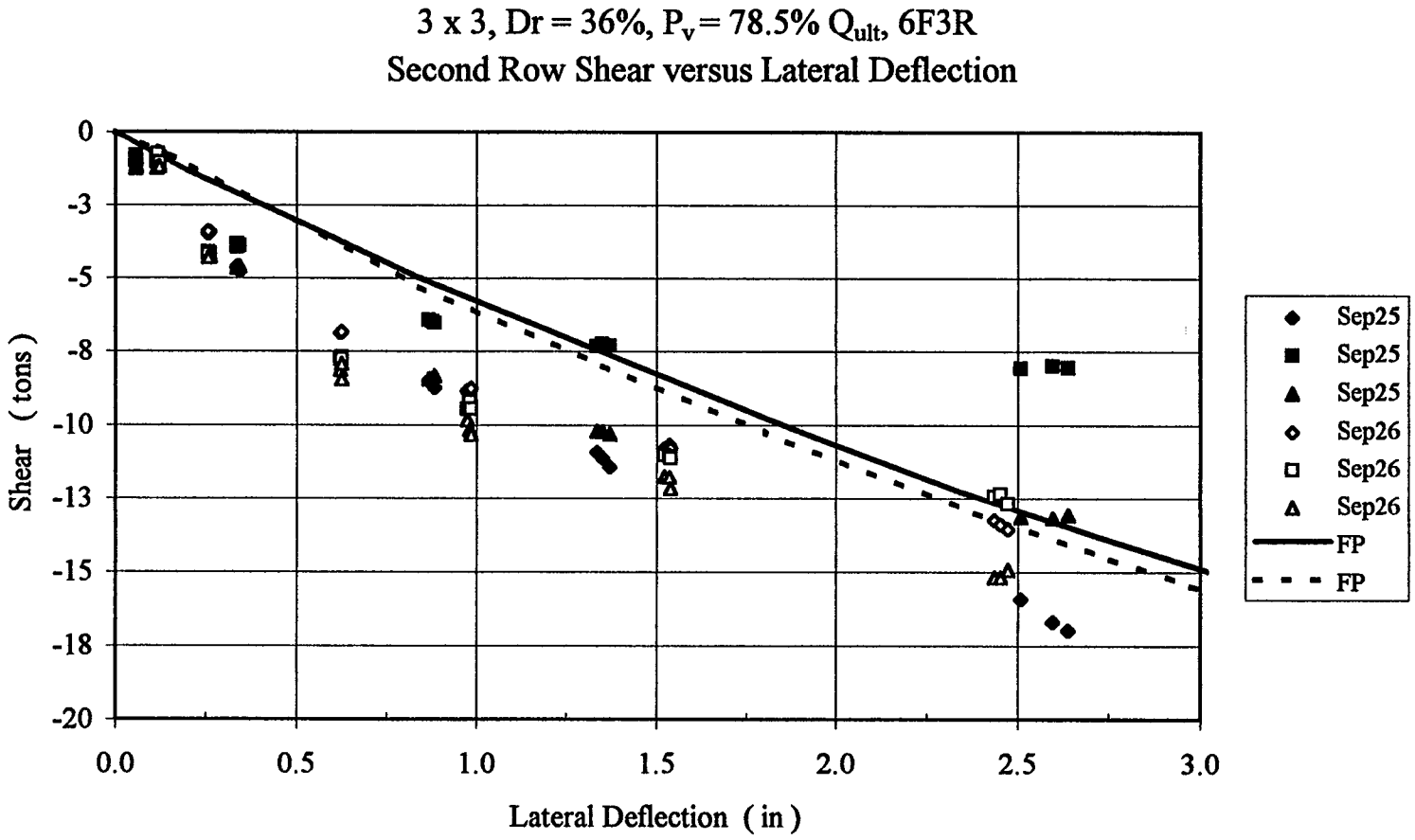

Figure B-47 Second Row Shear versus Lateral Deflection

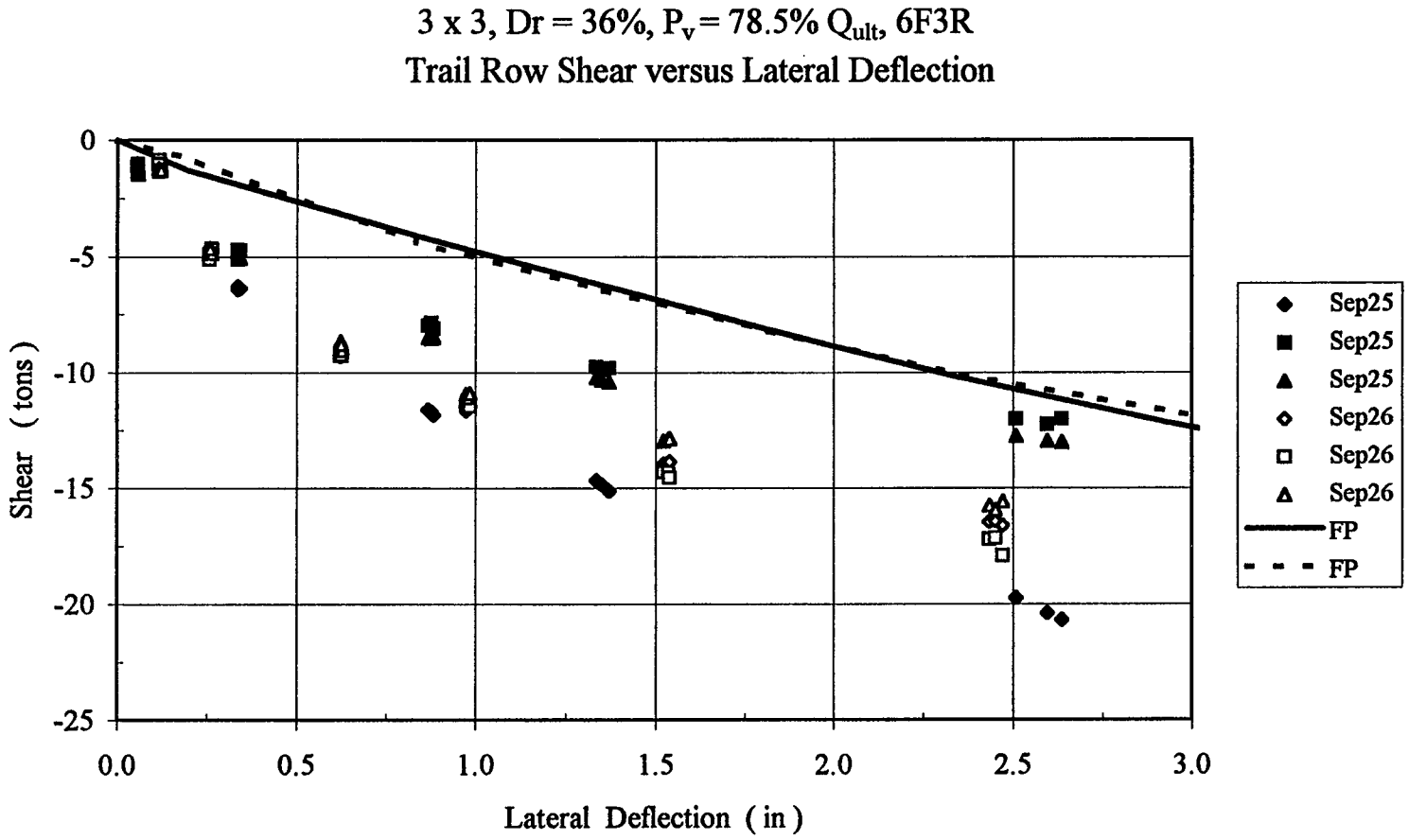

Figure B-48 Trail Row Shear versus Lateral Deflection

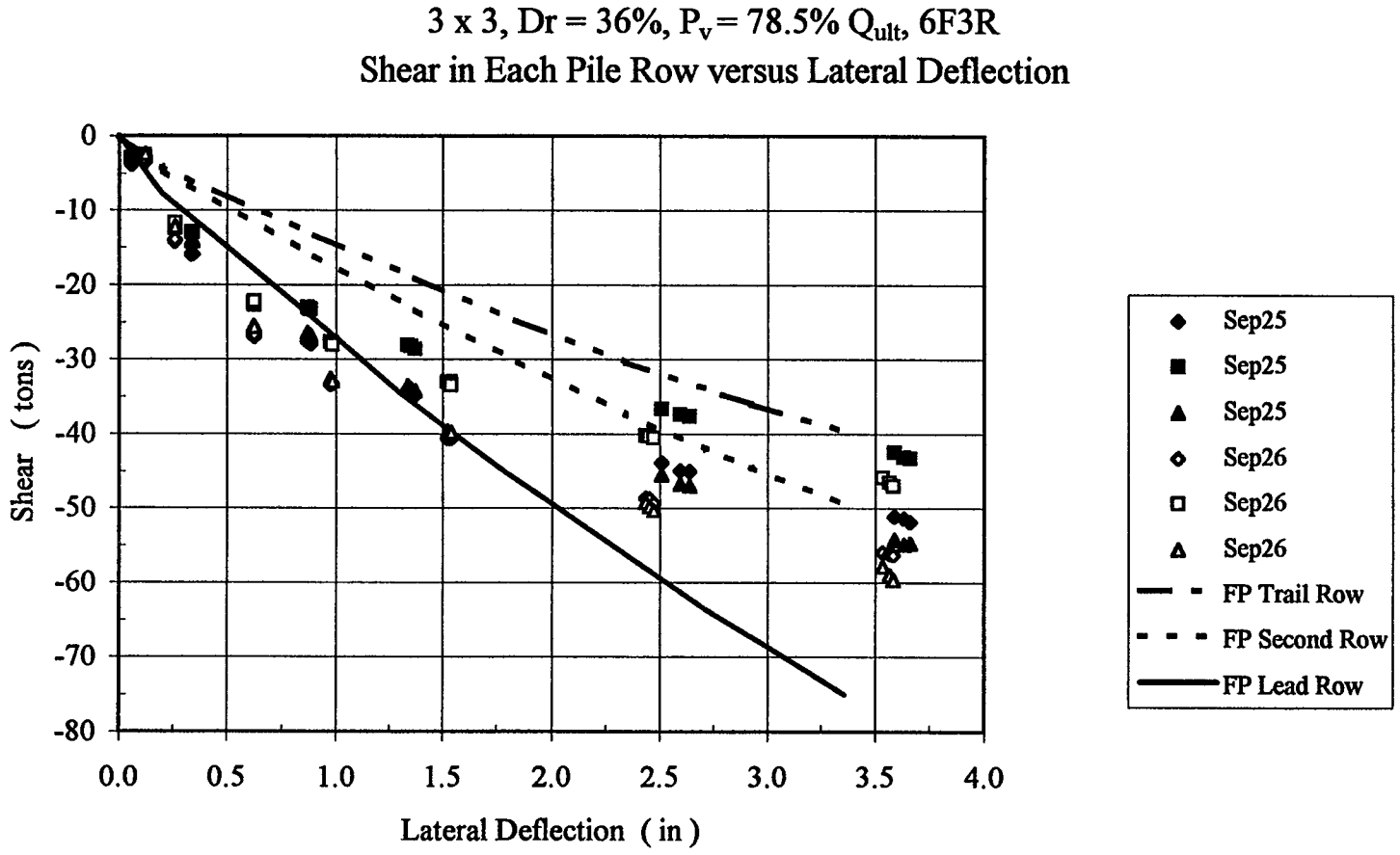

Figure B-49 Shear in Each Pile Row versus Lateral Deflection

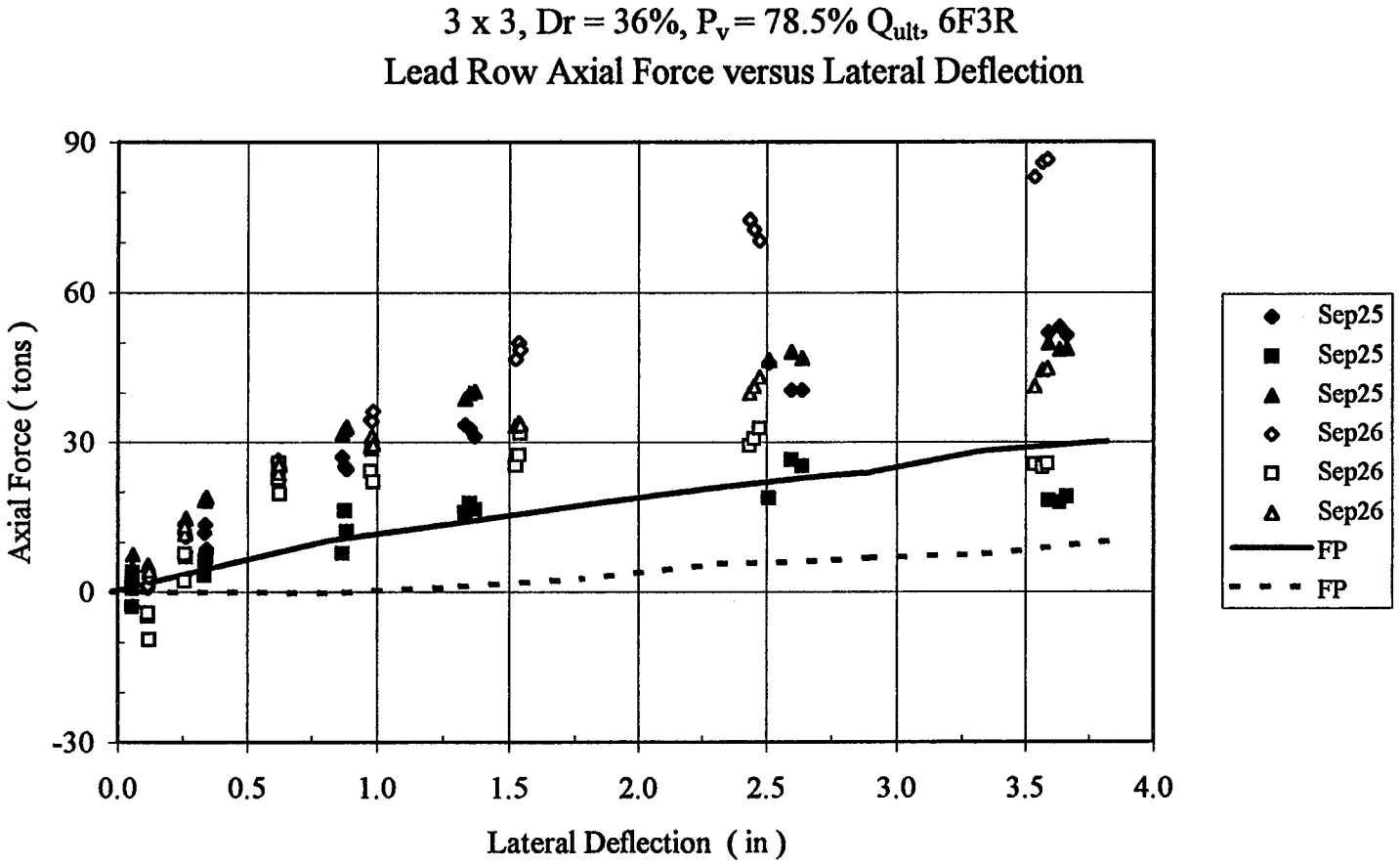

Figure B-50 Lead Row Axial Force versus Lateral Deflection

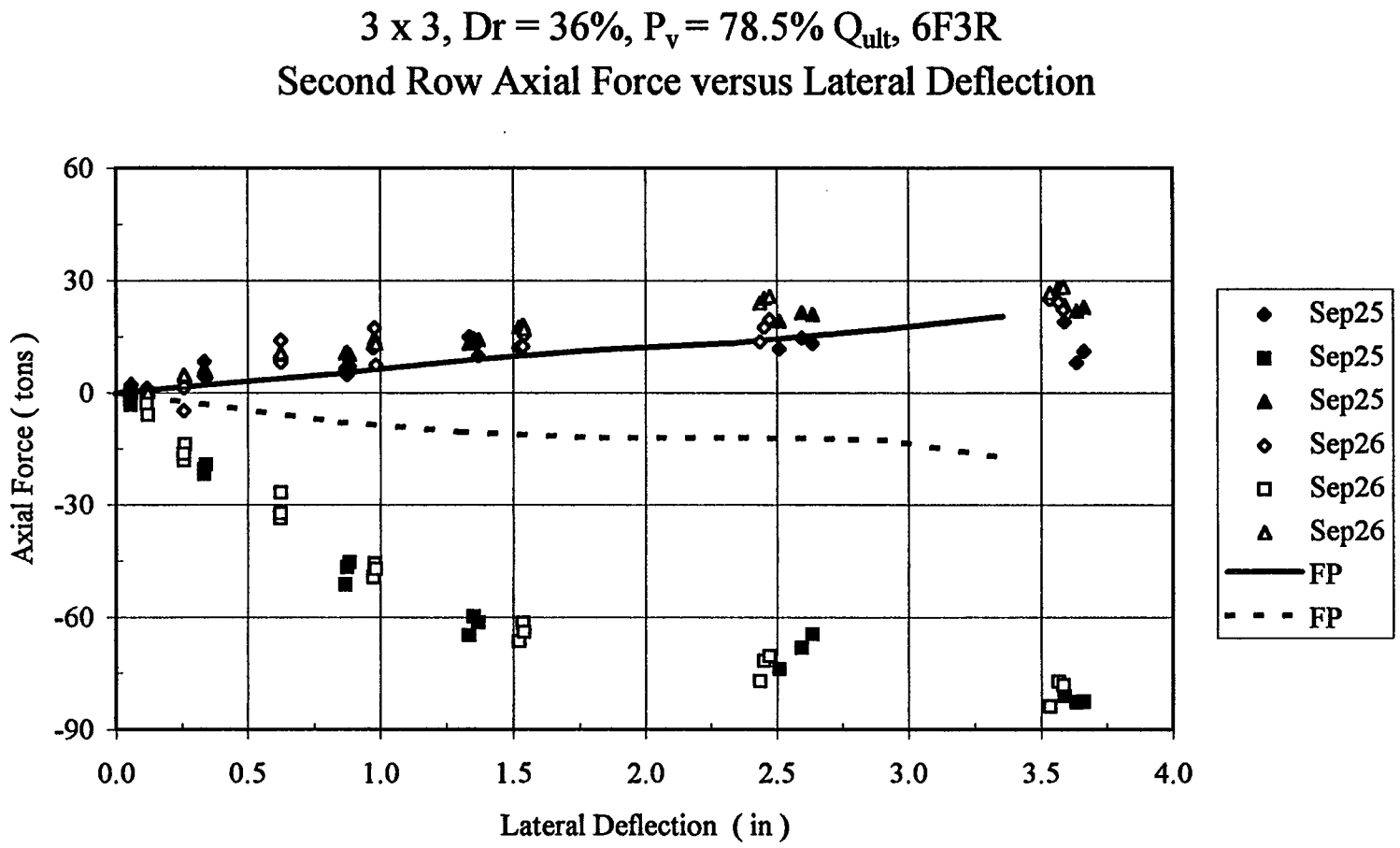

Figure B-51 Second Row Axial Force versus Lateral Deflection

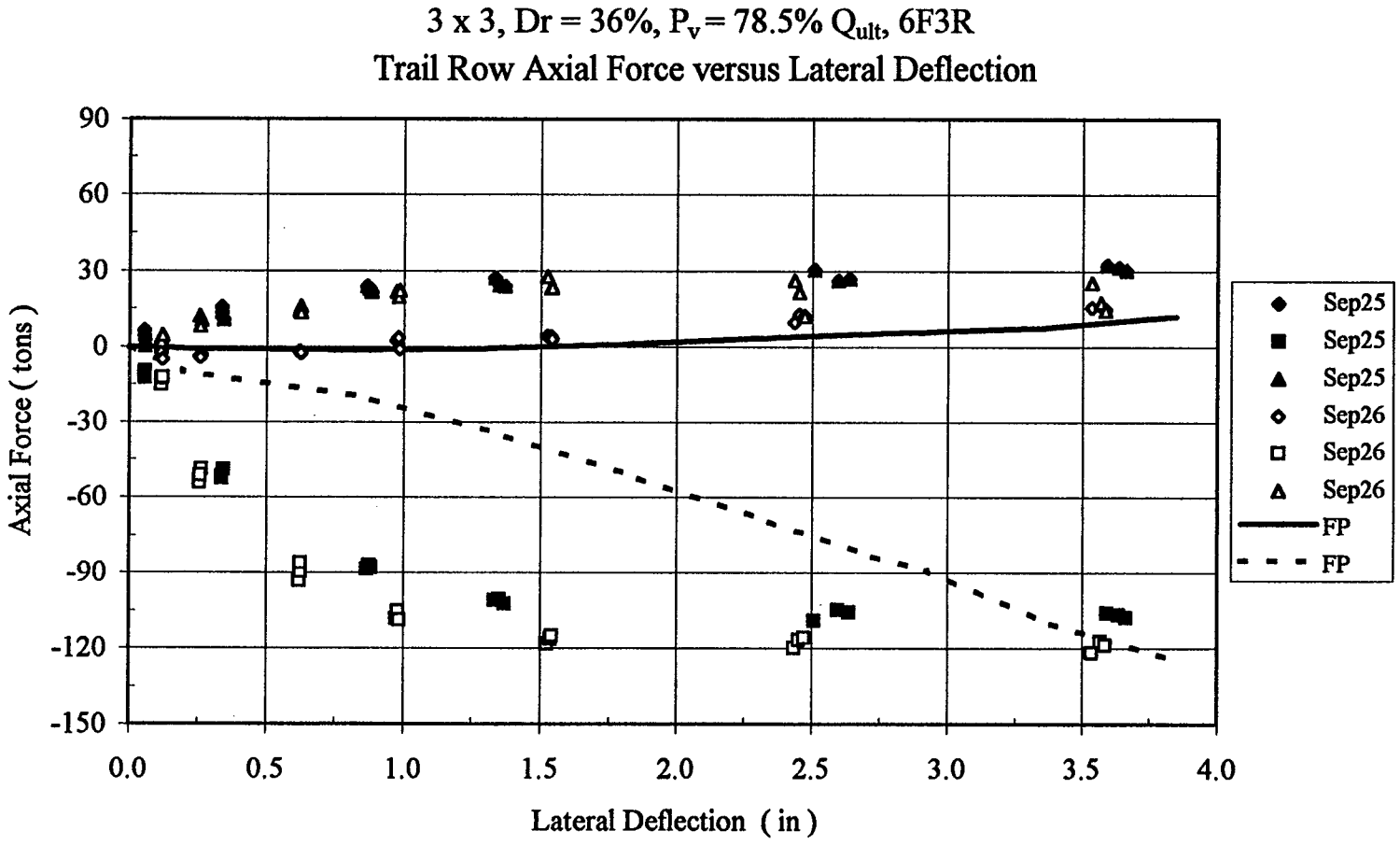

Figure B-52 Trail Row Axial Force versus Lateral Deflection

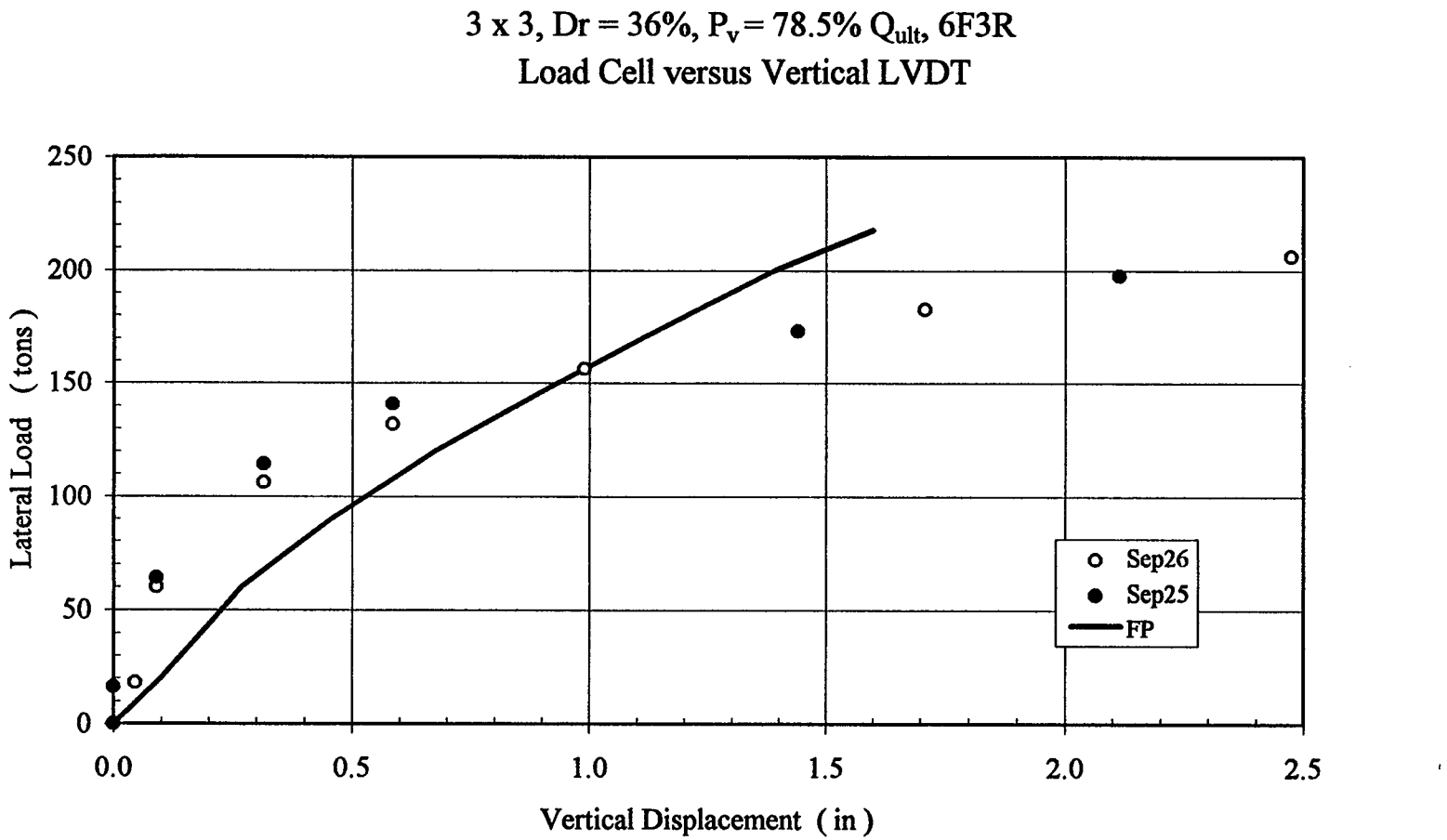

Figure B-53 Lateral Load versus Vertical Displacement

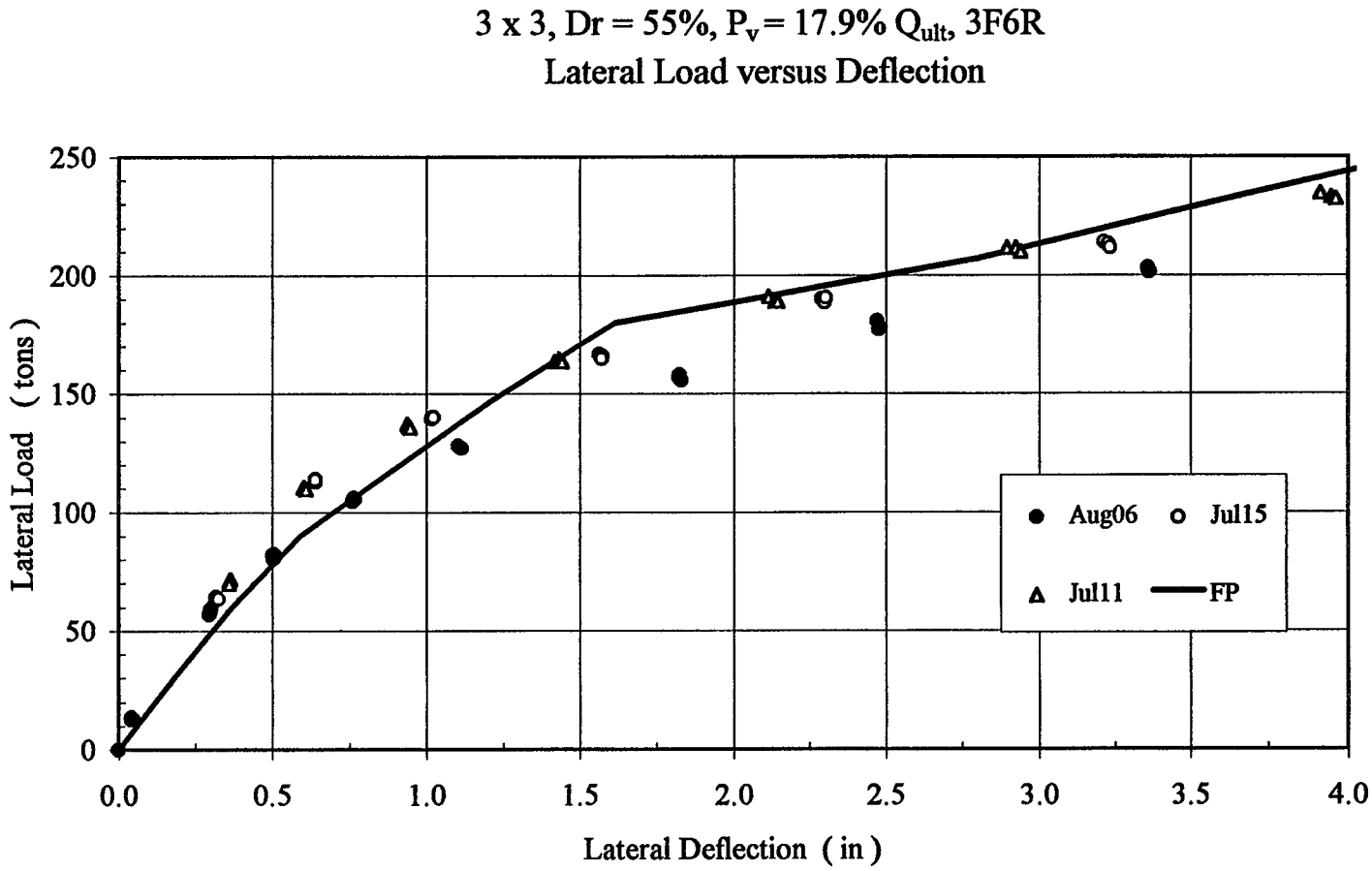

Figure B-54 Lateral Load versus Deflection

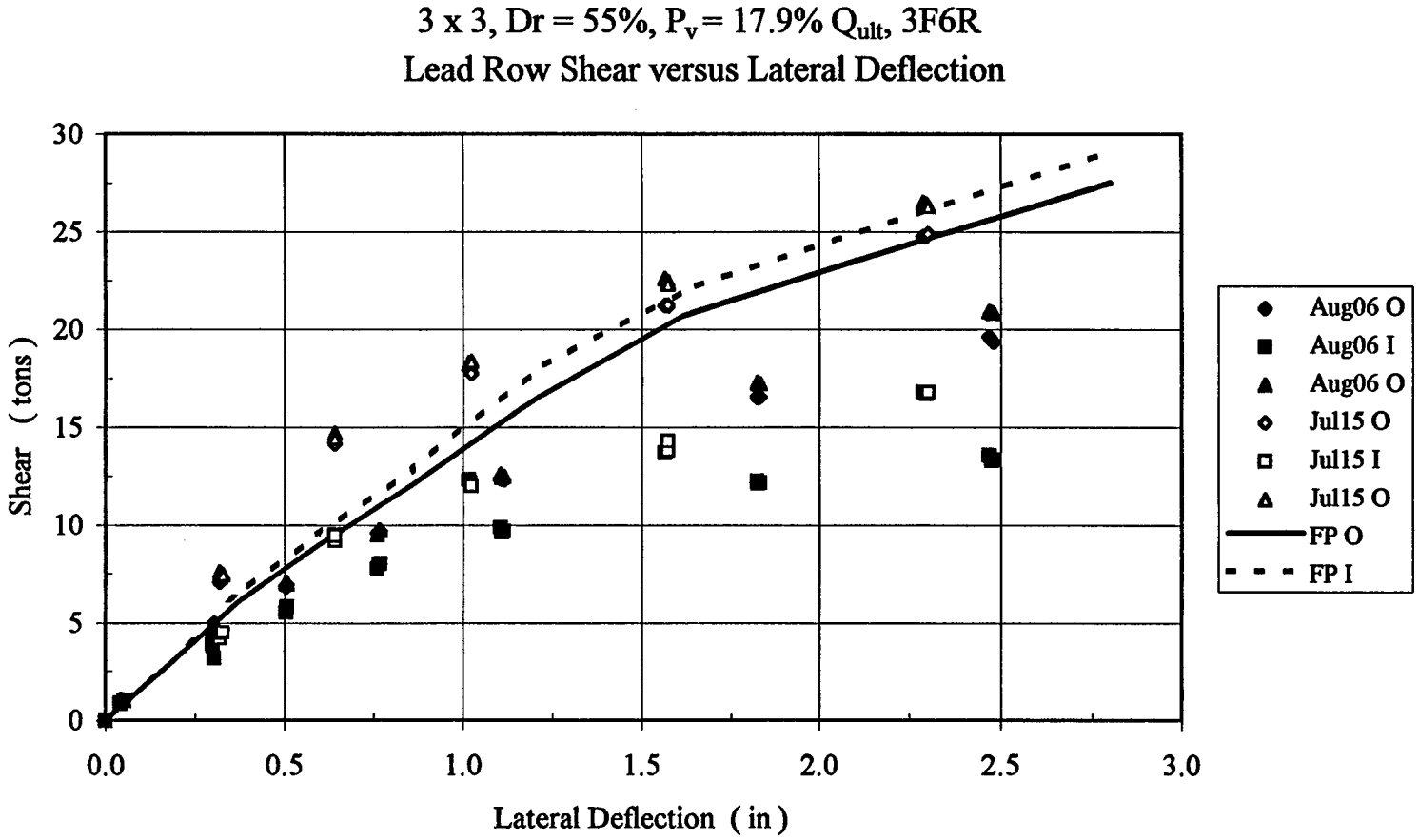

Figure B-55 Lead Row Shear versus Lateral Deflection

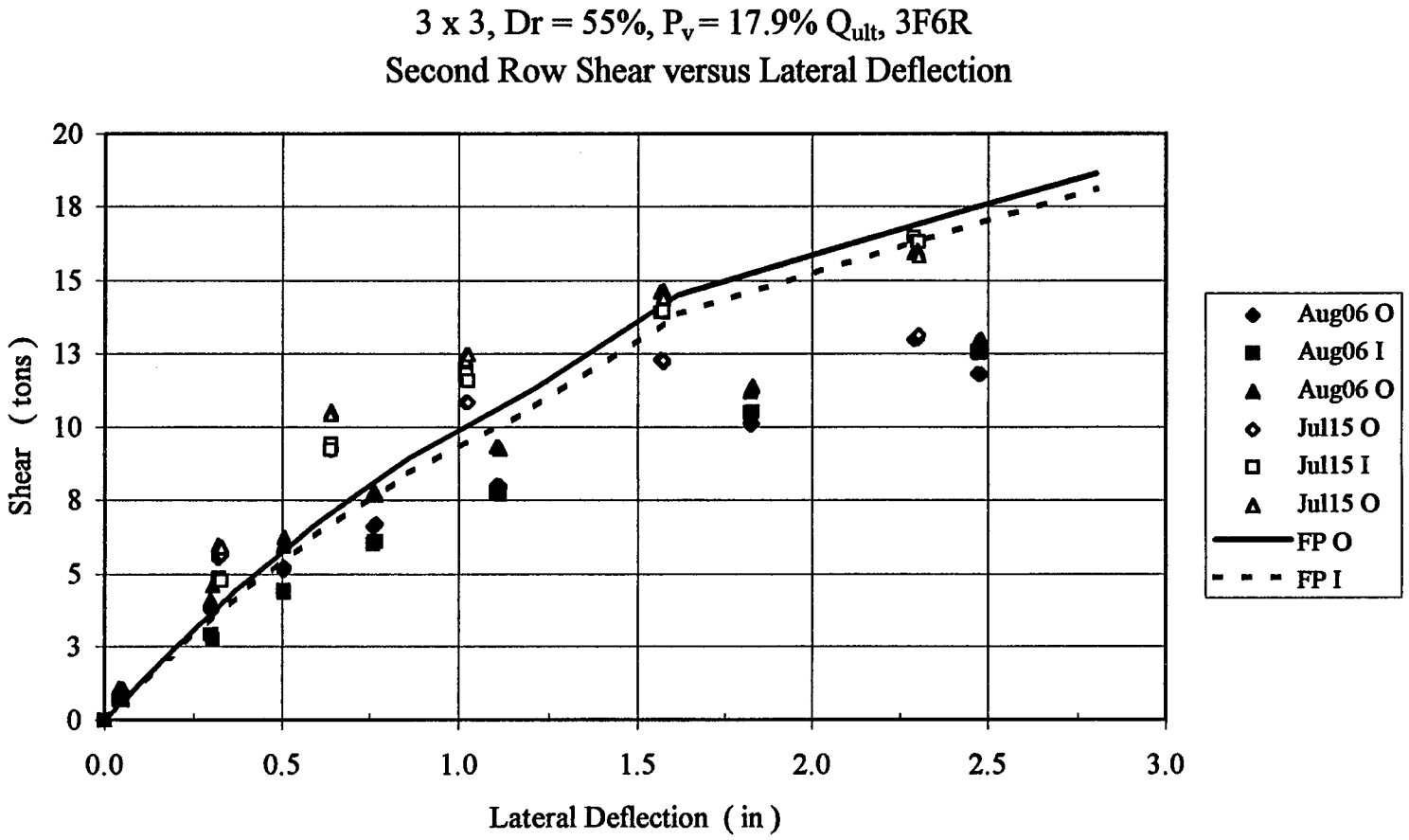

Figure B-56 Second Row Shear versus Lateral Deflection

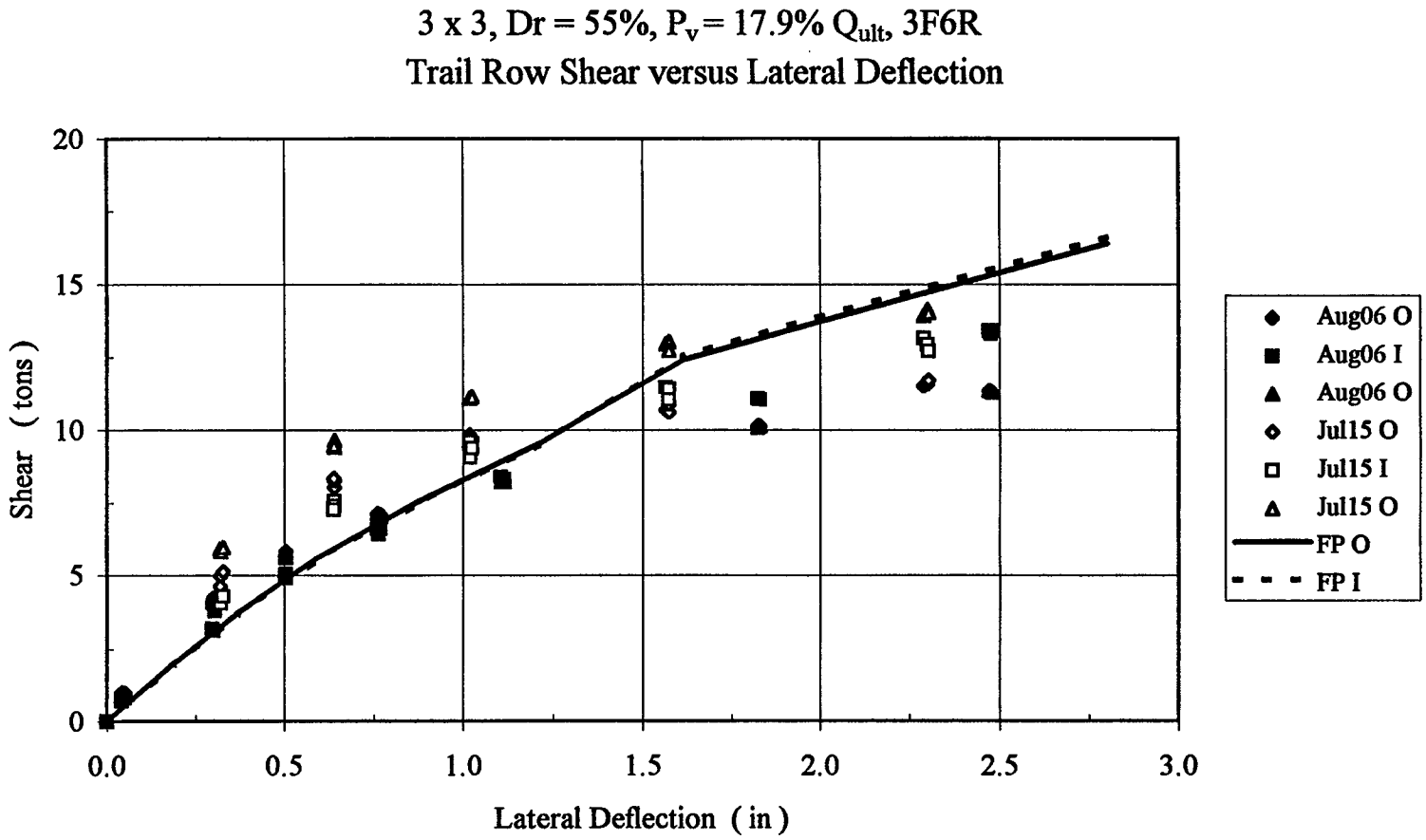

Figure B-57 Trail Row Shear versus Lateral Deflection

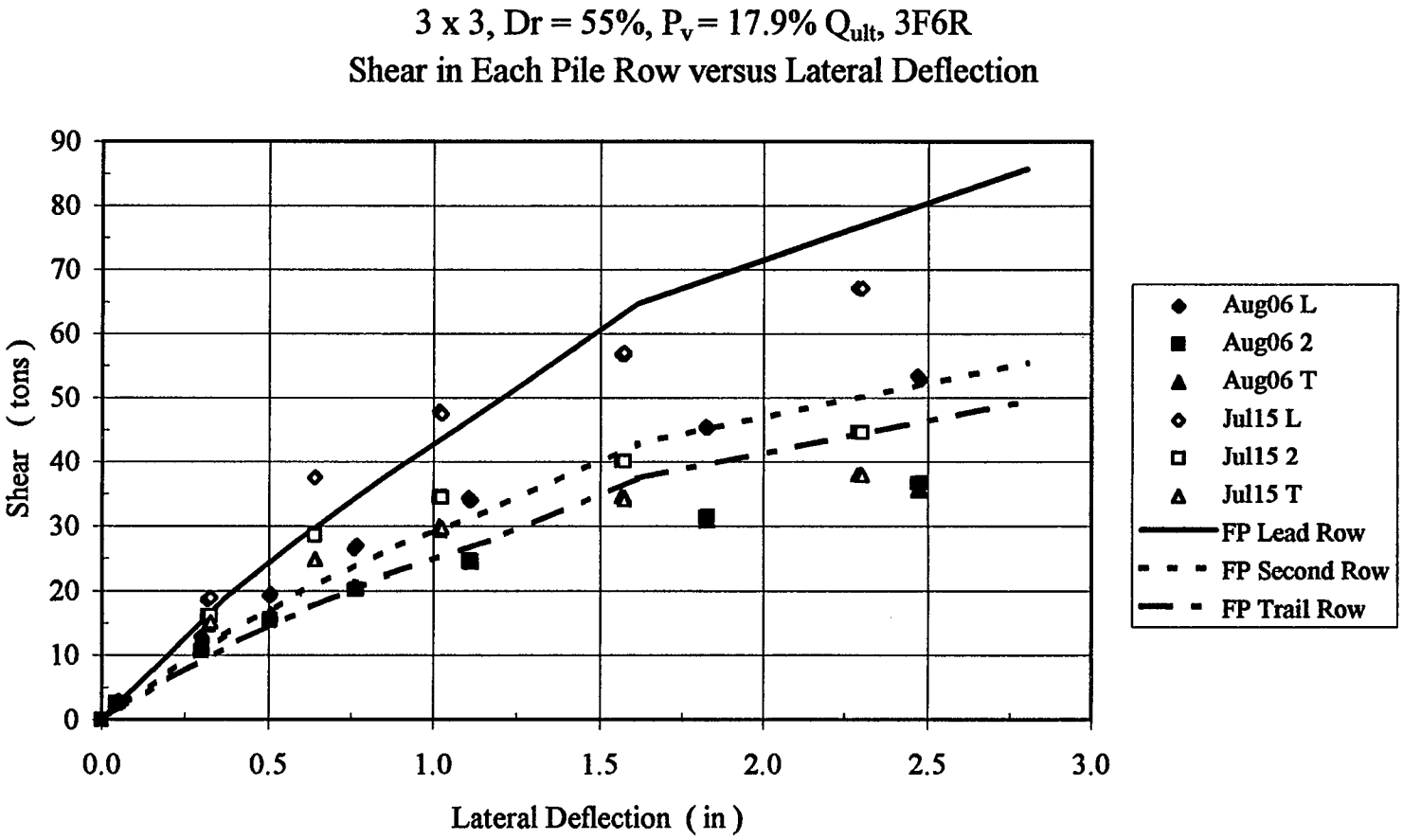

Figure B-58 Shear in Each Pile Row versus Lateral Deflection

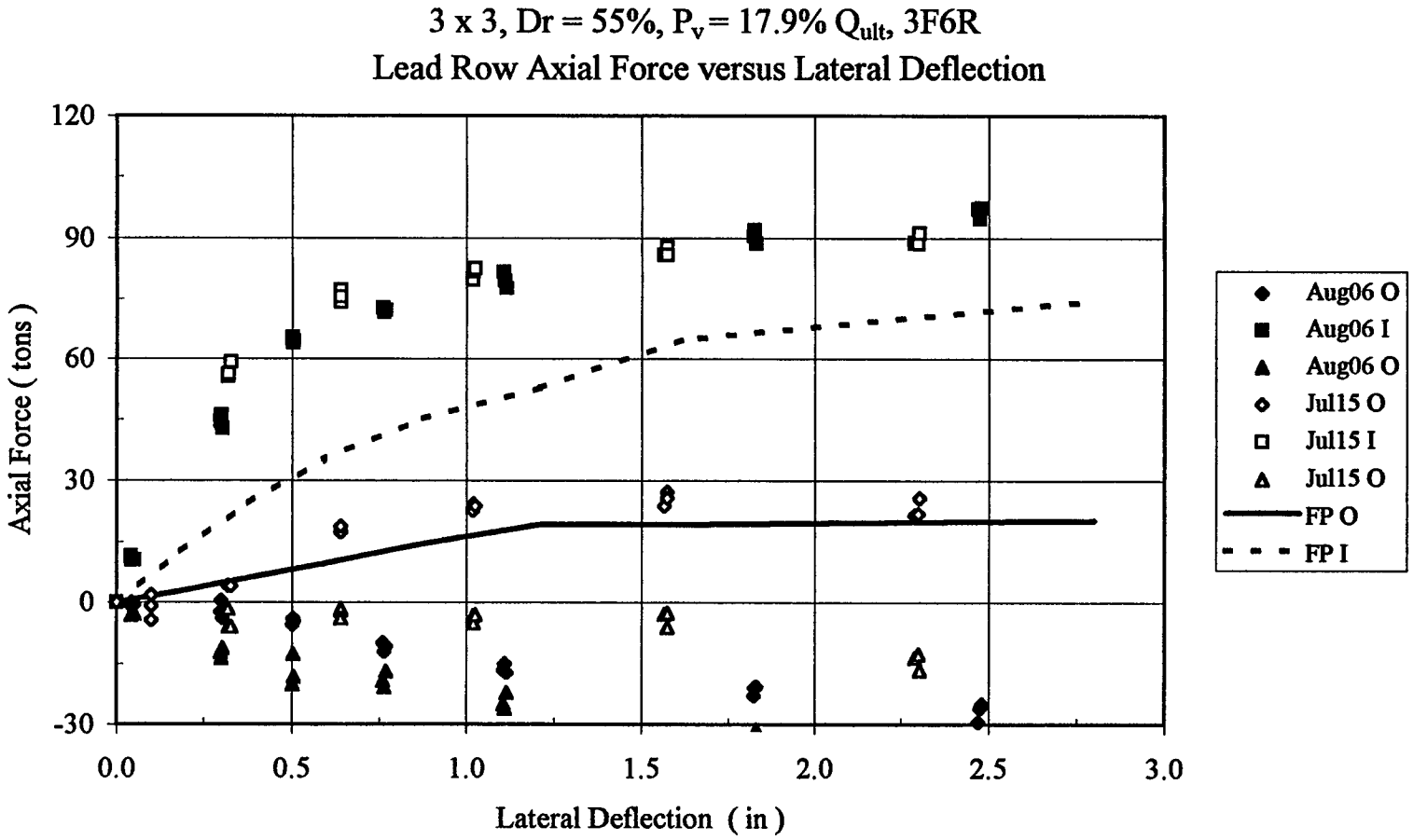

Figure B-59 Lead Row Axial Force versus Lateral Deflection

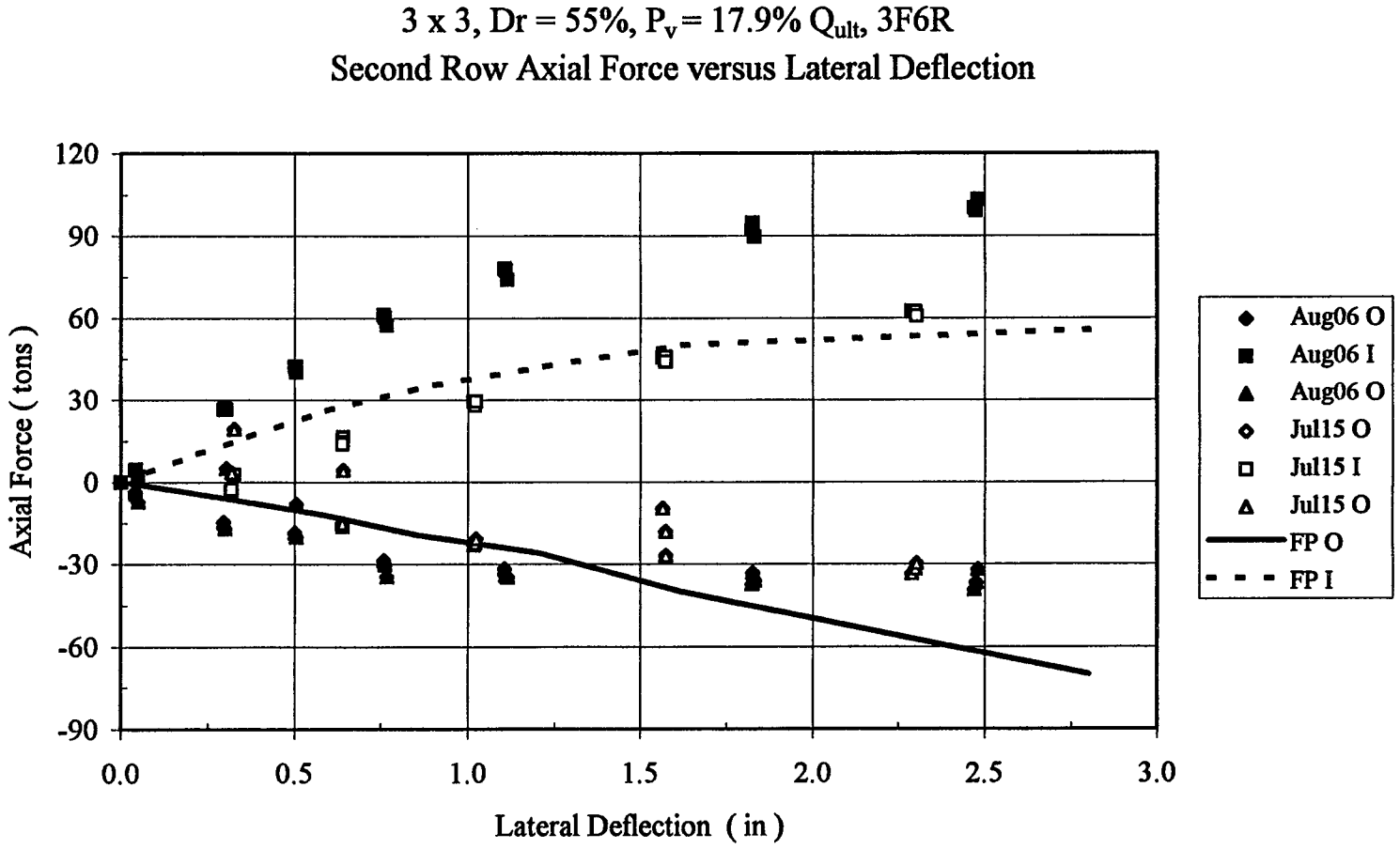

Figure B-60 Lead Row Axial Force versus Lateral Deflection

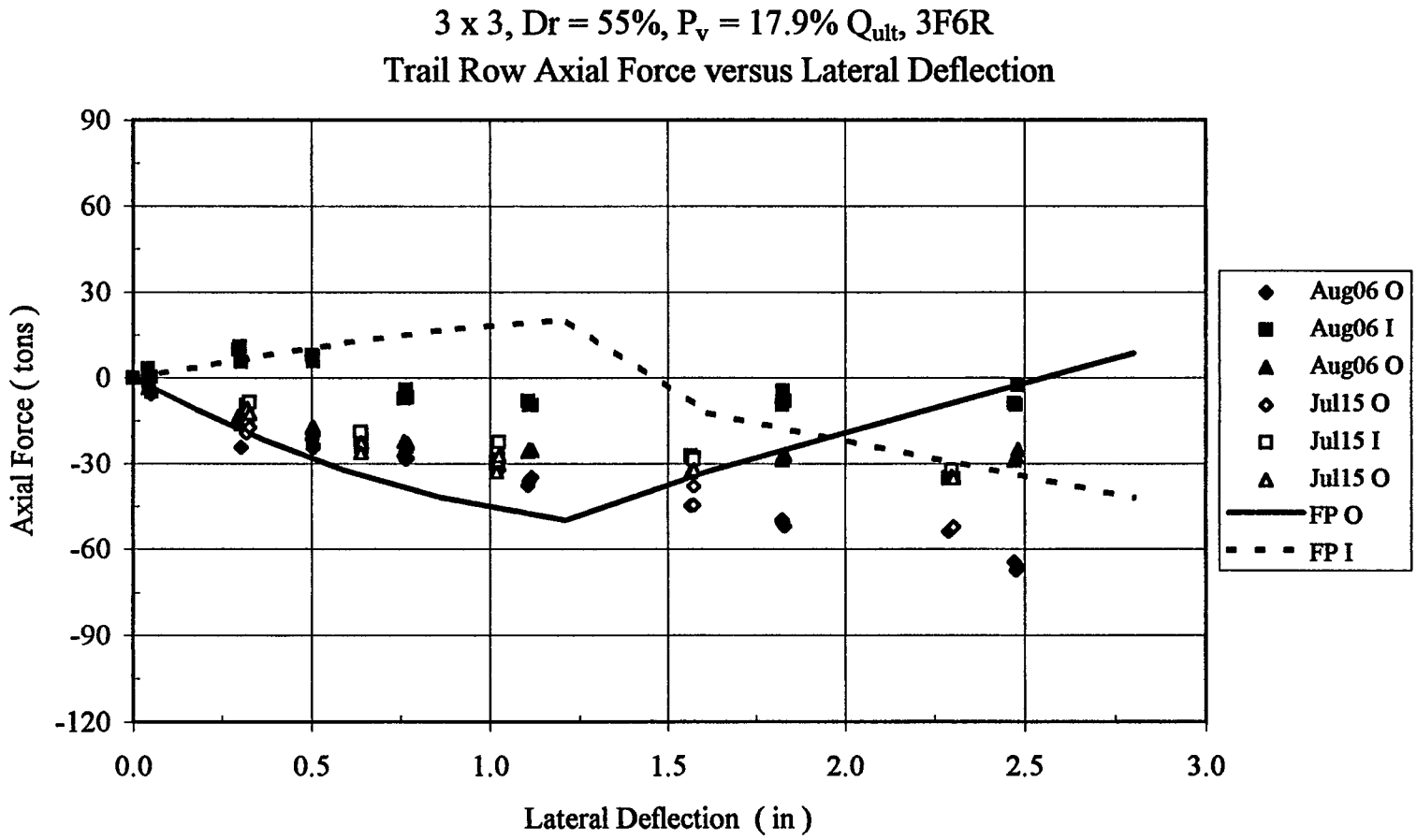

Figure B-61 Trail Row Axial Force versus Lateral Deflection

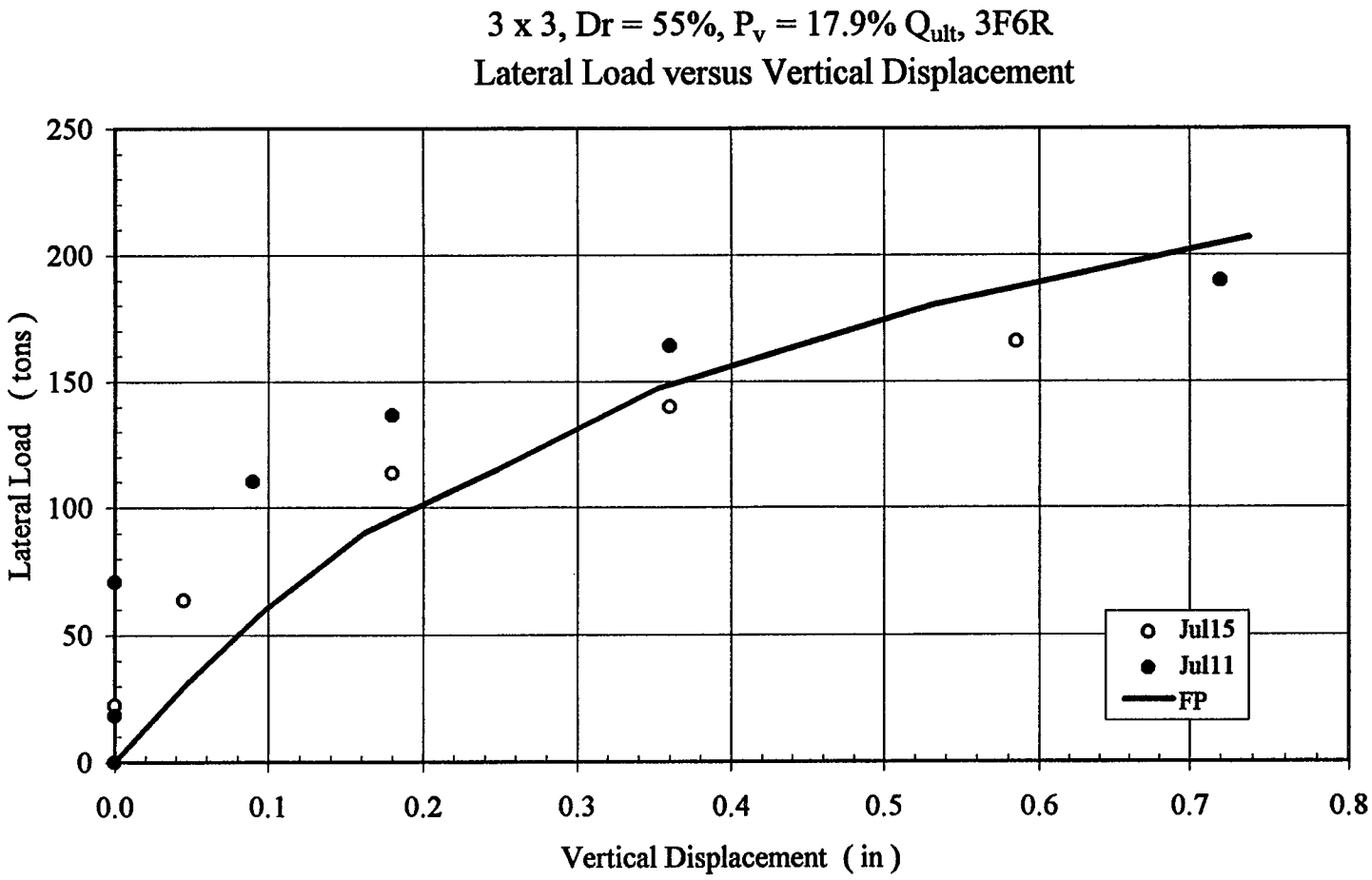

Figure B-62 Lateral Load versus Vertical Displacement

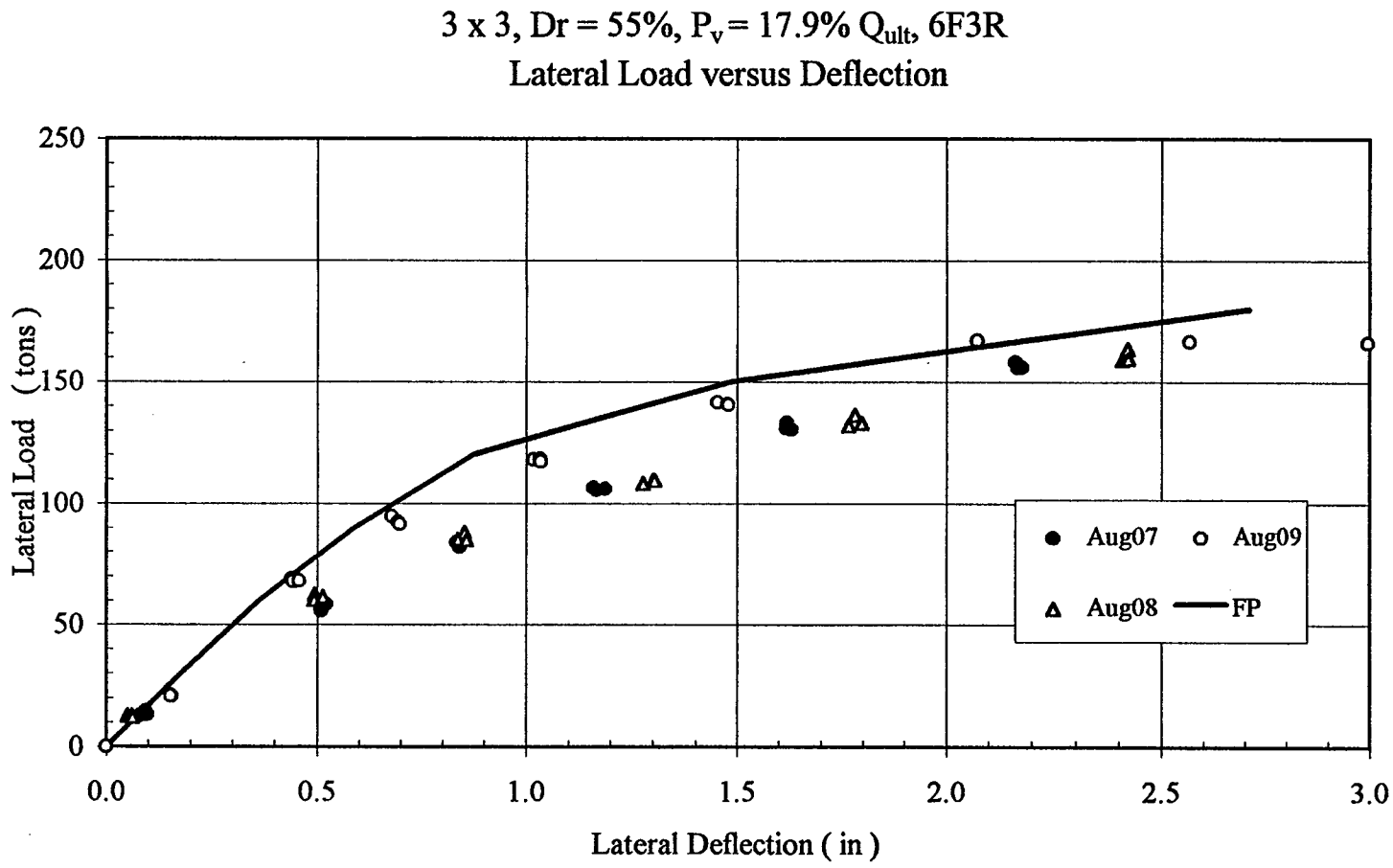

Figure B-63 Lateral Load versus Deflection

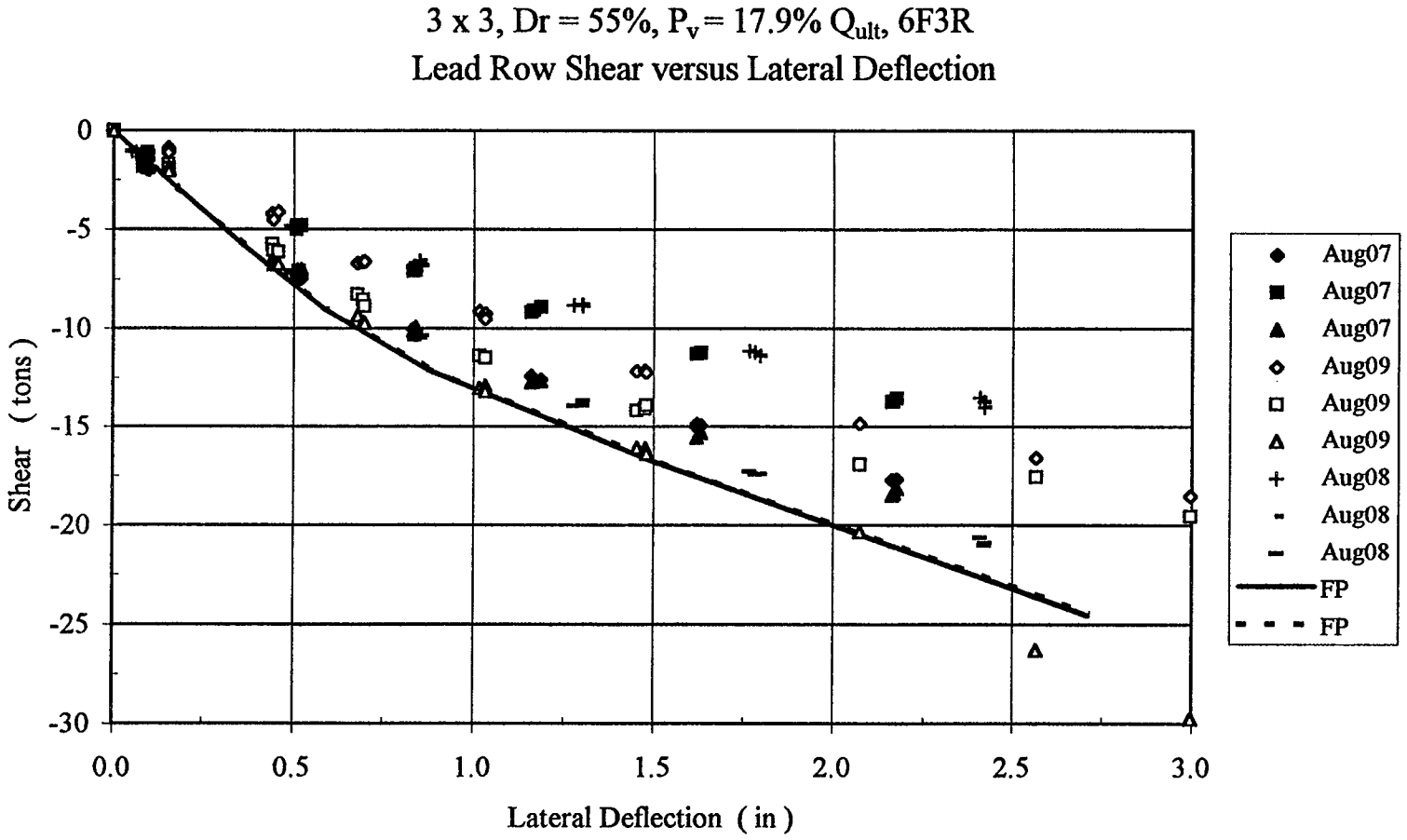

Figure B-64 Lead Row Shear versus Lateral Deflection

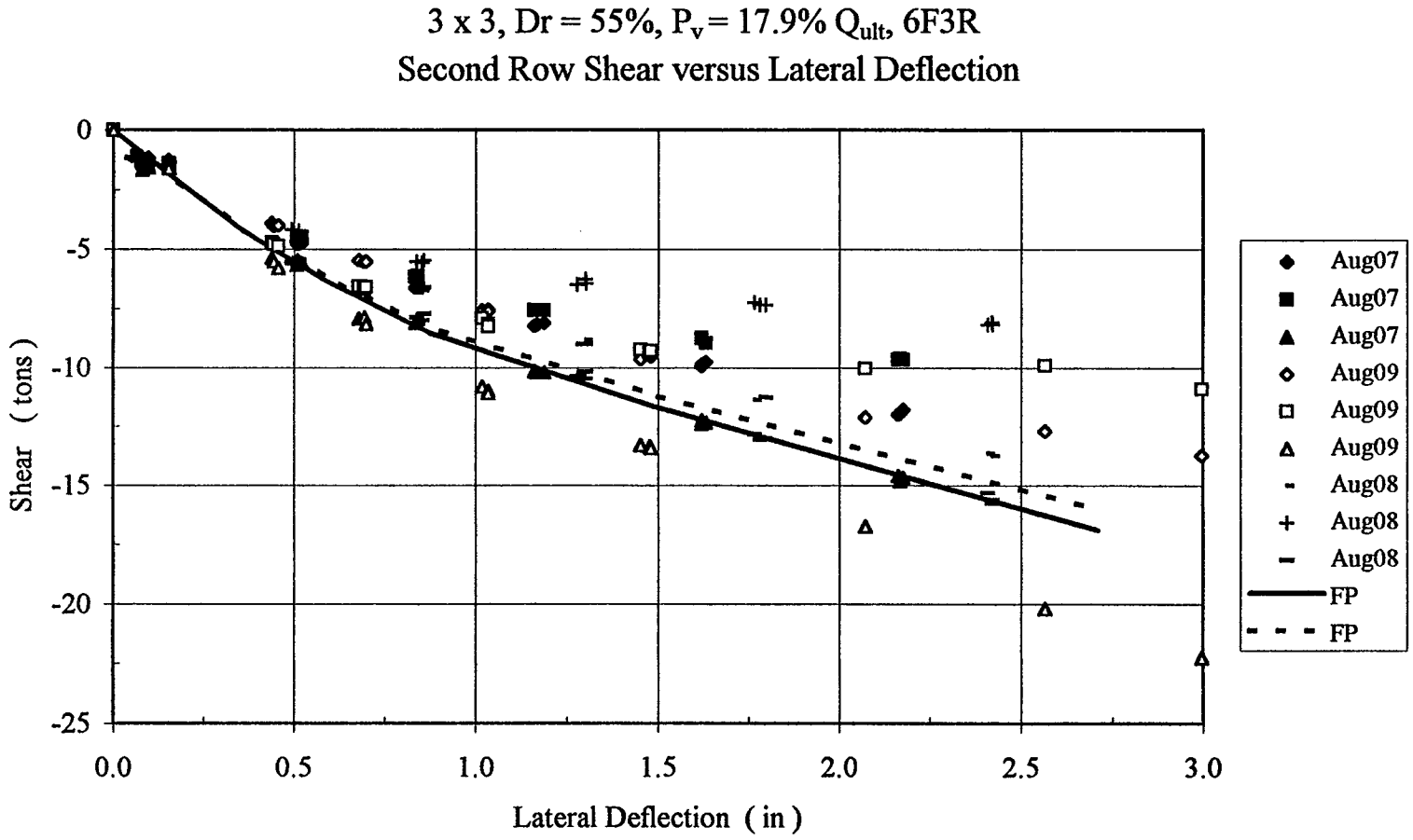

Figure B-65 Second Row Shear versus Lateral Deflection

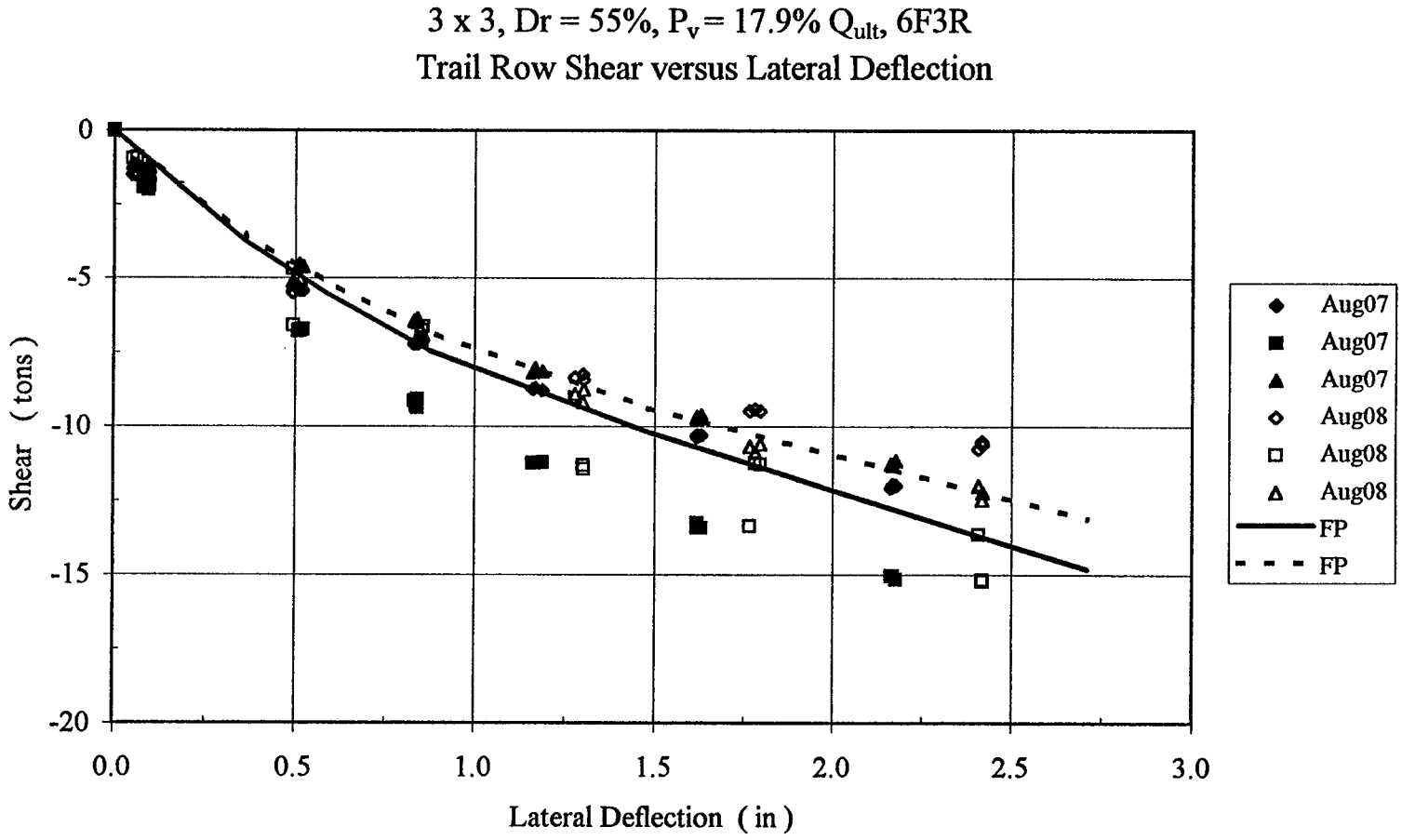

Figure B-66 Trail Row Shear versus Lateral Deflection

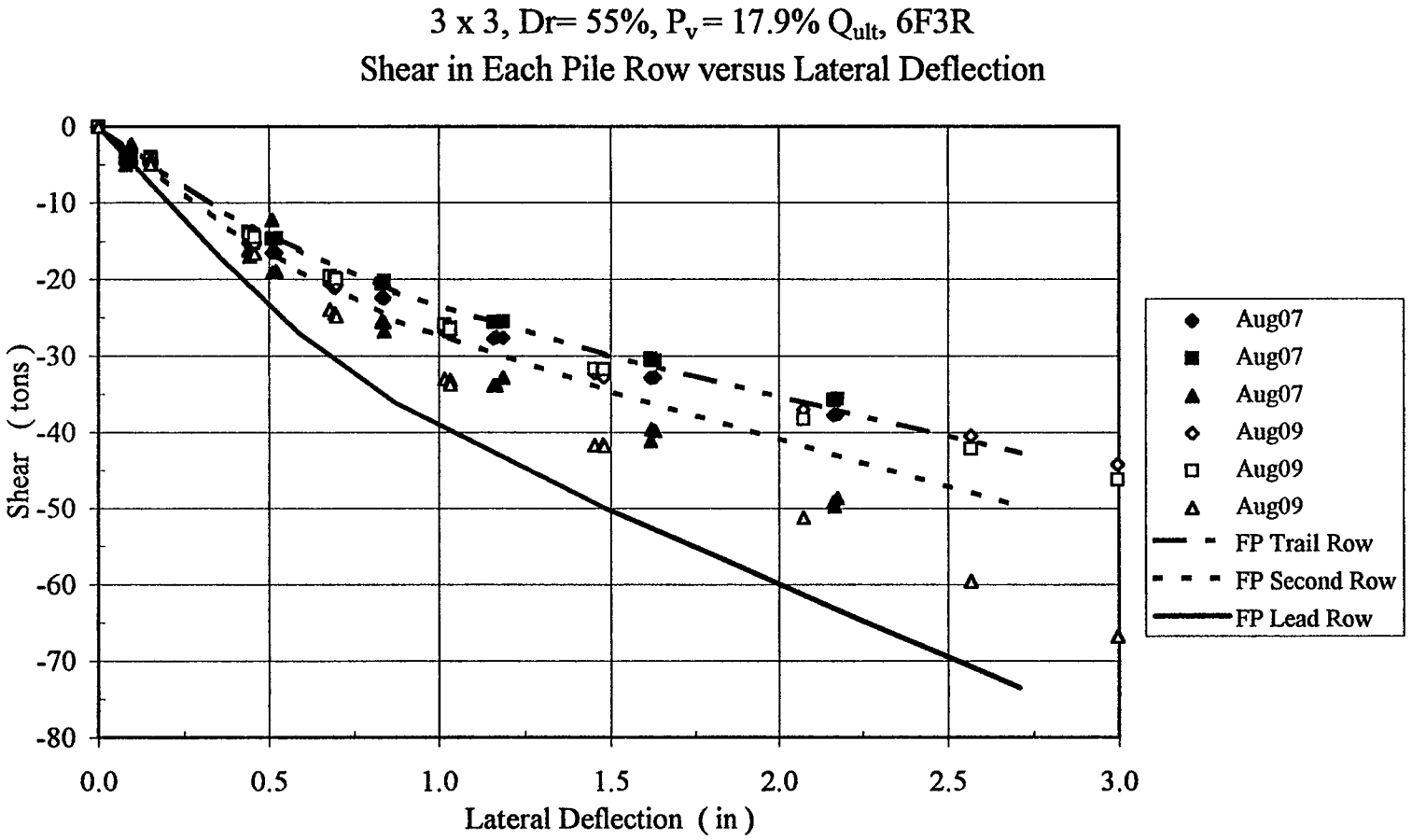

Figure B-67 Shear in Each Pile Row versus Lateral Deflection

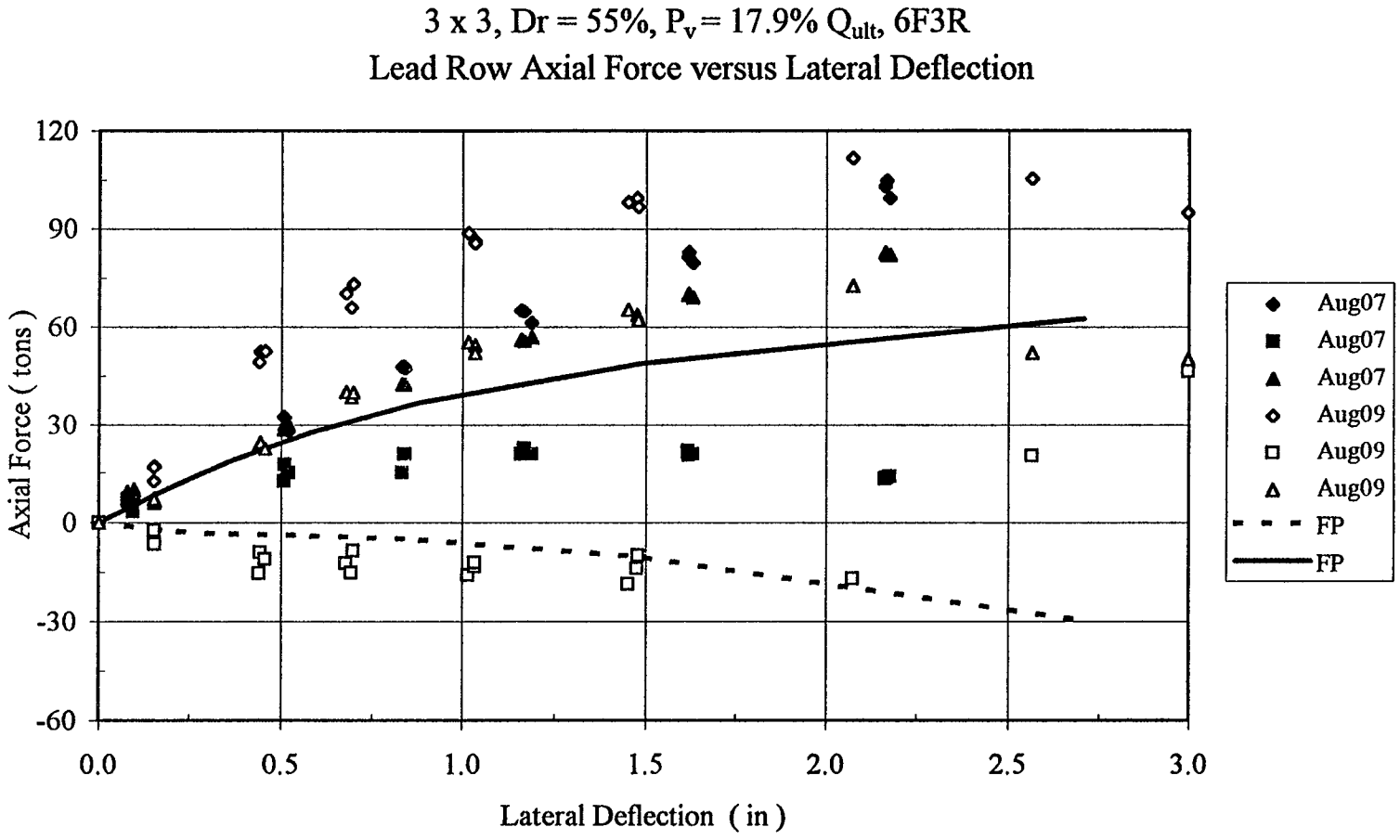

Figure B-68 Lead Row Axial Force versus Lateral Deflection

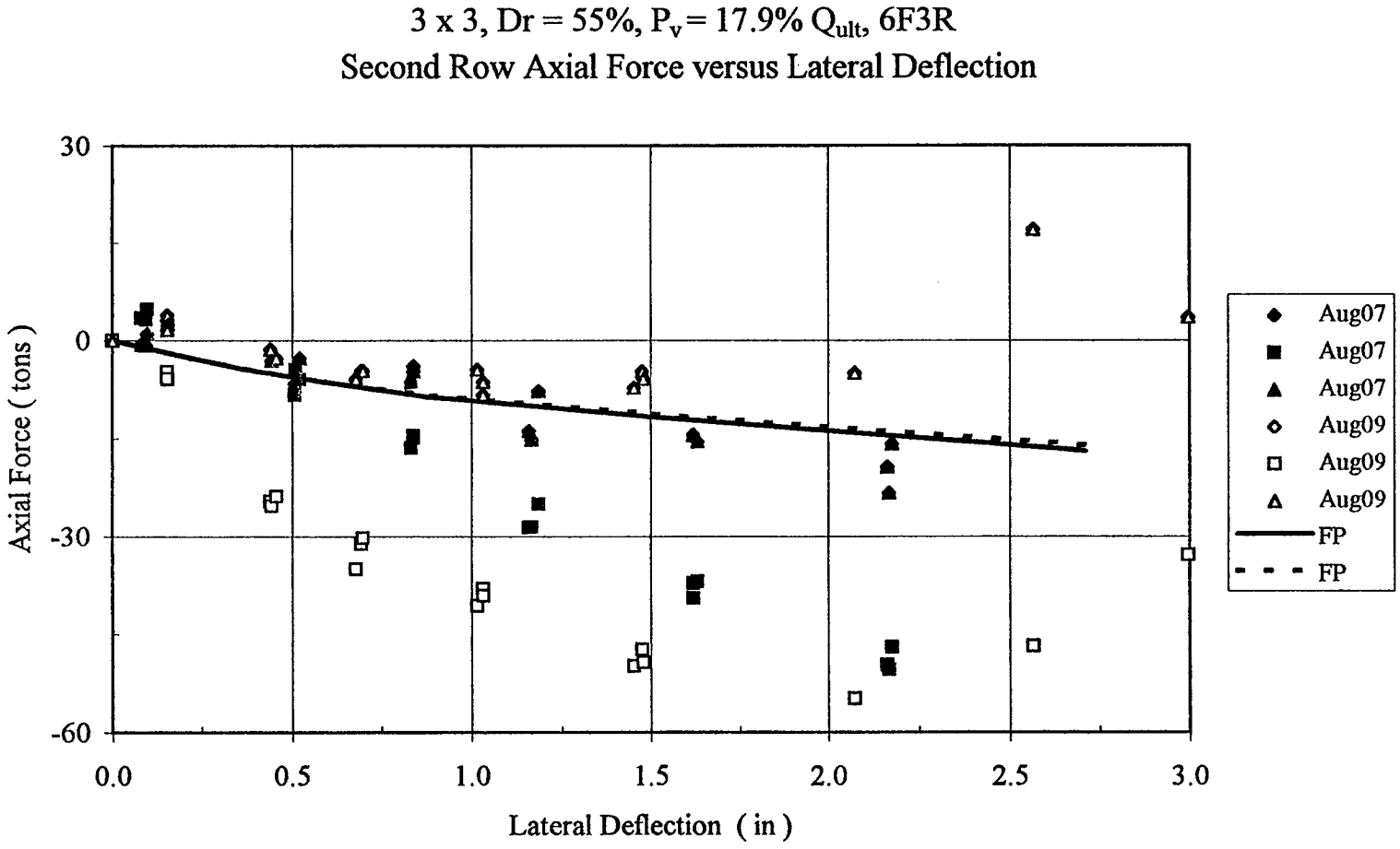

Figure B-69 Second Row Axial Force versus Lateral Deflection

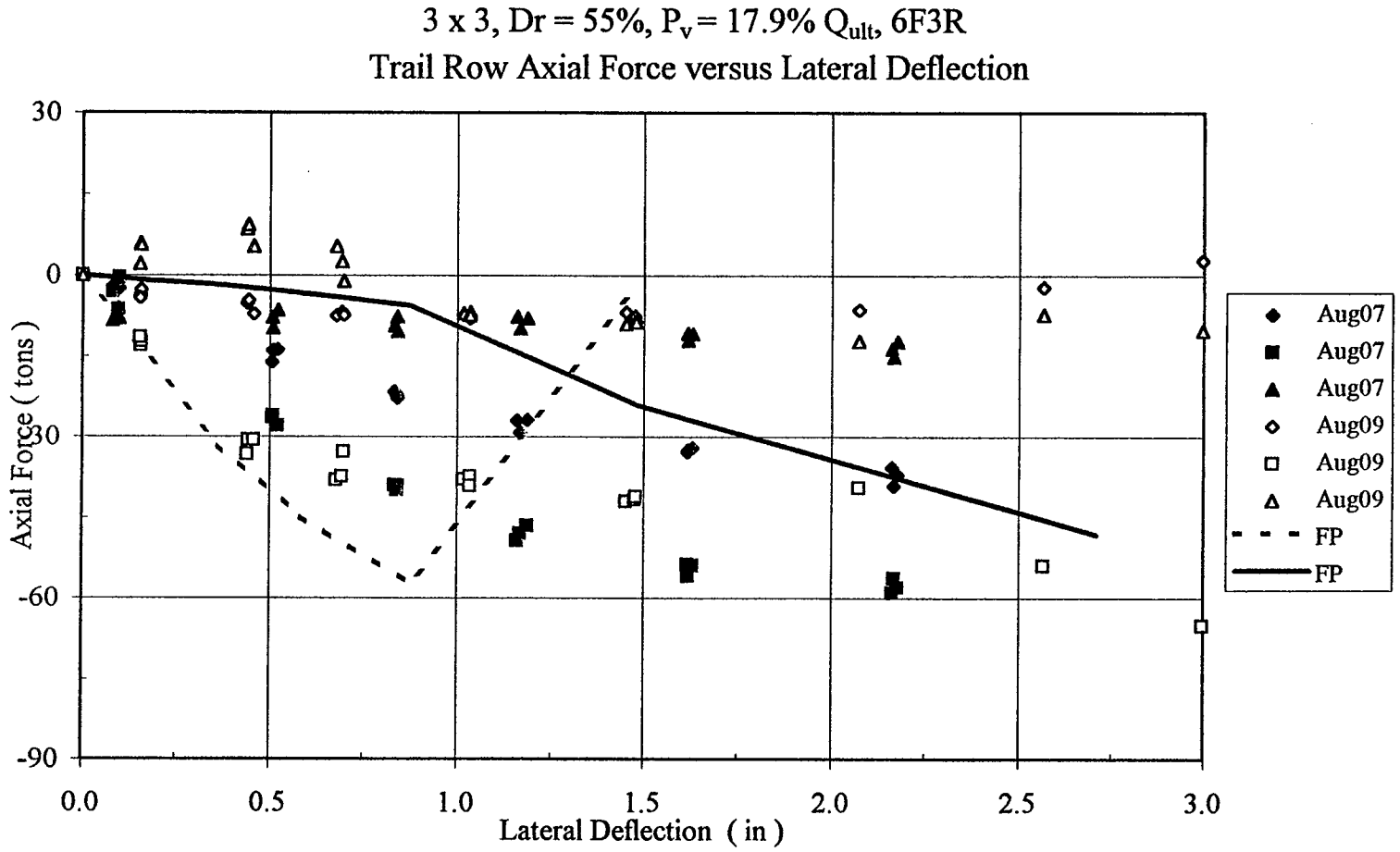

Figure B-70 Trail Row Axial Force versus Lateral Deflection

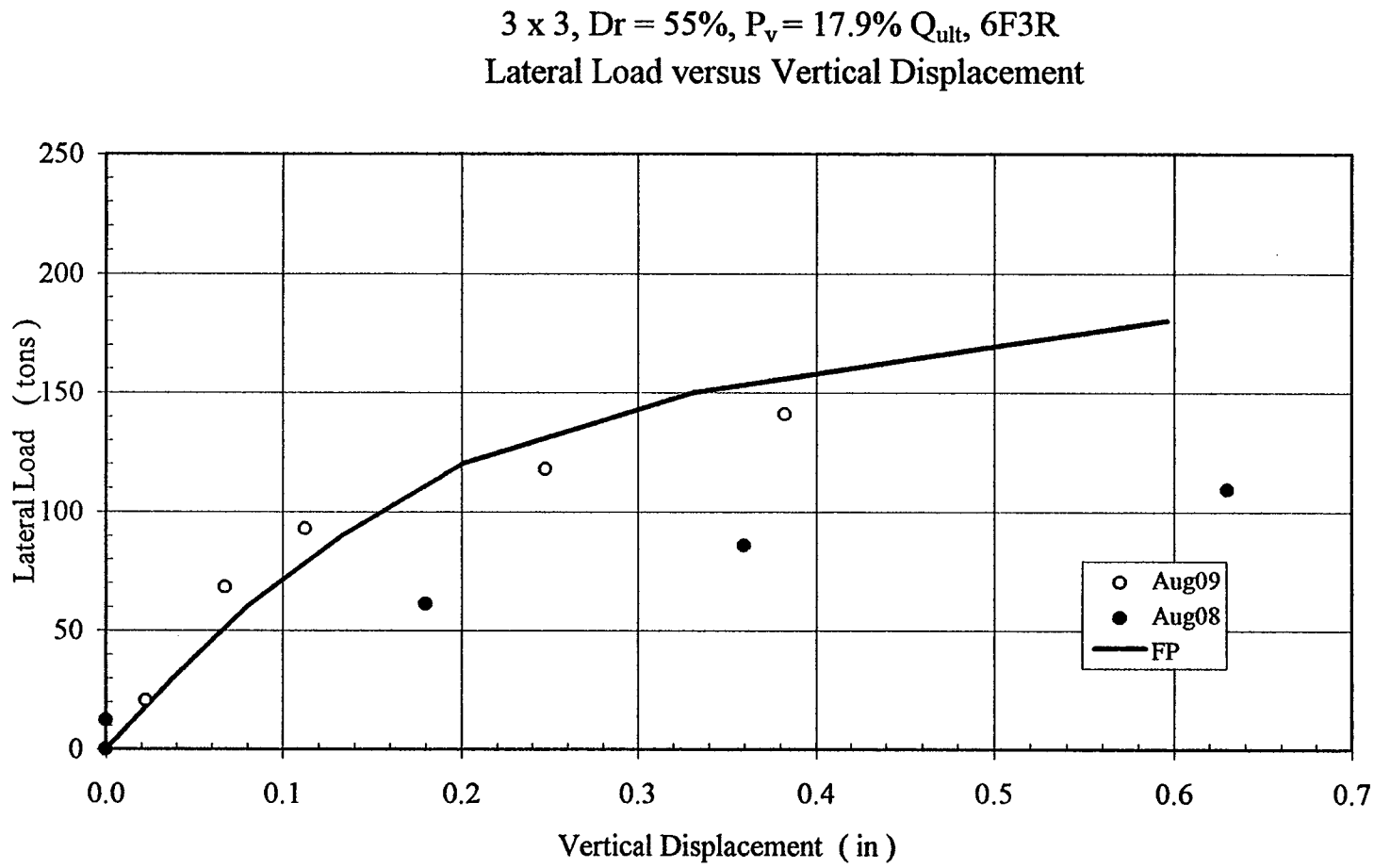

Figure B-71 Lateral Load versus Vertical Displacement

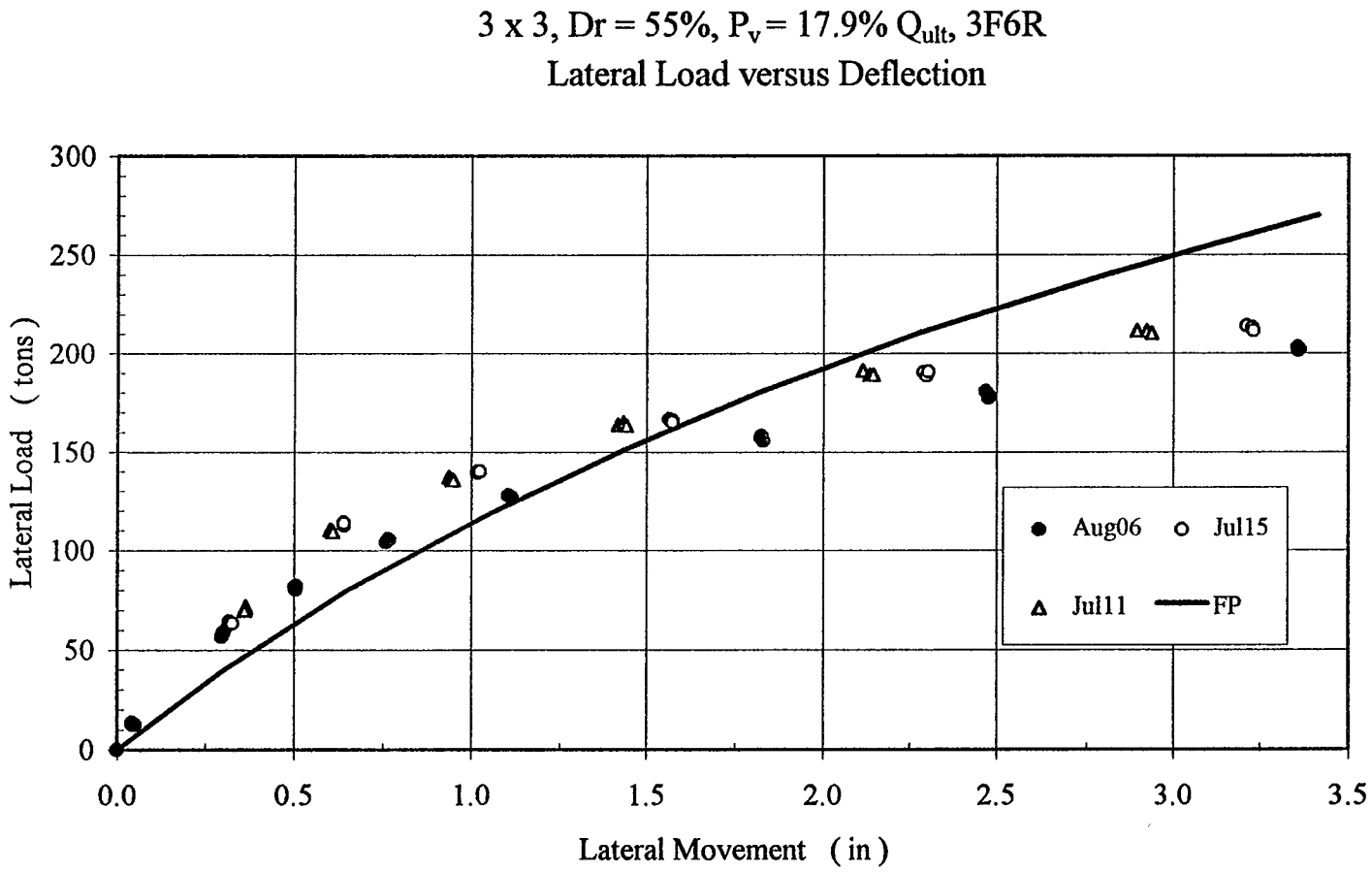

Figure B-72 Lateral Load versus Deflection

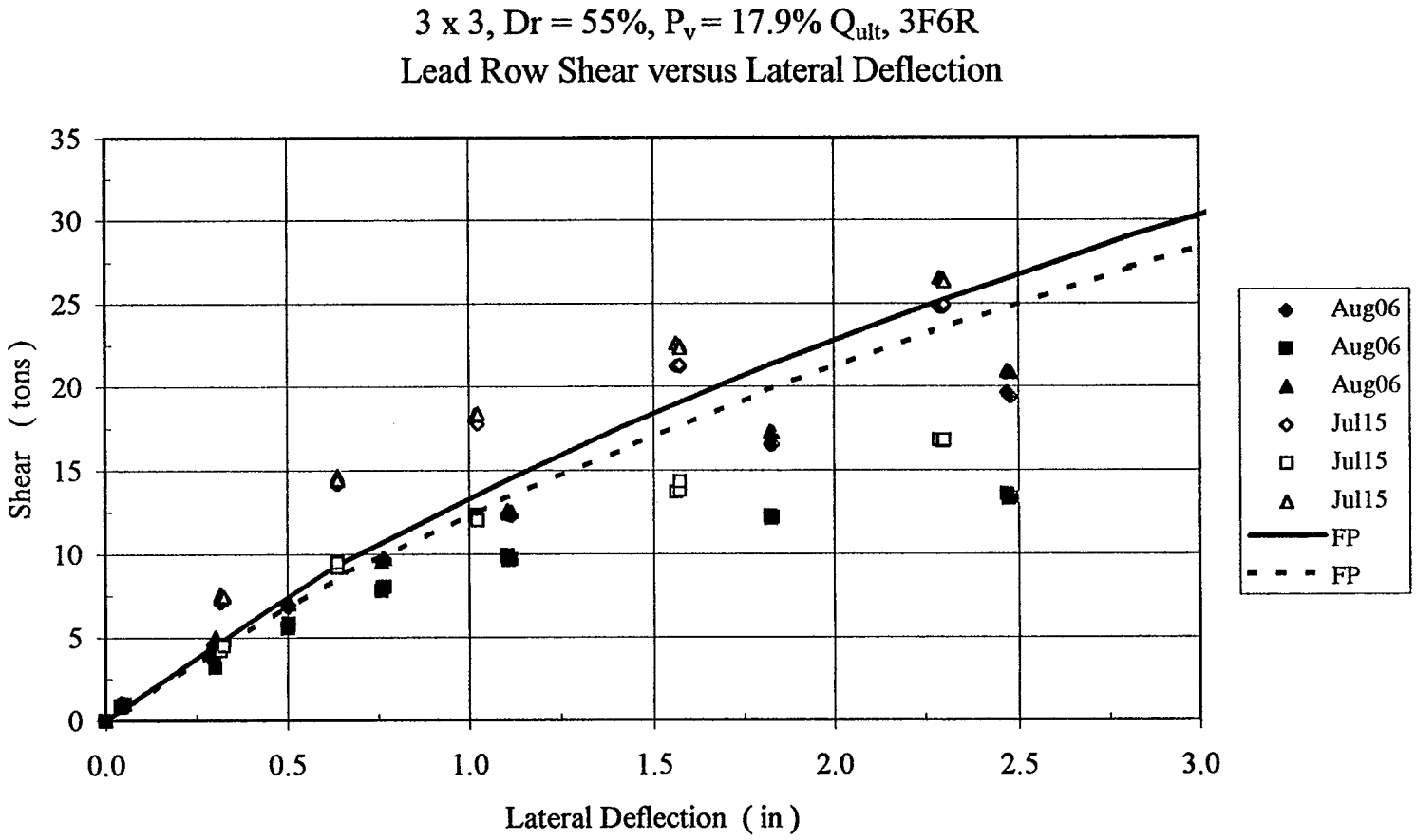

Figure B-73 Lead Row Shear versus Lateral Deflection

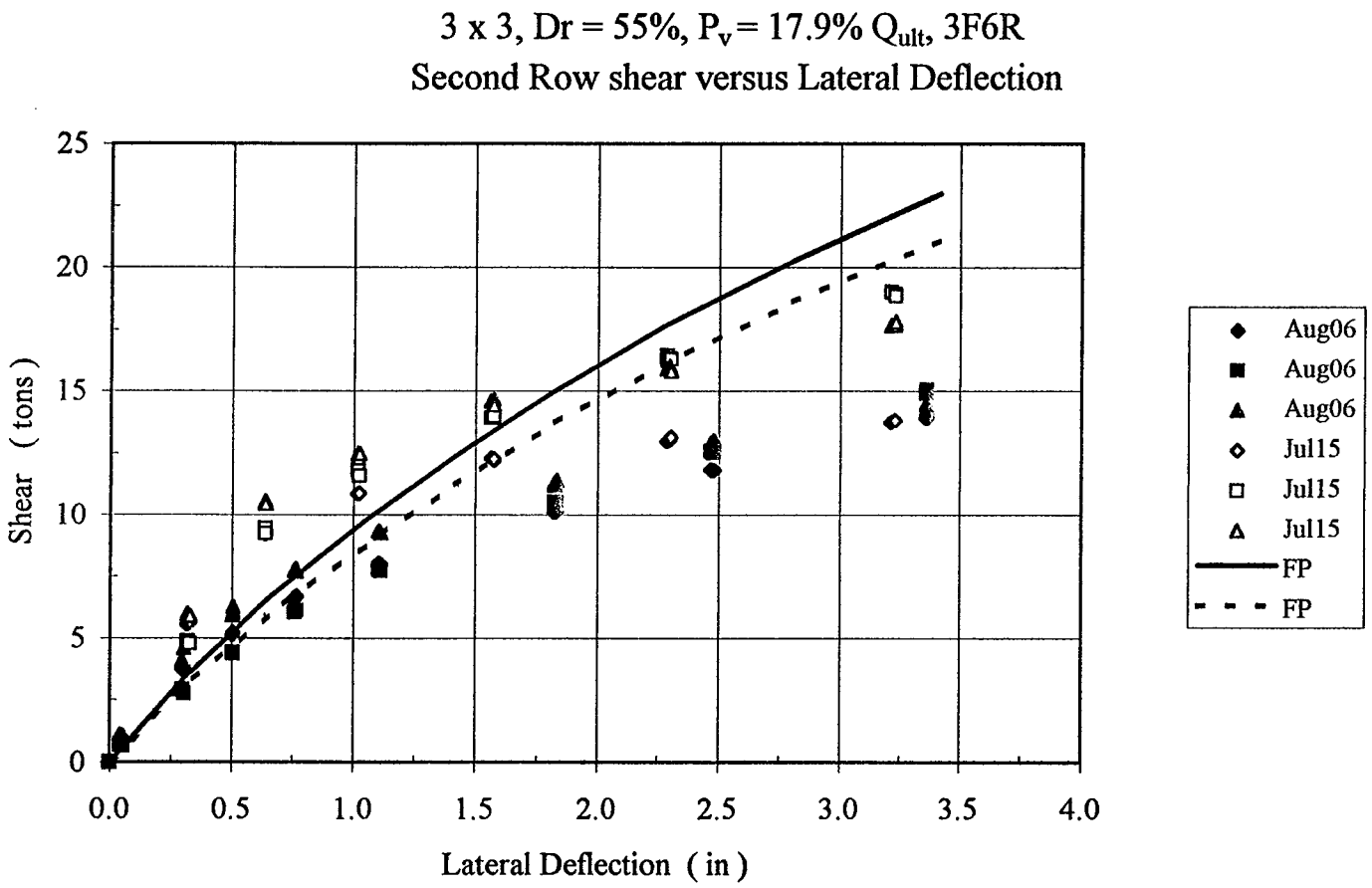

Figure B-74 Second Row Shear versus Lateral Deflection

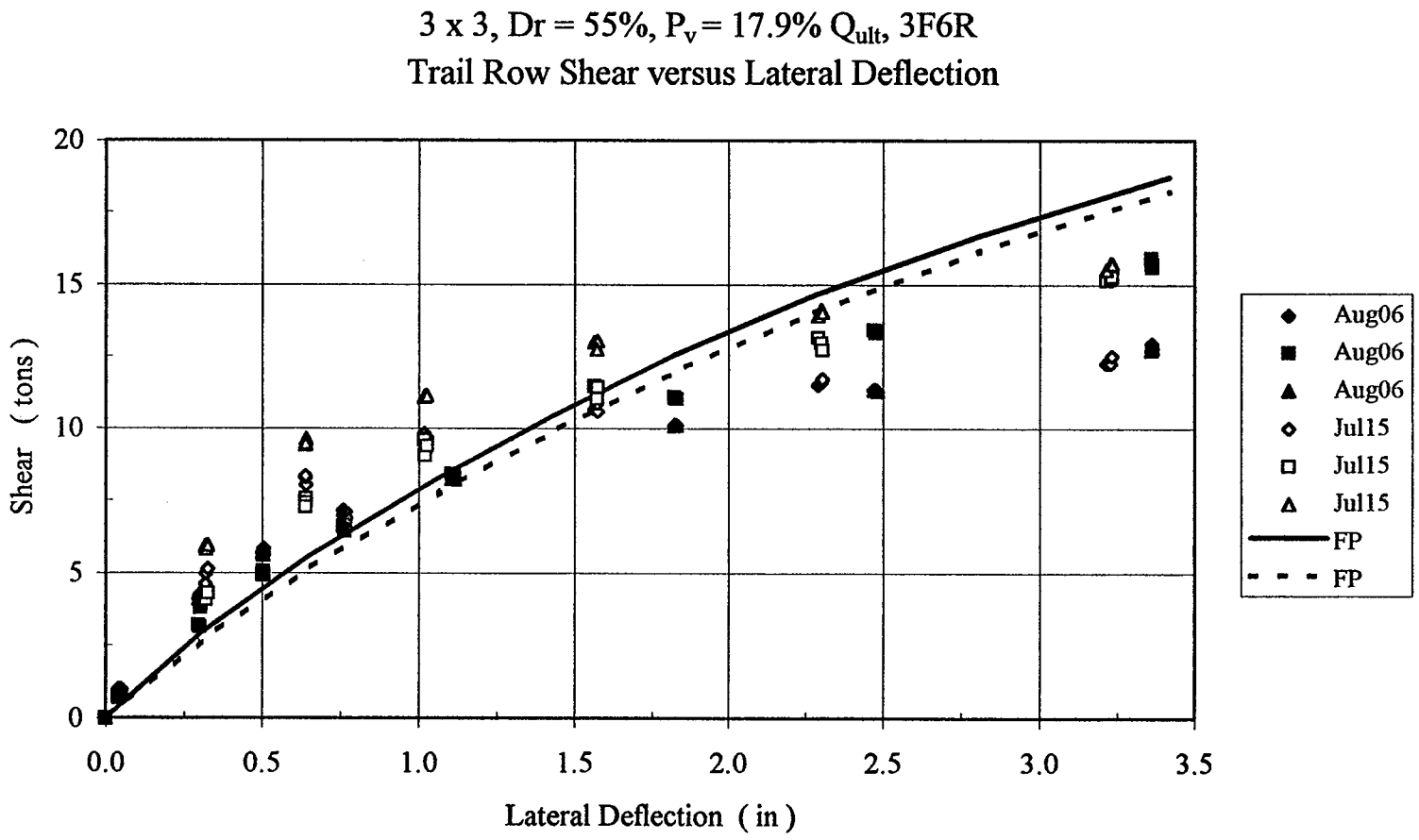

Figure B-75 Trail Row Shear versus Lateral Deflection

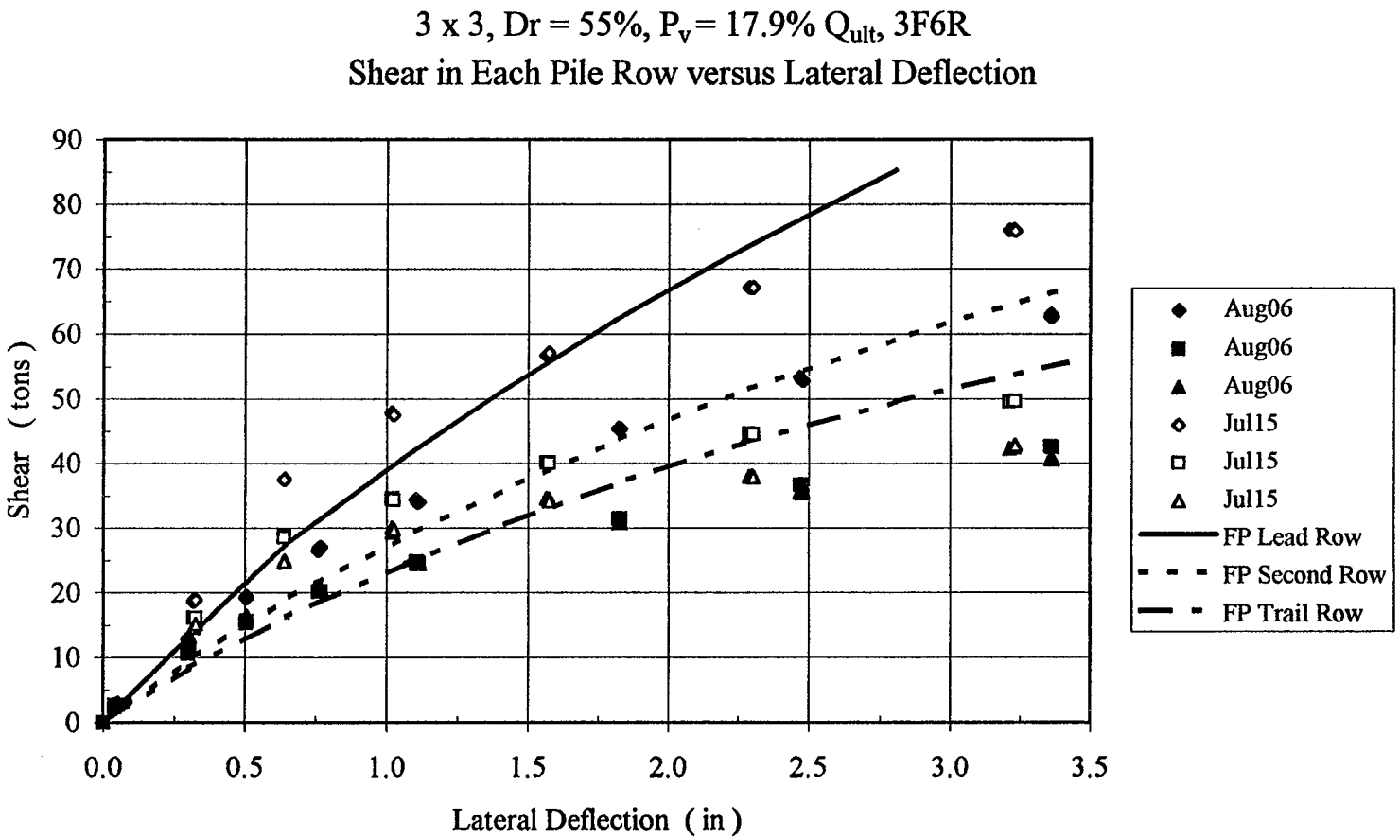

Figure B-76 Shear in Each Row versus Lateral Deflection

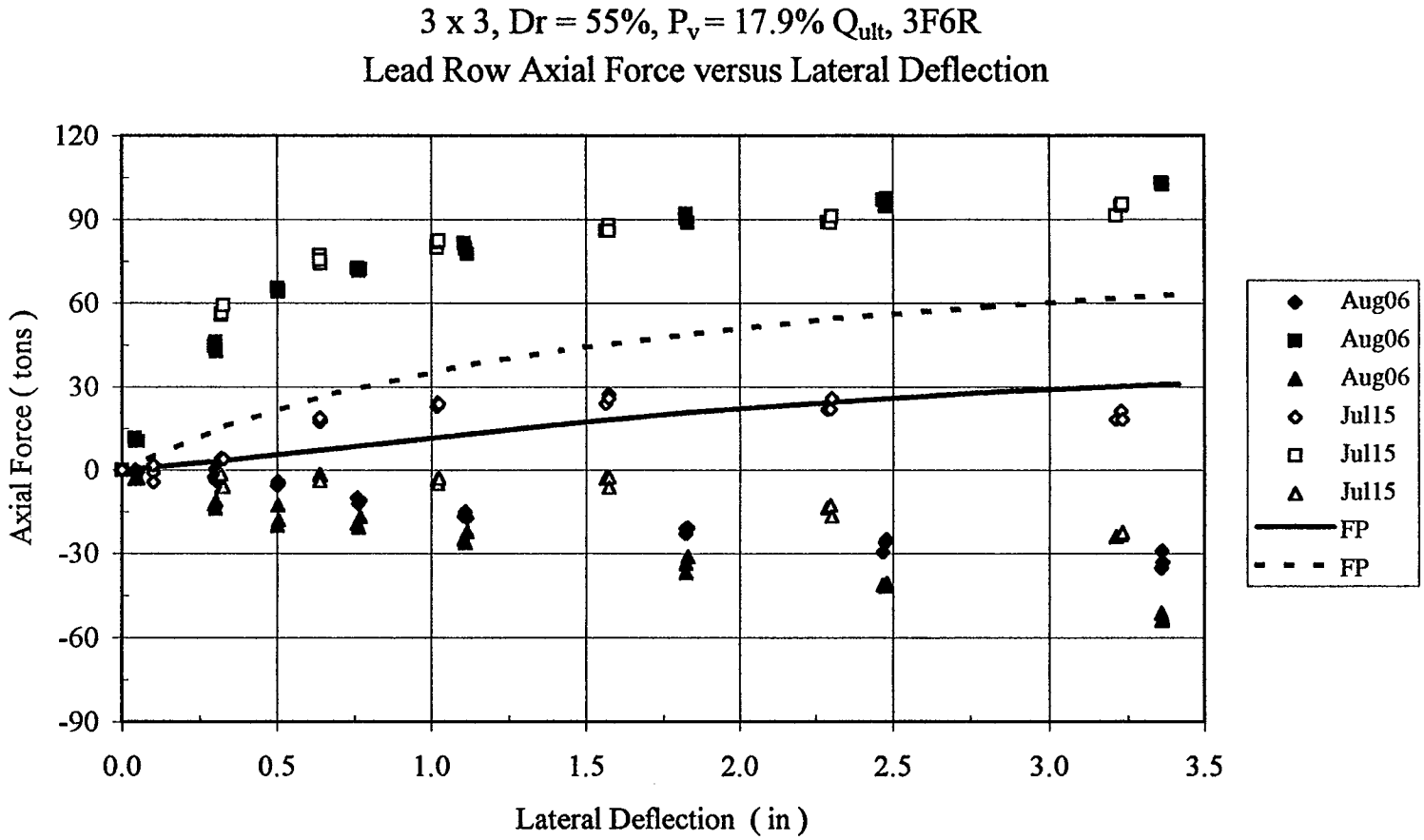

Figure B-77 Lead Row Axial Force versus Lateral Deflection

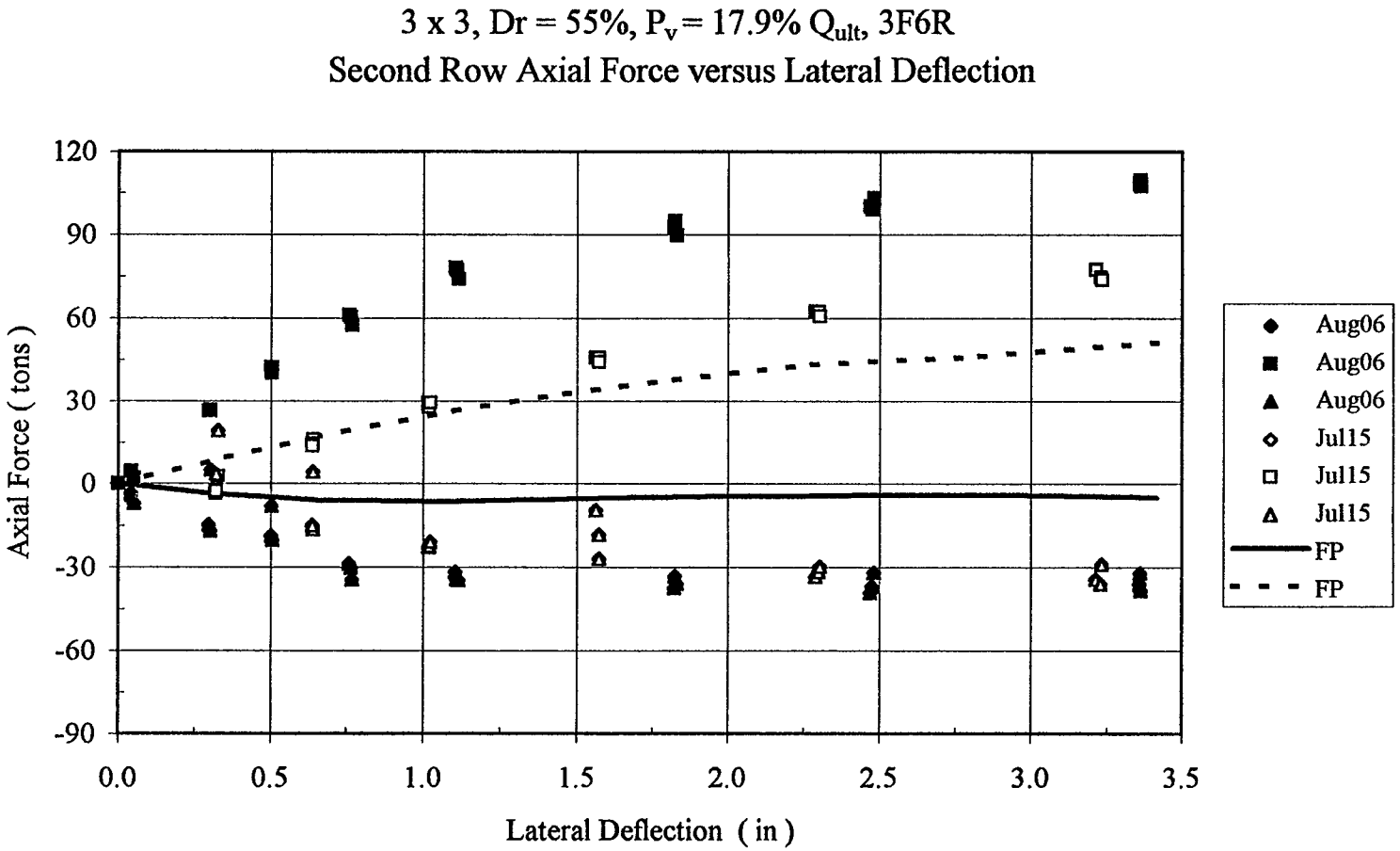

Figure B-78 Second Row Axial Force versus Lateral Deflection

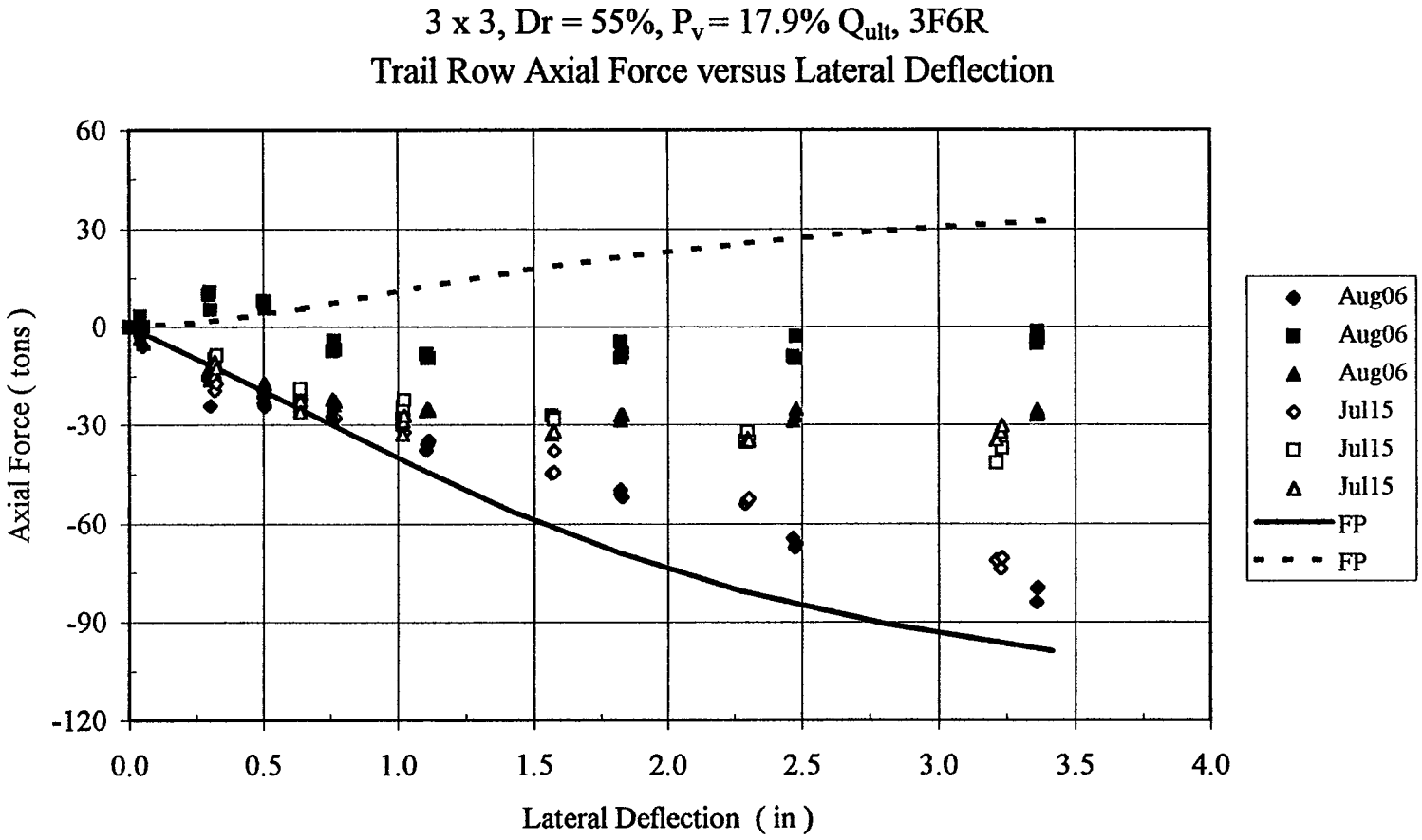

Figure B-79 Trail Row Axial Force versus Lateral Deflection

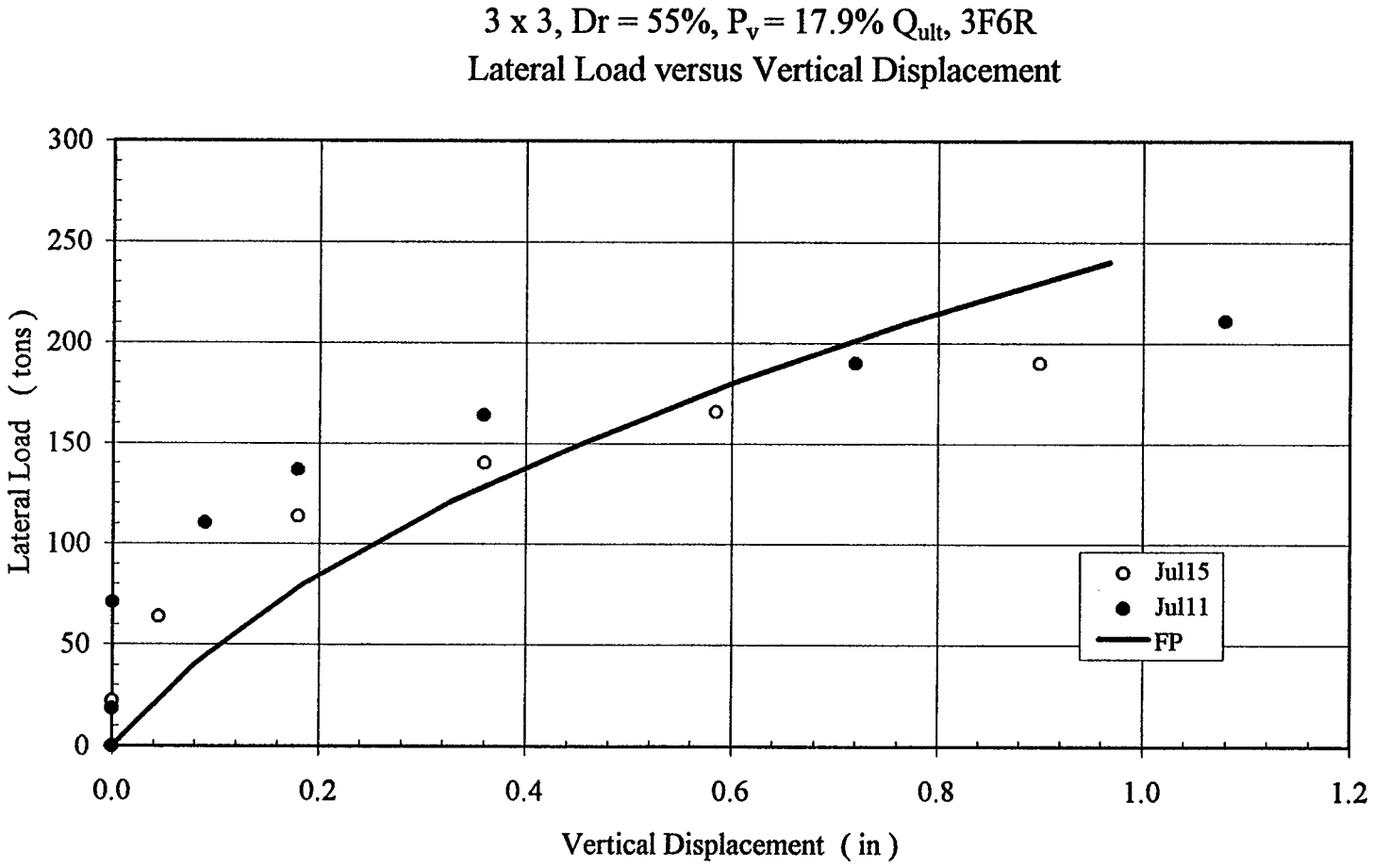

Figure B-80 Lateral Load versus Vertical Deflection

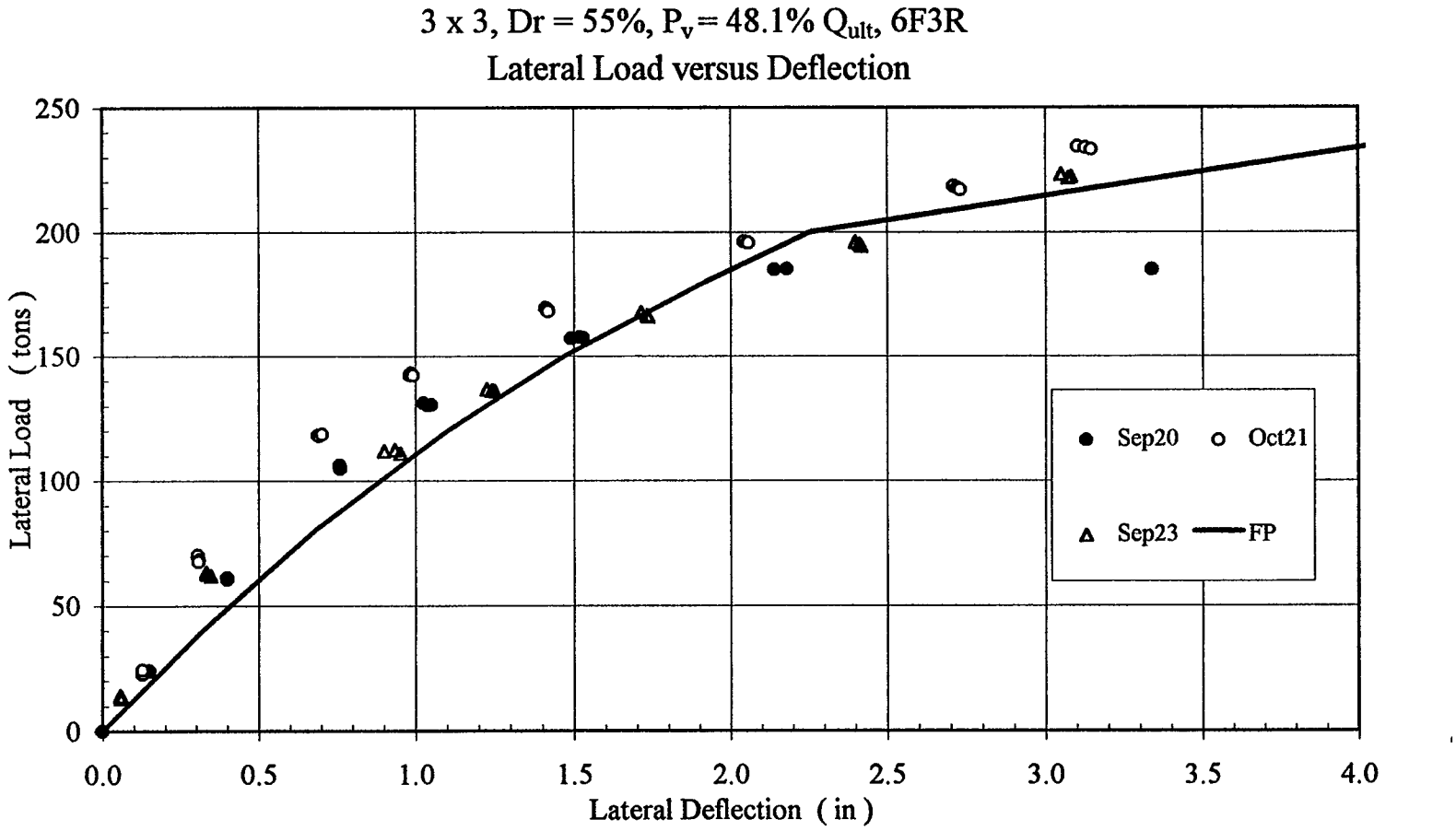

Figure B-81 Lateral Load versus Deflection

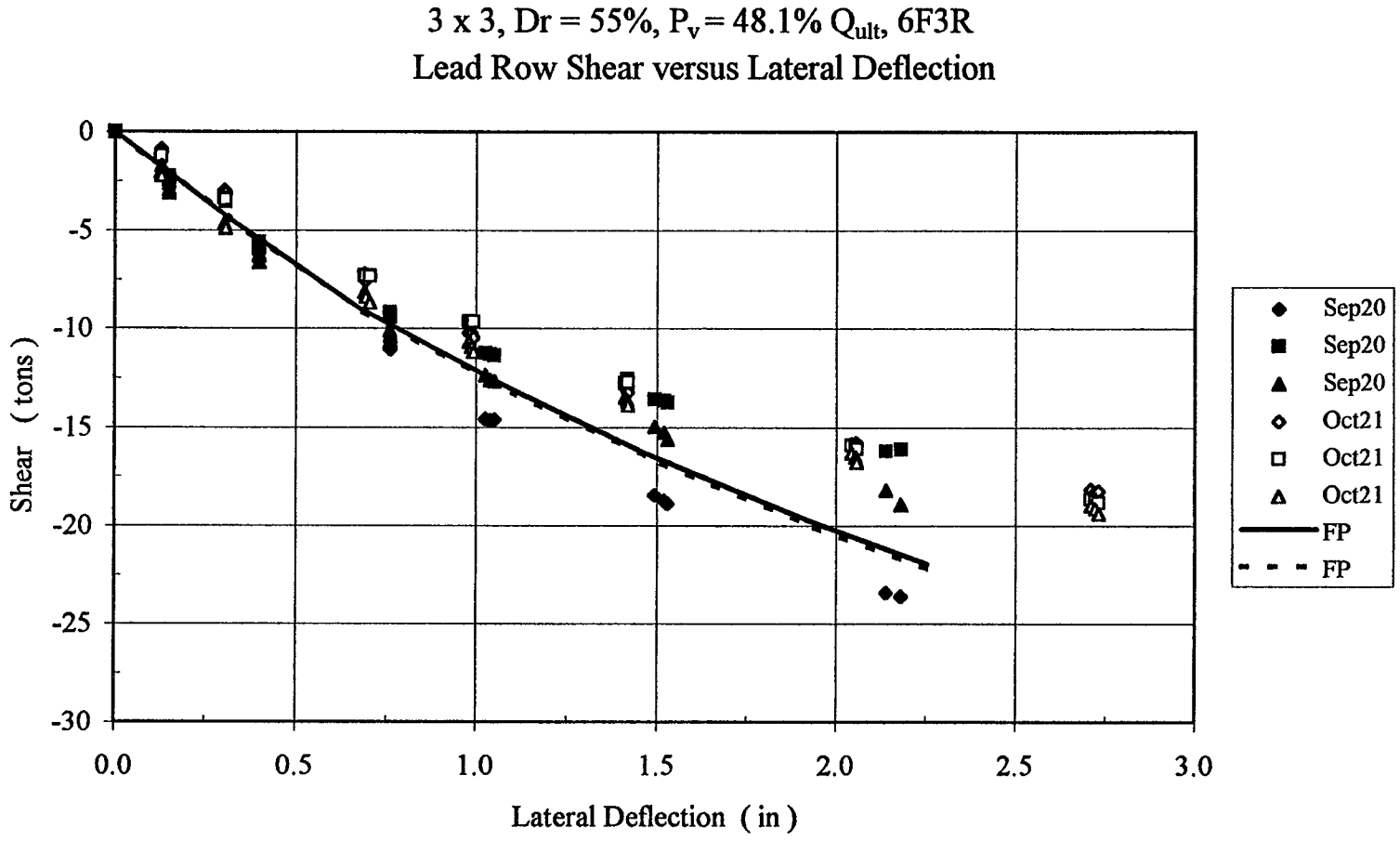

Figure B-82 Lead Row Shear versus Lateral Deflection

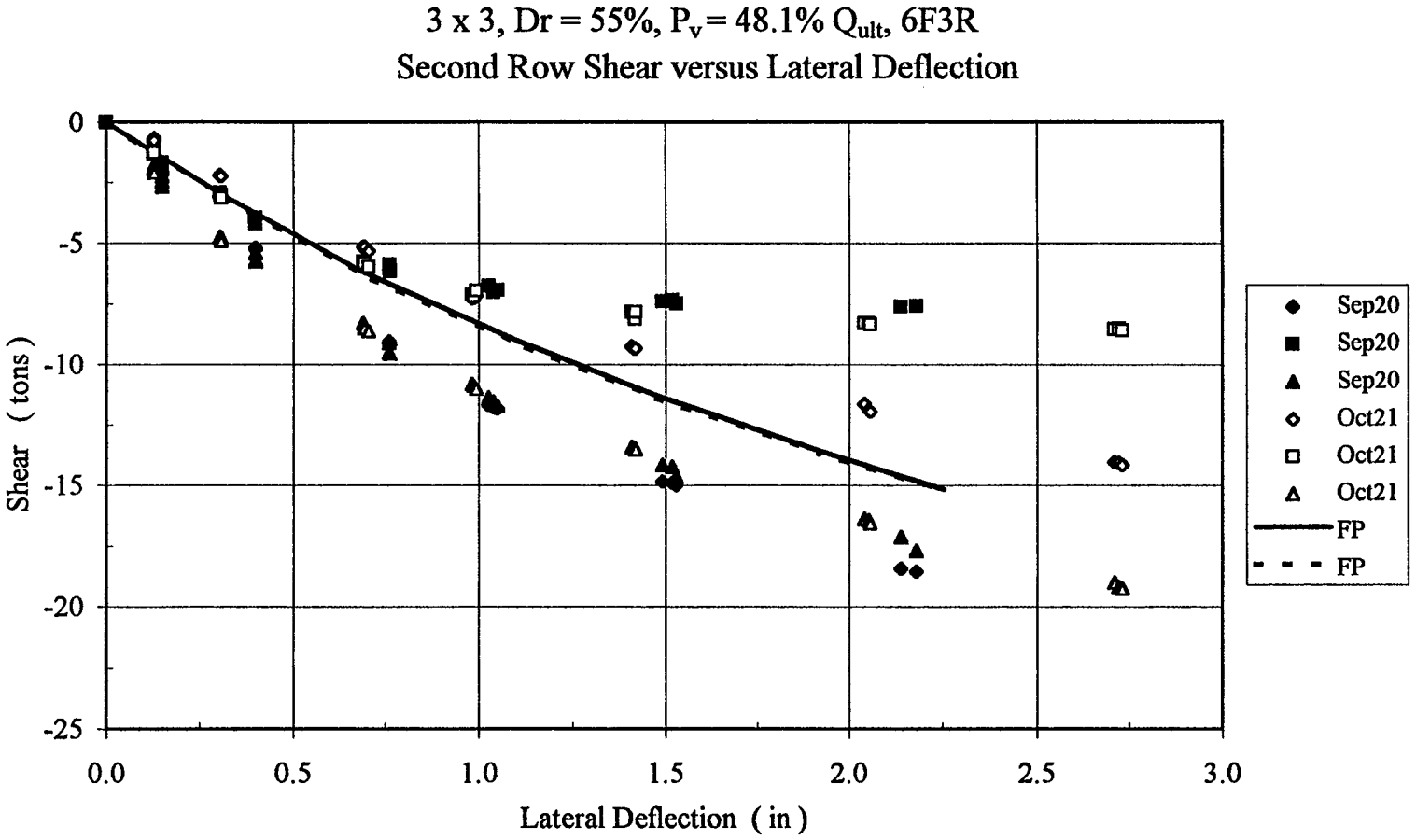

Figure B-83 Second Row Shear versus Lateral Deflection

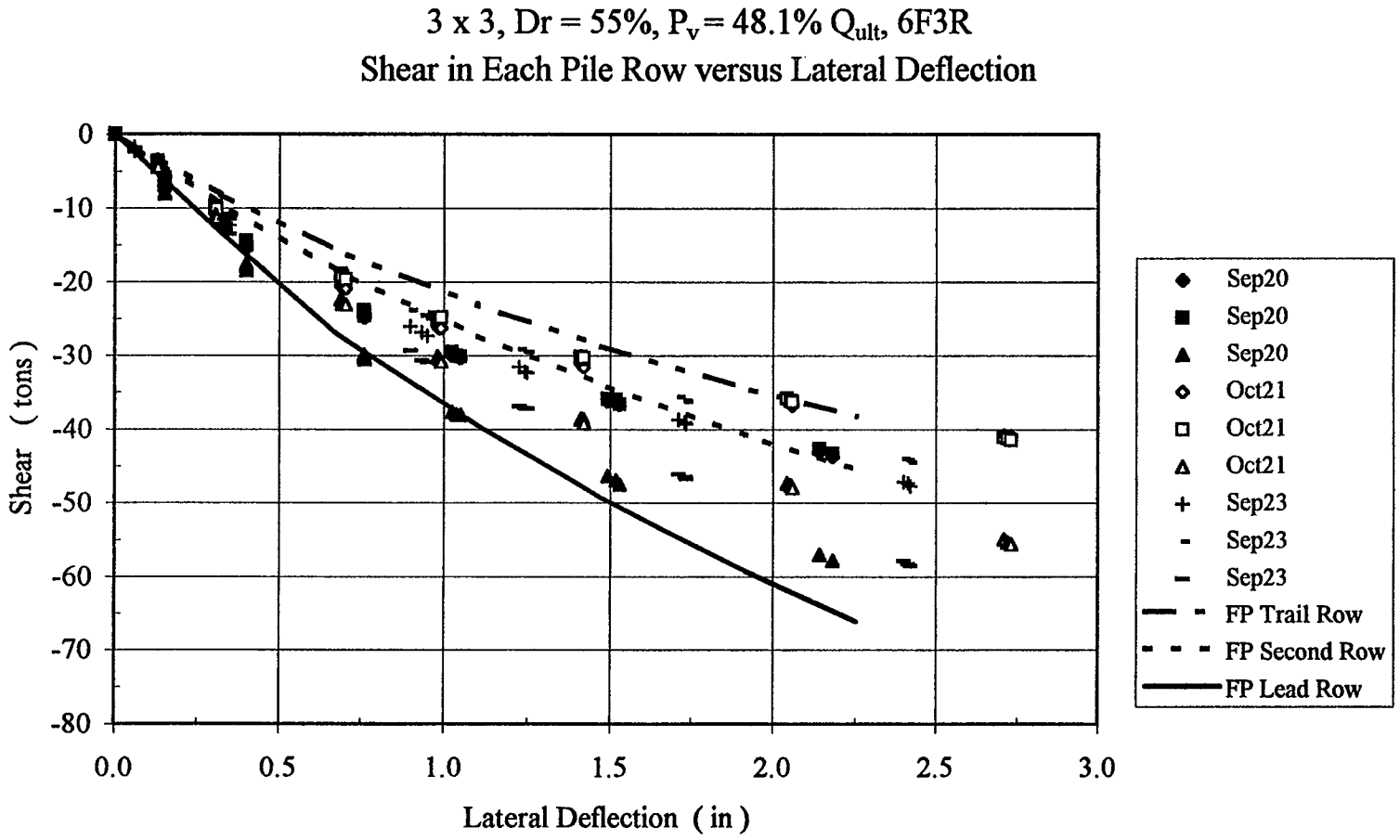

Figure B-84 Shear in Each Pile Row versus Lateral Deflection

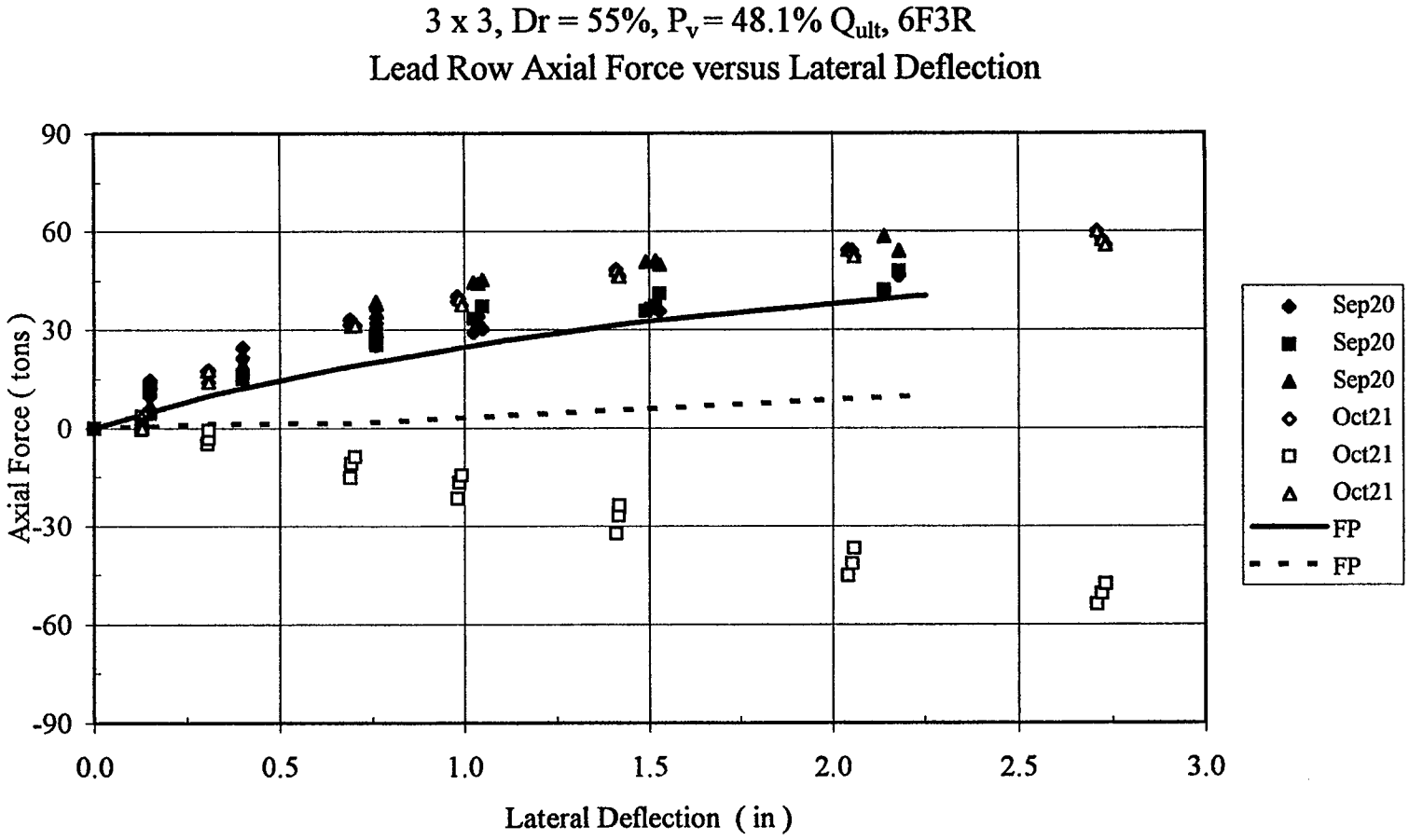

Figure B-85 Lead Row Axial Force versus Lateral Deflection

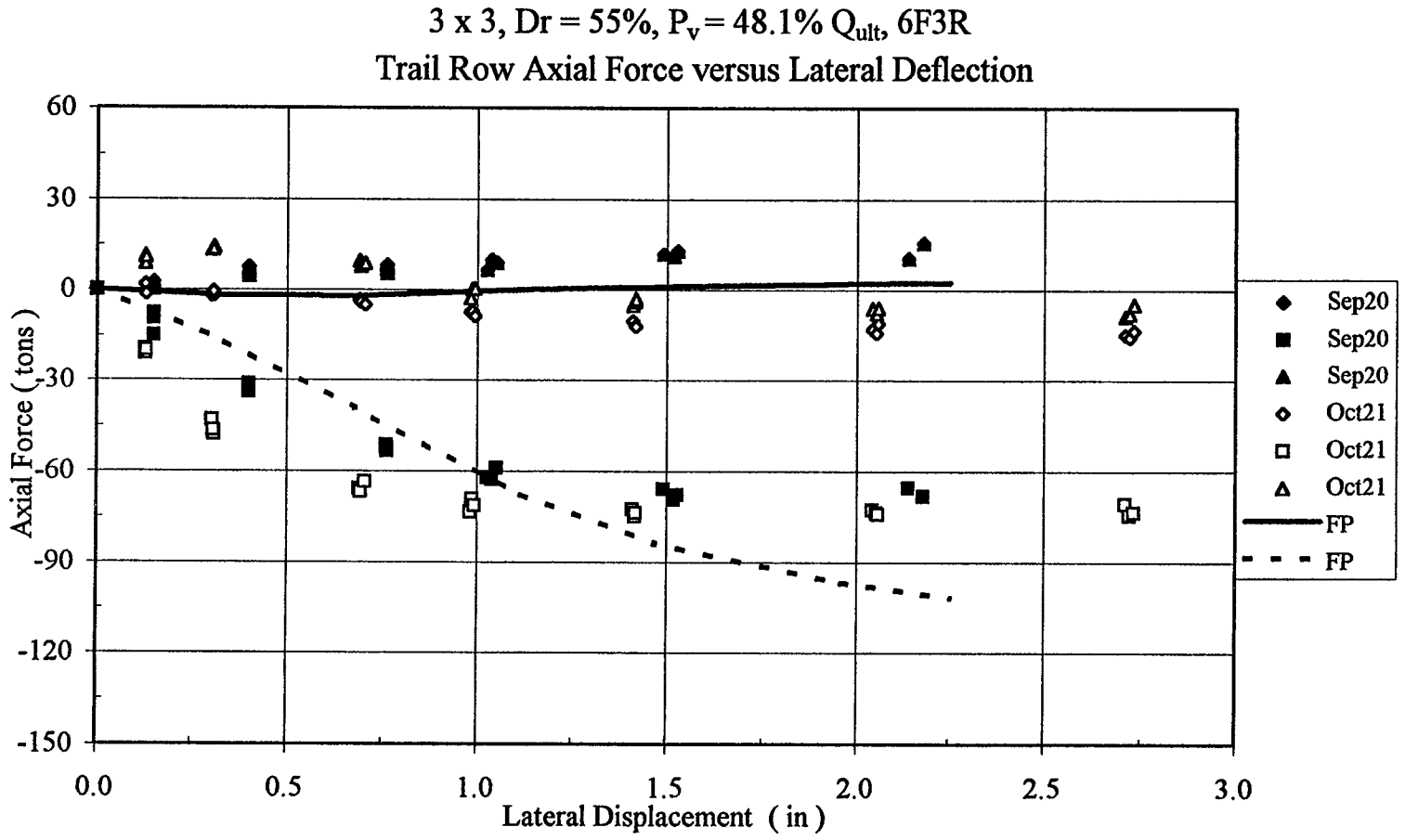

Figure B-86 Trail Row Axial Force versus Lateral Deflection

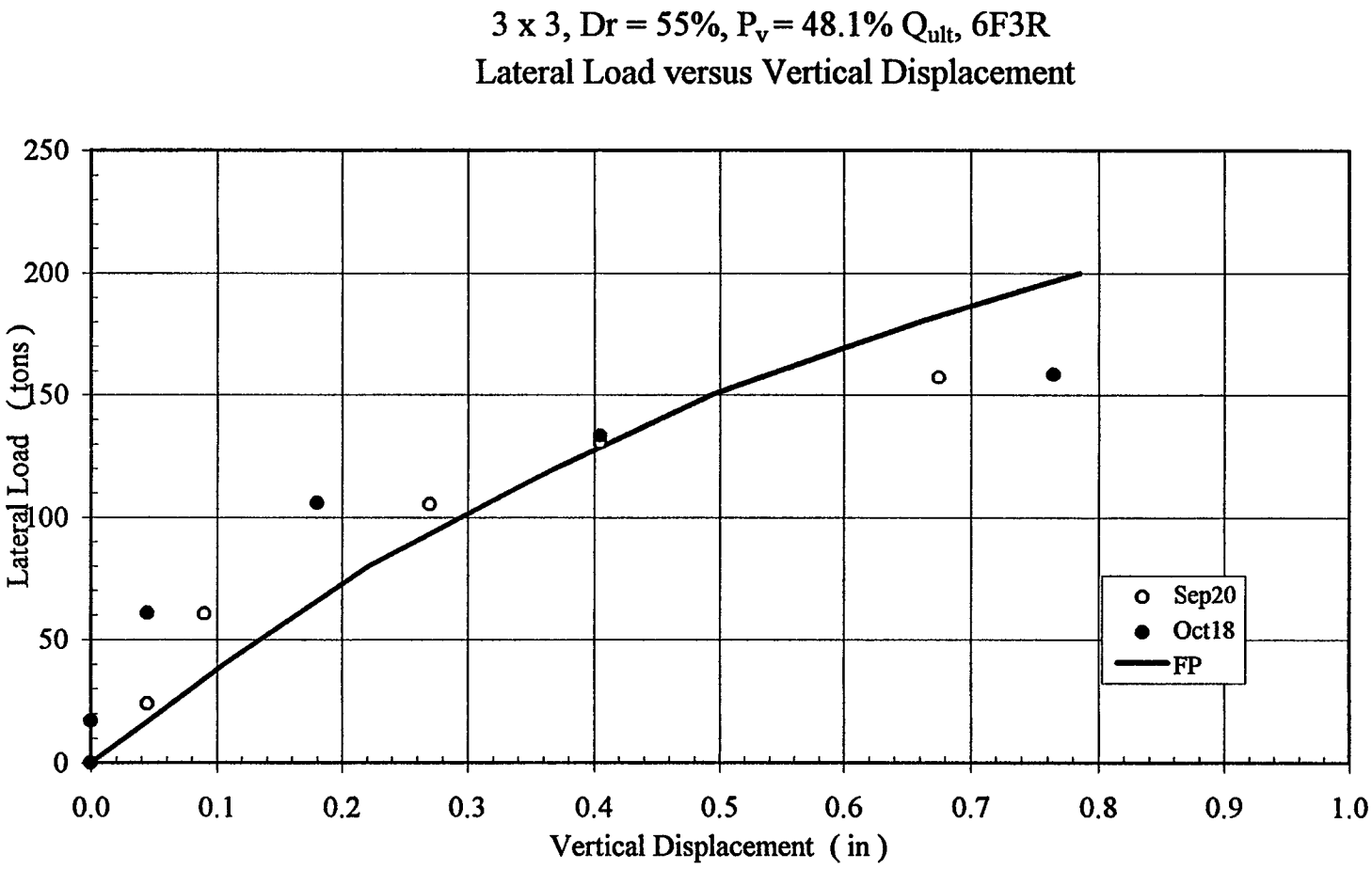

Figure B-87 Lateral Load versus Vertical Displacement

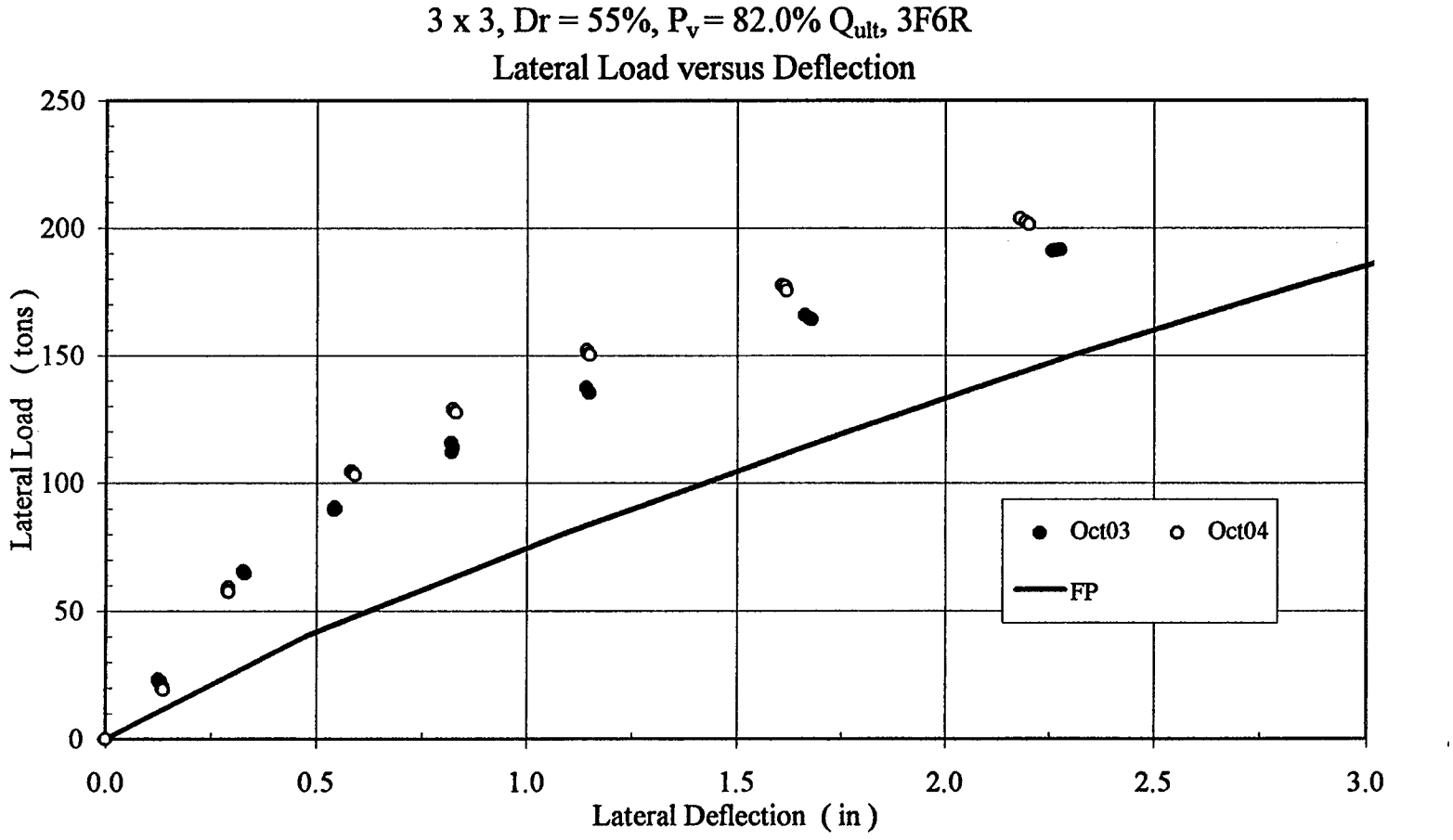

Figure B-88 Lateral Load versus Deflection

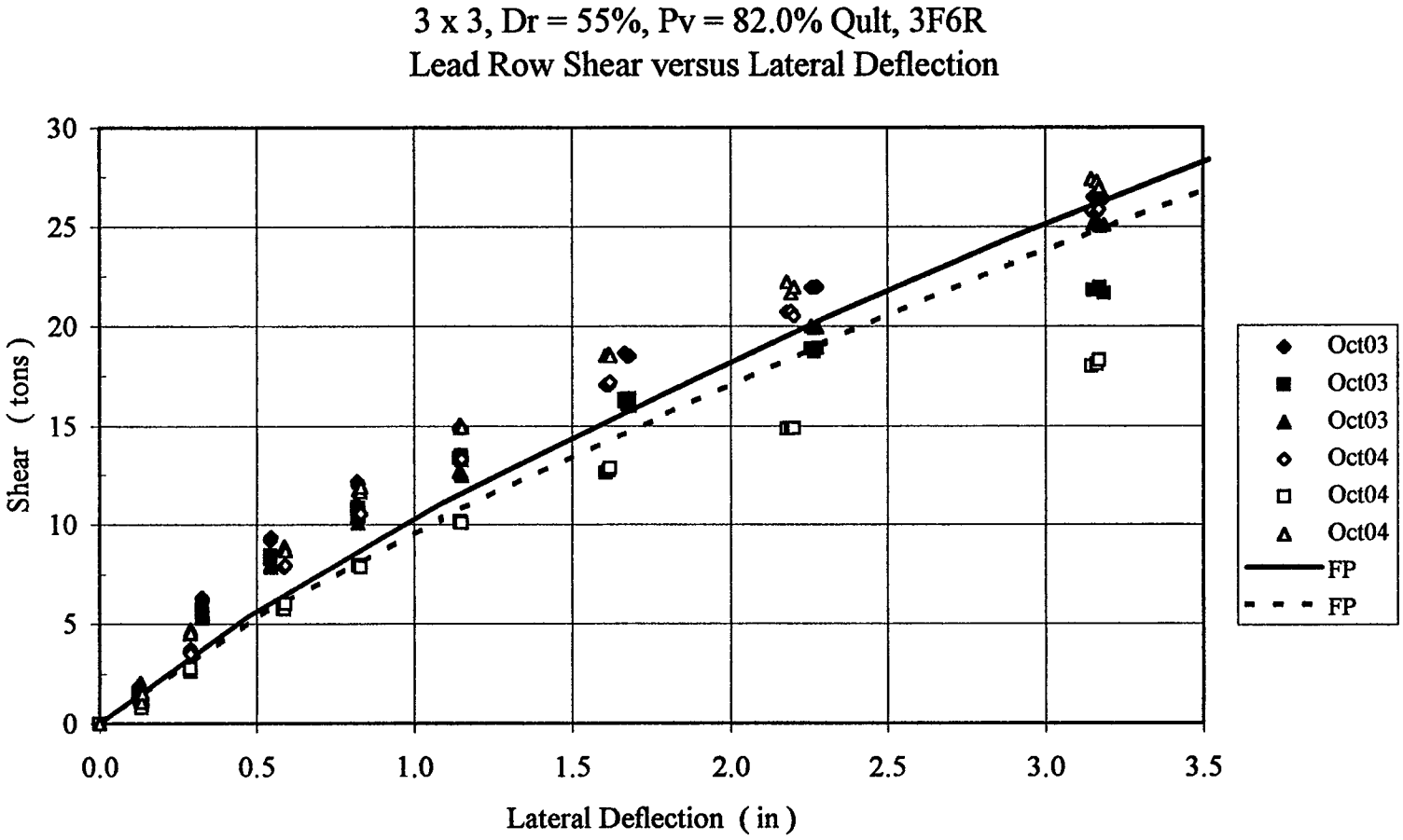

Figure B-89 Lead Row Shear versus Deflection

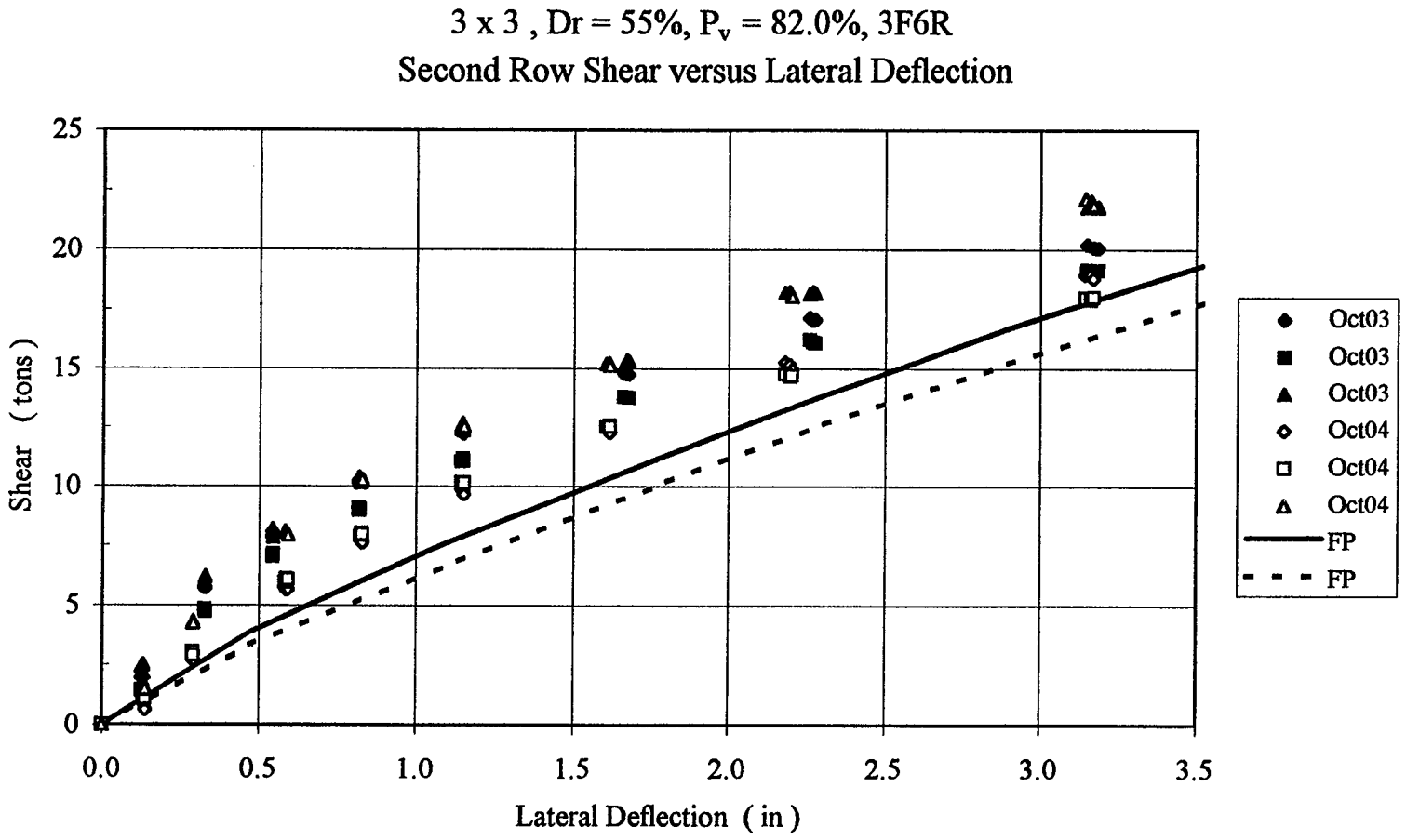

Figure B-90 Second Row Shear versus Lateral Deflection

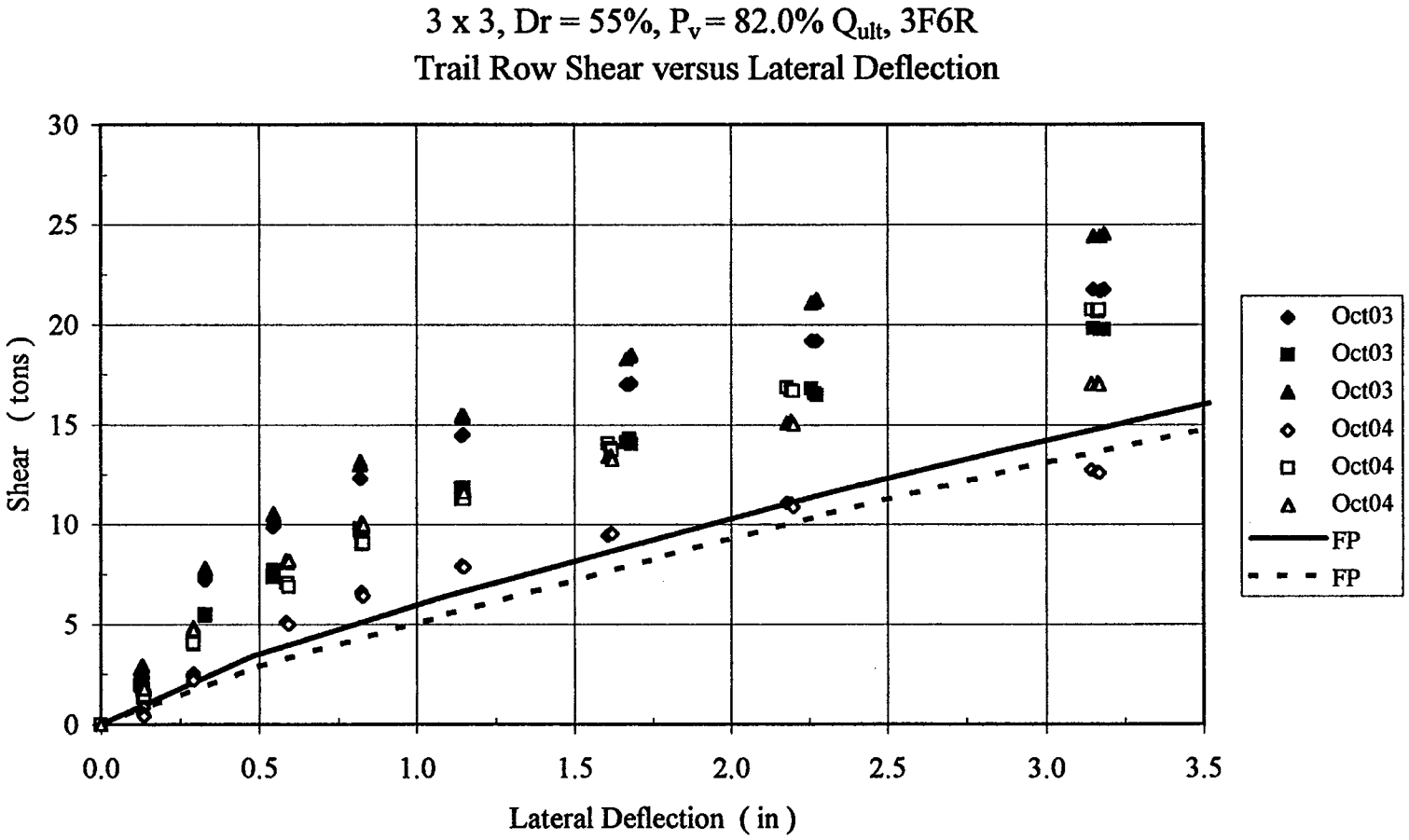

Figure B-91 Trail Row Shear versus Lateral Deflection

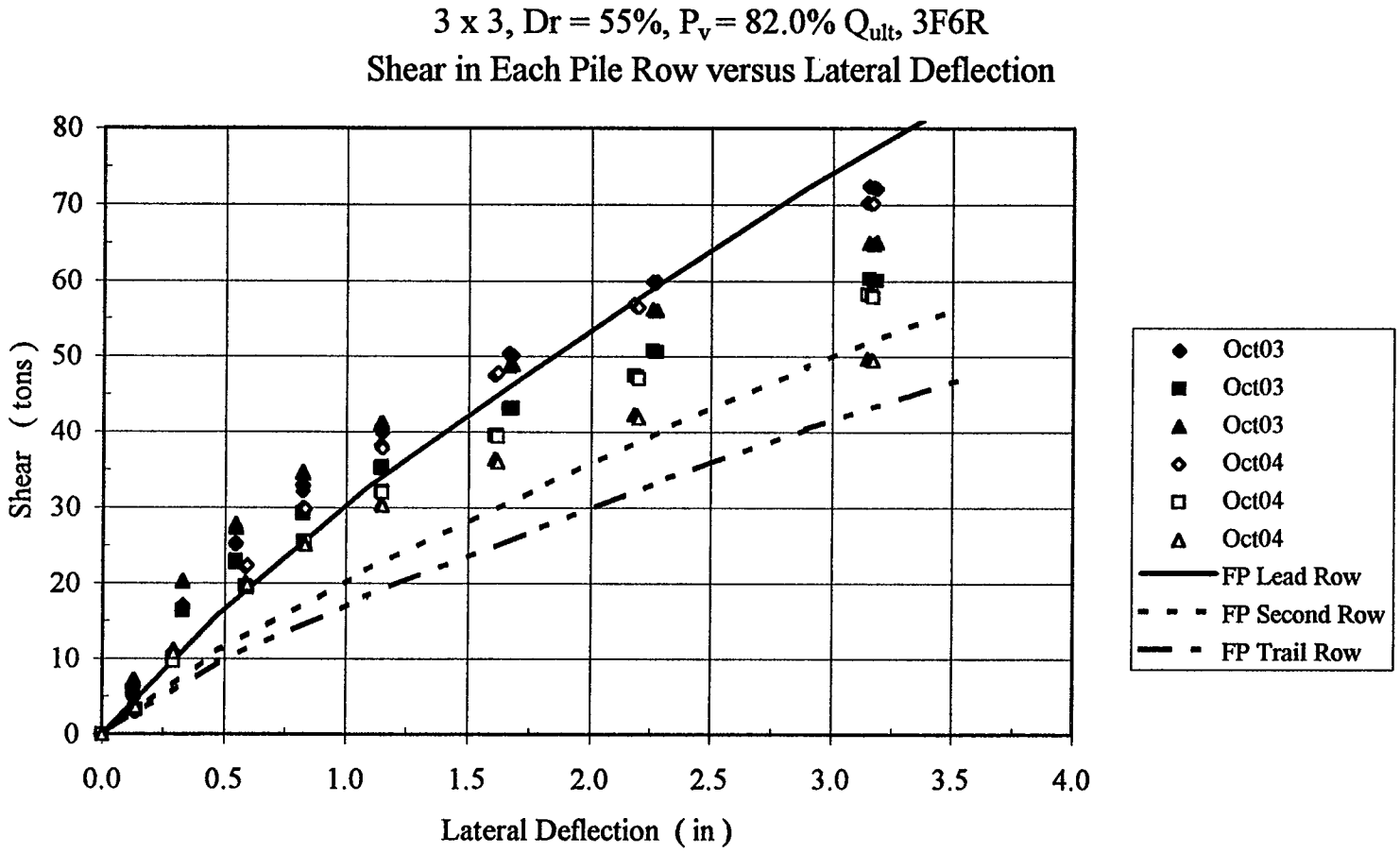

Figure B-92 Shear in Each Pile Row versus Lateral Deflection

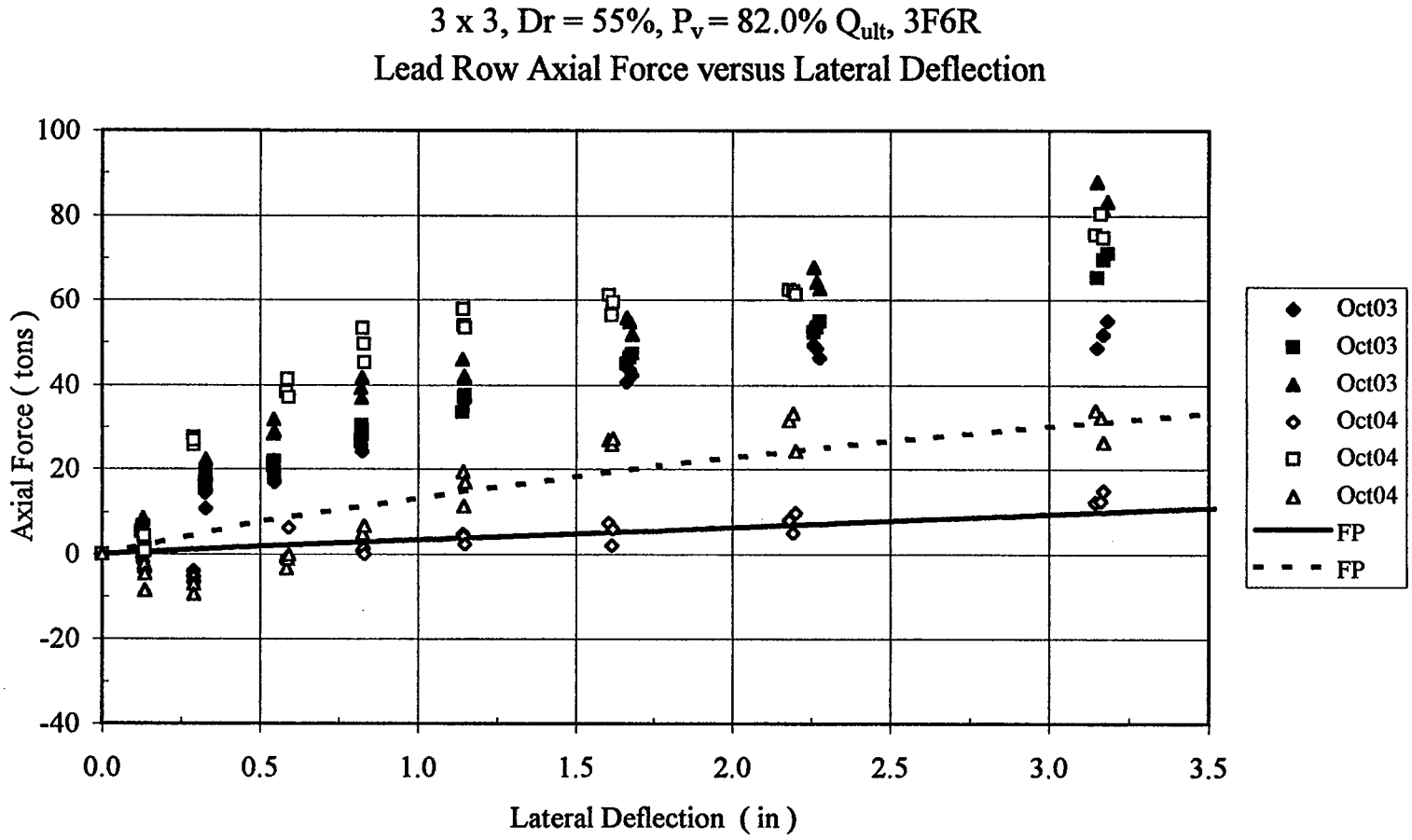

Figure B-93 Lead Row Axial Force versus Lateral Deflection

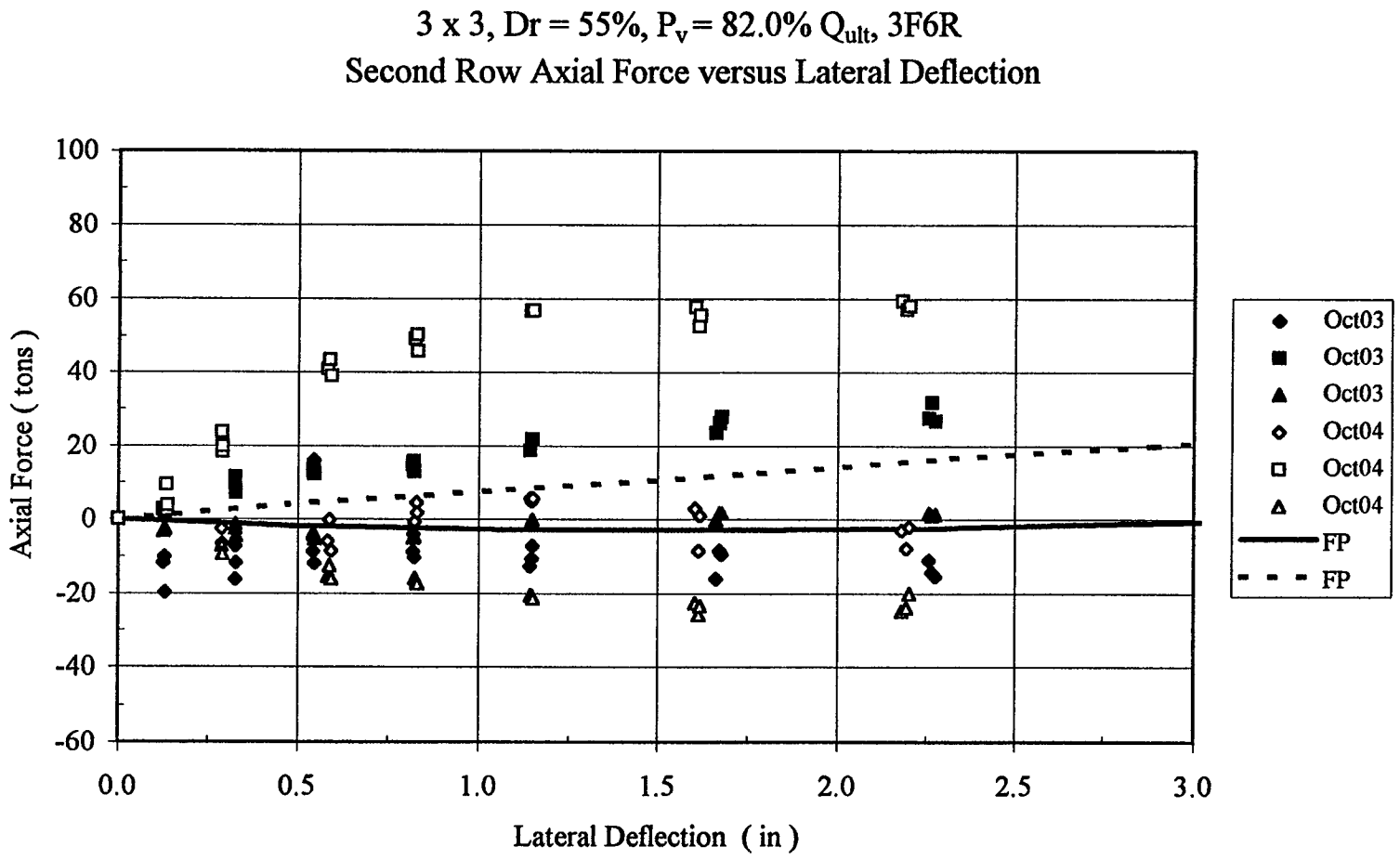

Figure B-94 Second Row Axial Force versus Lateral Deflection

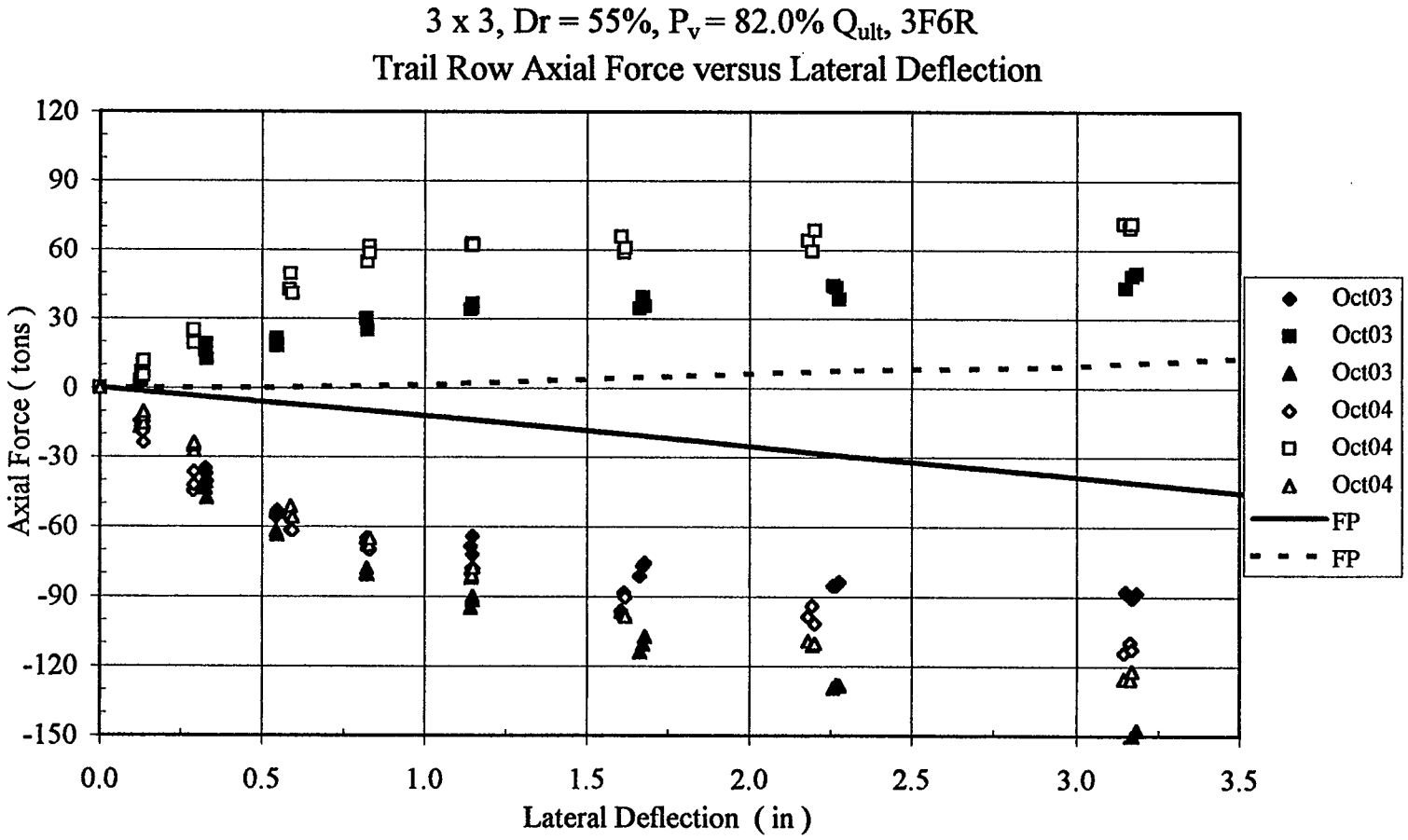

Figure B-95 Trail Row Axial Force versus Lateral Deflection

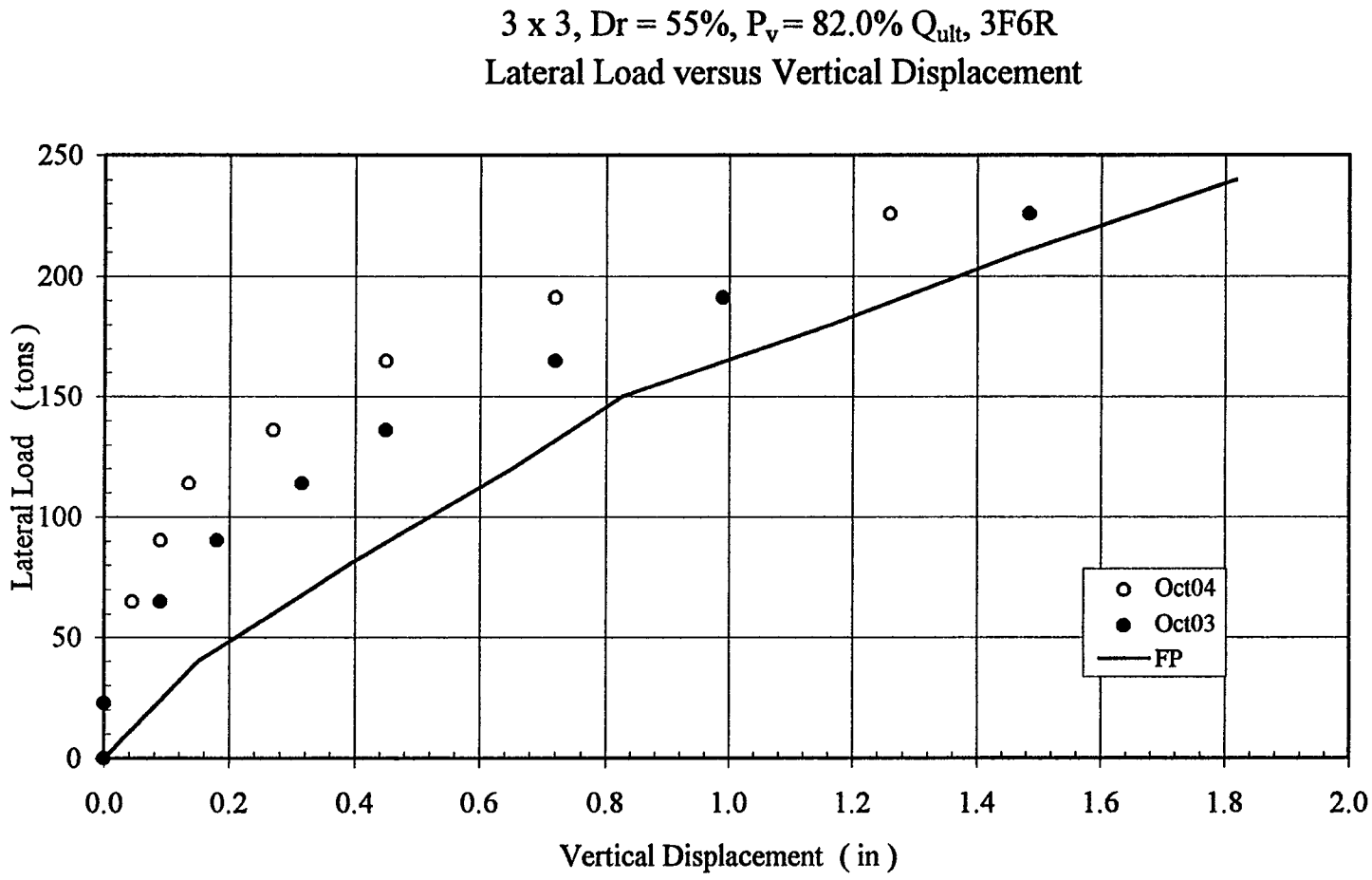

Figure B-96 Lateral Load versus Vertical Displacement

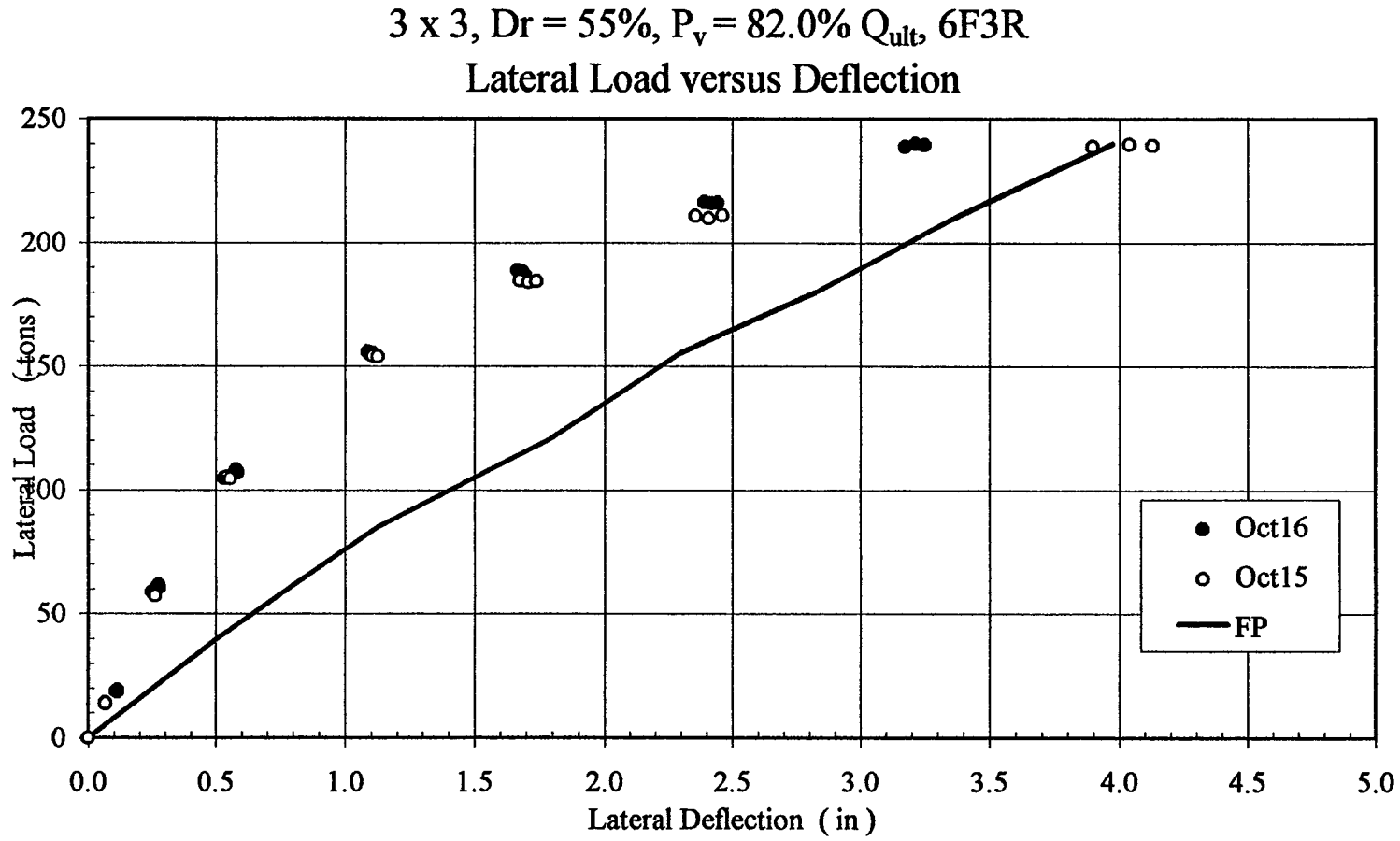

Figure B-97 Lateral Load versus Deflection

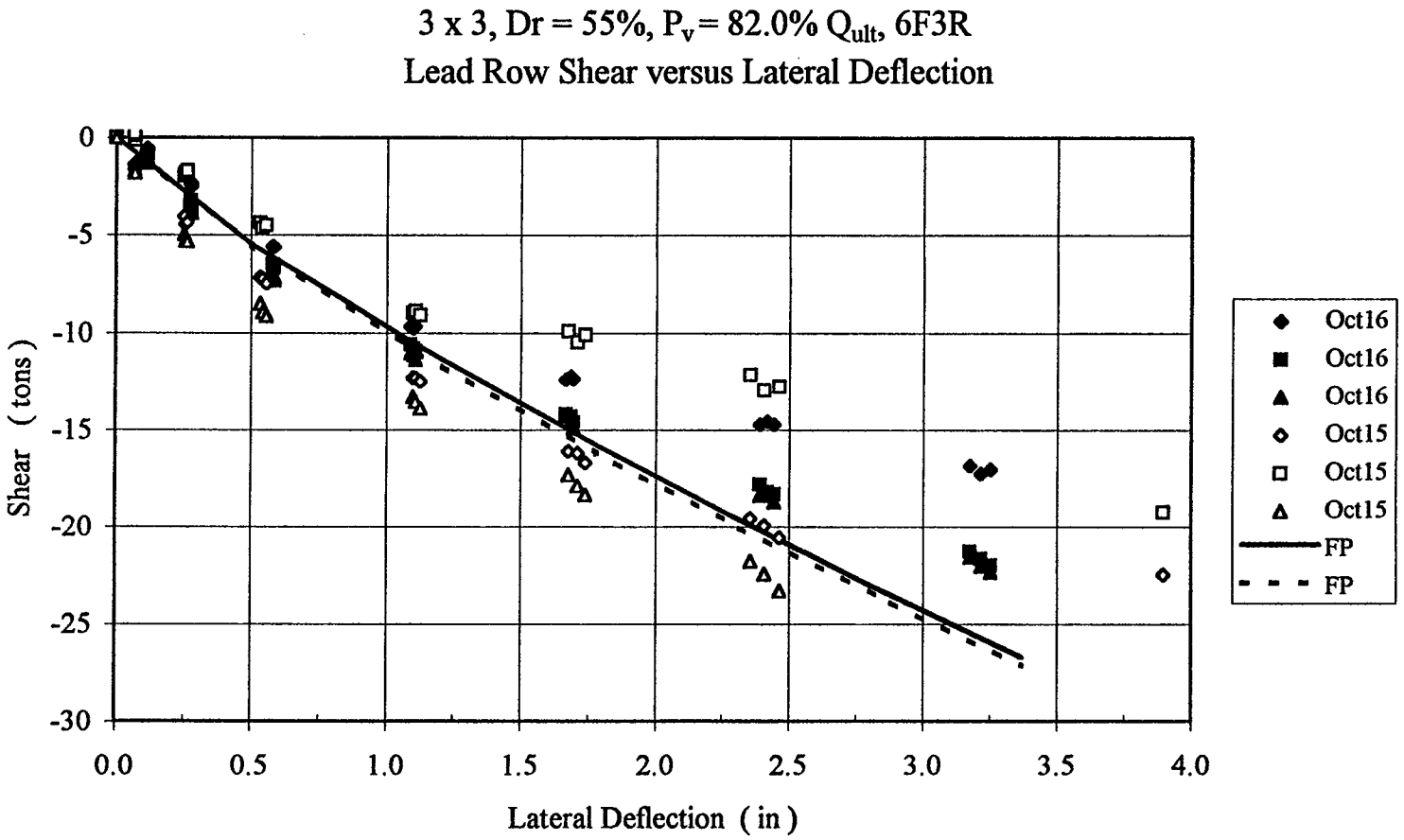

Figure B-98 Lead Row Shear versus Lateral Deflection

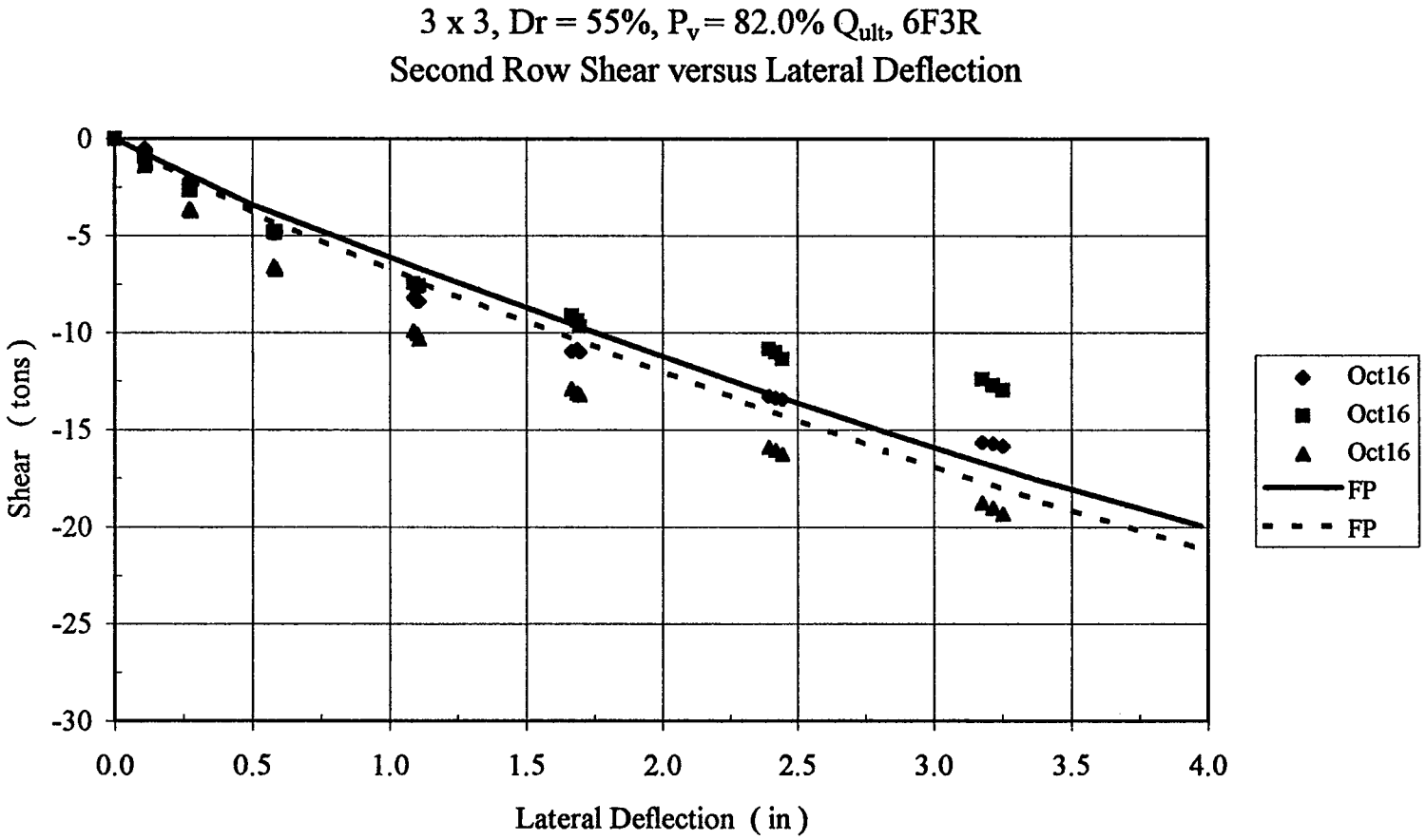

Figure B-99 Second Row Shear versus Lateral Deflection

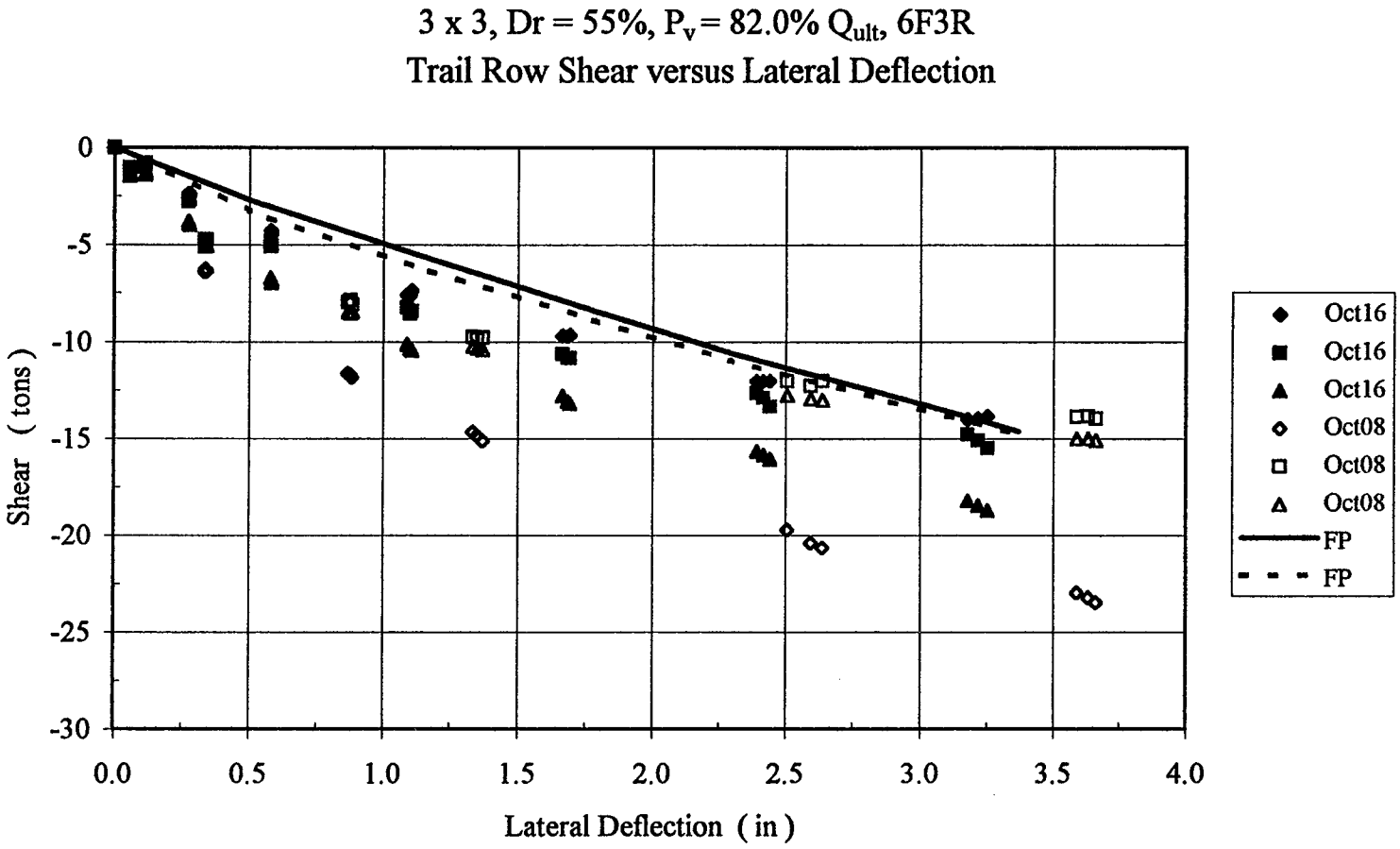

Figure B-100 Trail Row Shear versus Lateral Deflection

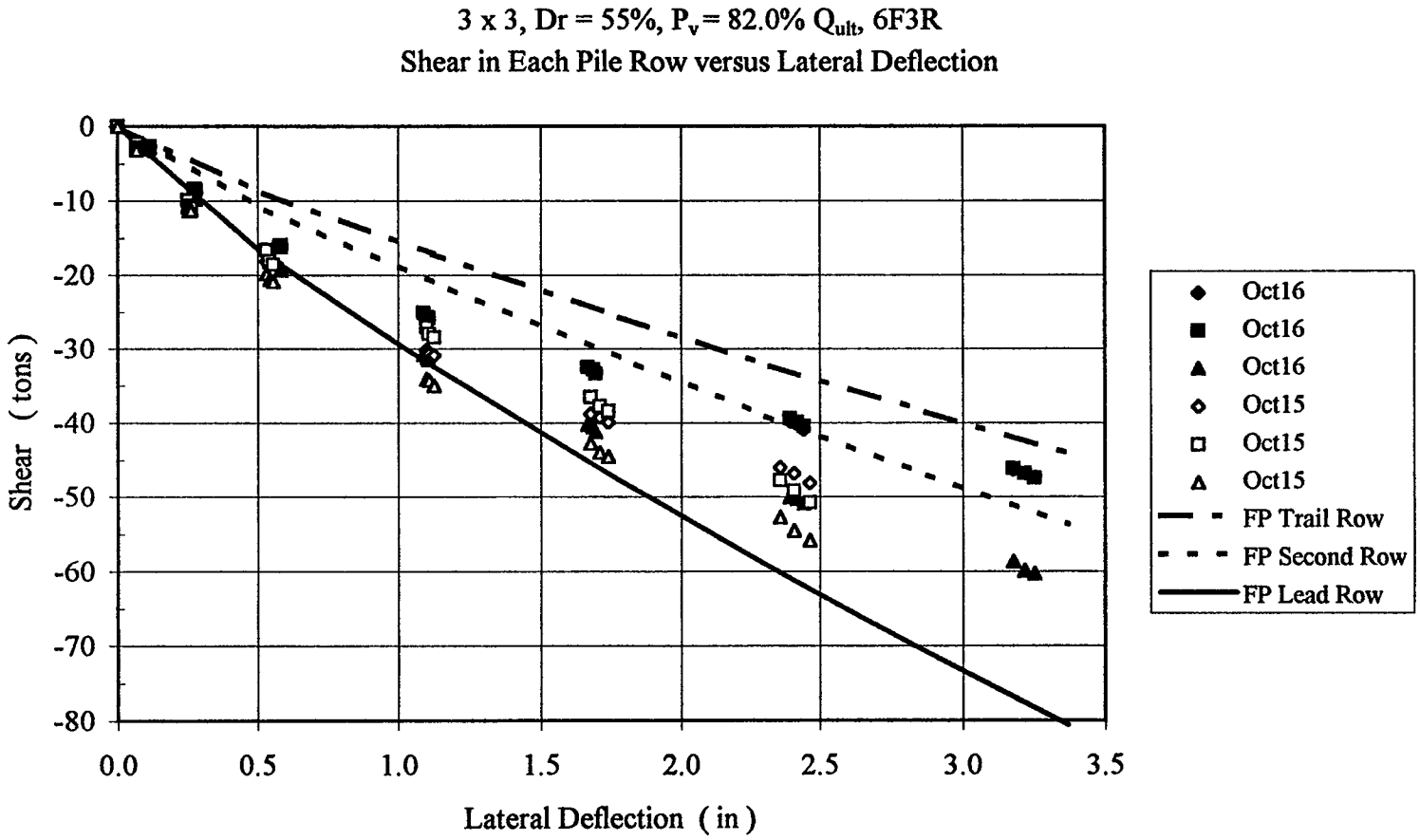

Figure B-101 Shear in Each Pile Row versus Lateral Deflection

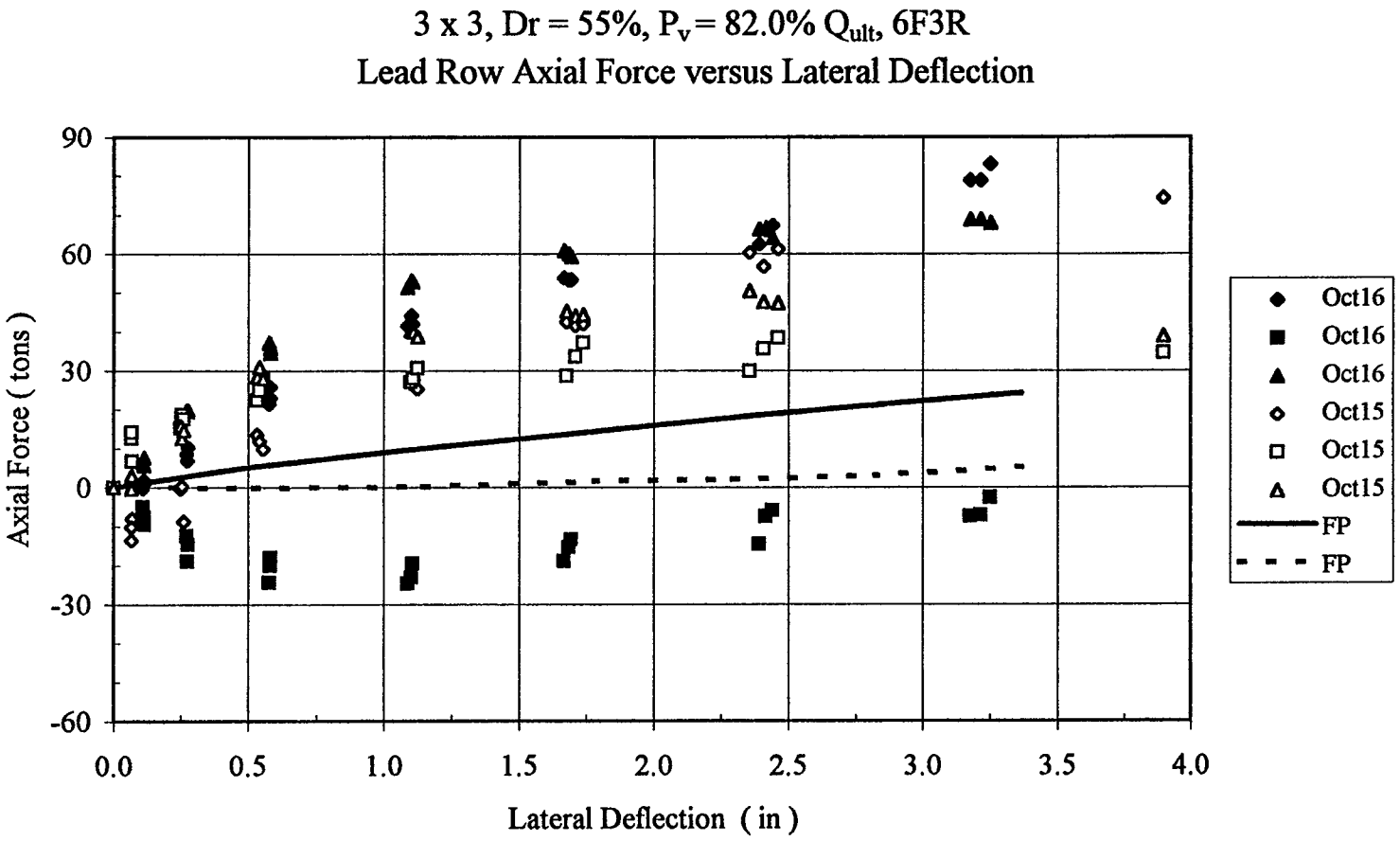

Figure B-102 Lead Row Axial Force versus Lateral Deflection

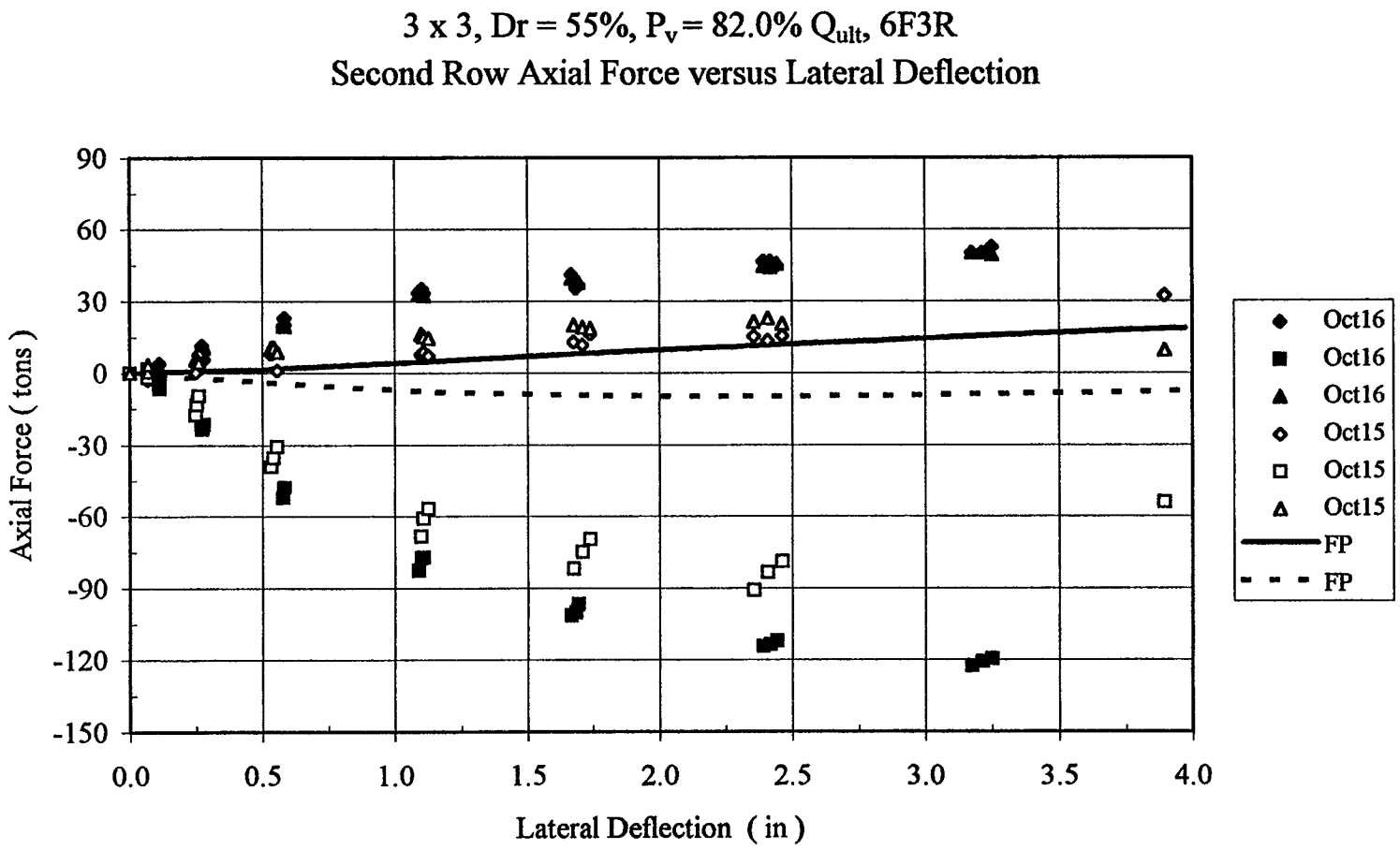

Figure B-103 Second Row Axial Force versus Lateral Deflection

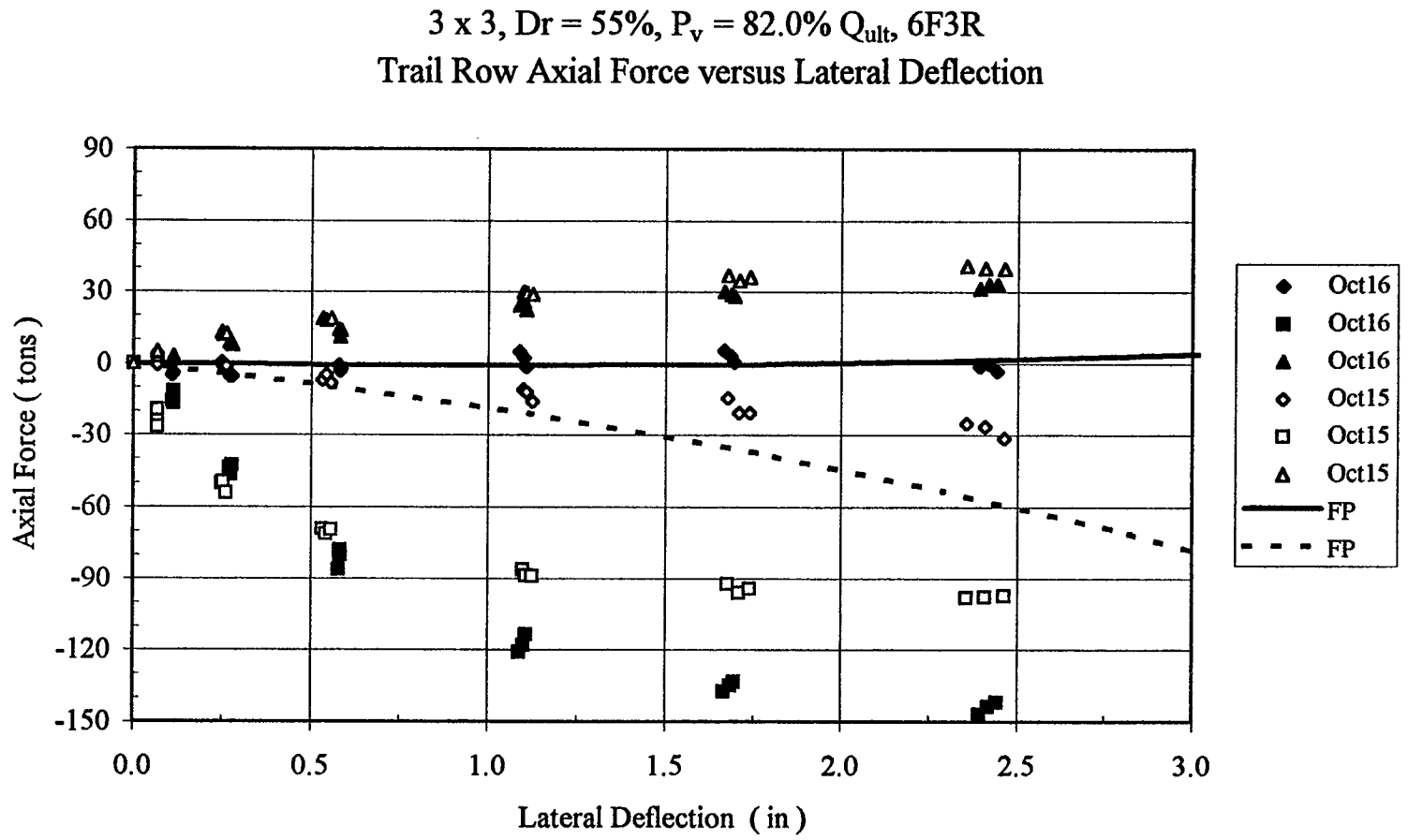

Figure B-104 Trail Row Axial Force versus Lateral Deflection

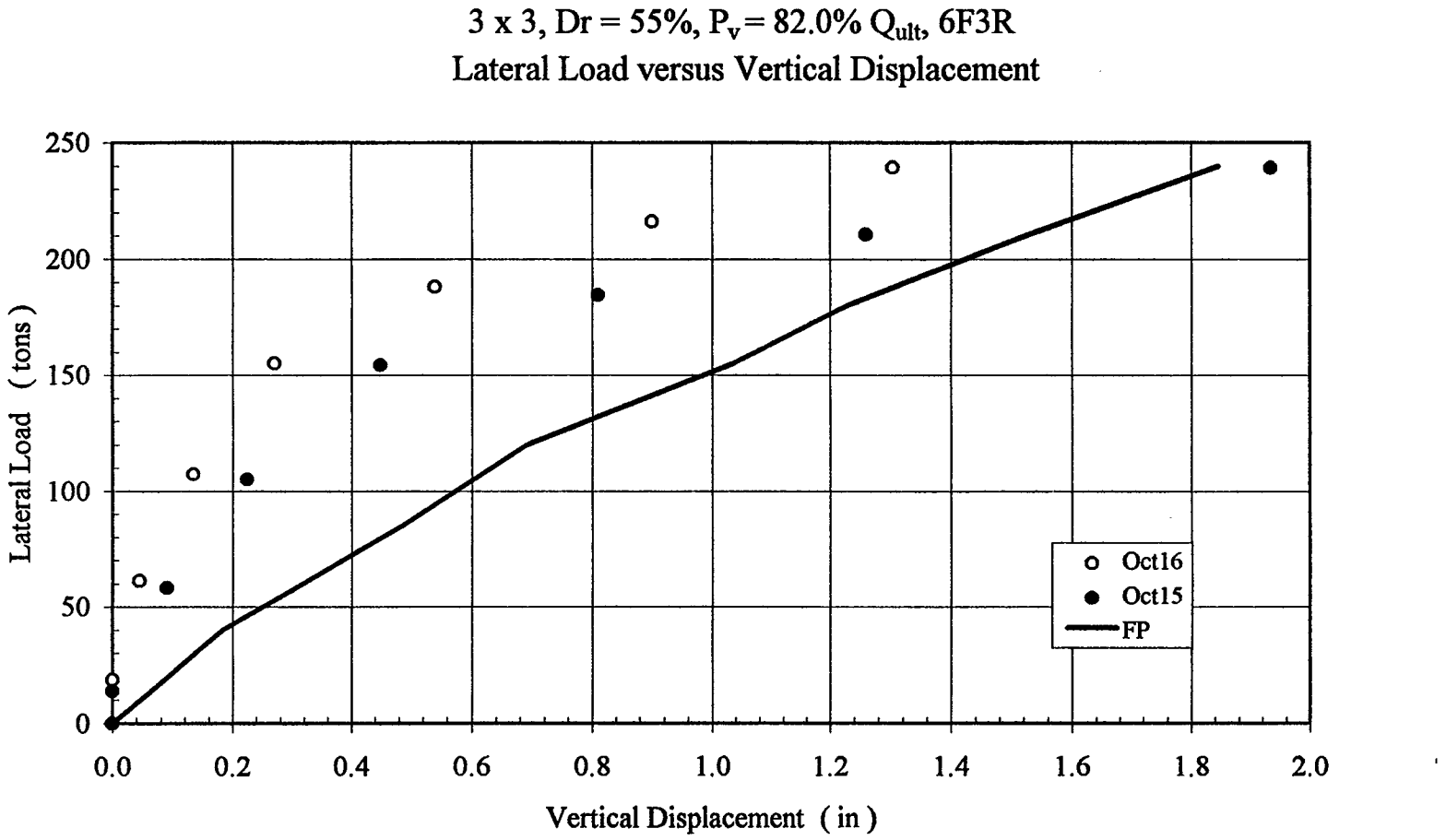

Figure B-105
Lateral Load versus Vertical Displacement

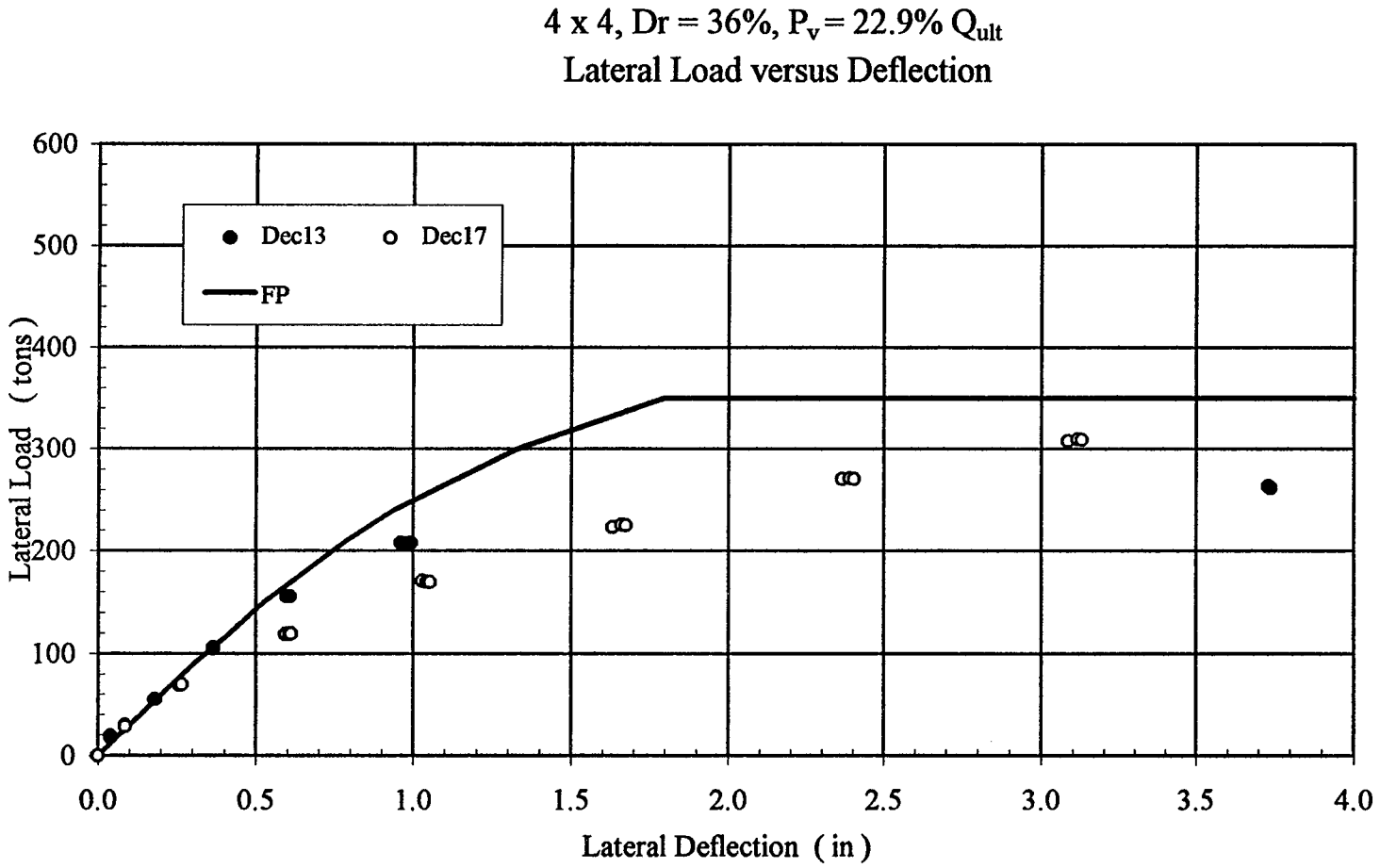

Figure B-106 Lateral Load versus Deflection

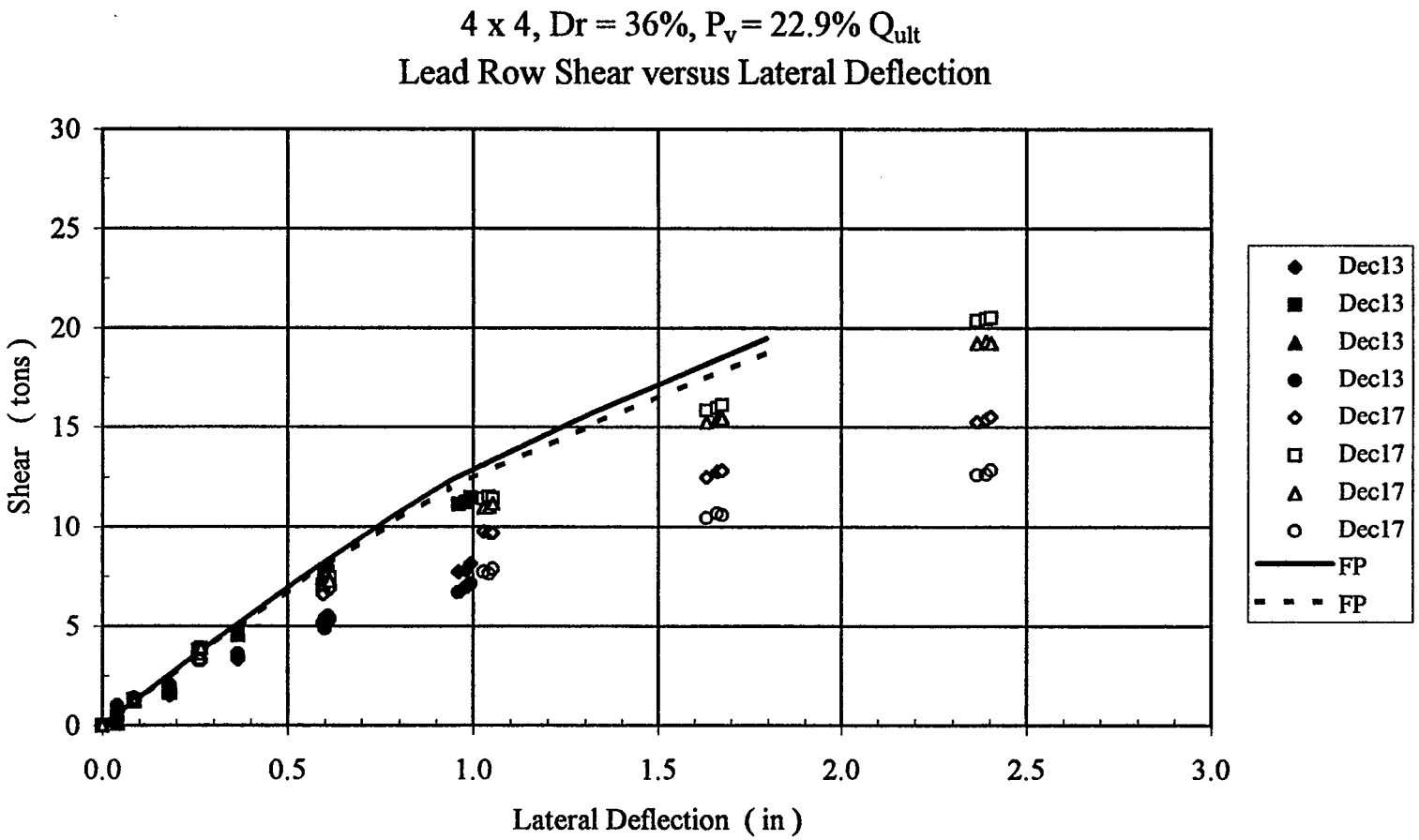

Figure B-107 Lead Row Shear versus Lateral Deflection

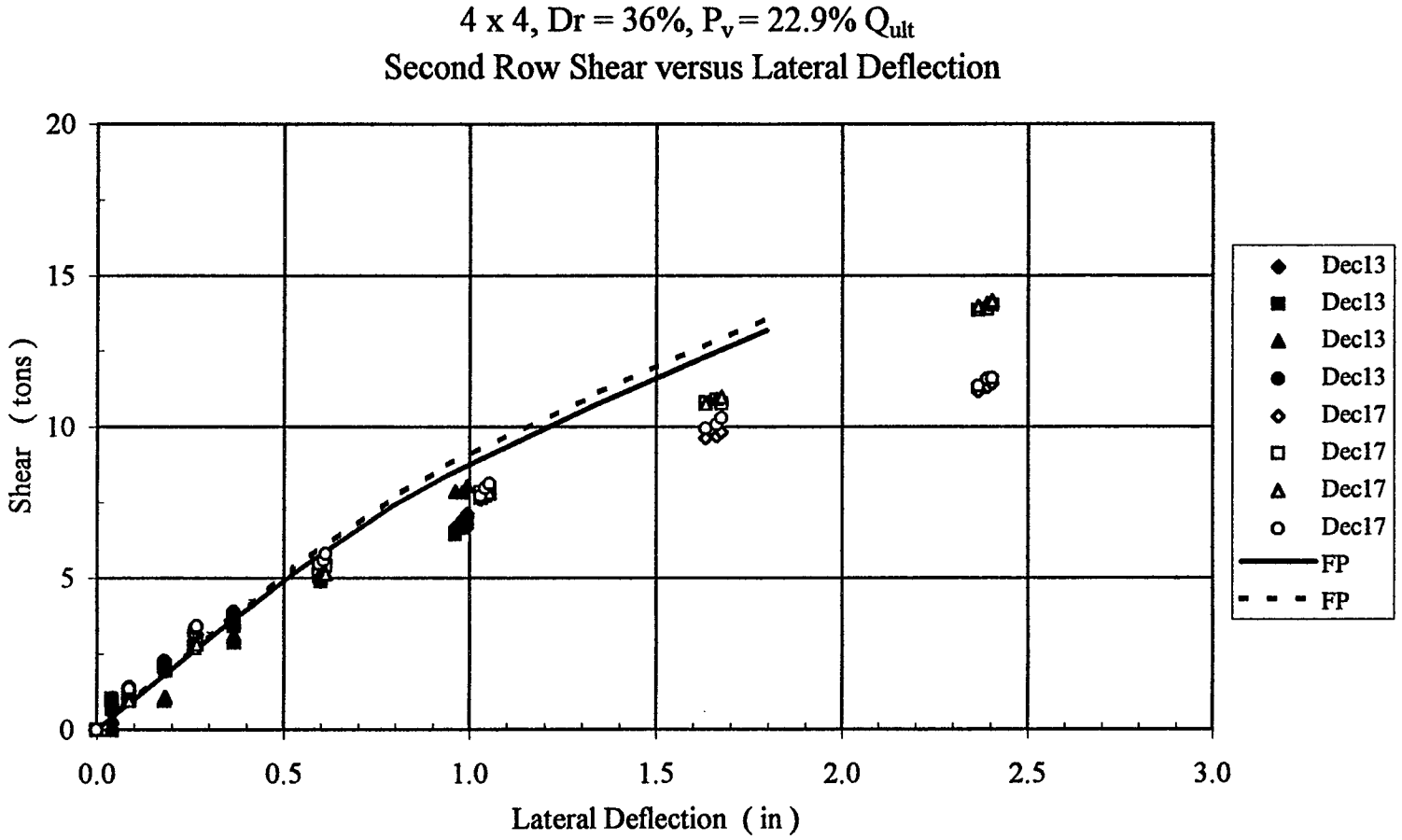

Figure B-108 Second Row Shear versus Lateral Deflection

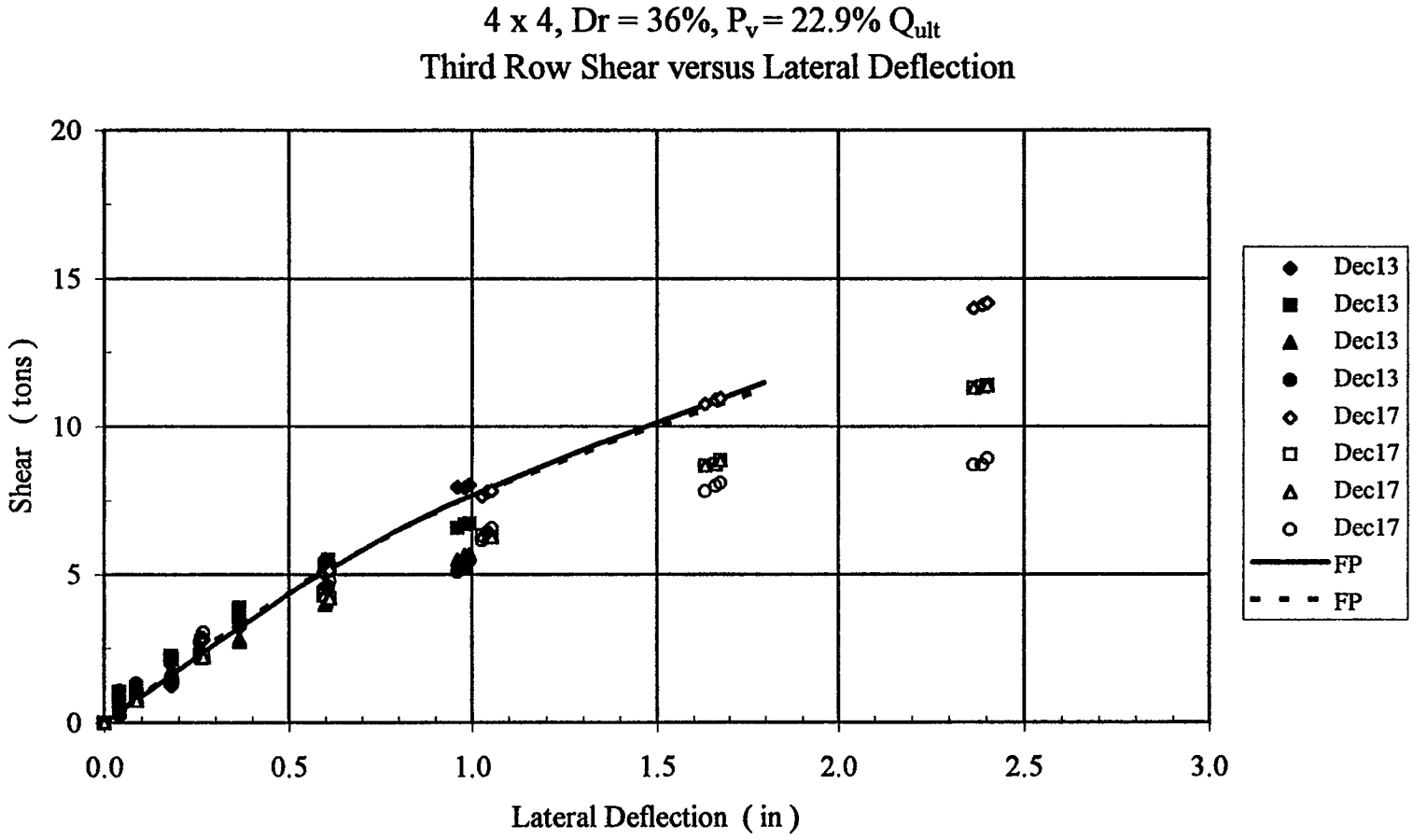

Figure B-109 Third Row Shear versus Lateral Deflection

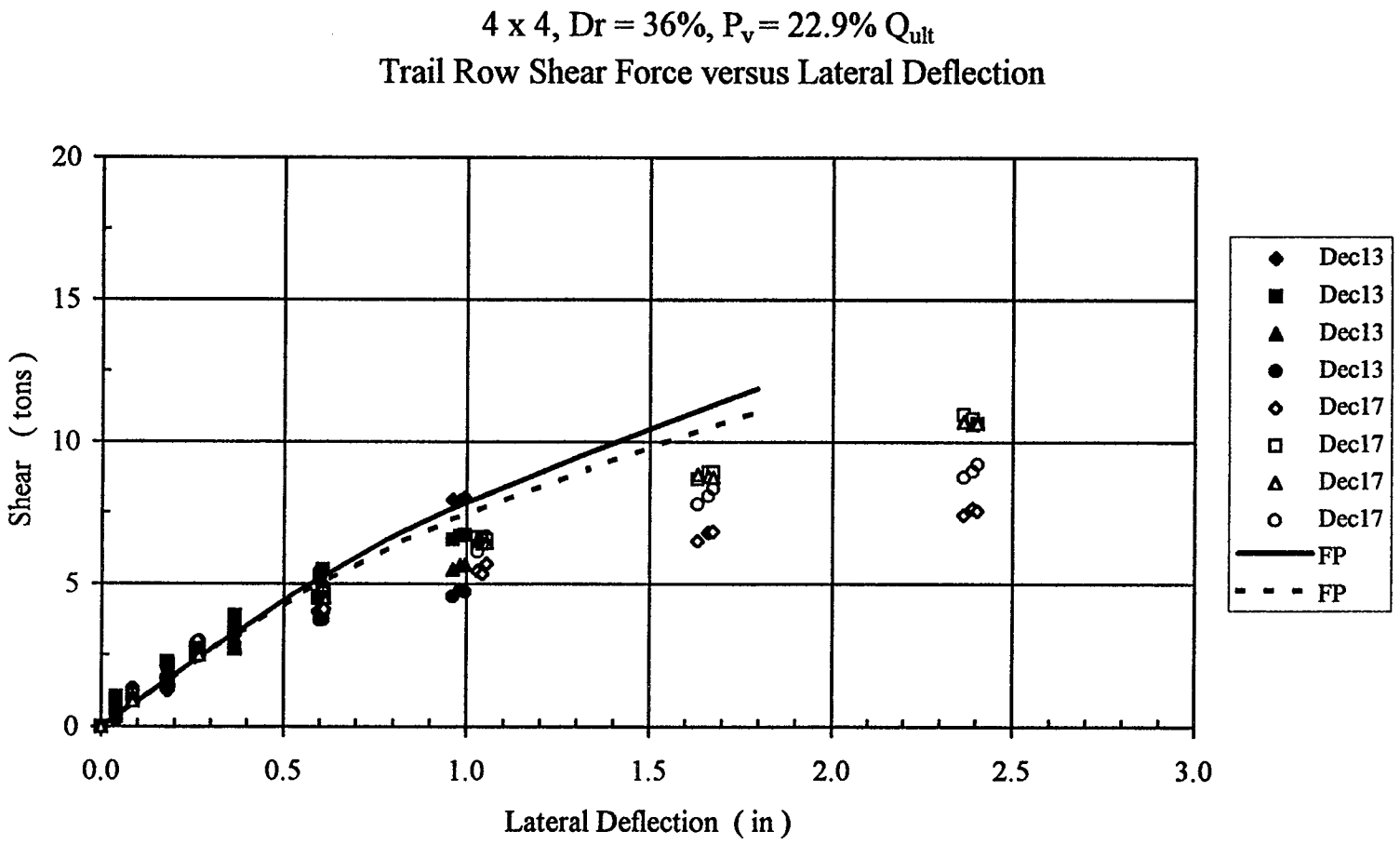

Figure B-110 Trail Row Shear versus Lateral Deflection

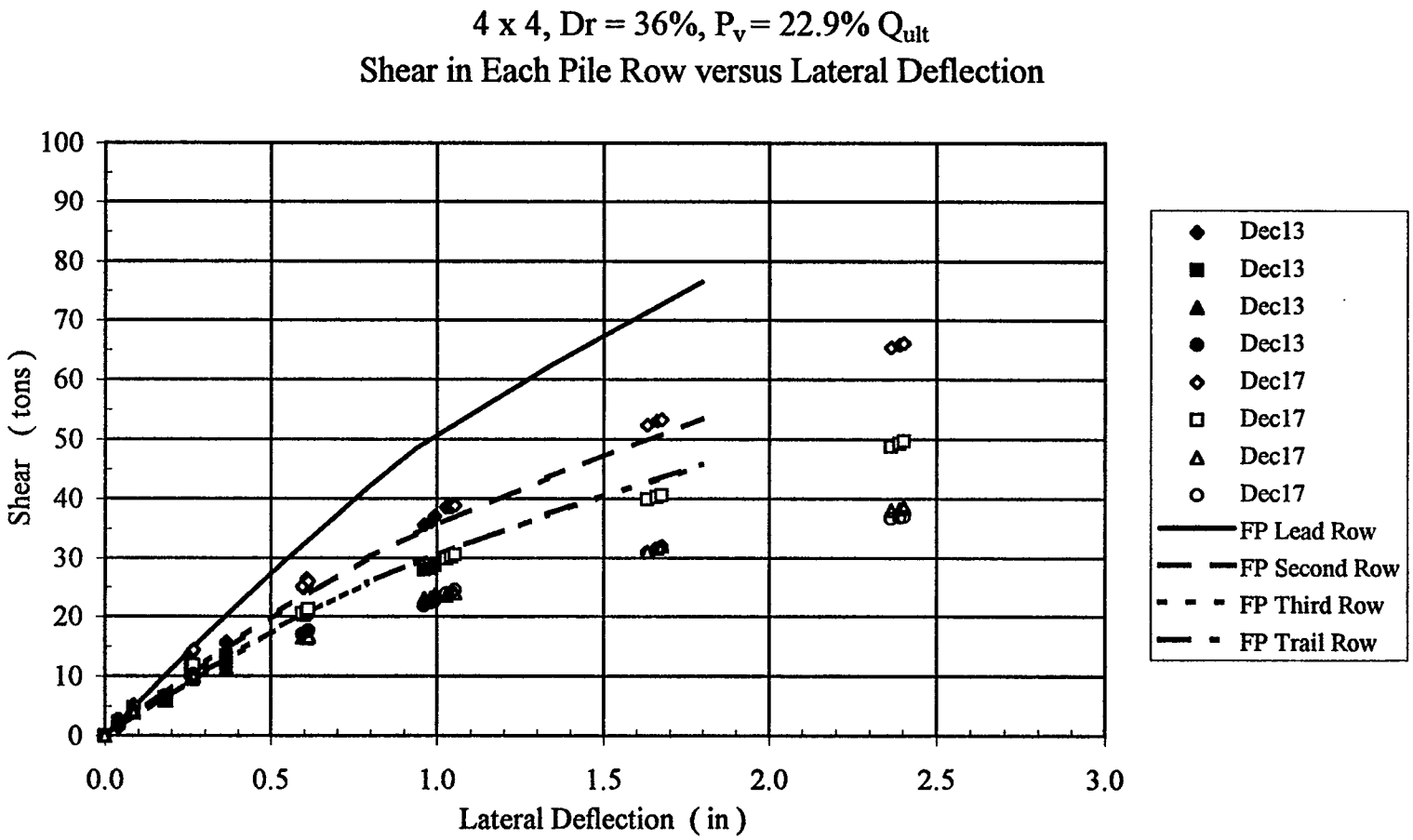

Figure B-111 Shear in Each PIle Row versus Lateral Deflection

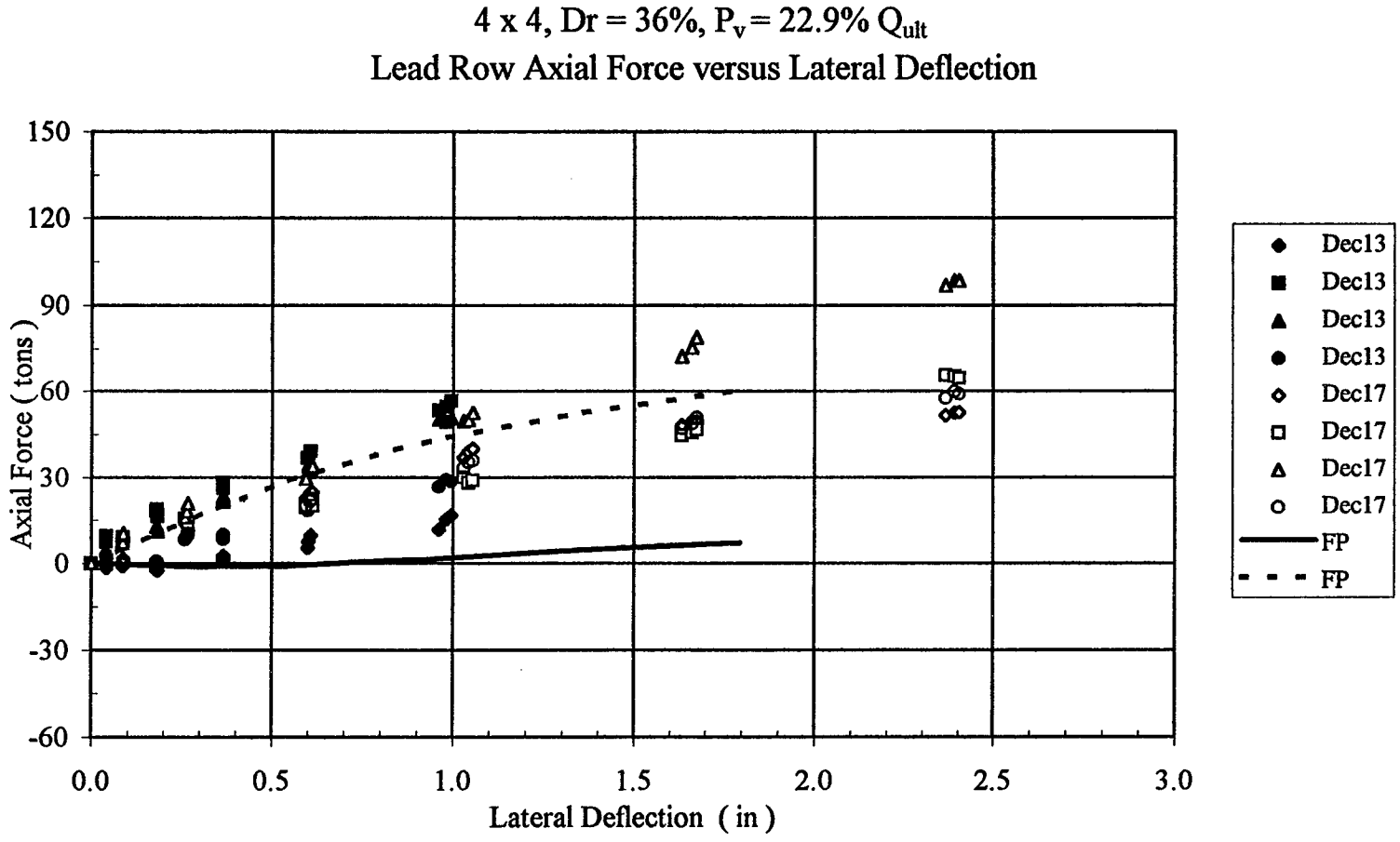

Figure B-112 Lead Row Axial Force versus Lateral Deflection

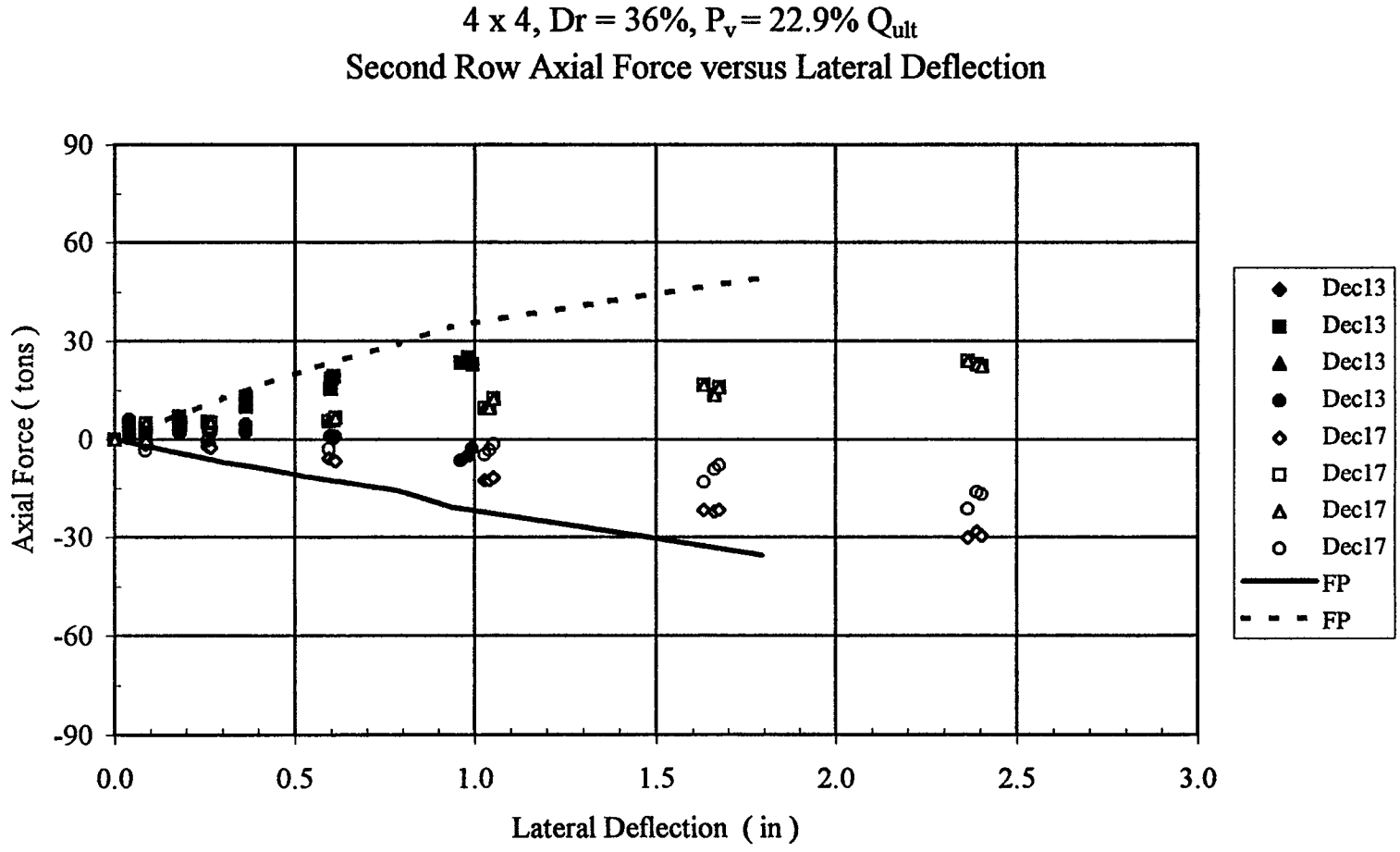

Figure B-113 Second Row Axial Force versus Lateral Deflection

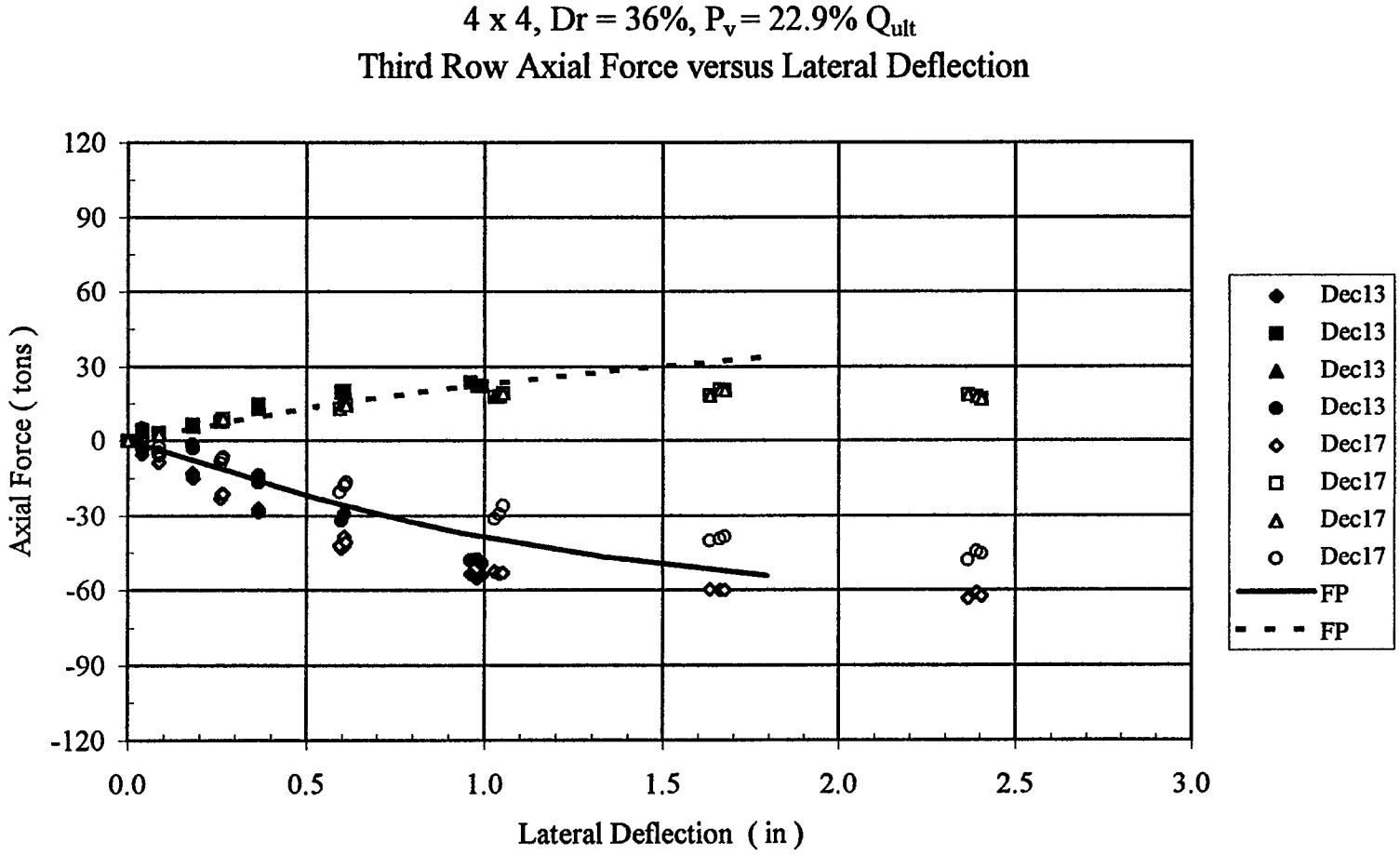

Figure B-114 Third Row Axial Force versus Lateral Deflection

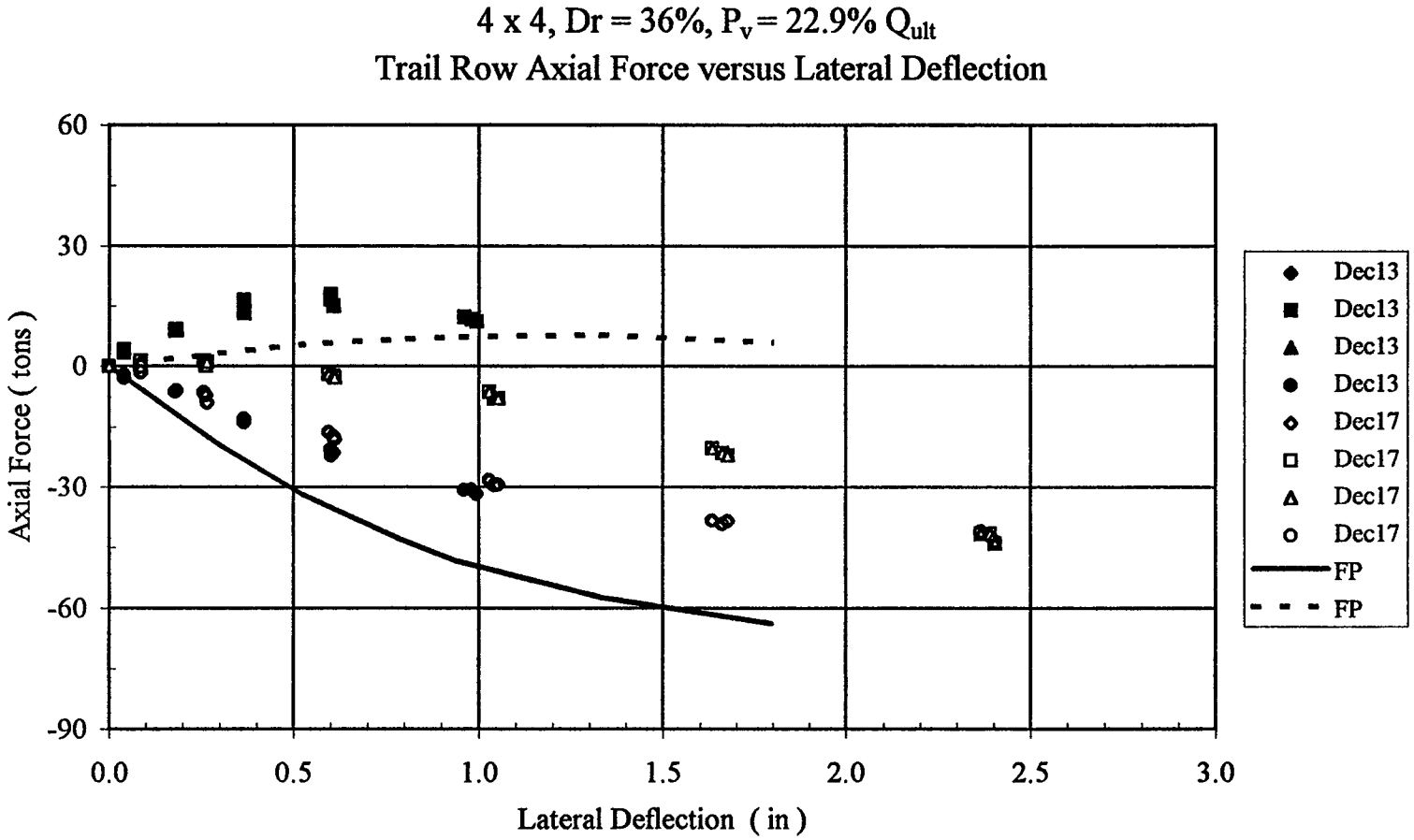

Figure B-115 Trail Row Axial Force versus Lateral Deflection

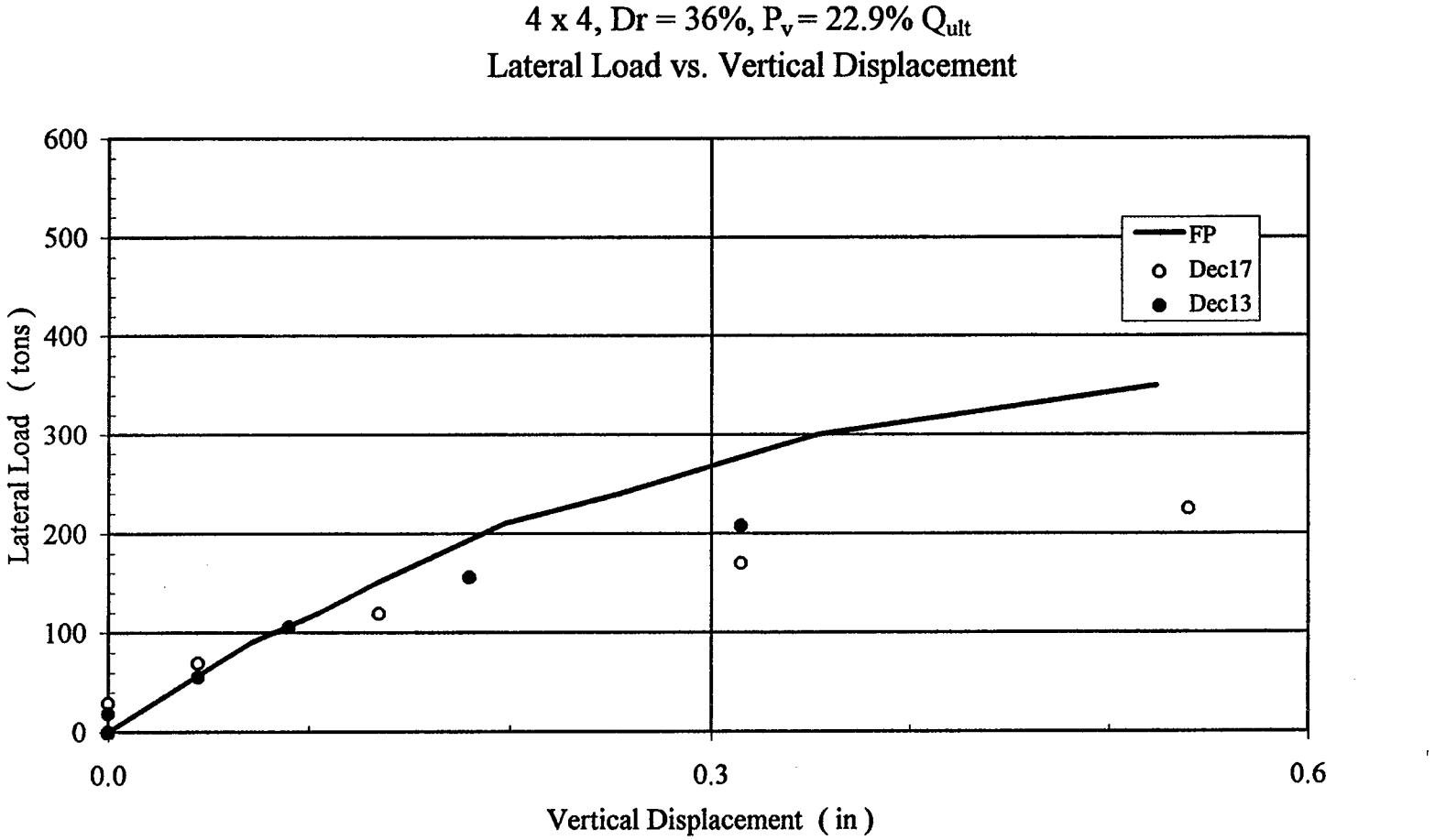

Figure B-116 Lateral Load versus Vertical Displacement

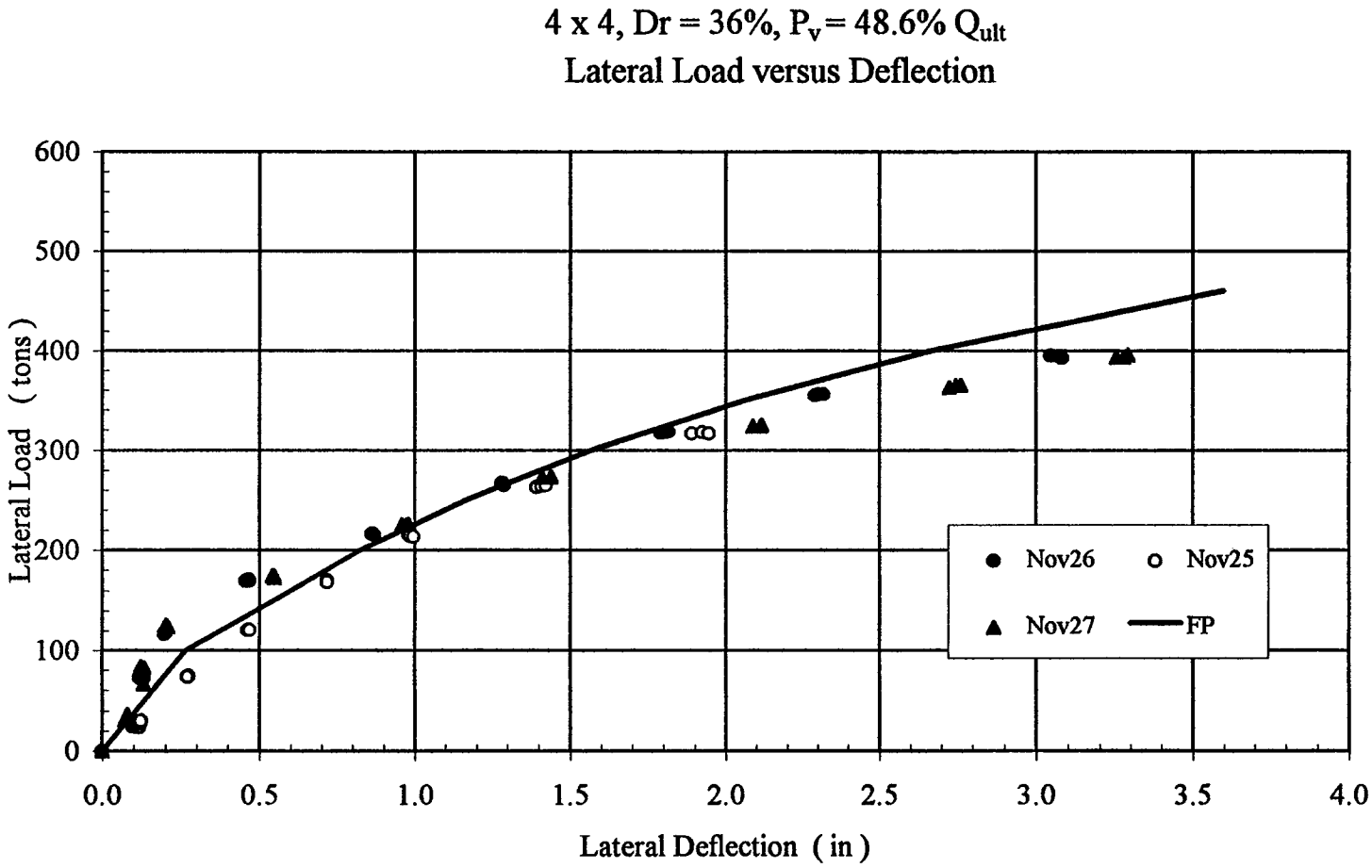

Figure B-117 Lateral Load versus Deflection

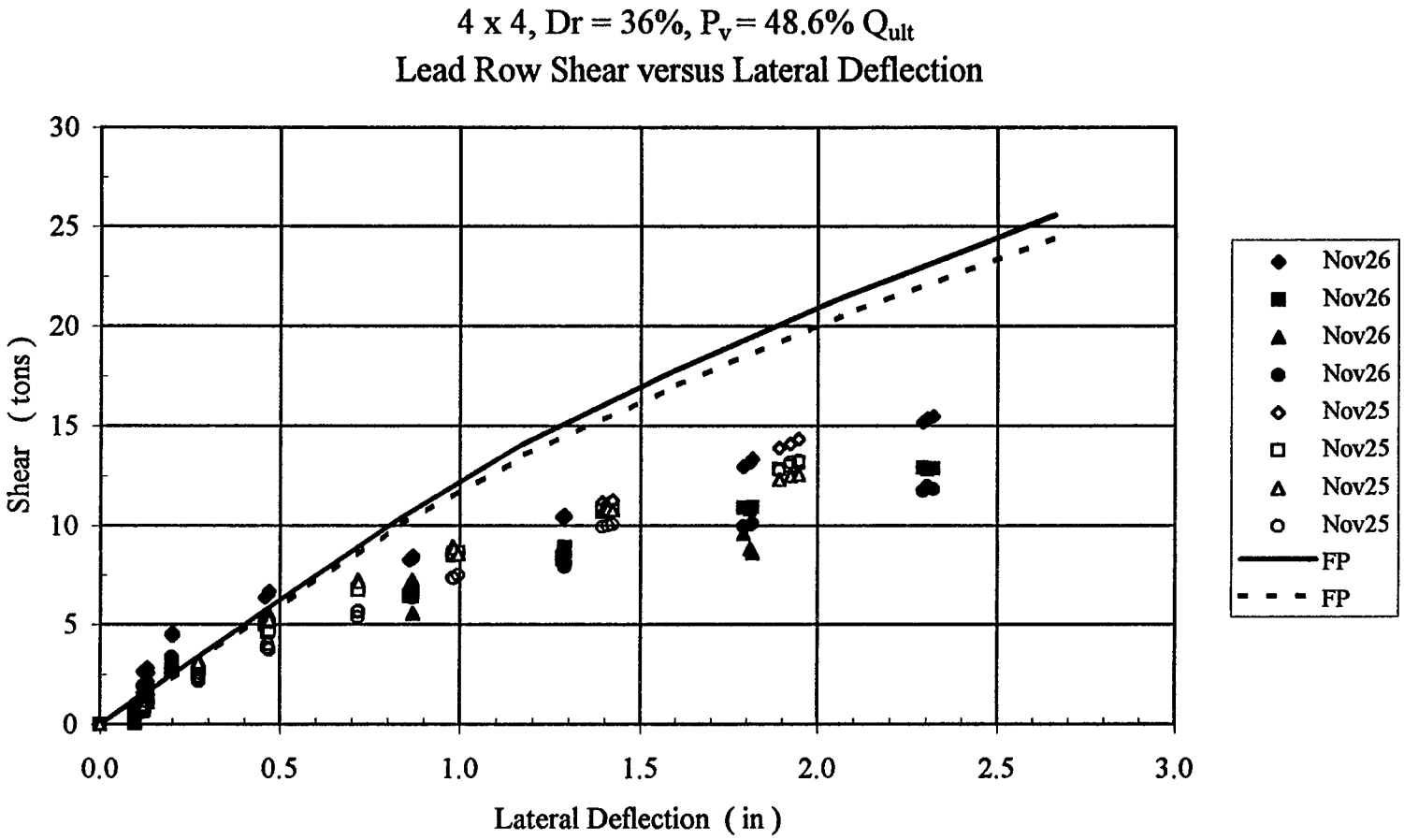

Figure B-118 Lead Row Shear versus Lateral Deflection

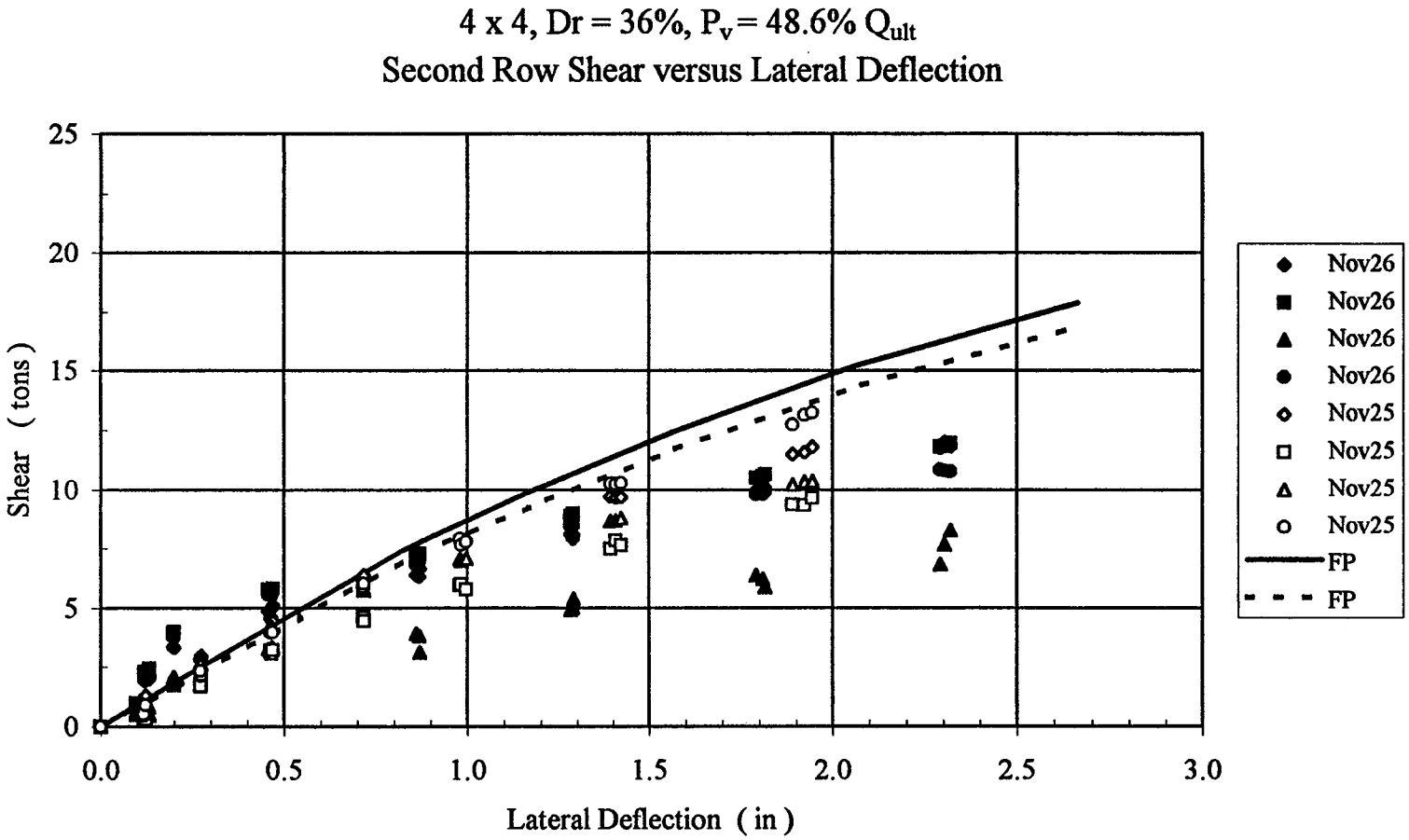

Figure B-119 Second Row Shear versus Lateral Deflection

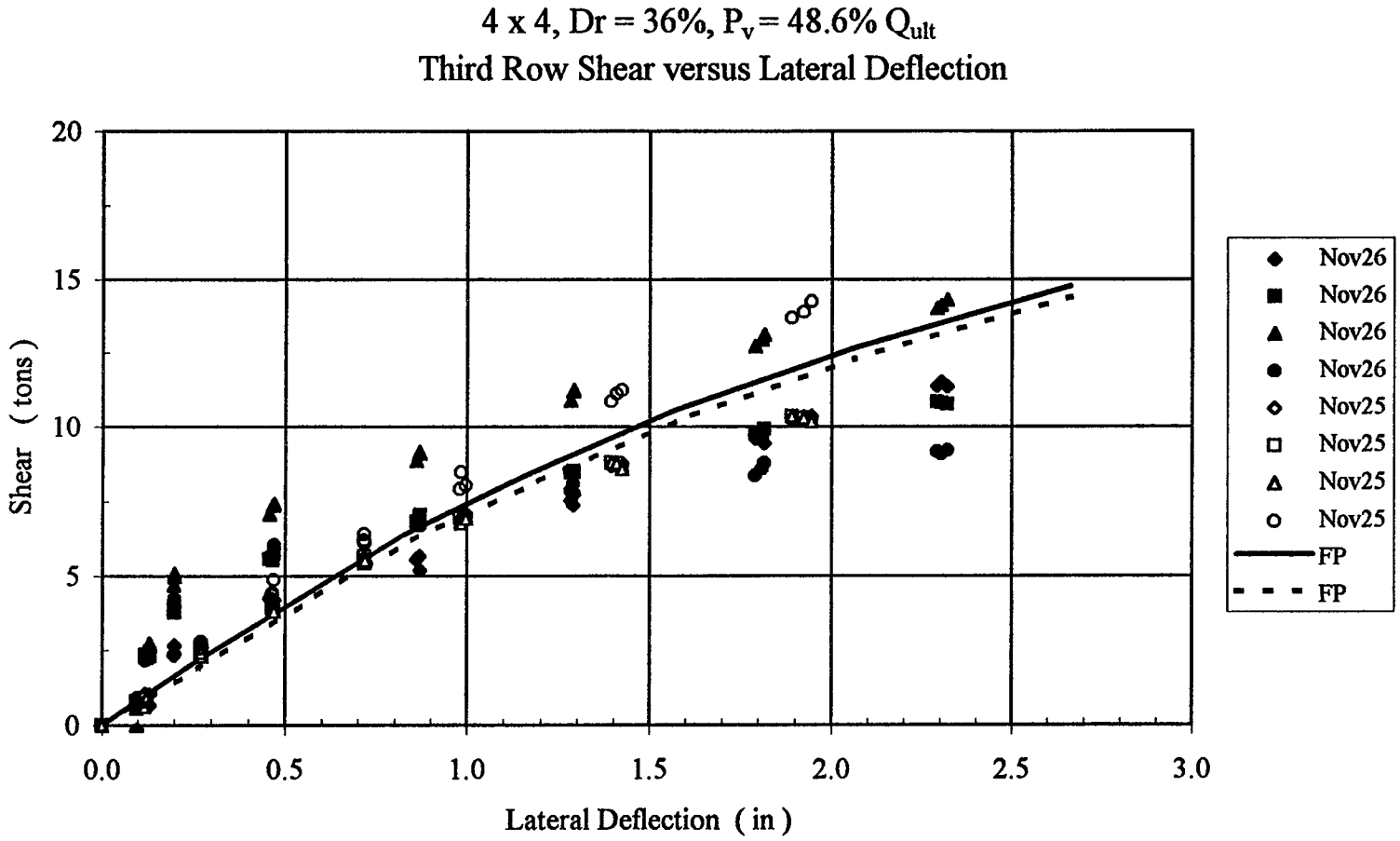

Figure B-120 Third Row Shear versus Lateral Deflection

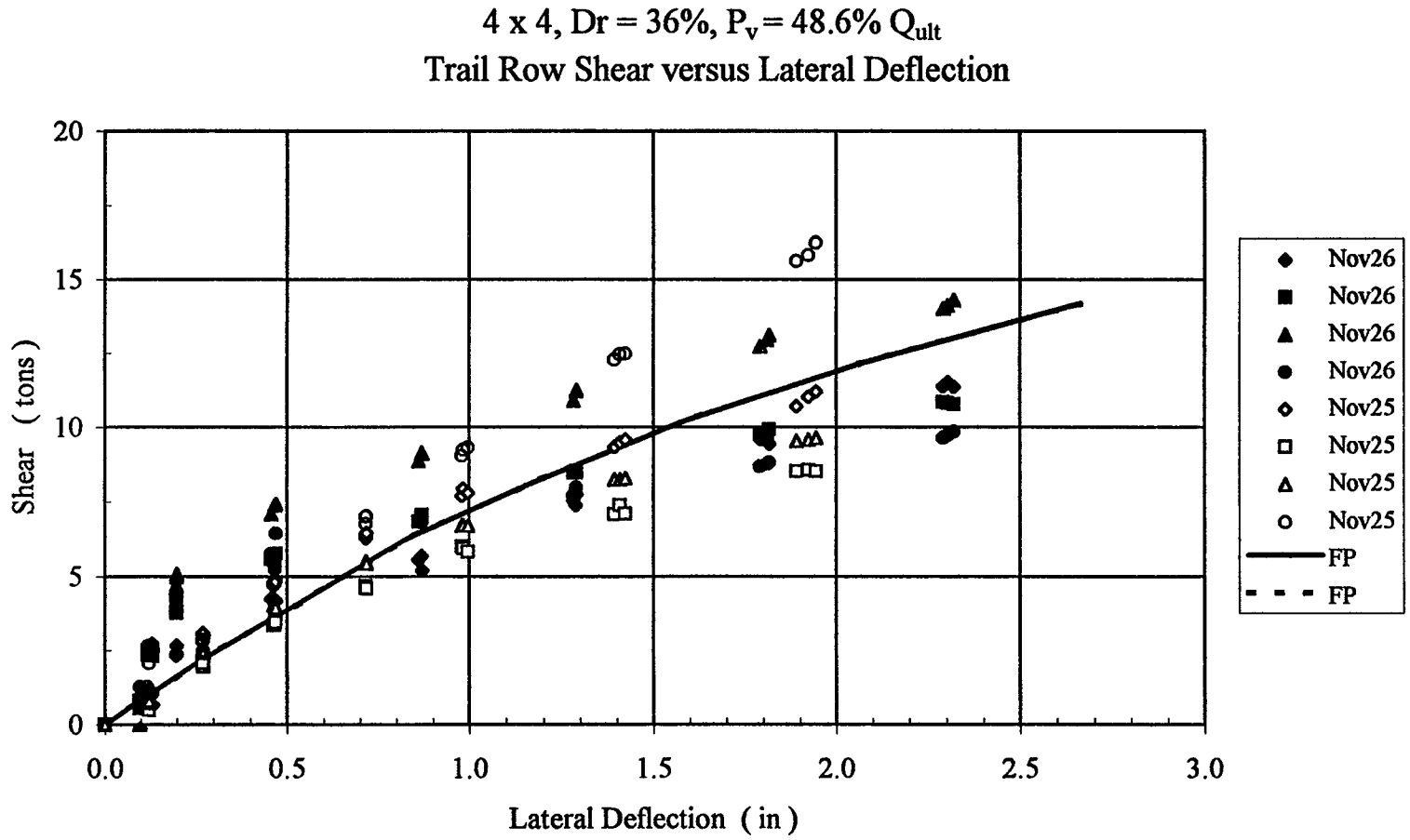

Figure B-121 Trail Row Shear versus Lateral Deflection

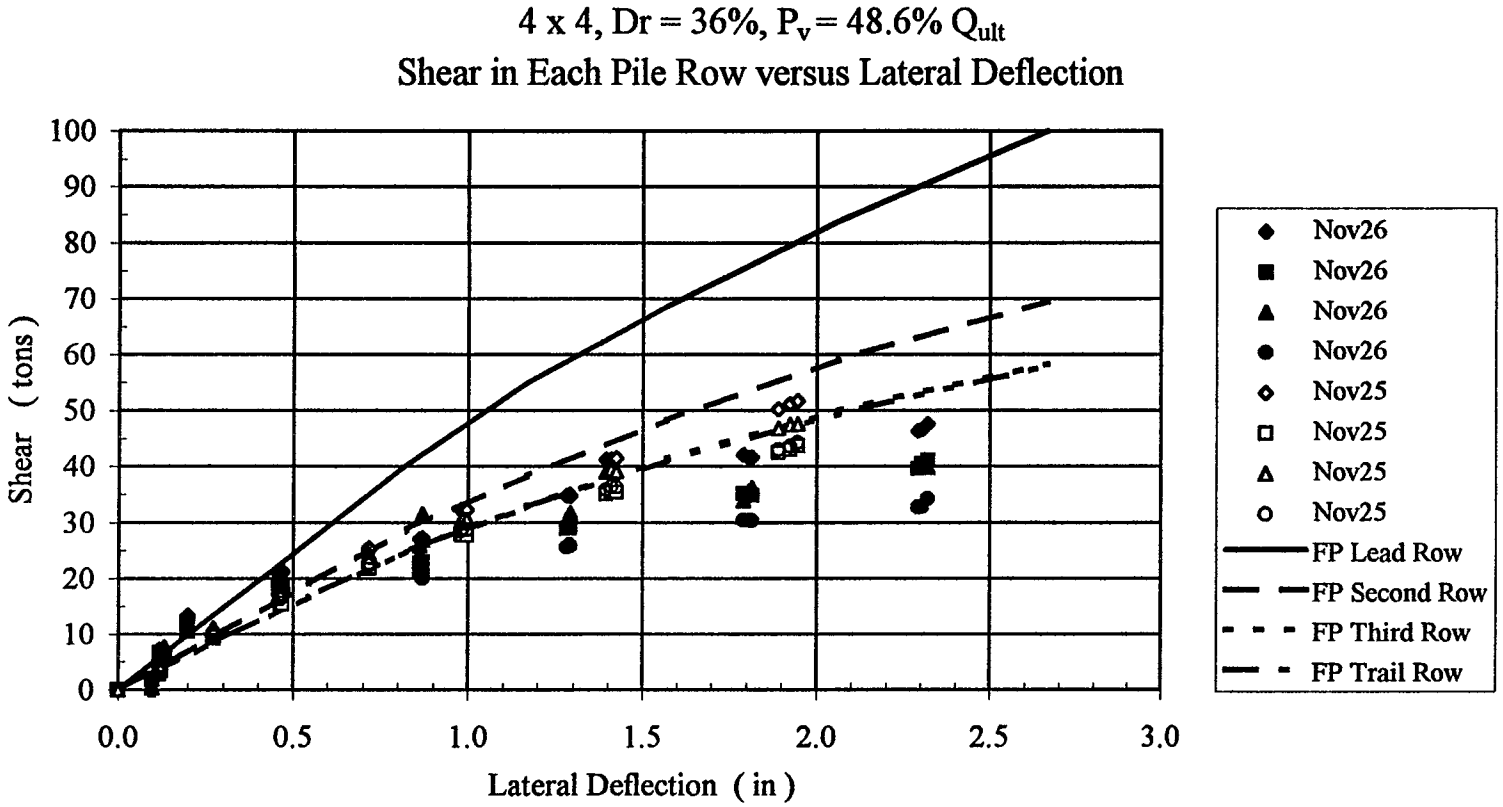

Figure B-122 Shear in Each Pile Row versus Lateral Deflection

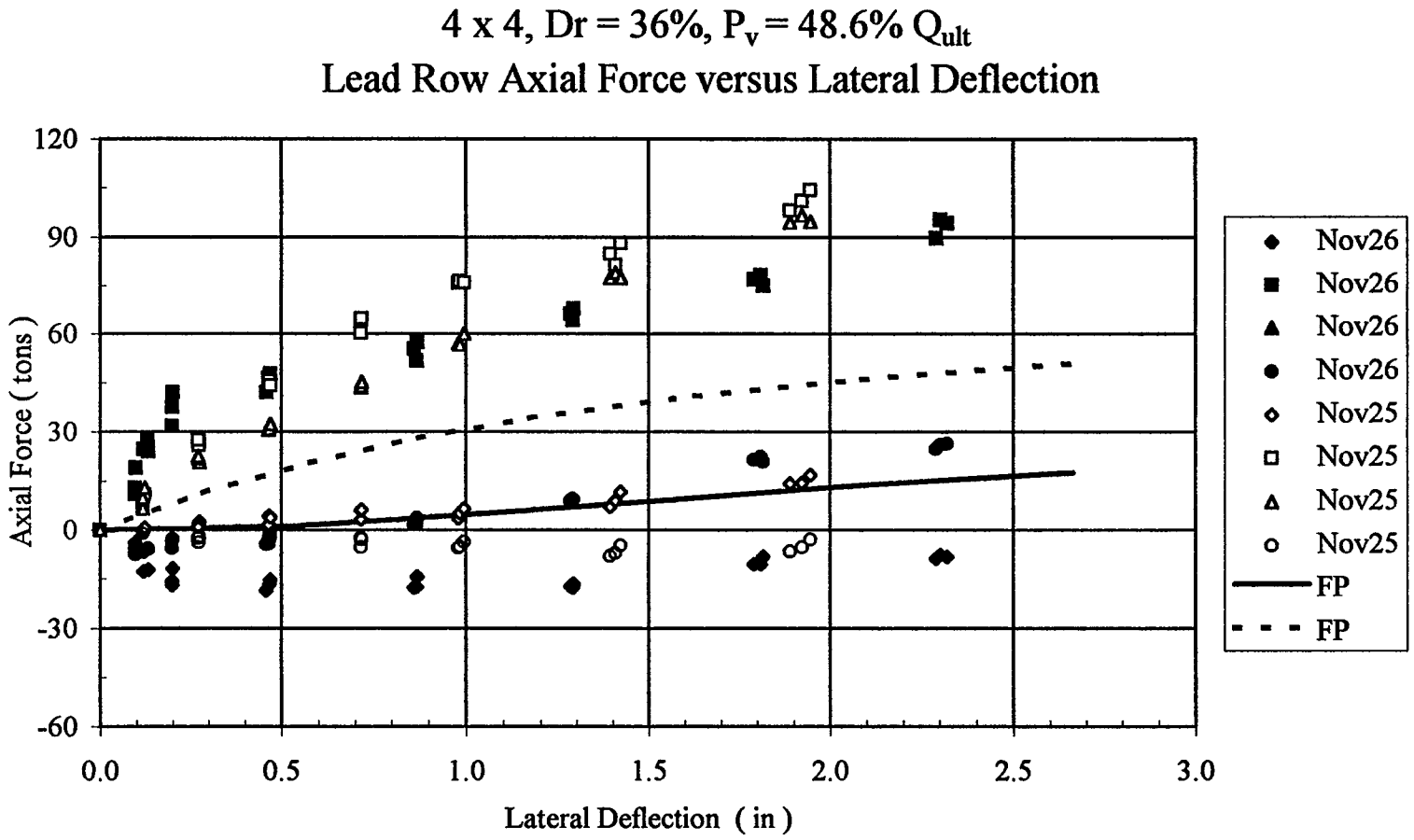

Figure B-123 Lead Row Axial Force versus Lateral Deflection

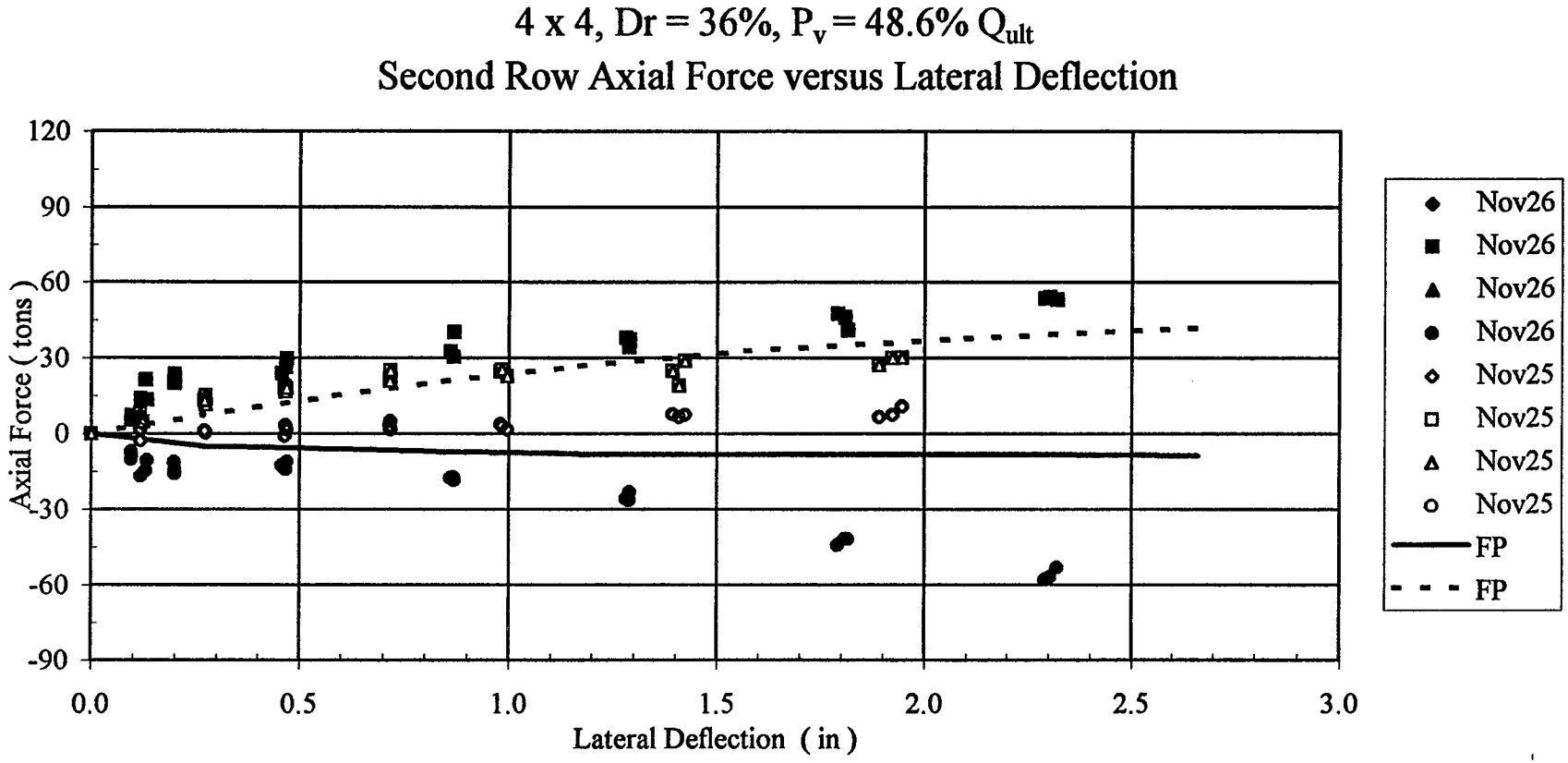

Figure B-124 Second Row Axial Force versus Lateral Deflection

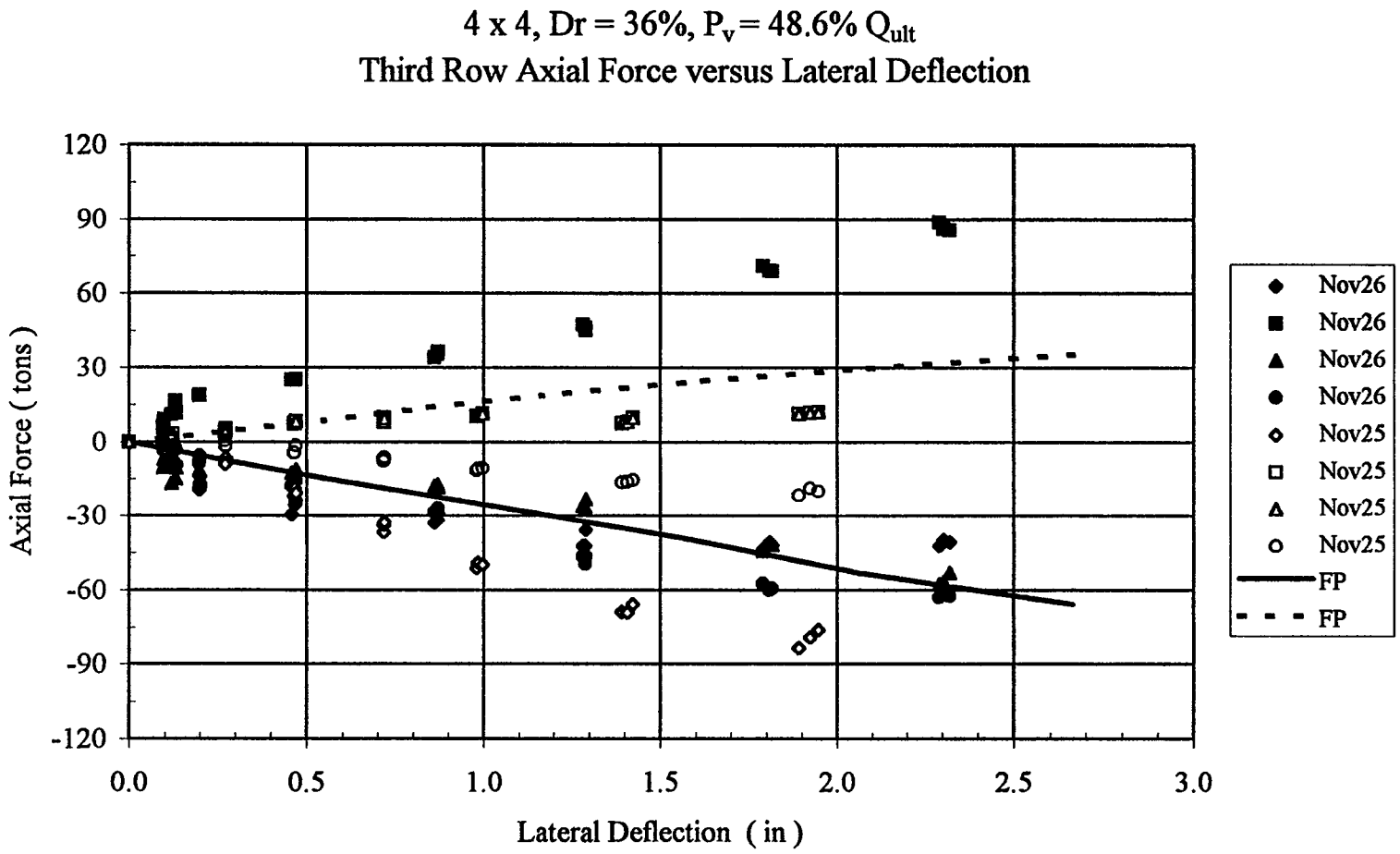

Figure B-125 Third Row Axial Force versus Lateral Deflection

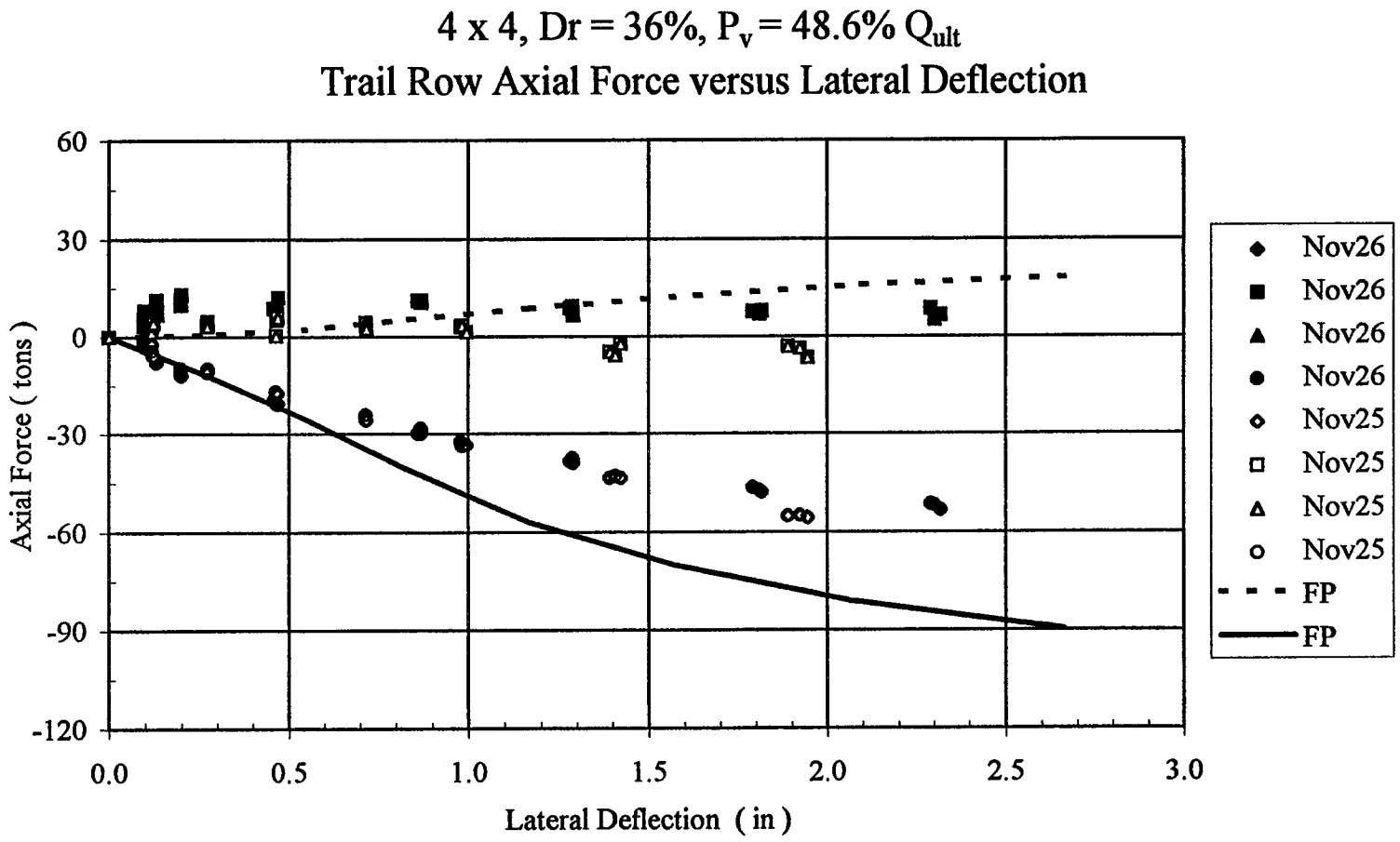

Figure B-126 Trail Row Axial Force versus Lateral Deflection

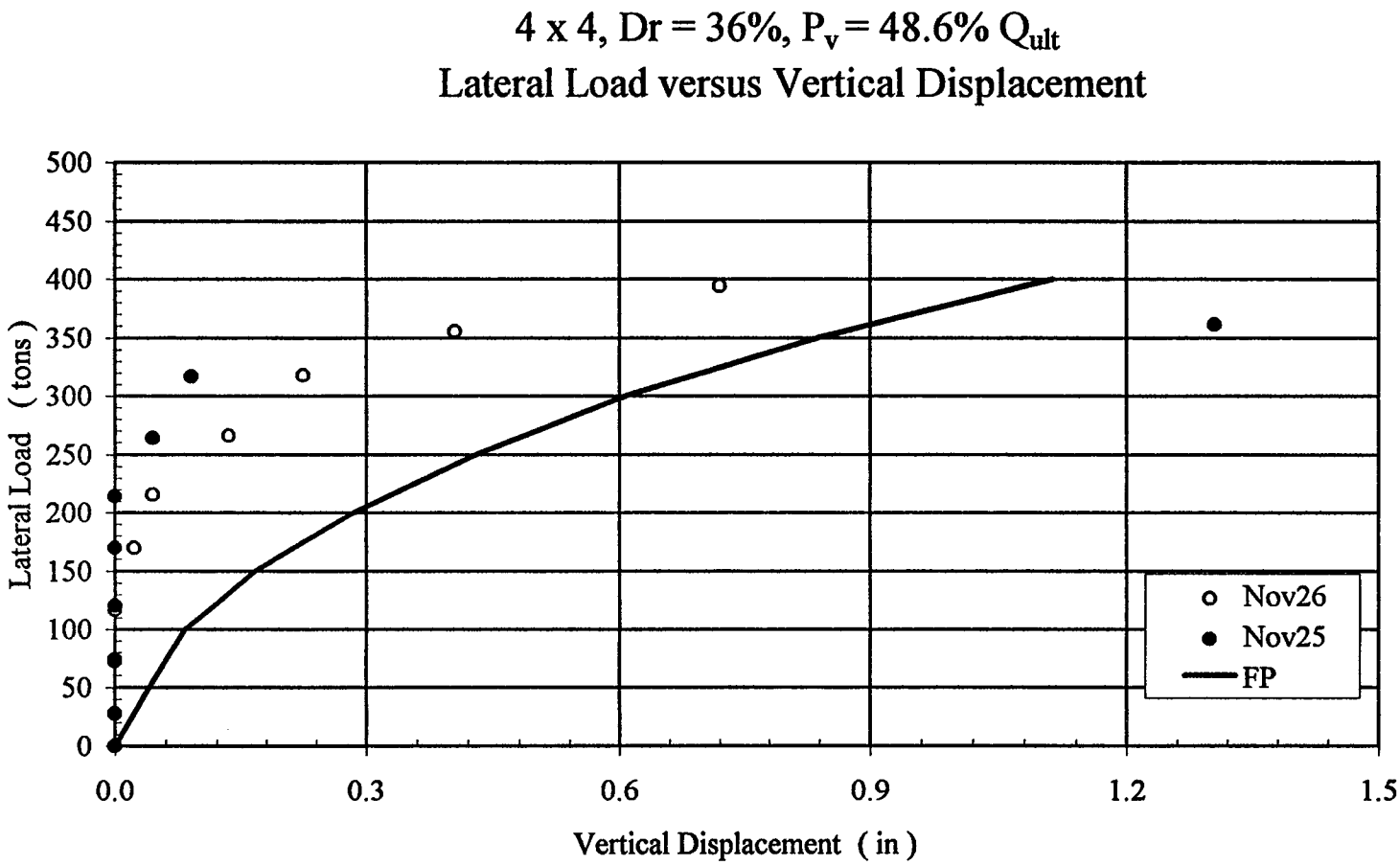

Figure B-127 Lateral Load versus Vertical Displacement

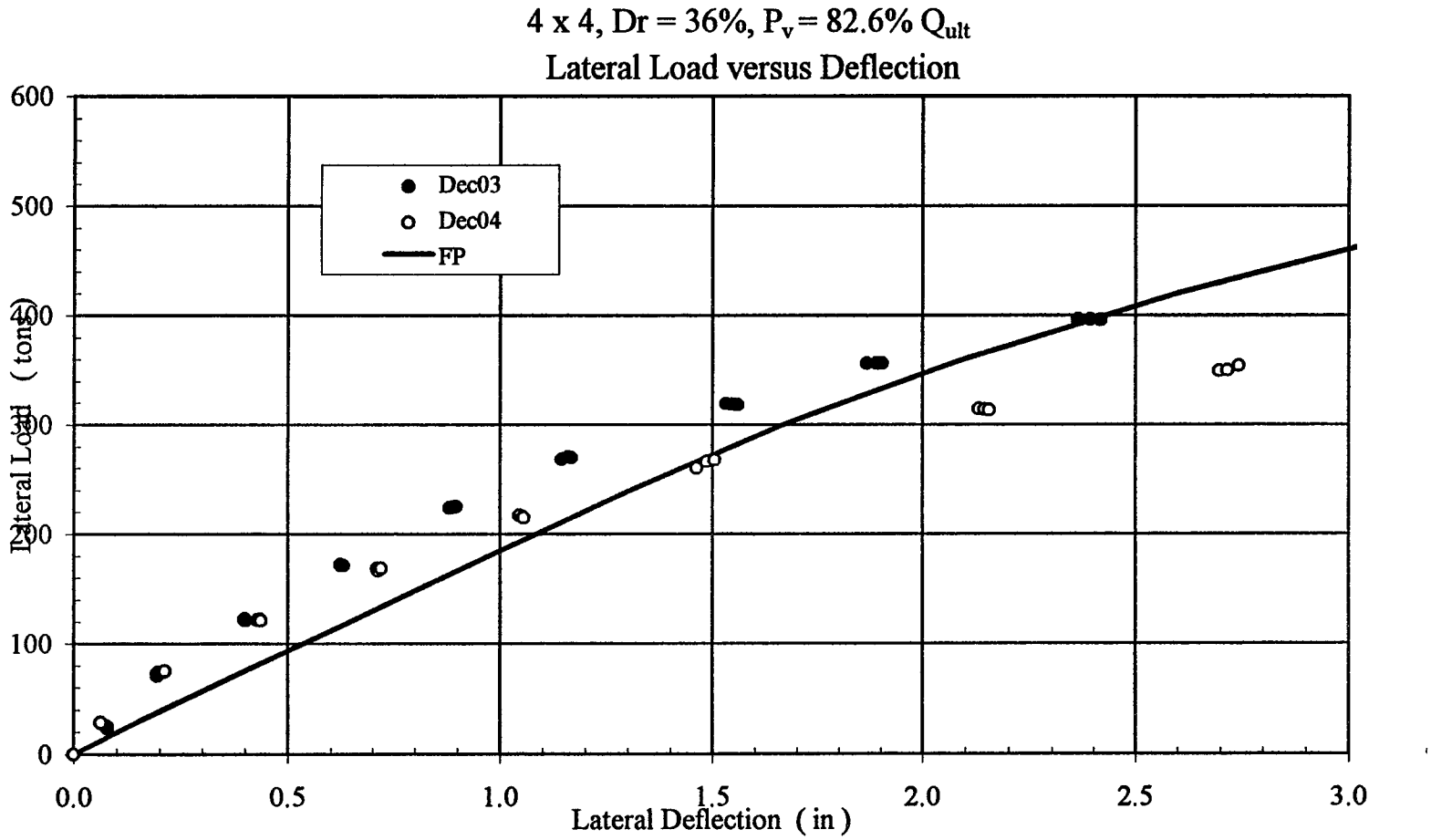

Figure B-128 Lateral Load versus Deflection

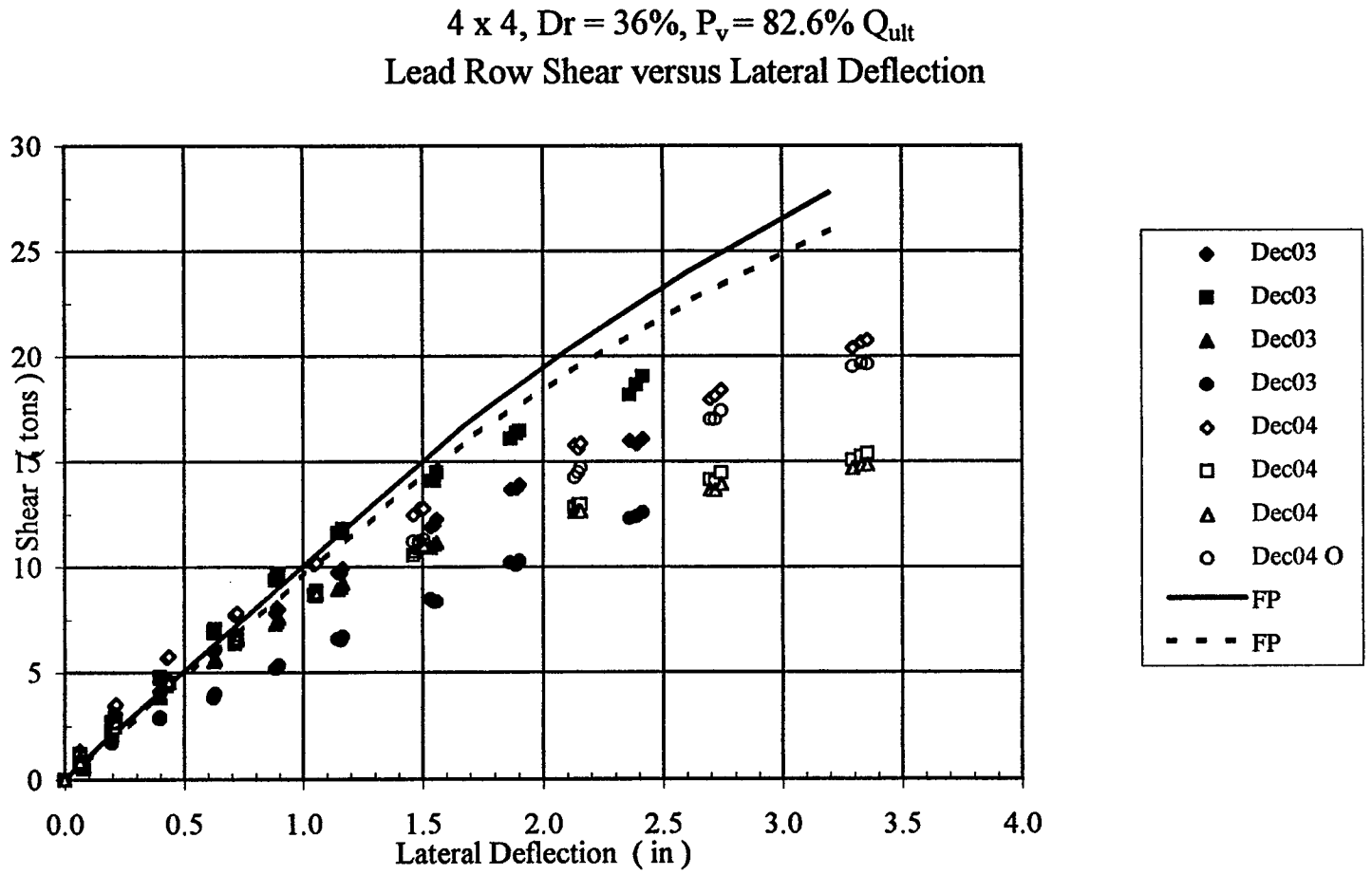

Figure B-129 Lead Row Shear versus Lateral Deflection

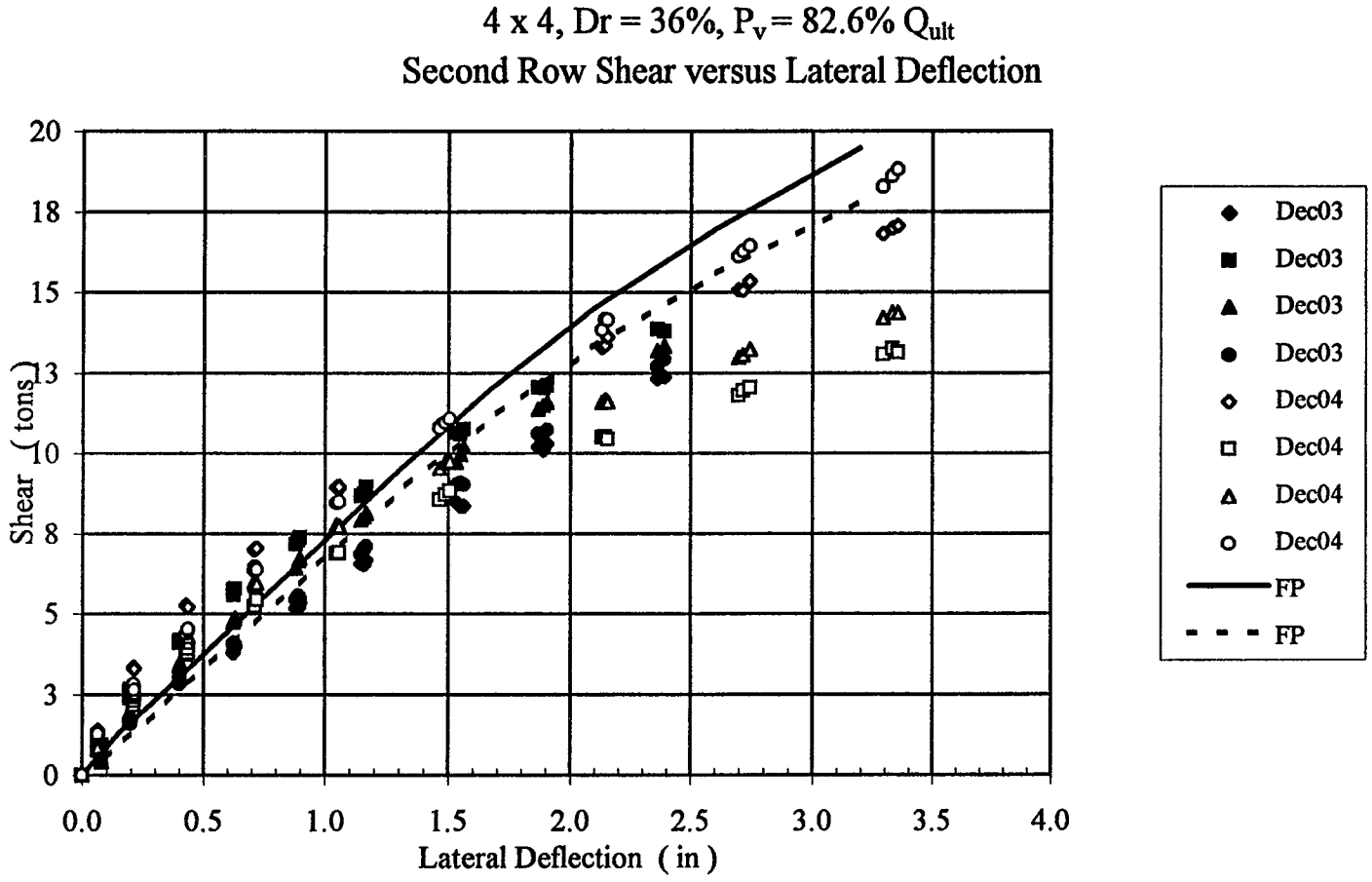

Figure B-130 Second Row Shear versus Lateral Deflection

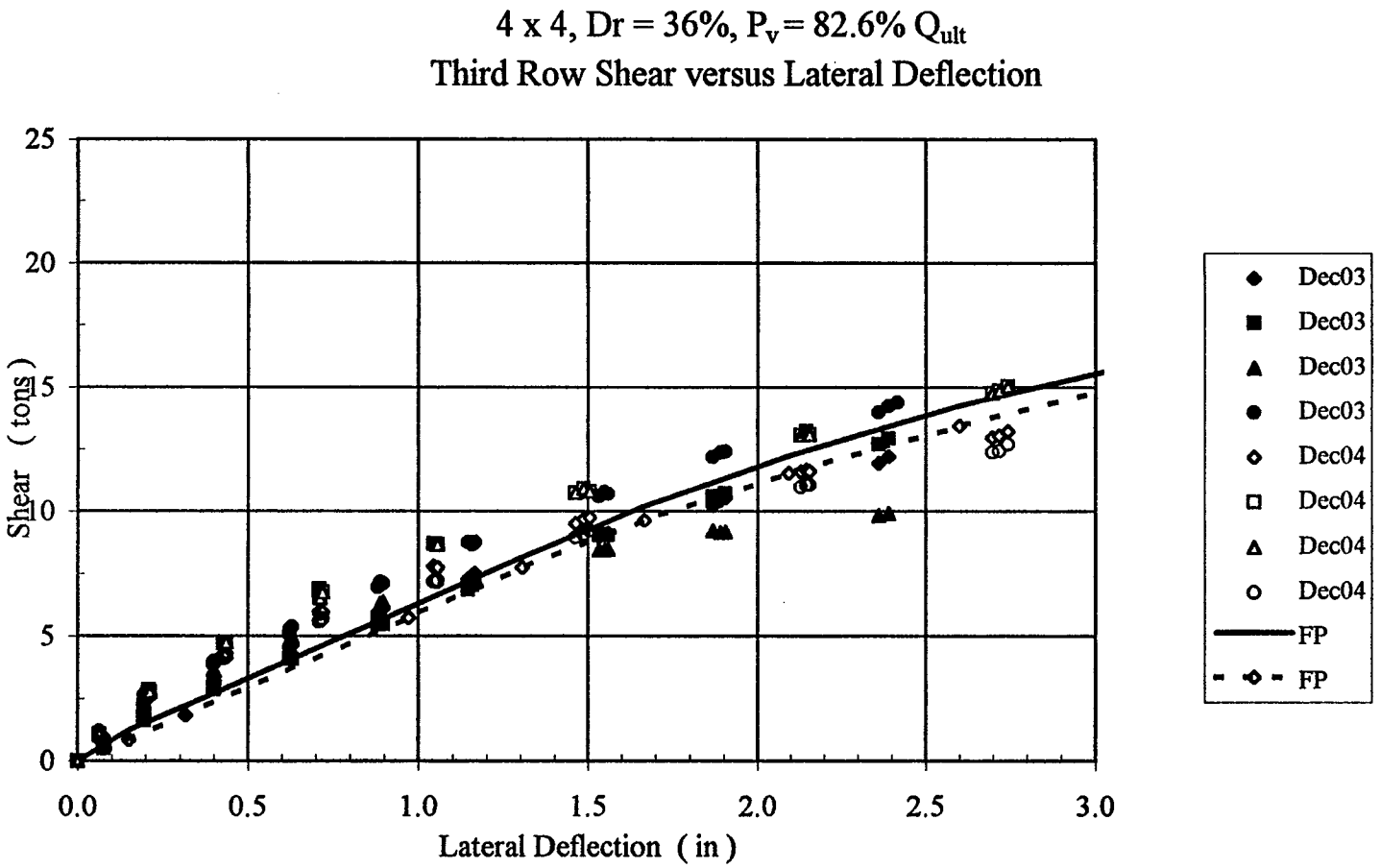

Figure B-131 Third Row Shear versus Lateral Deflection

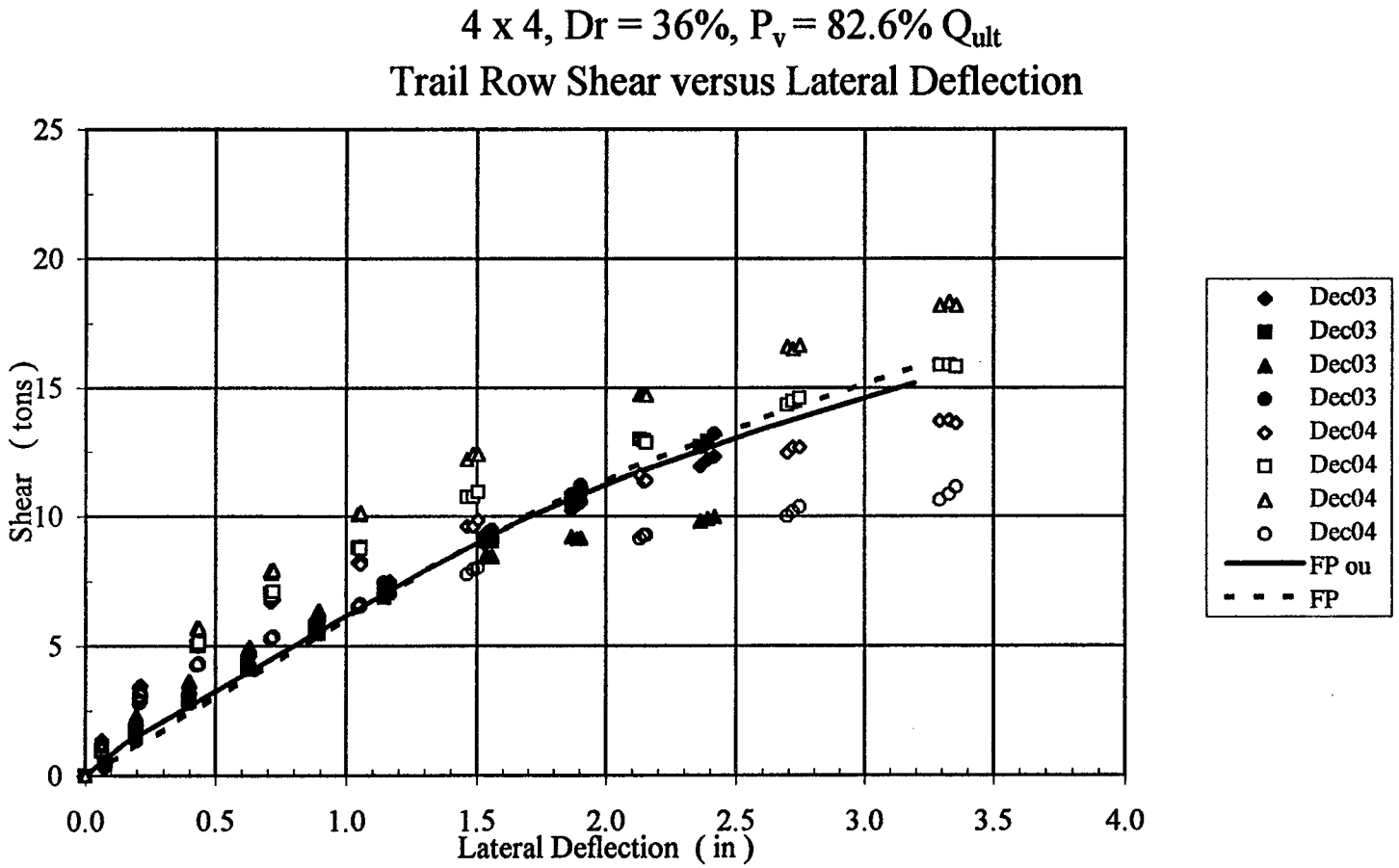

Figure B-132 Trail Row Shear versus Lateral Deflection

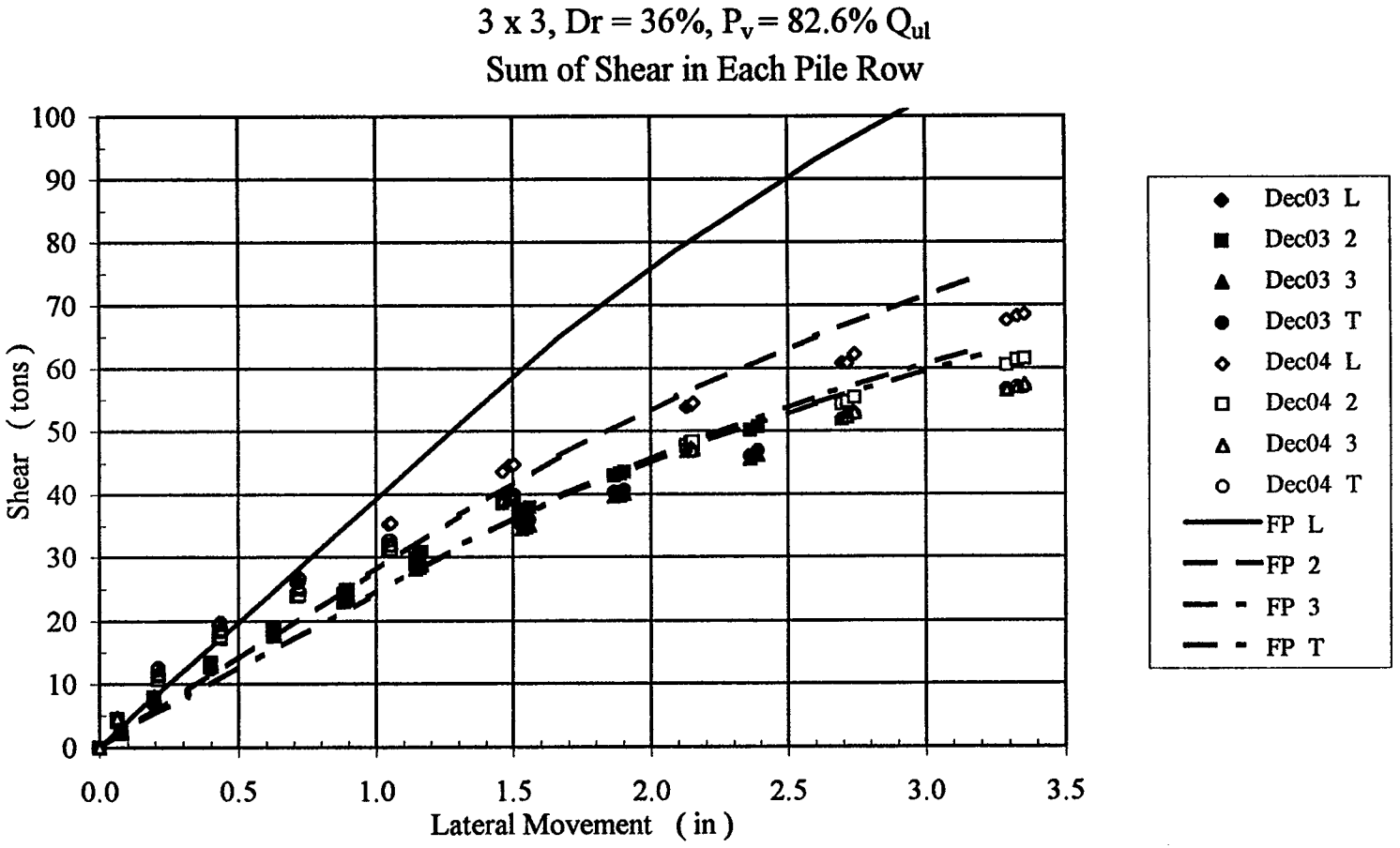

Figure B-133 Shear in Each Pile Row versus Lateral Deflection

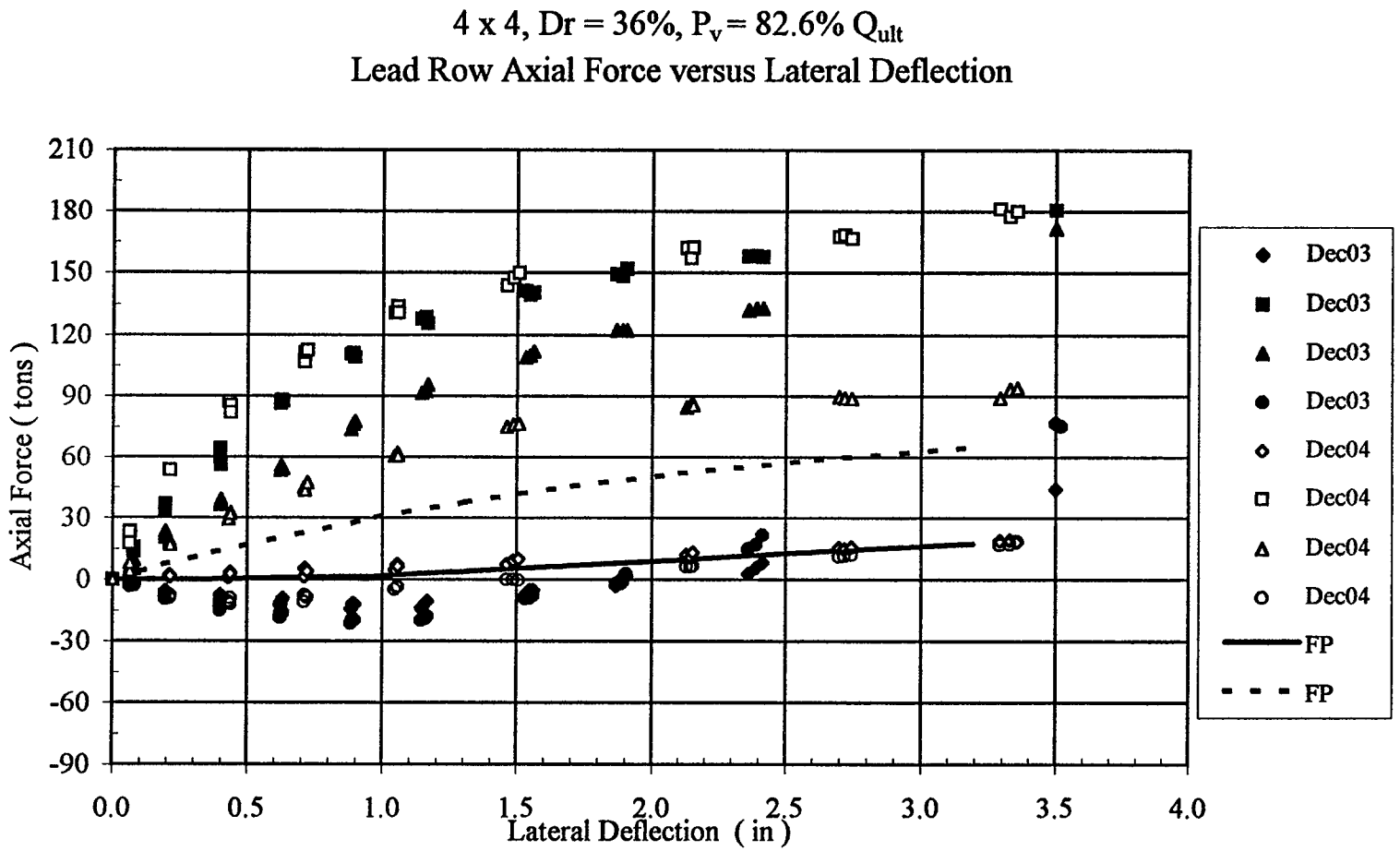

Figure B-134 Lead Row Axial Force versus Lateral Deflection

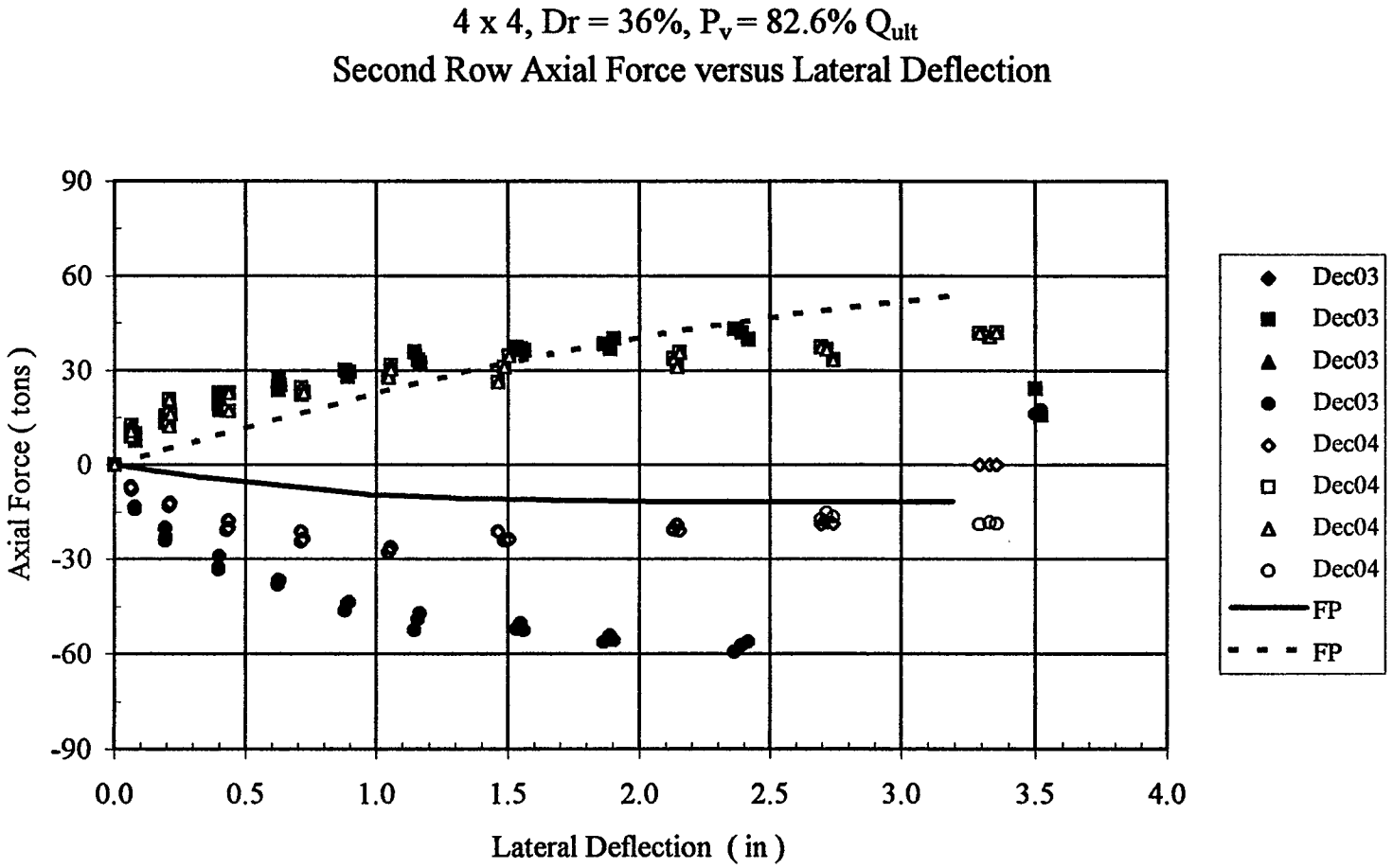

Figure B-135 Second Row Axial Force versus Lateral Deflection

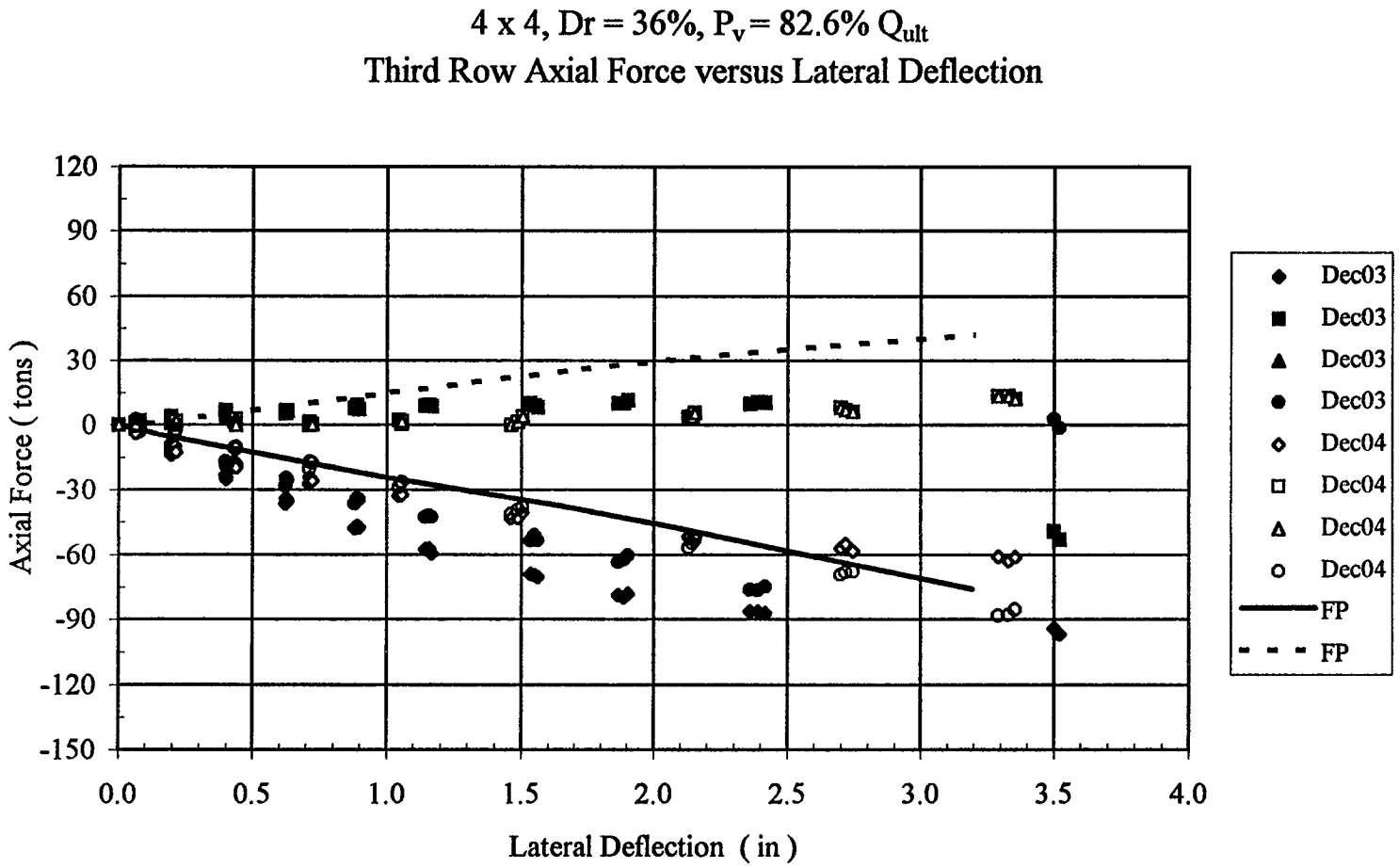

Figure B-136 Third Row Axial Force versus Lateral Deflection

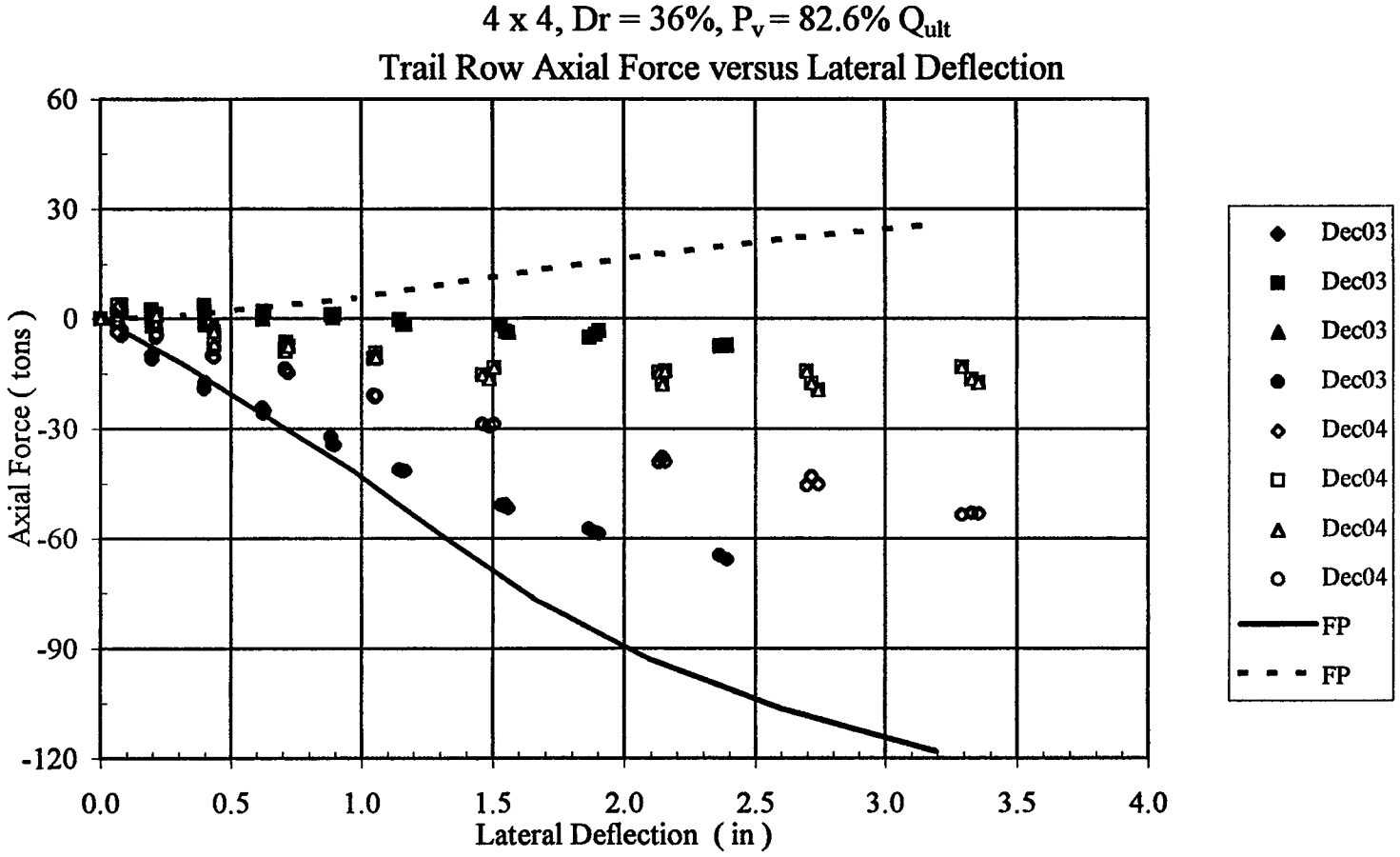

Figure B-137 Trail Row Axial Force versus Lateral Deflection

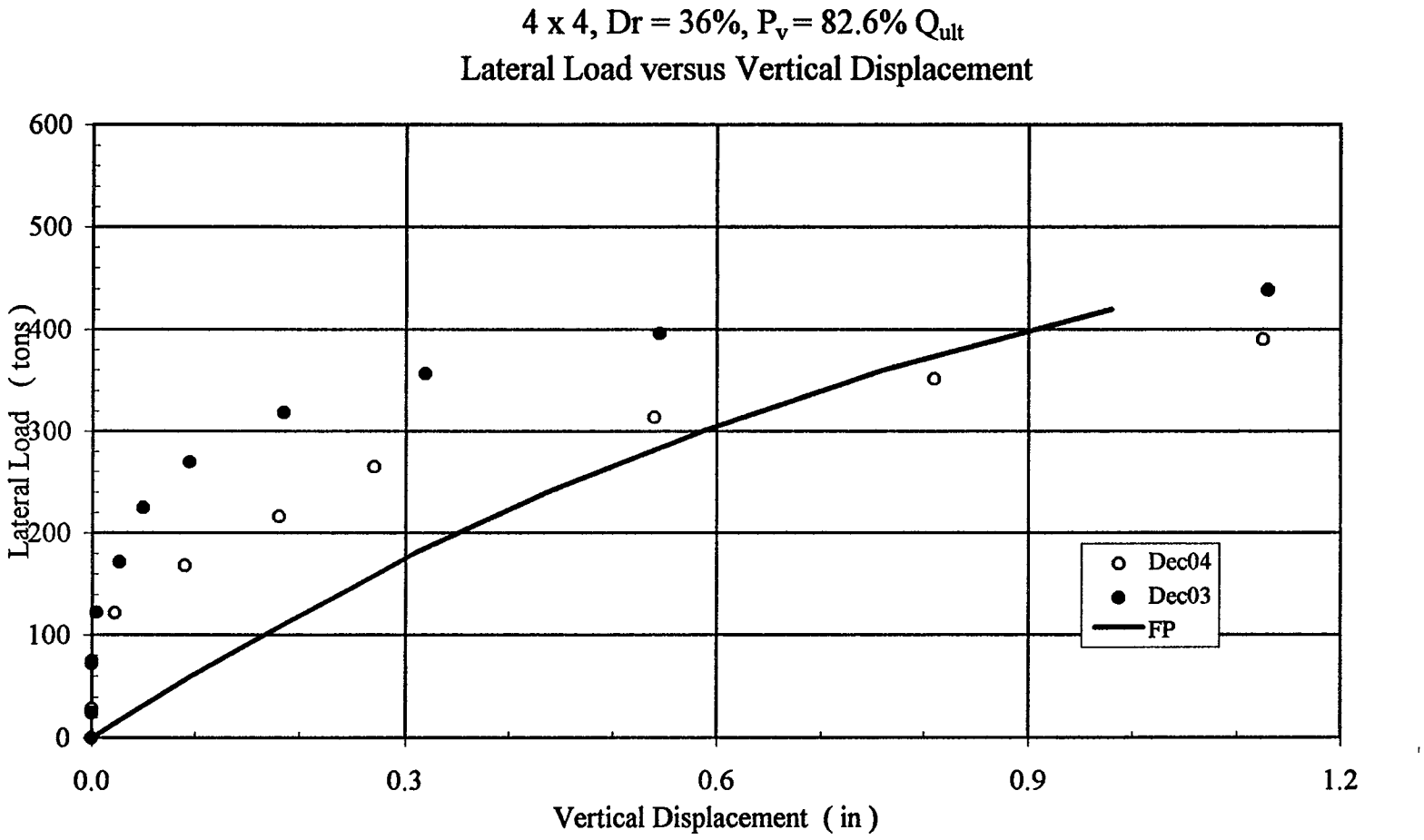

Figure B-138 Lateral Load versus Vertical Displacement

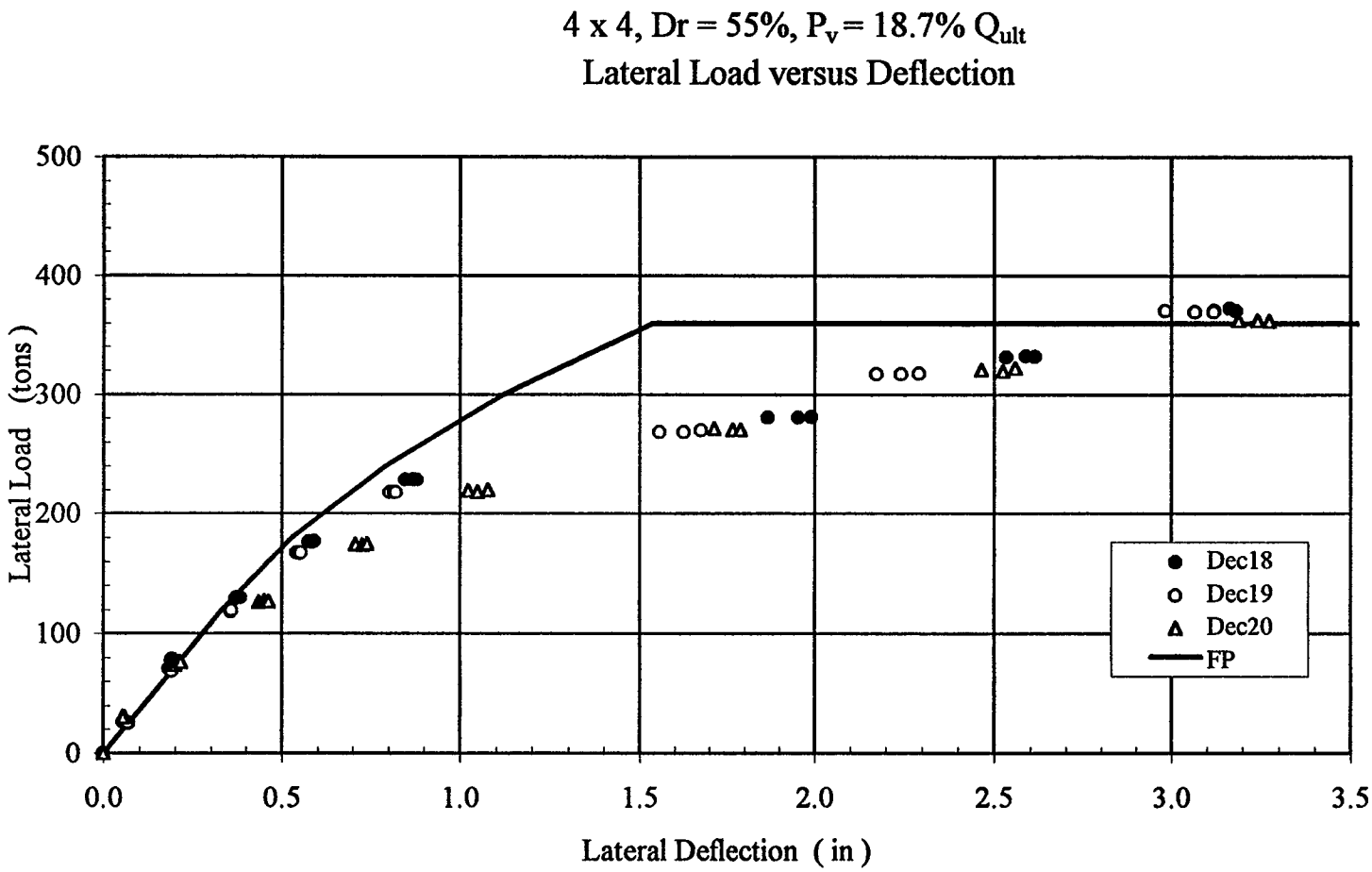

Figure B-139 Lateral Load versus Deflection

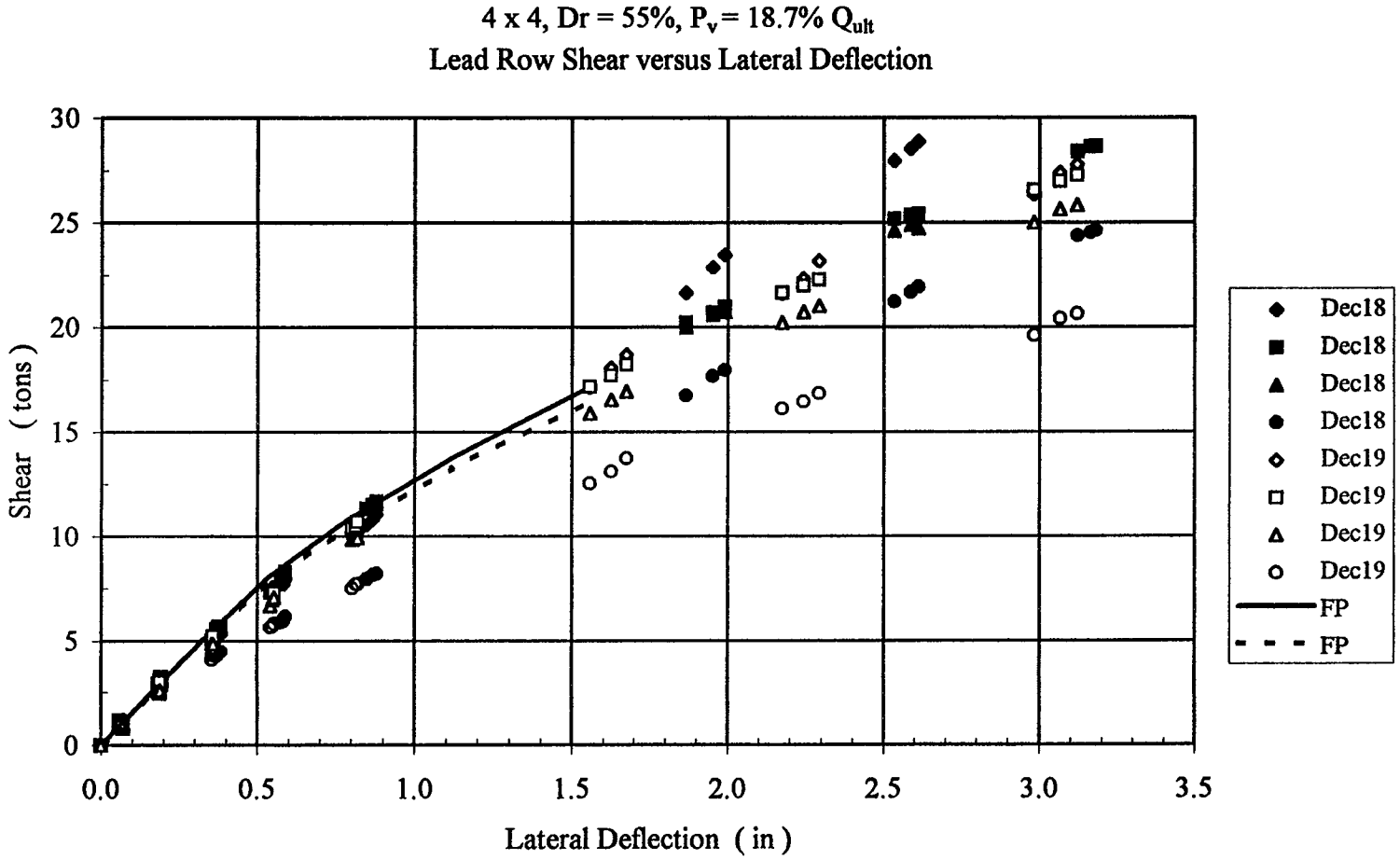

Figure B-140 Lead Row Shear versus Lateral Deflection

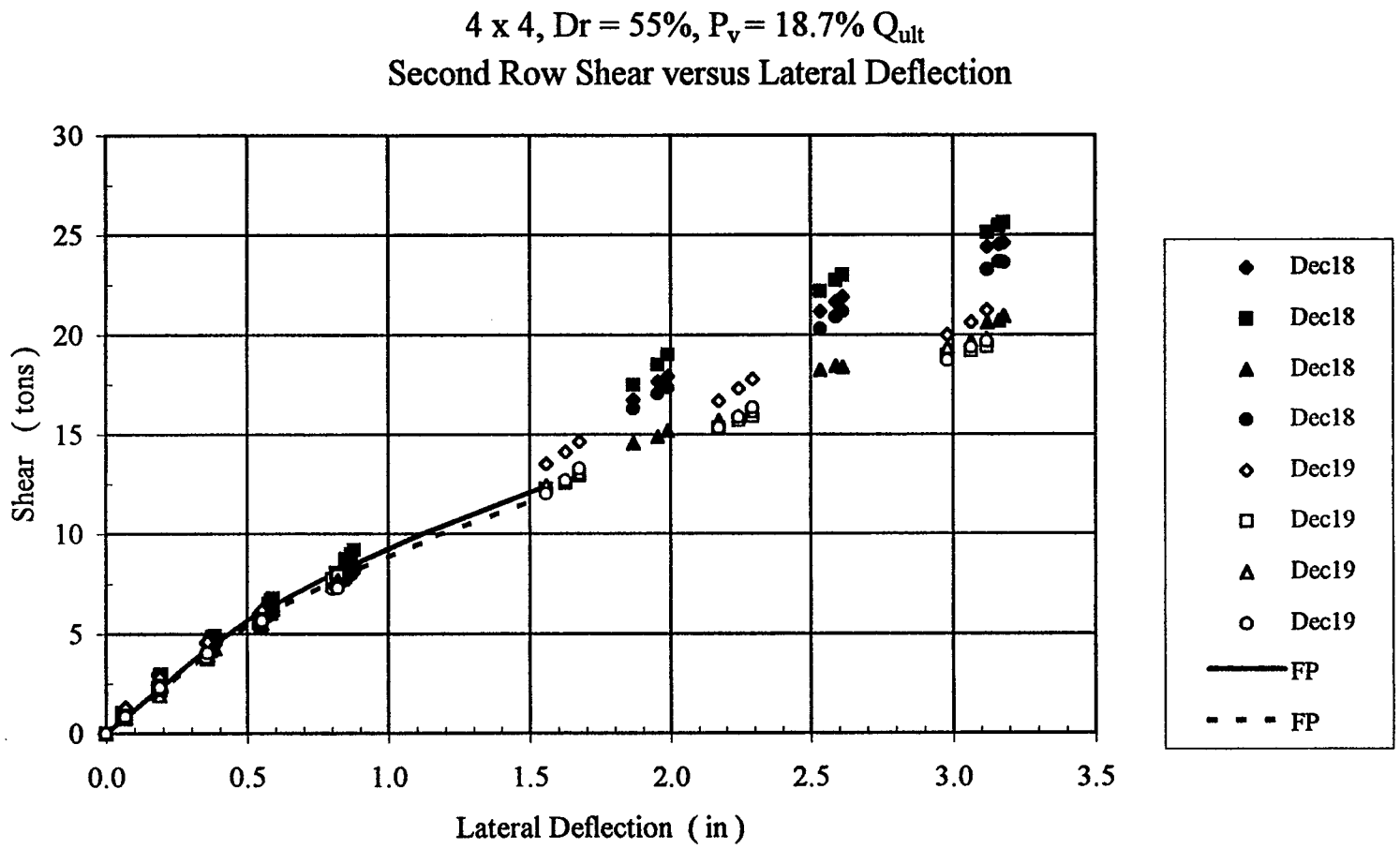

Figure B-141 Second Row versus Lateral Deflection

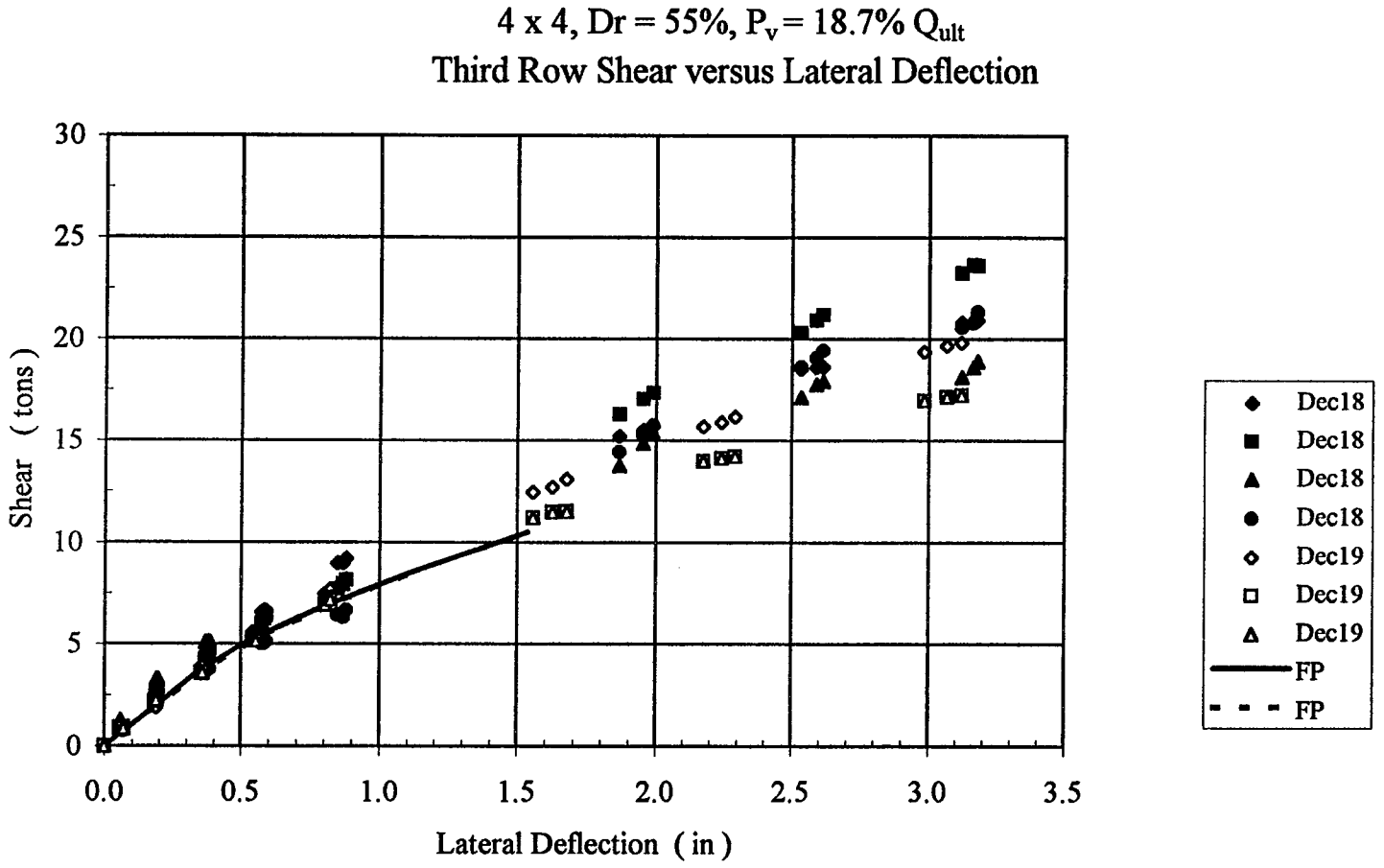

Figure B-142 Third Row Shear versus Lateral Deflection

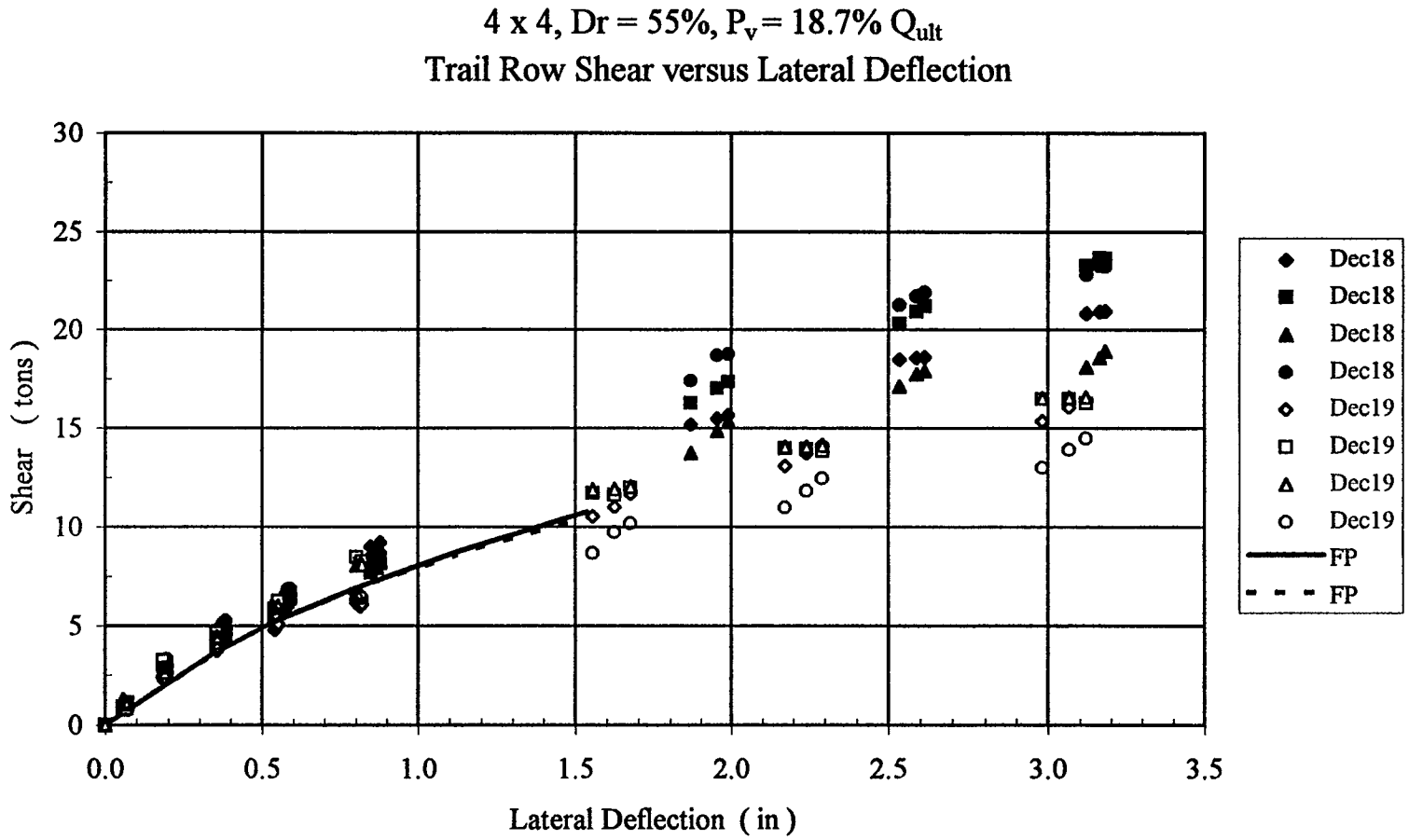

Figure B-143 Trail Row Shear versus Lateral Deflection

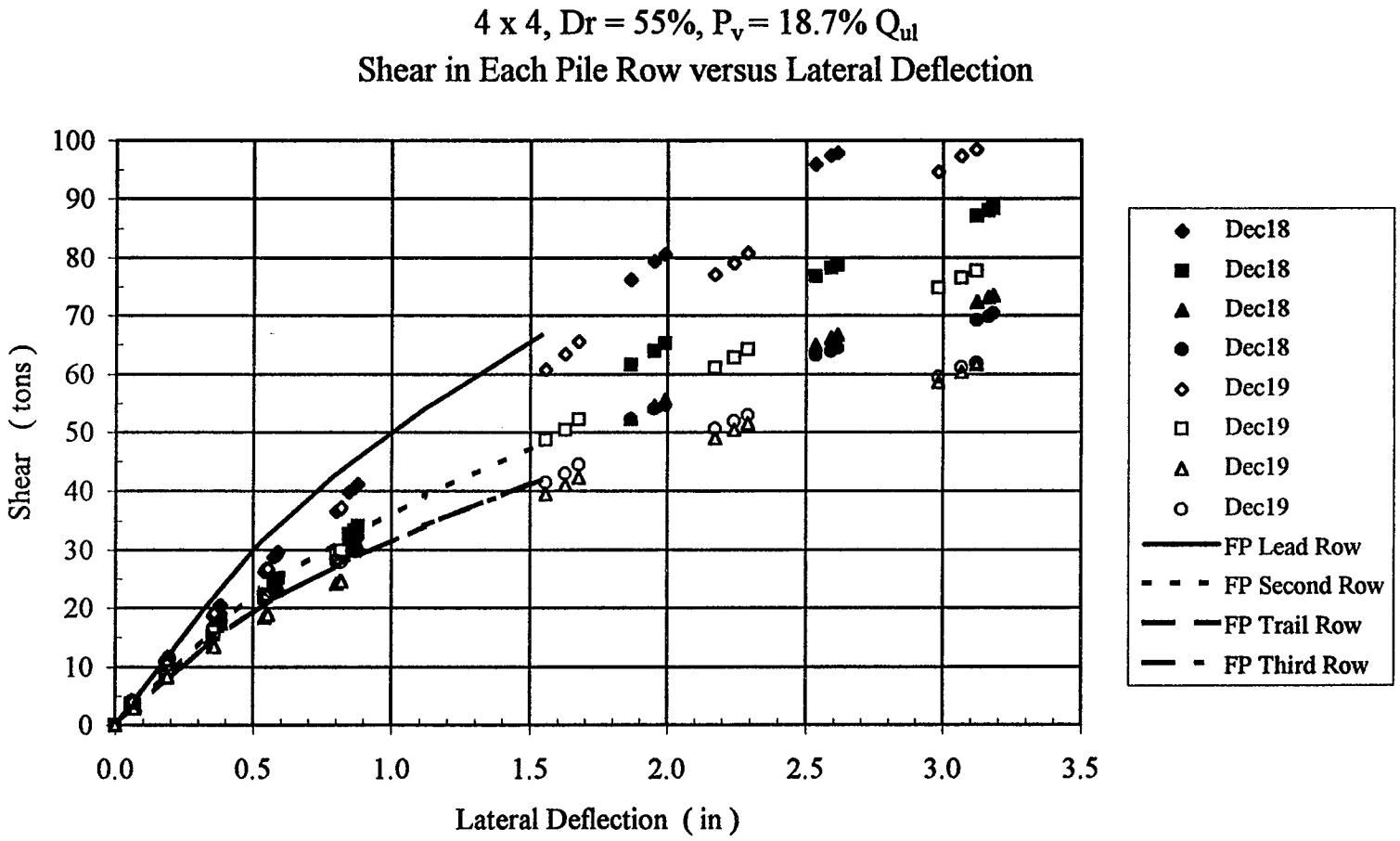

Figure B-144 Shear in Each Pile Row versus Lateral Deflection

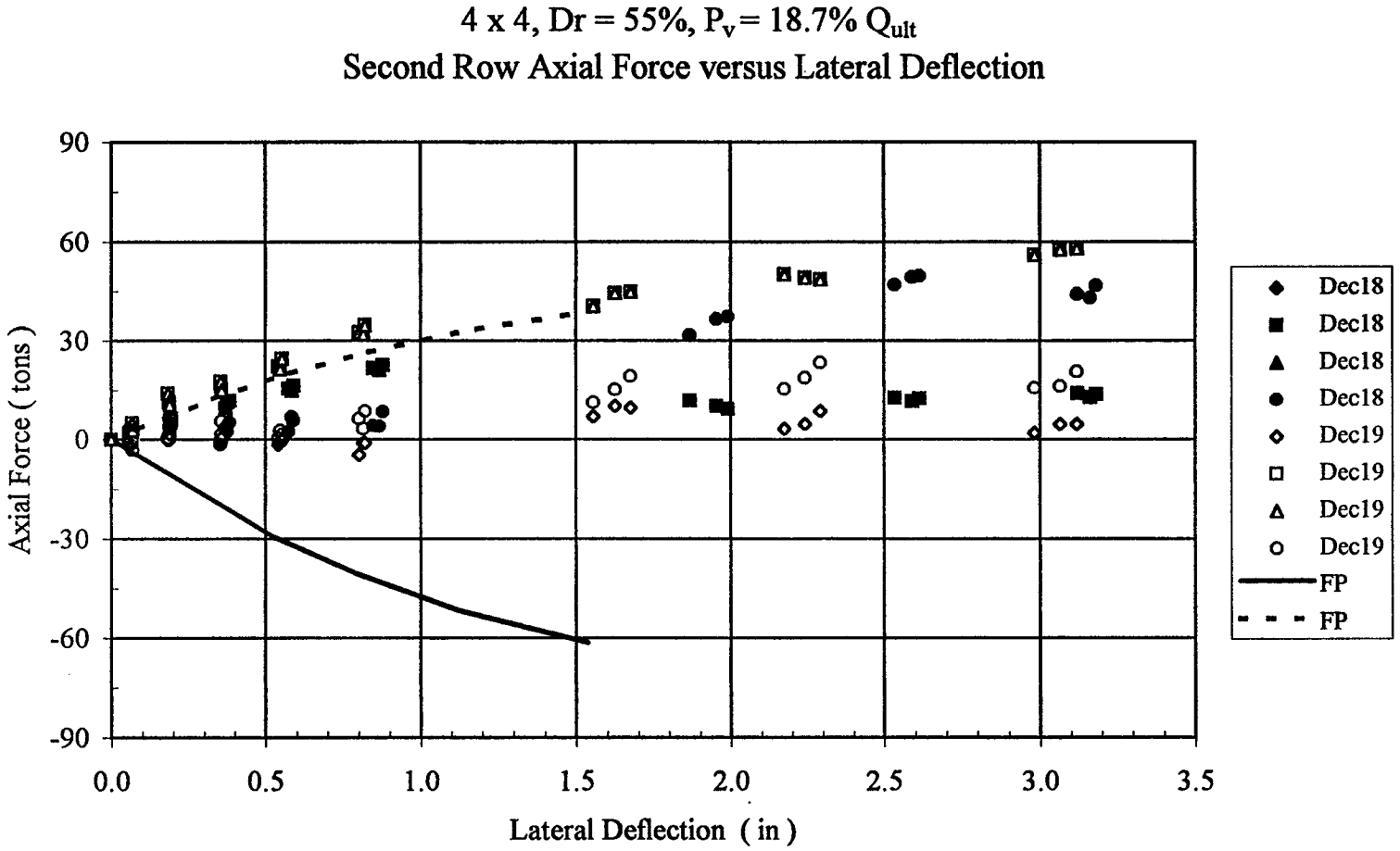

Figure B-145 Second Row Axial Force versus Lateral Deflection

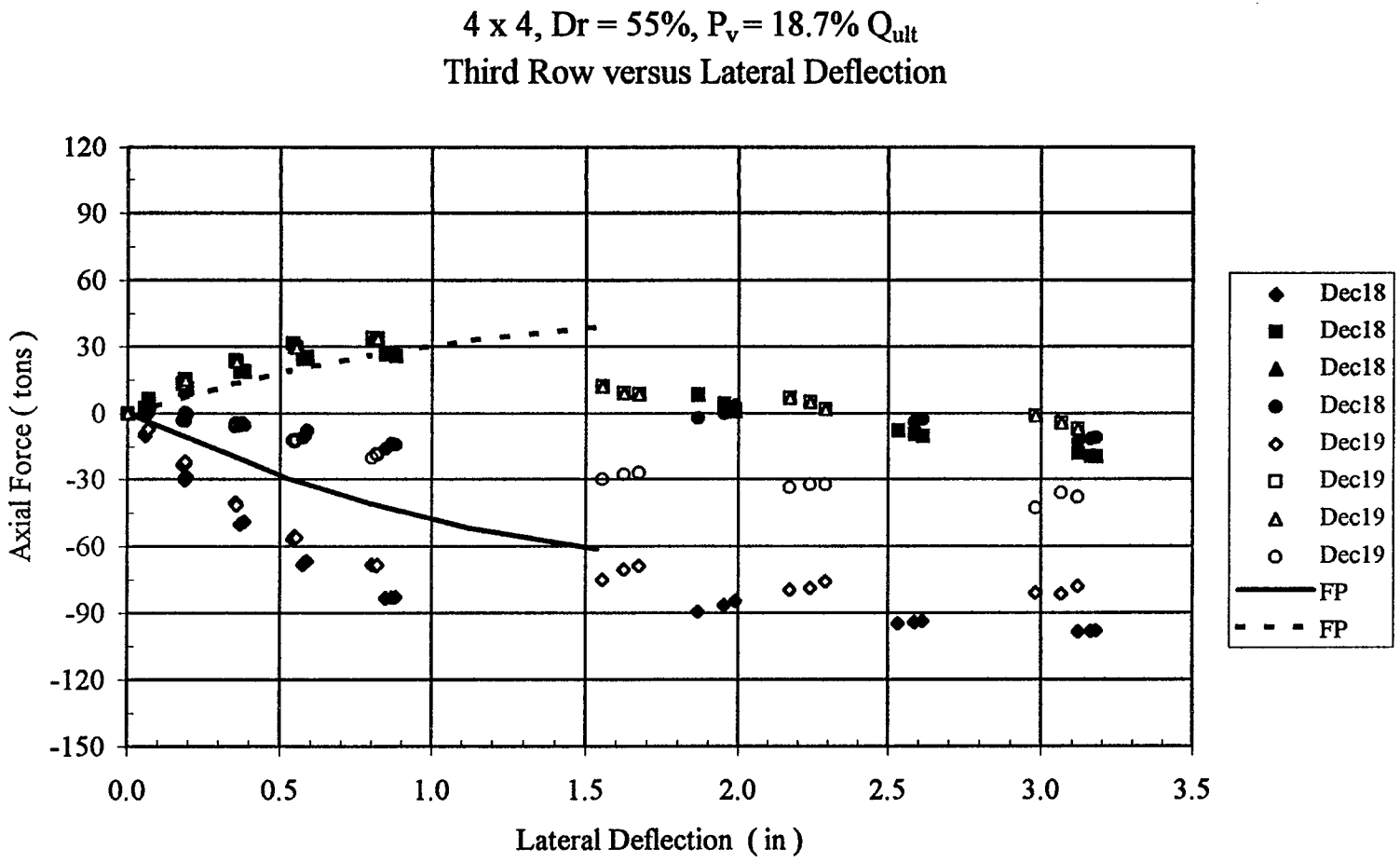

Figure B-146 Third Row versus Lateral Deflection

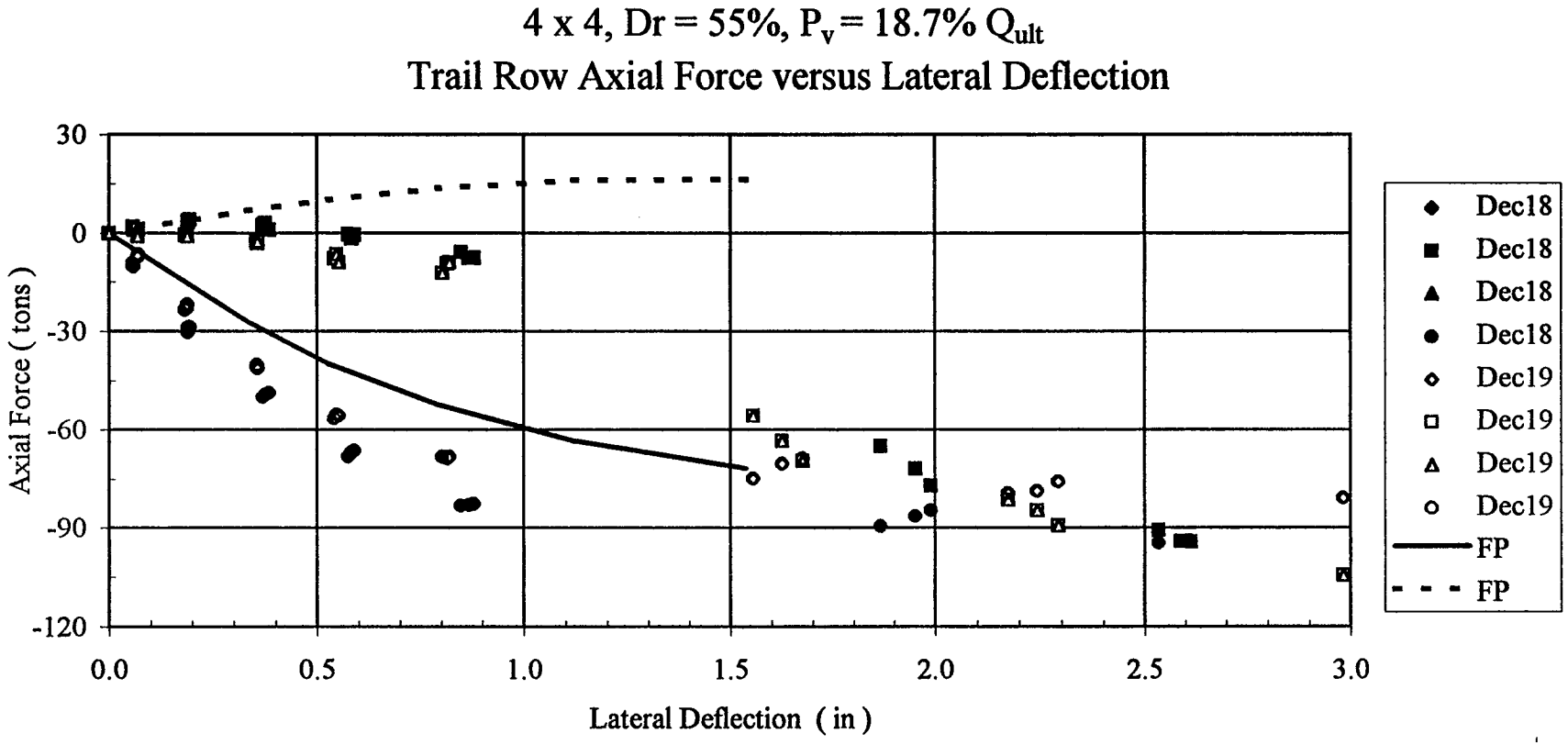

Figure B-147 Trail Row Axial Force versus Lateral Deflection

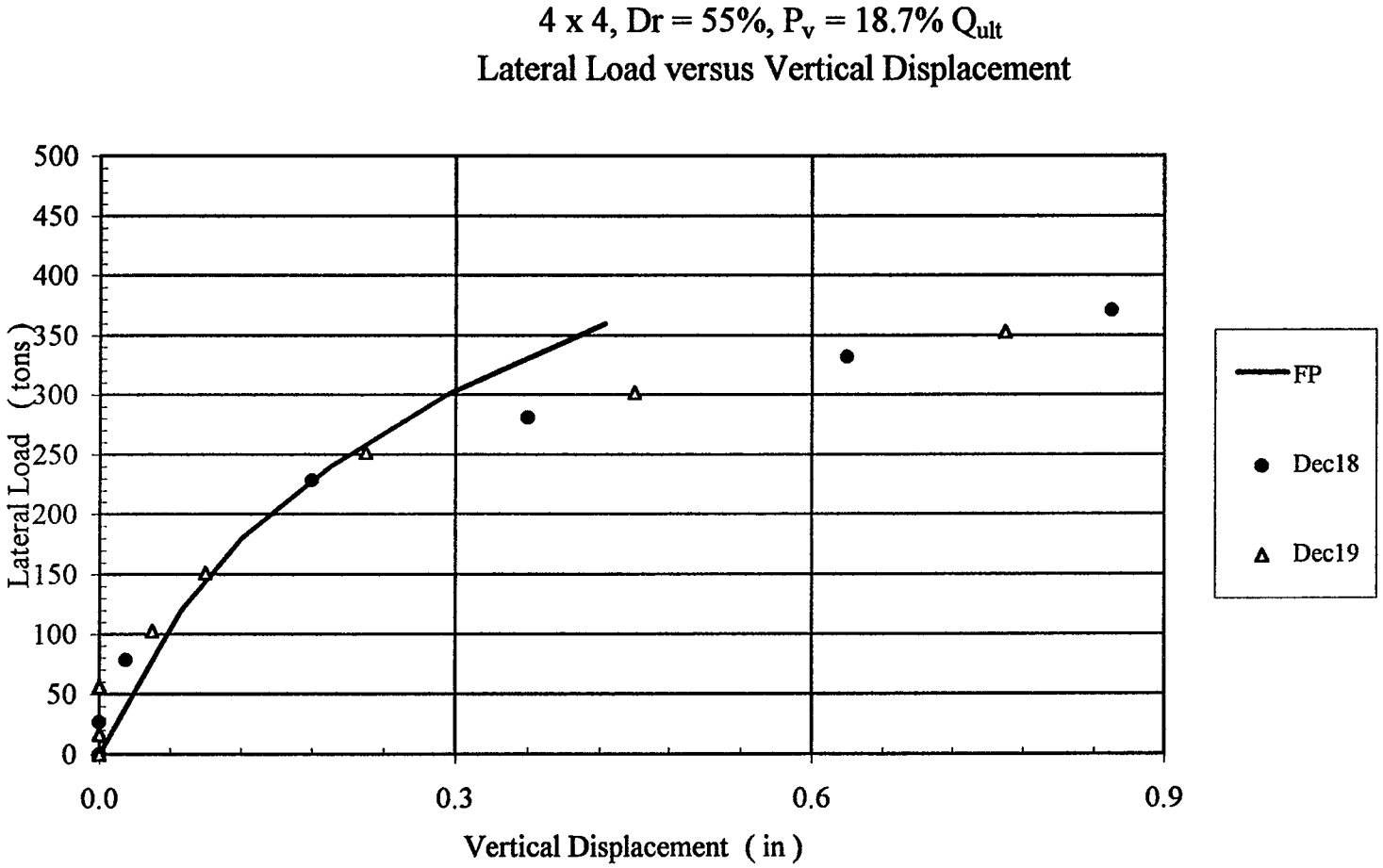

Figure B-148 Lateral Load versus Vertical Displacement

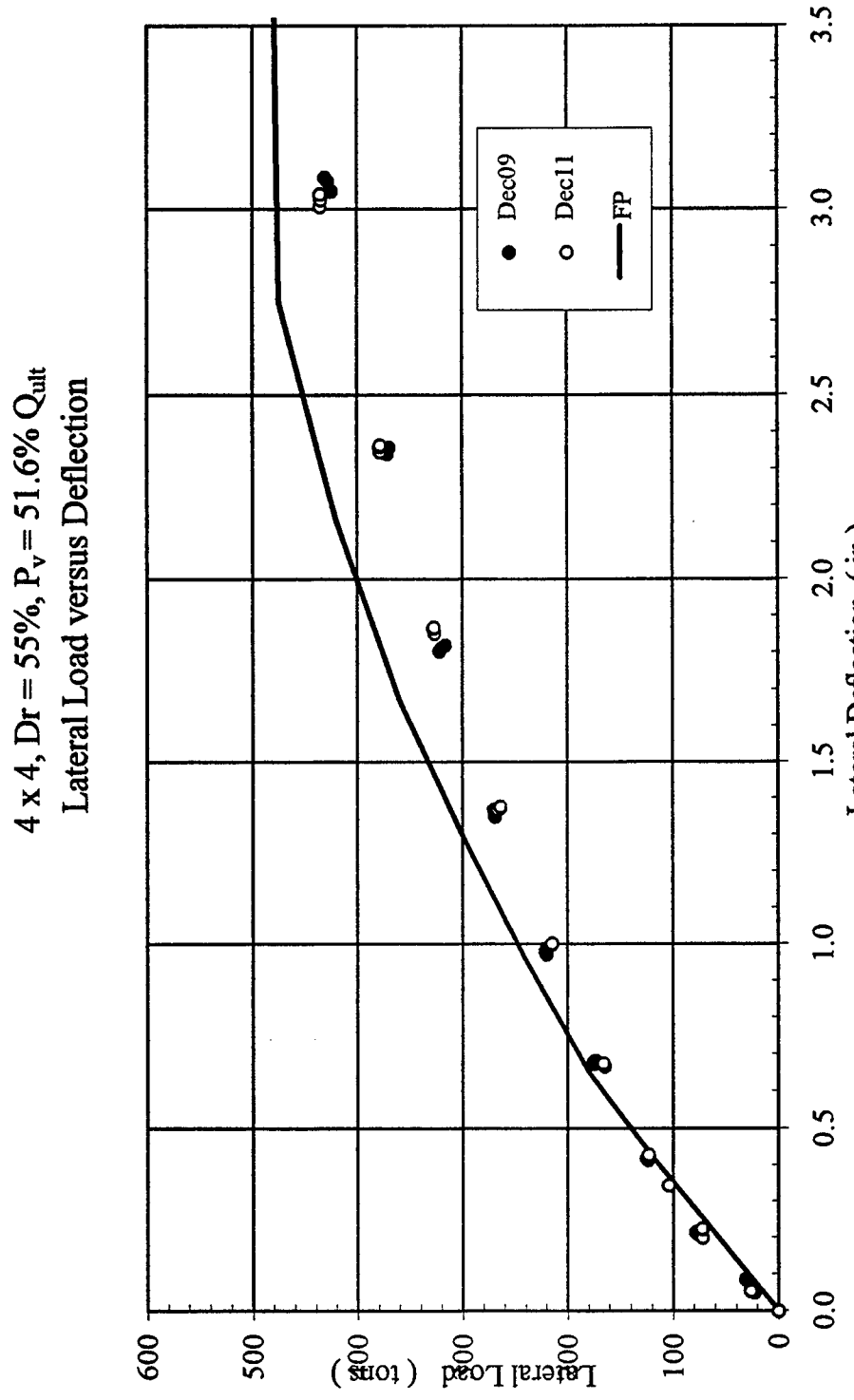

Figure B-149 Lateral Load versus Deflection

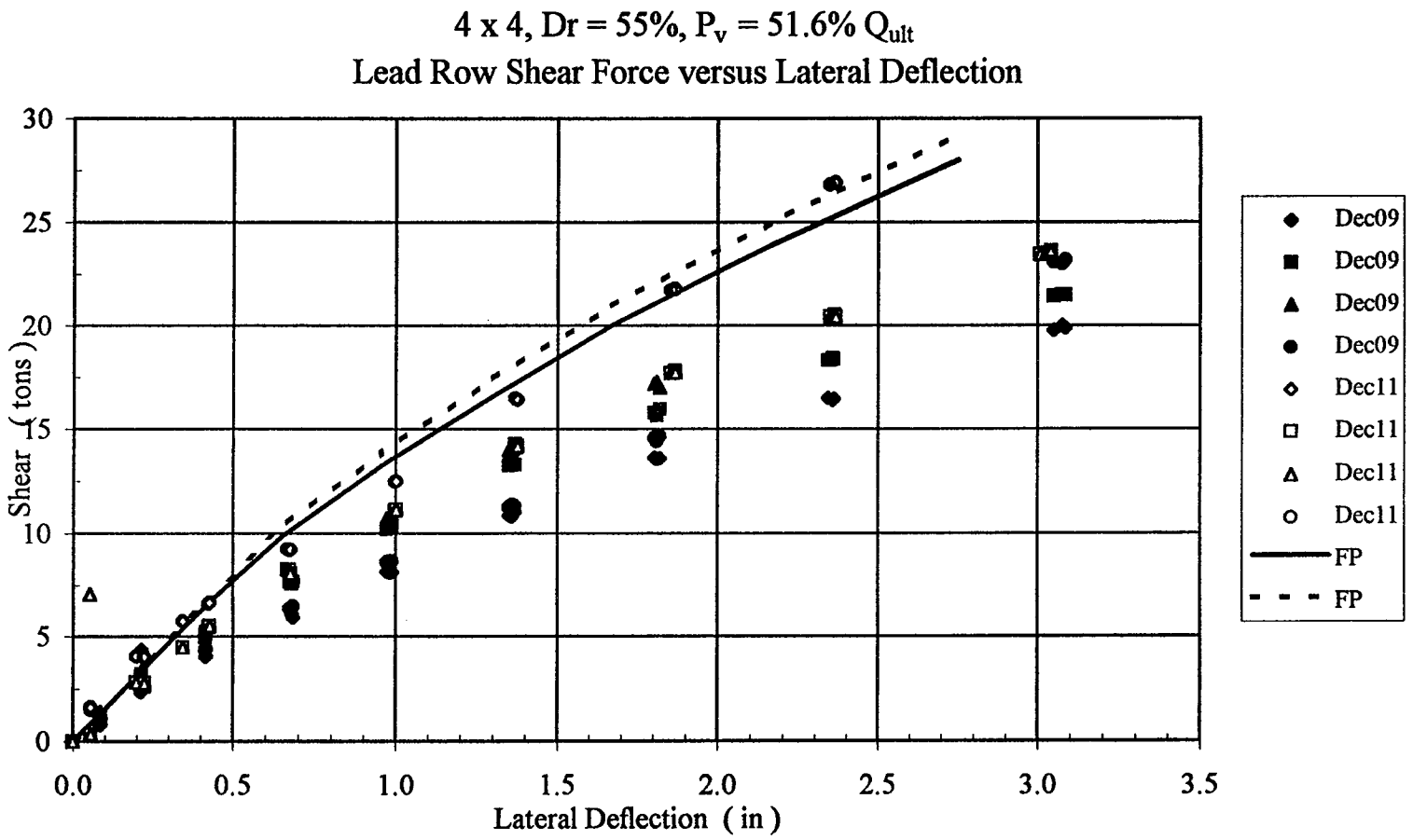

Figure B-150 Lead Row Shear versus Lateral Deflection

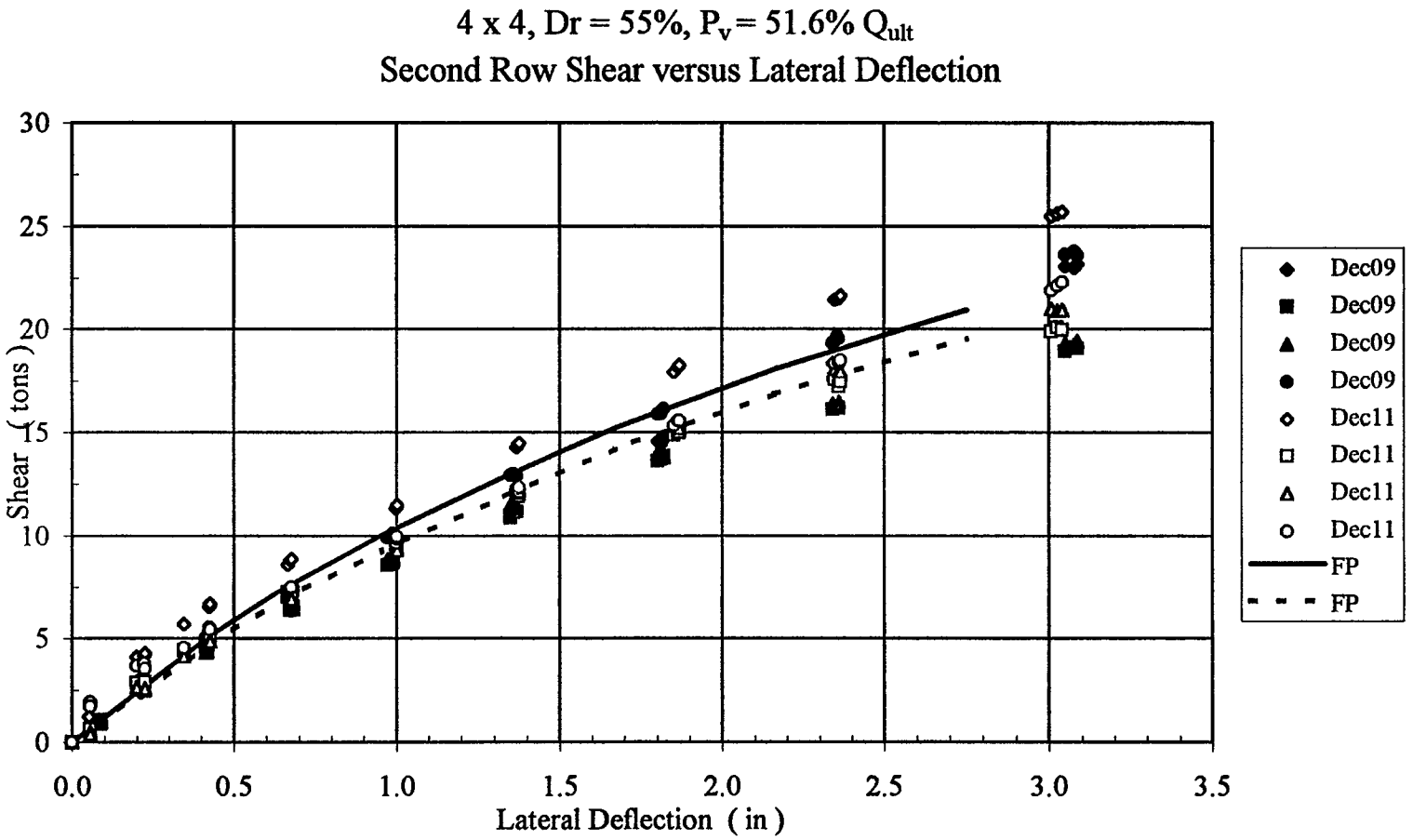

Figure B-151 Second Row Shear versus Lateral Deflection

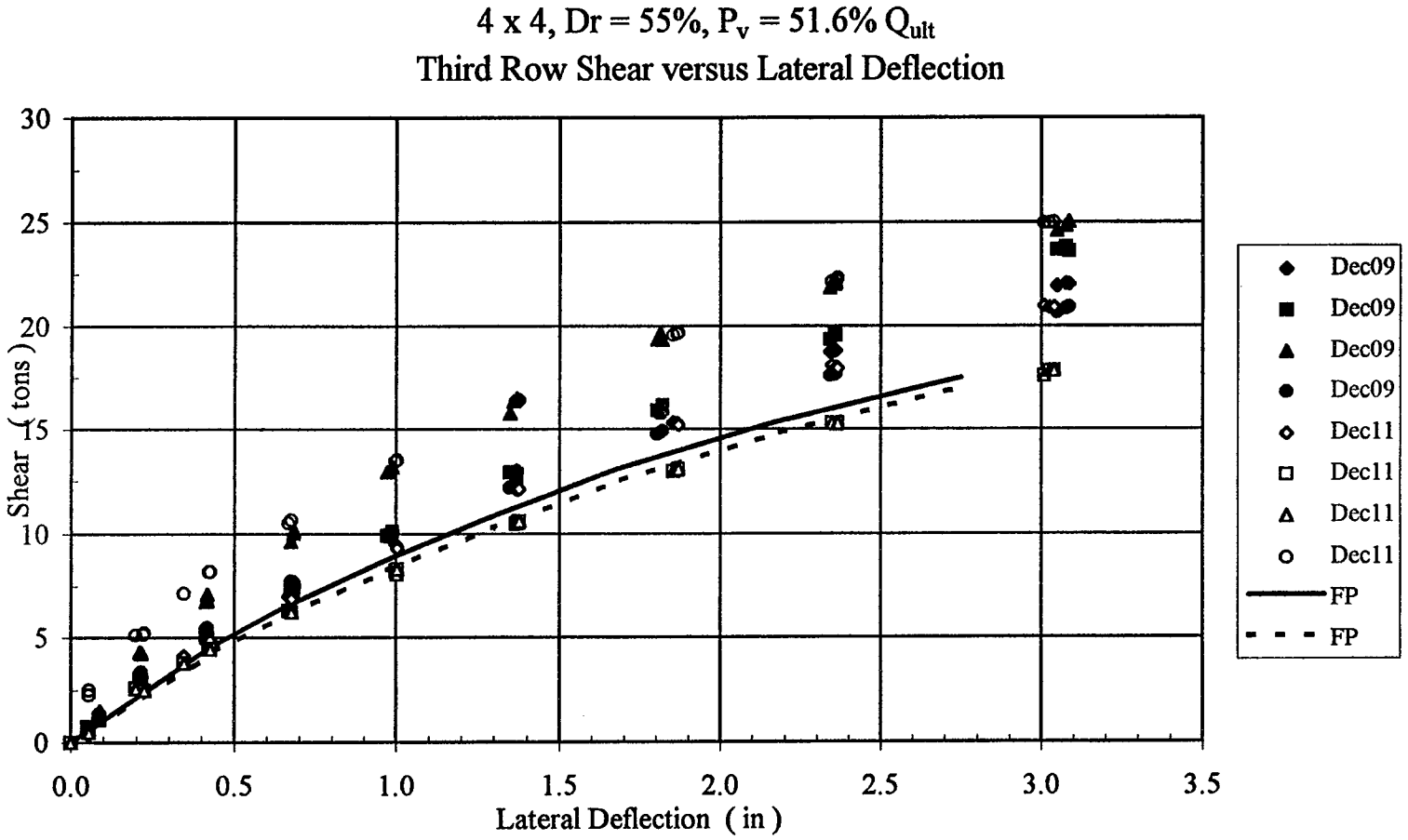

Figure B-152 Third Row Shear versus Lateral Deflection

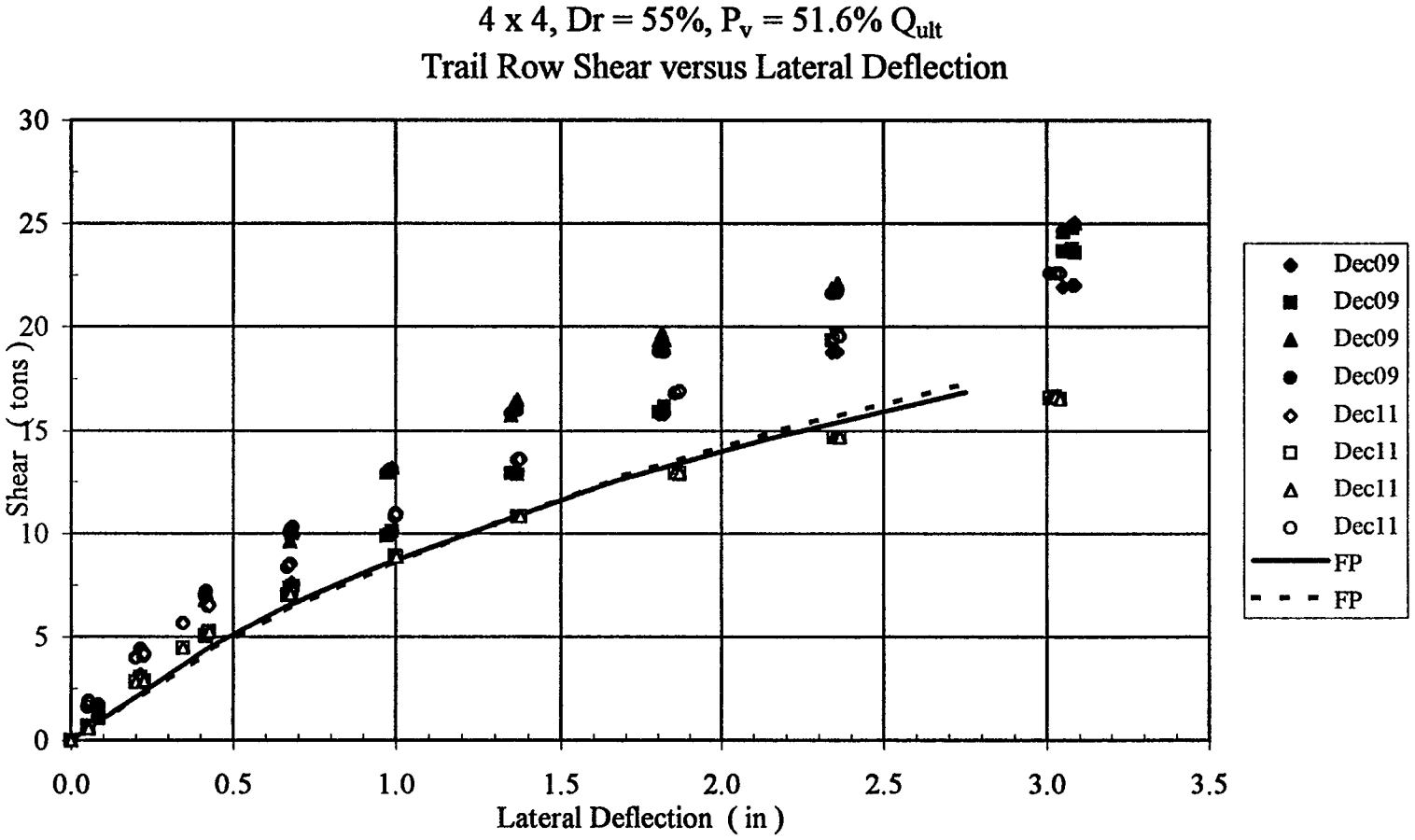

Figure B-153 Trail Row Shear versus Lateral Deflection

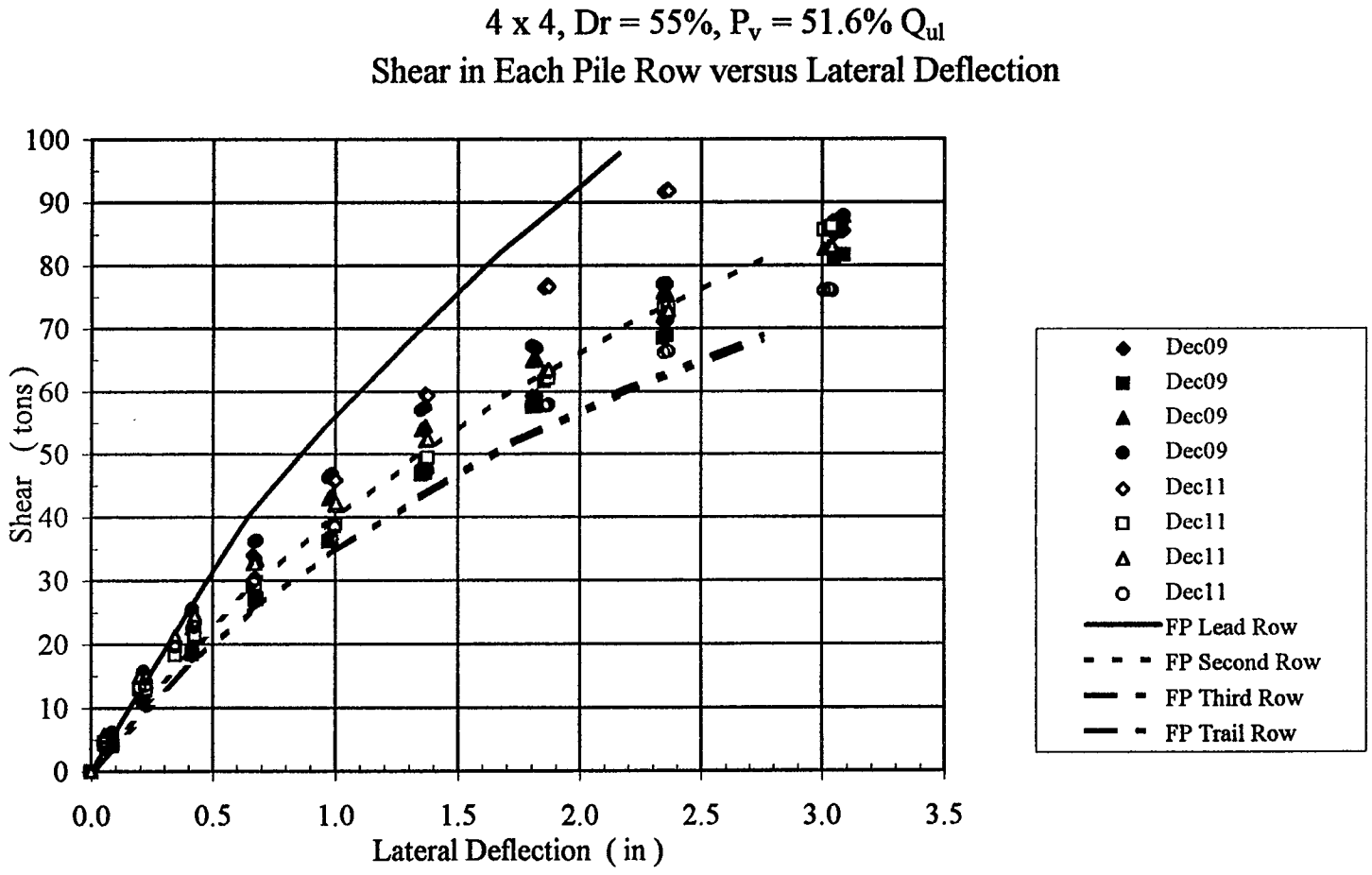

Figure B-154 Shear in Each Pile Row versus Lateral Deflection

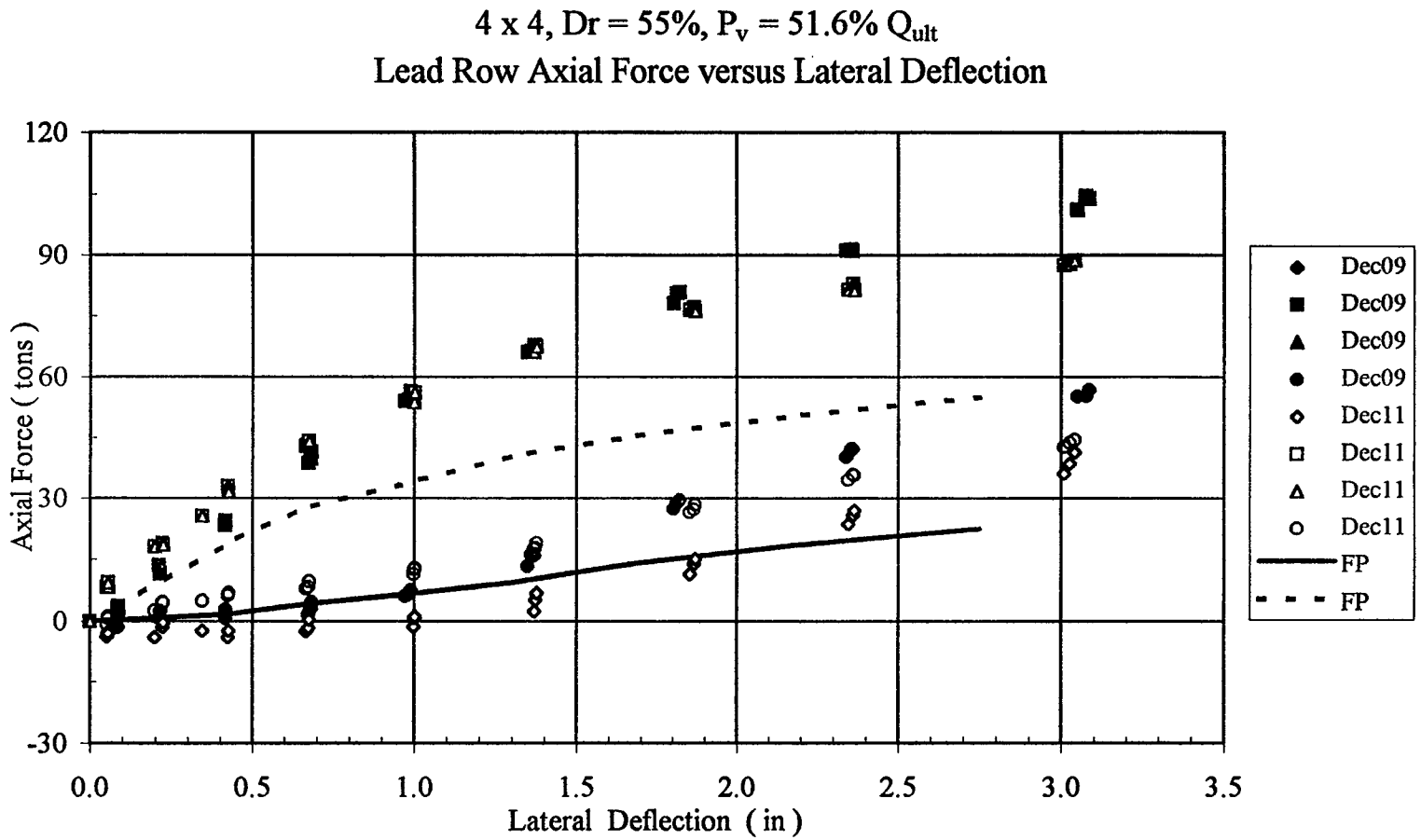

Figure B-155 Lead Row Axial Force versus Lateral Deflection

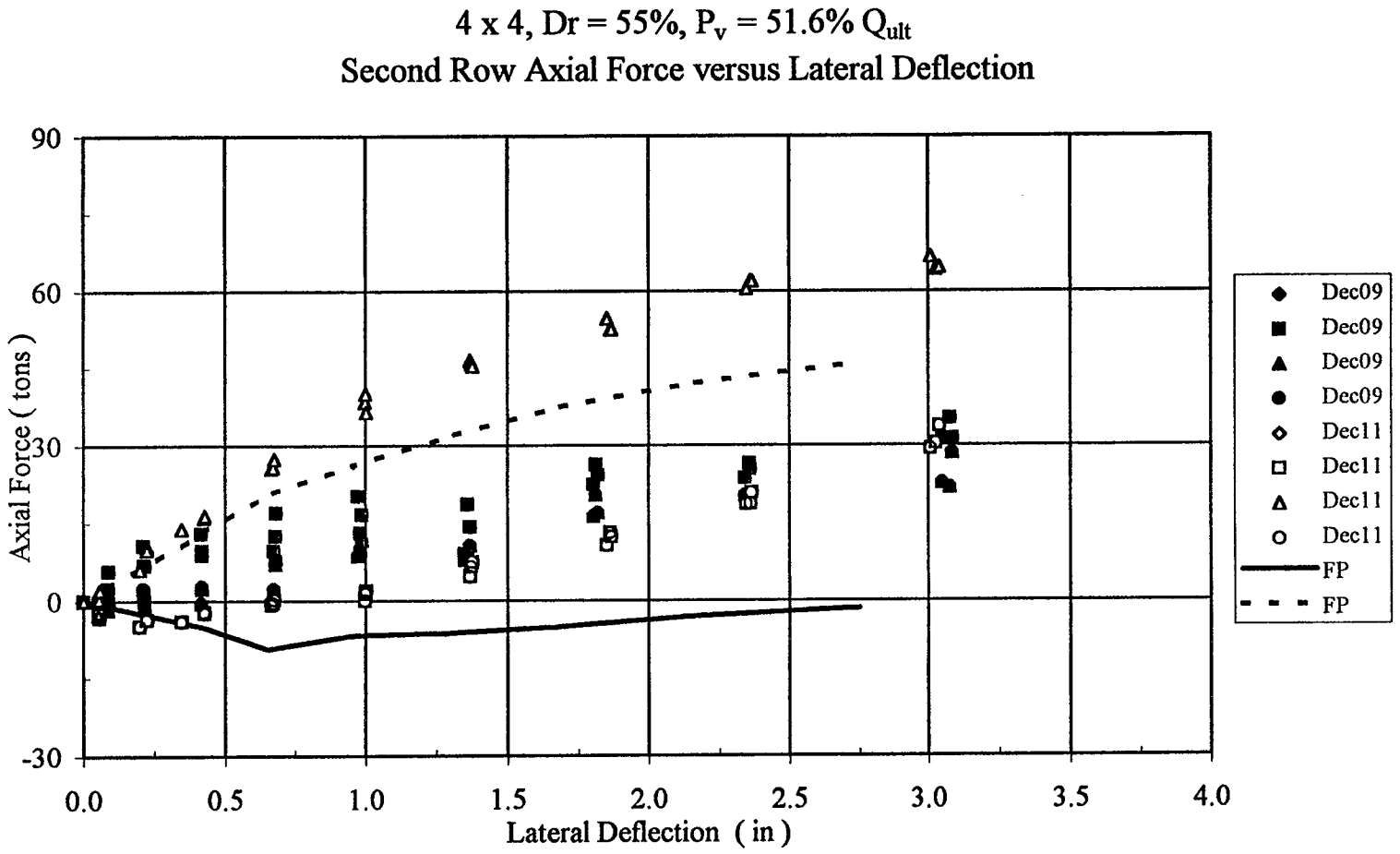

Figure B-156 Second Row Axial Force versus Lateral Deflection

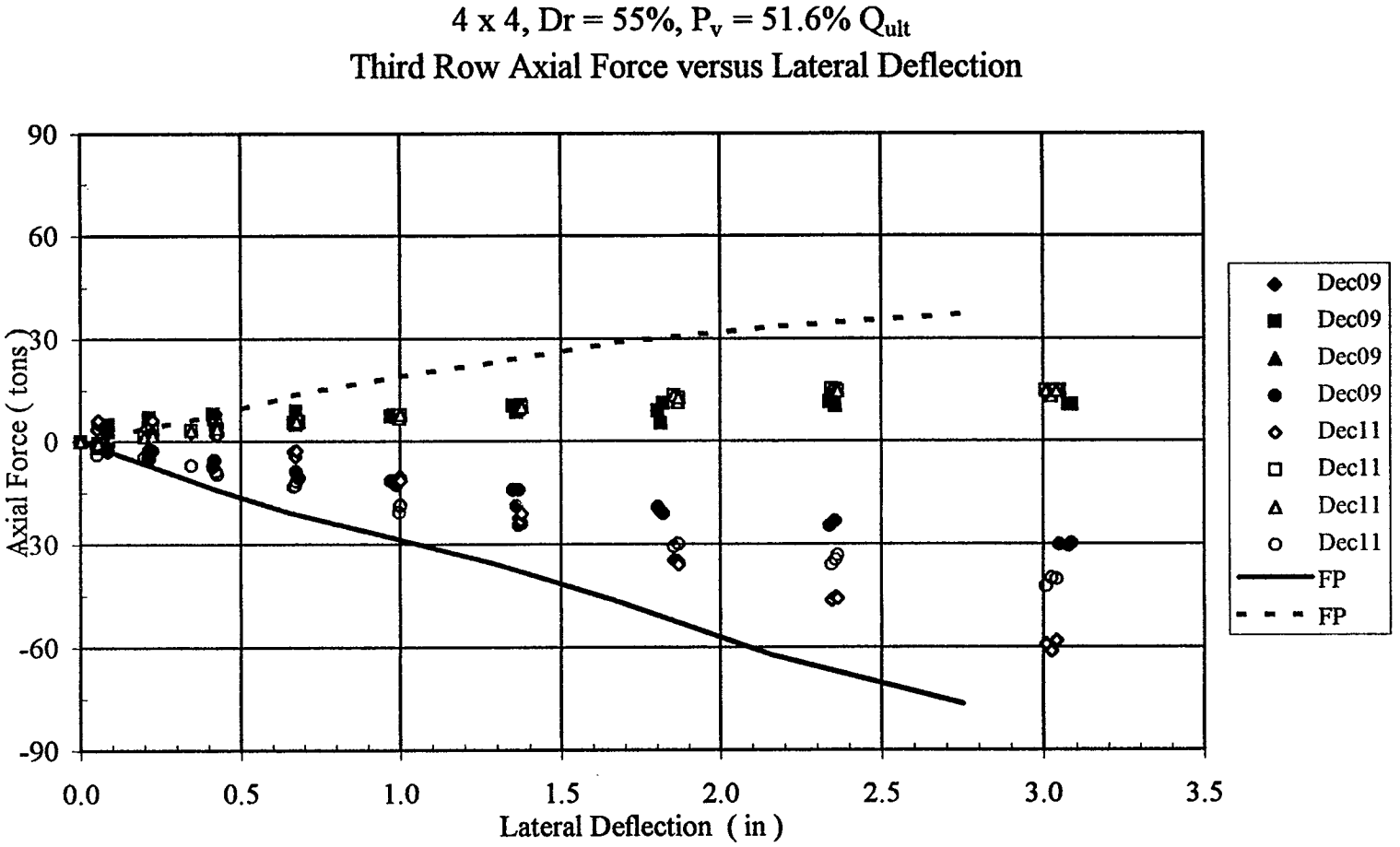

Figure B-157 Third Row Axial Force versus Lateral Deflection

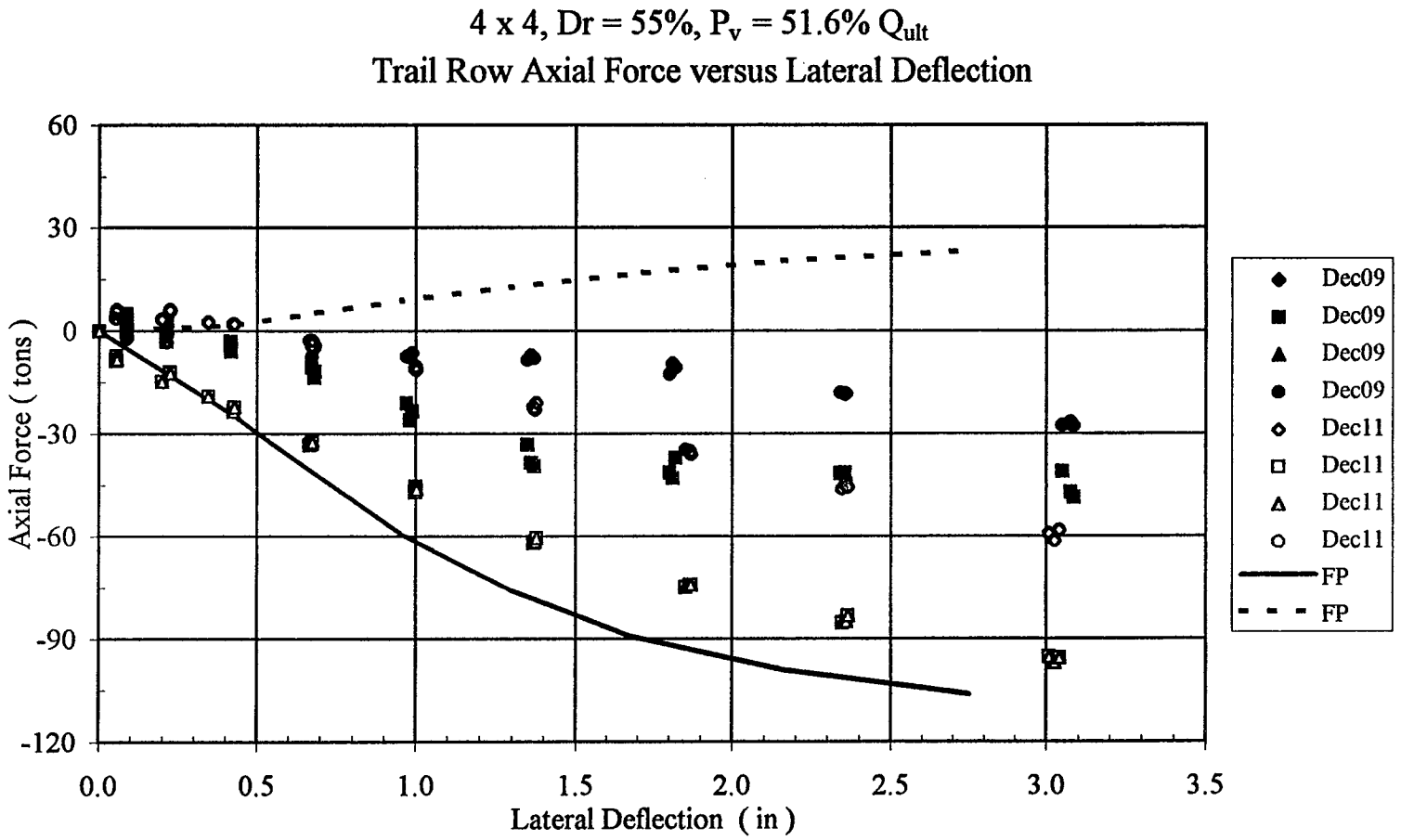

Figure B-158 Trail Row Axial Force versus Lateral Deflection

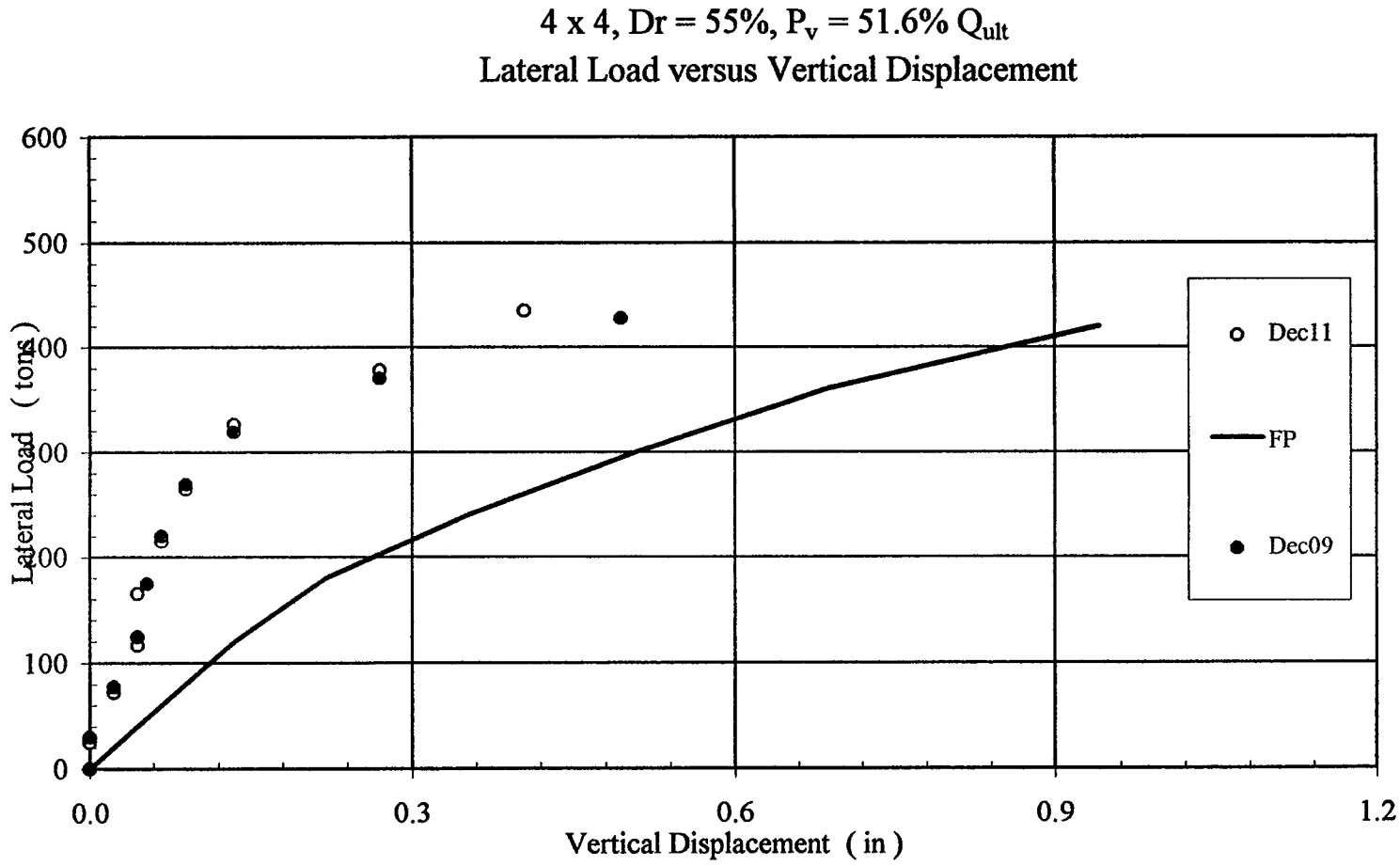

Figure B-159 Lateral Load versus Vertical Displacement

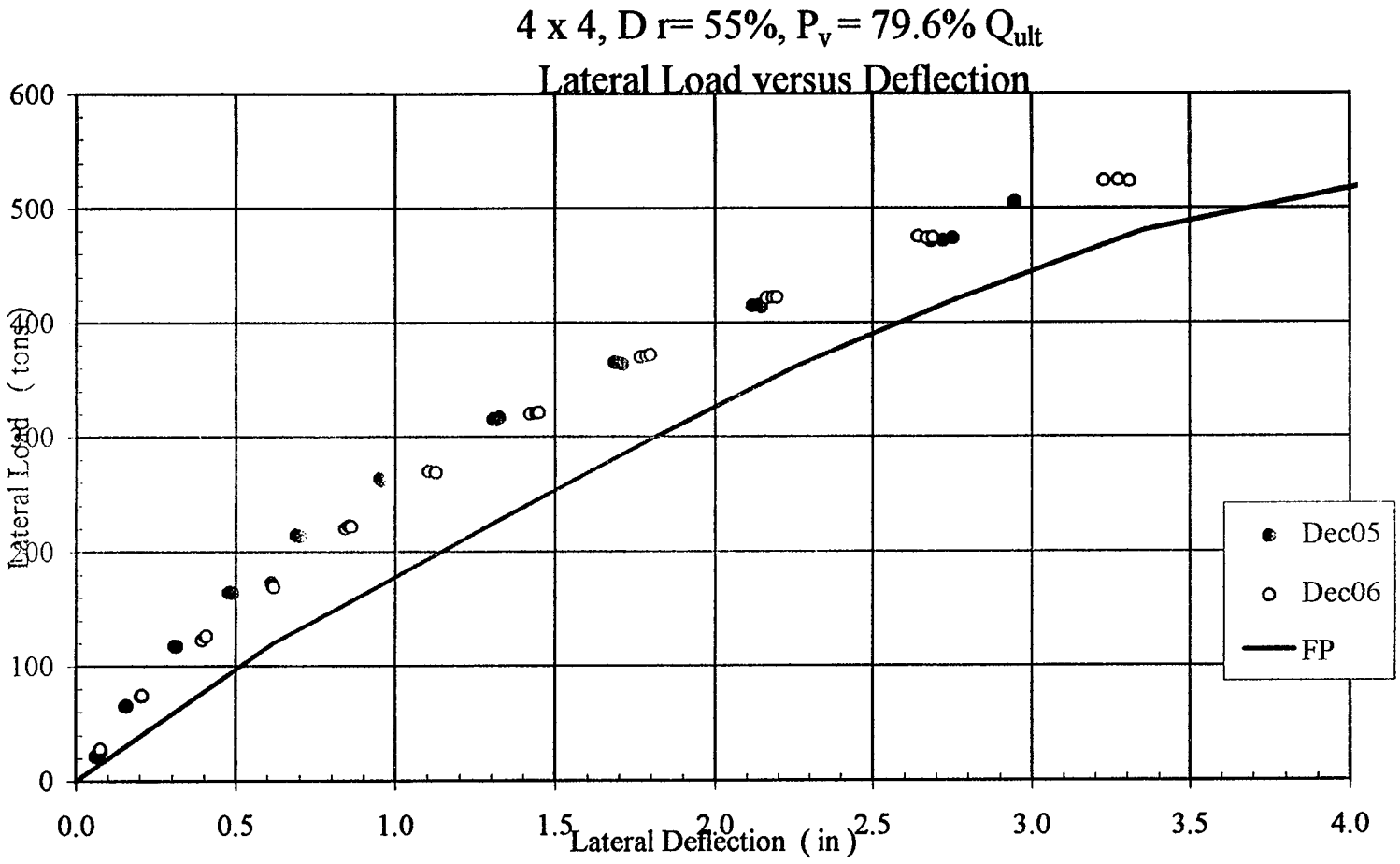

Figure B-160 Lateral Load versus Deflection

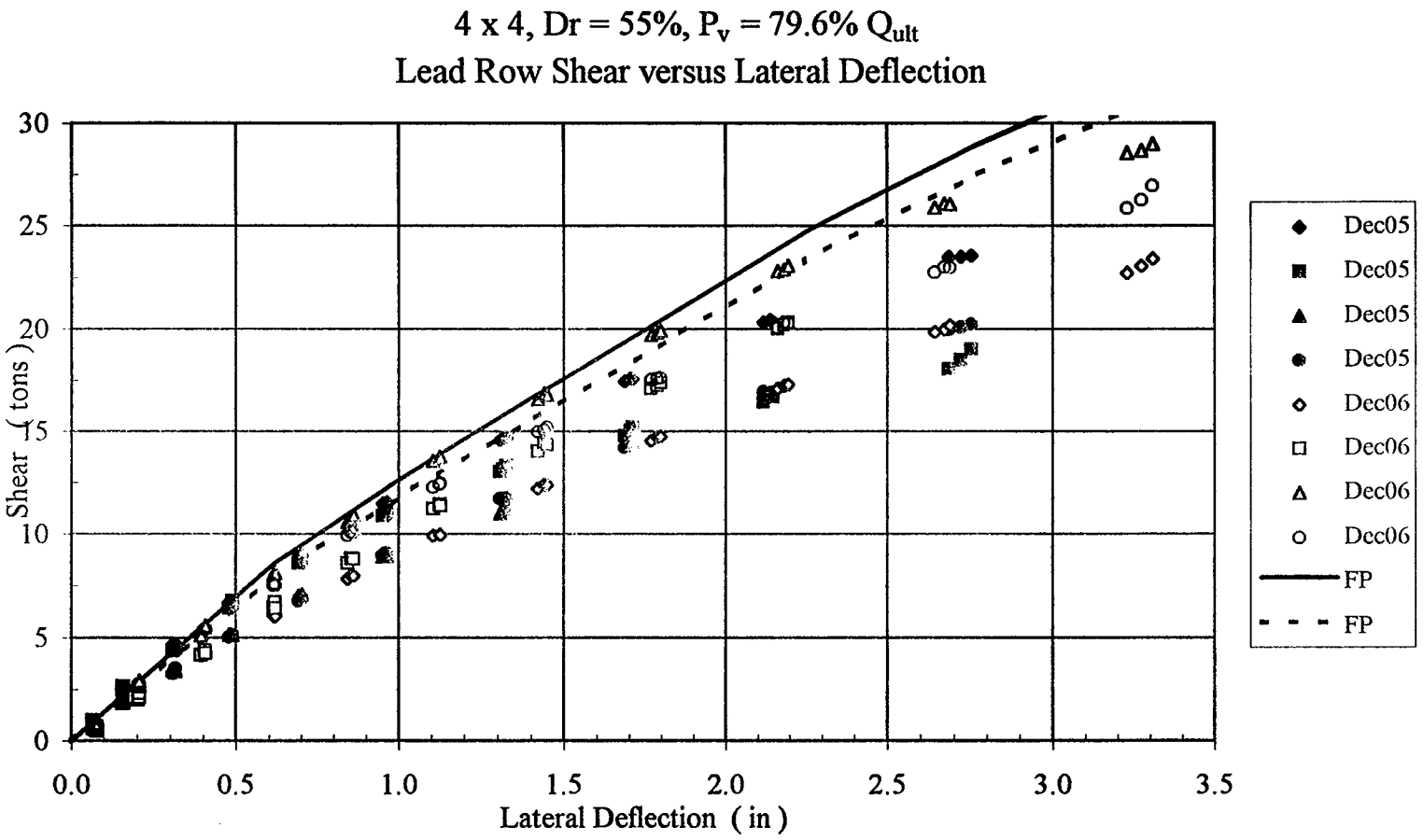

Figure B-161 Lead Row Shear versus Lateral Deflection

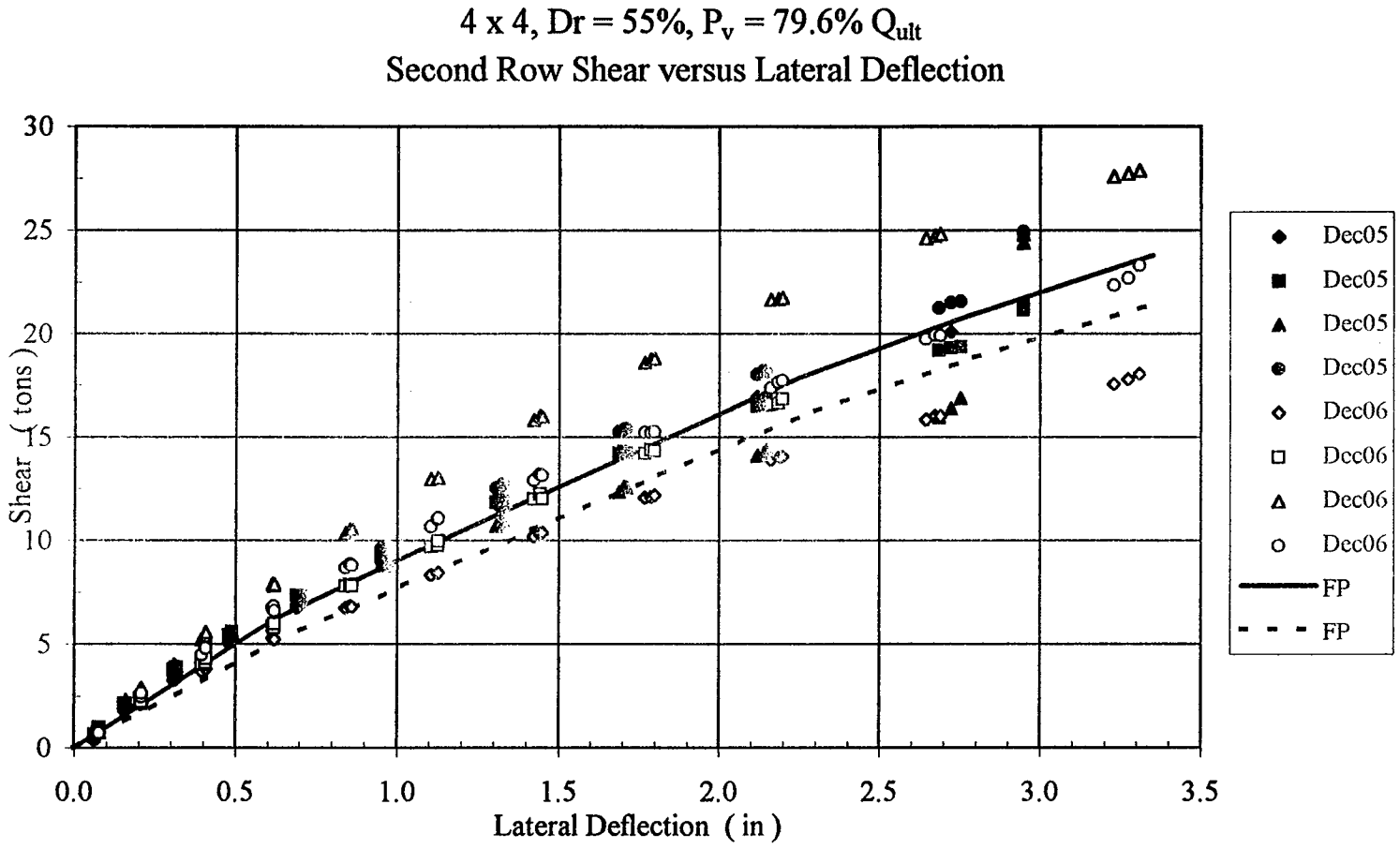

Figure B-162 Second Row Shear versus Lateral Deflection

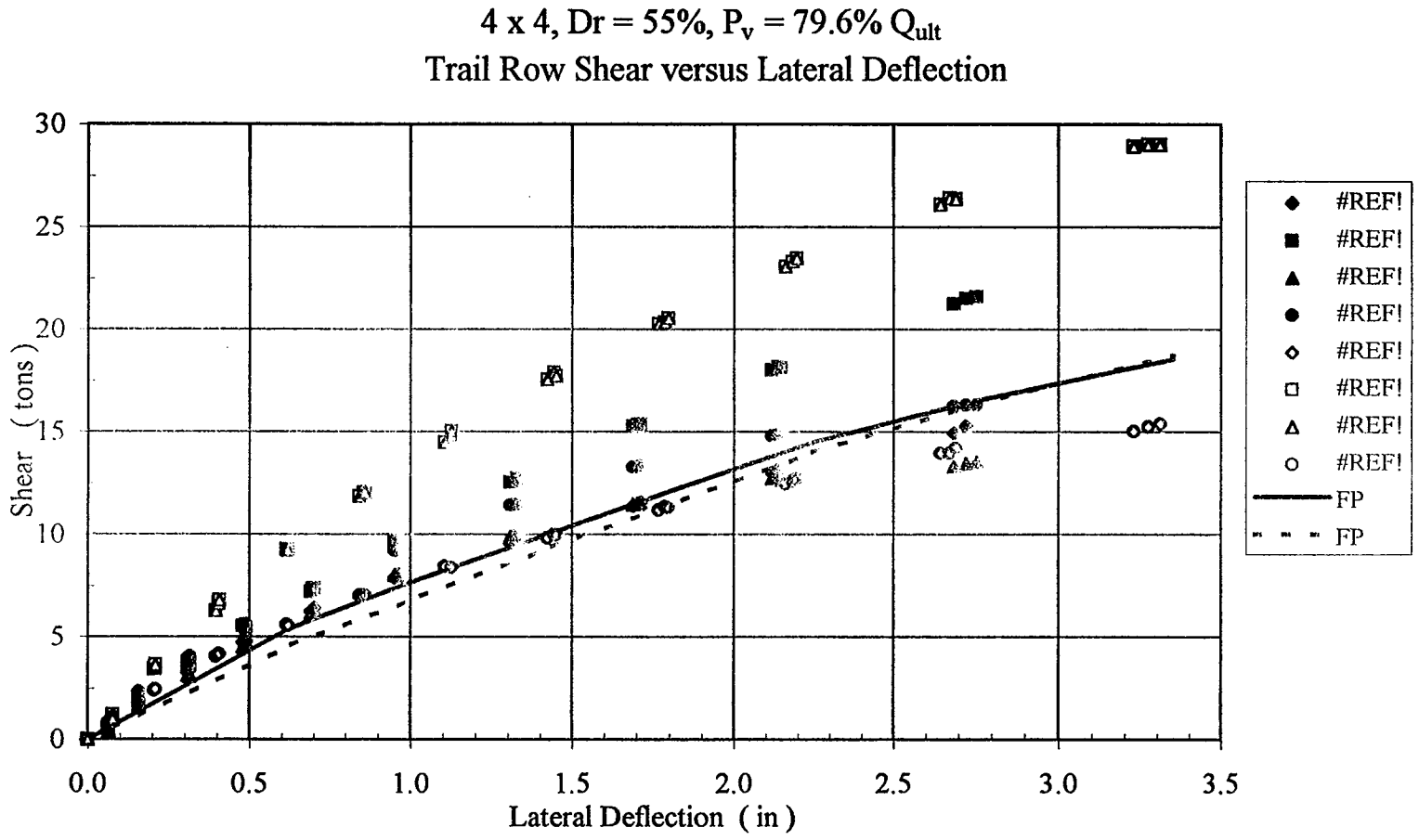

Figure B-163 Trail Row Shear versus Lateral Deflection

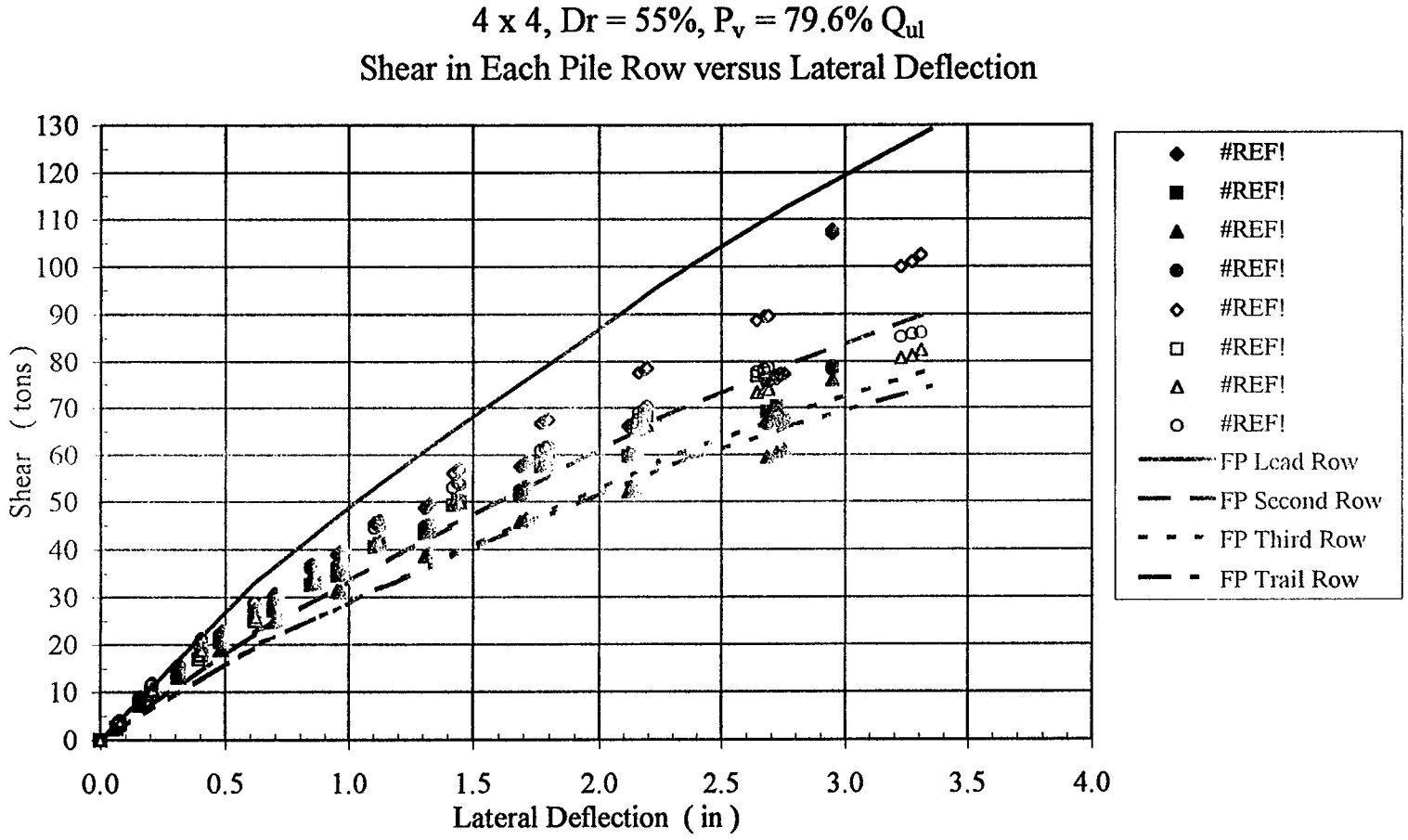

Figure B-164 Shear in Each Pile Row versus Lateral Deflection

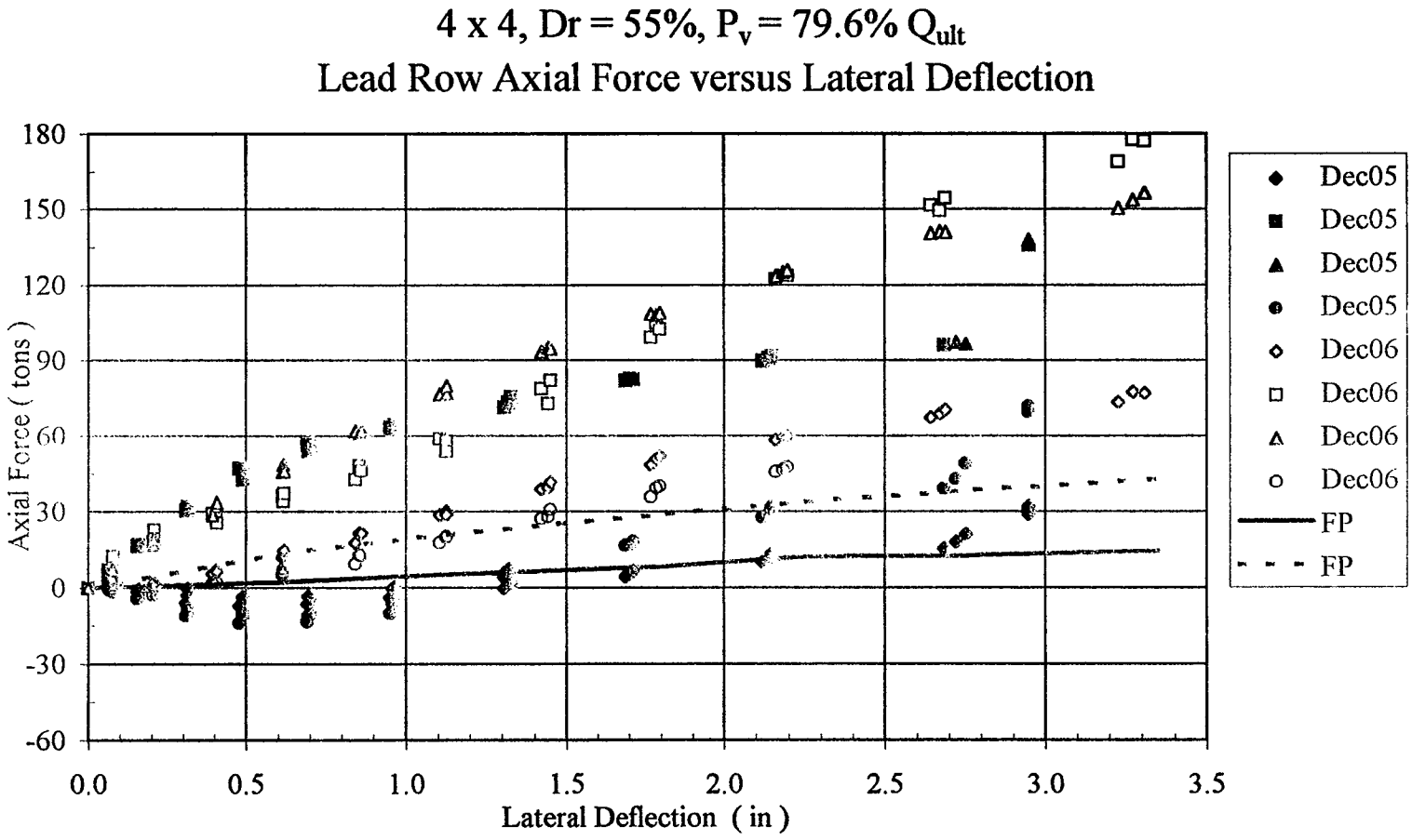

Figure B-165 Lead Row Axial Force versus Lateral Deflection

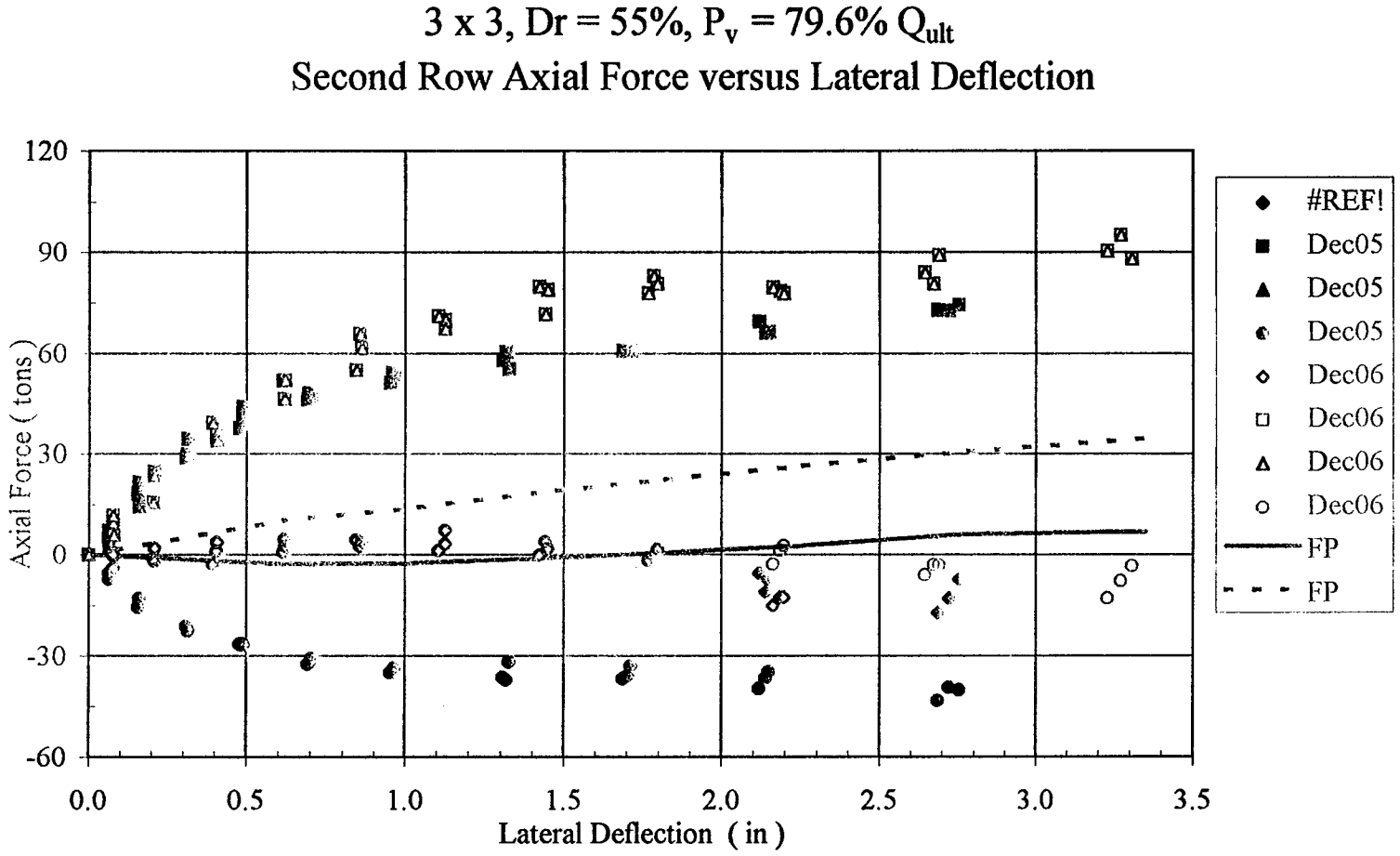

Figure B-166 Second Row Axial Force versus Lateral Deflection

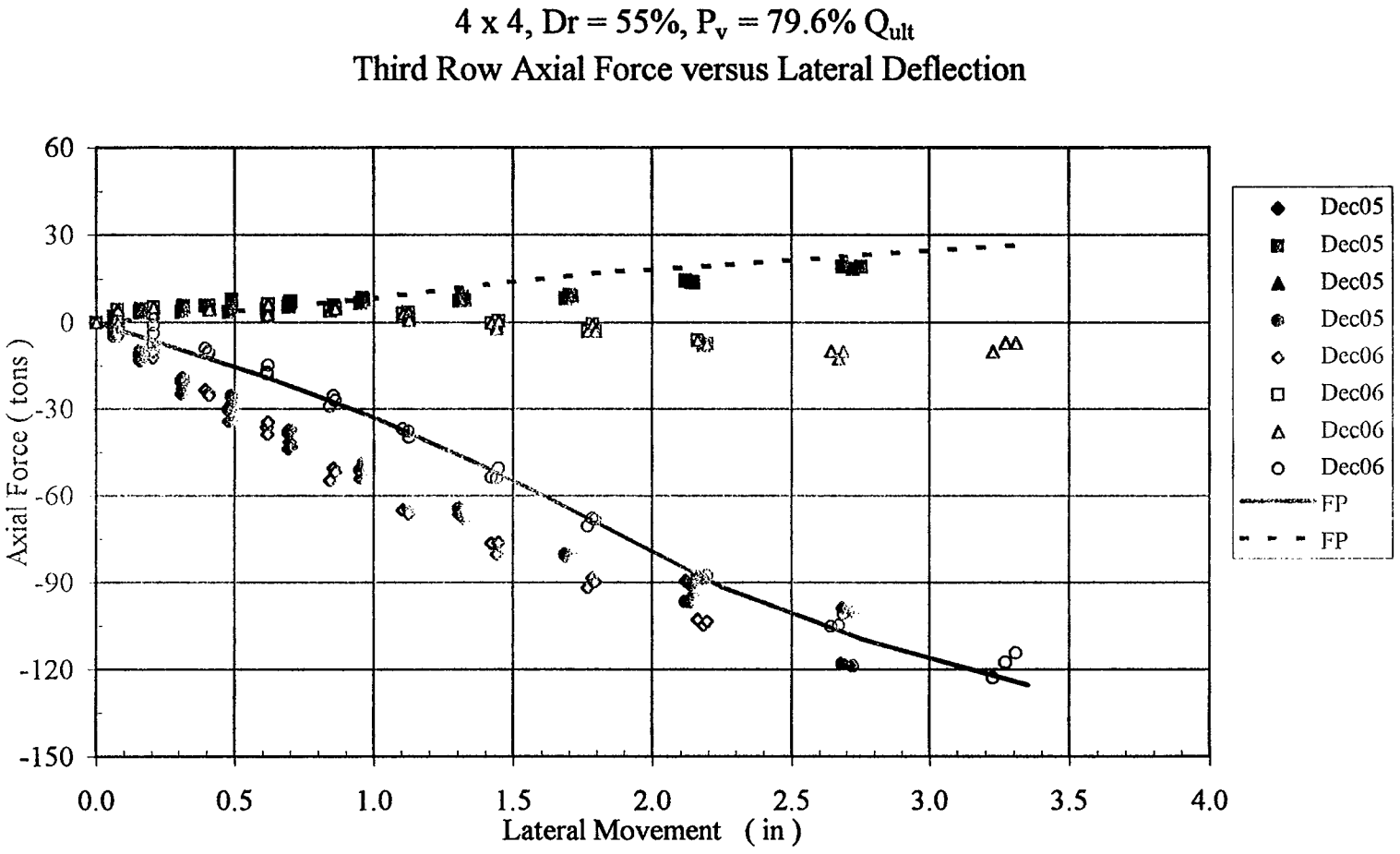

Figure B-167 Third Row Axial Force versus Lateral Deflection

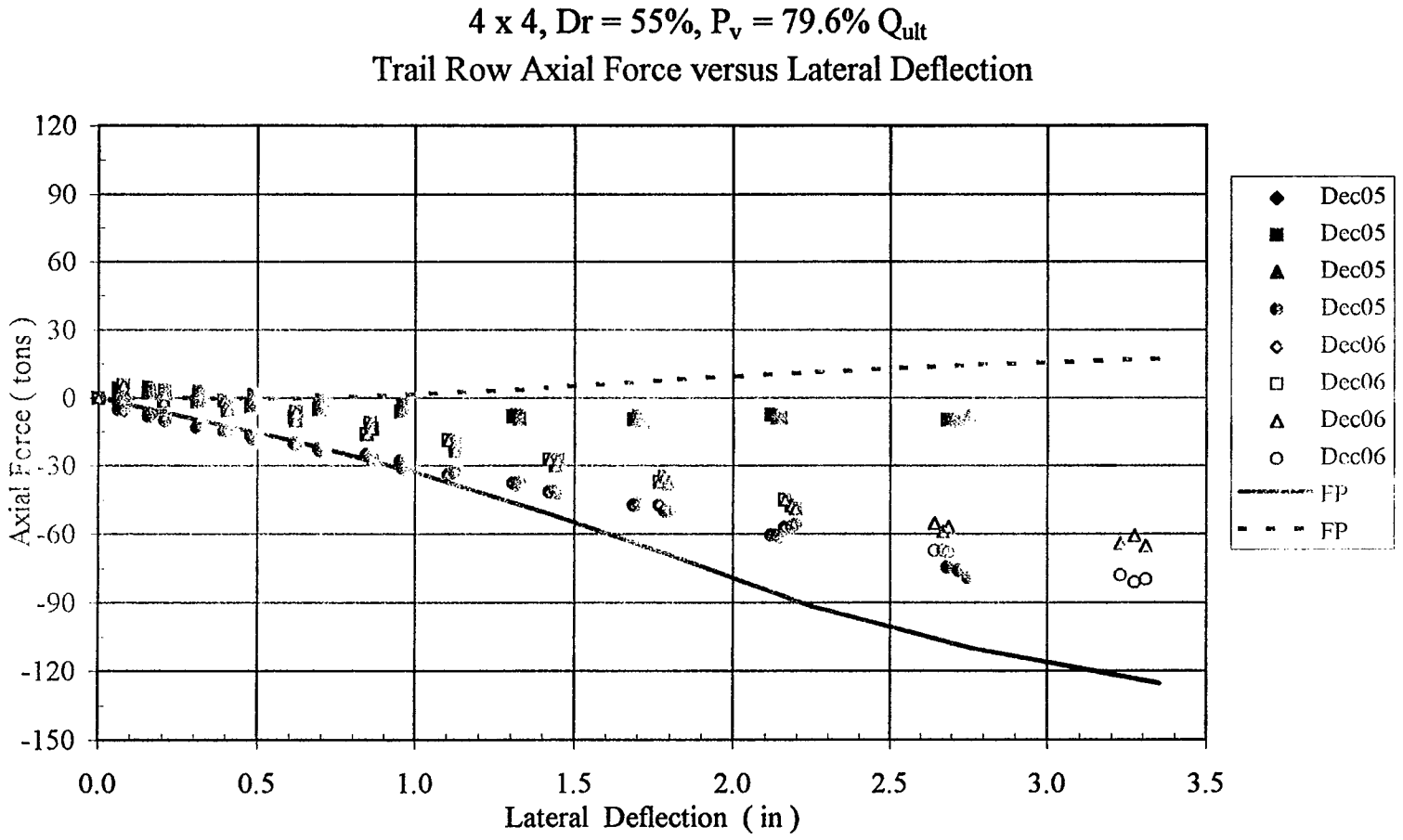

Figure B-168 Trail Row Axial Force versus Lateral Deflection

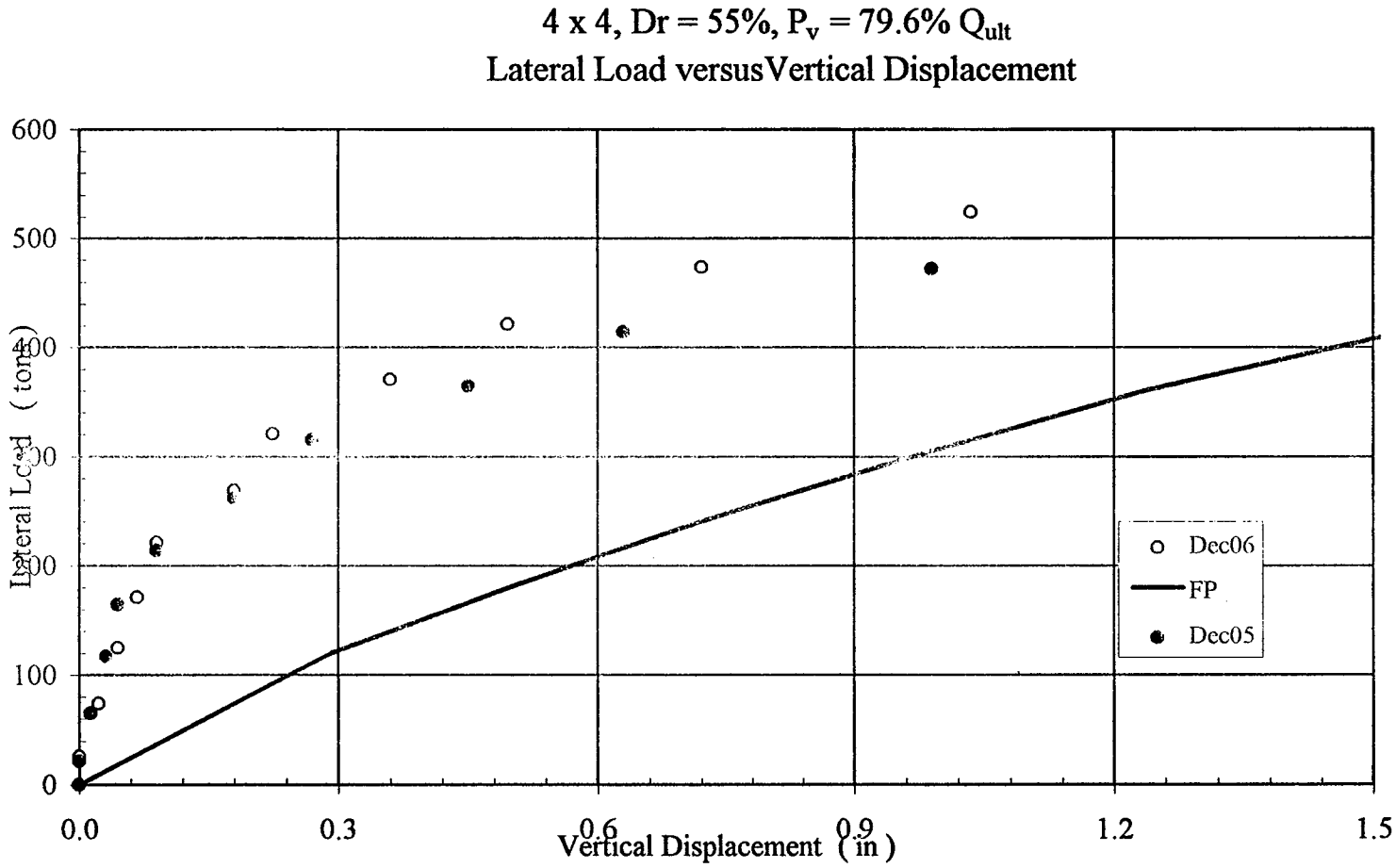

Figure B-169 Lateral Load versus Vertical Displacement

NTIS does not permit return of items for credit or refund. A replacement will be provided if an error is made in filling your order, if the item was received in damaged condition, or if the item is defective.

Reproduced by NTIS

National Technical Information Service
Springfield, VA 22161

This report was printed specifically for your order from nearly 3 million titles available in our collection.

For economy and efficiency, NTIS does not maintain stock of its vast collection of technical reports. Rather, most documents are printed for each order. Documents that are not in electronic format are reproduced from master archival copies and are the best possible reproductions available. If you have any questions concerning this document or any order you have placed with NTIS, please call our Customer Service Department at (703) 605-6050.

About NTIS

NTIS collects scientific, technical, engineering, and business related information — then organizes, maintains, and disseminates that information in a variety of formats — from microfiche to online services. The NTIS collection of nearly 3 million titles includes reports describing research conducted or sponsored by federal agencies and their contractors; statistical and business information; U.S. military publications; multimedia/training products; computer software and electronic databases developed by federal agencies; training tools; and technical reports prepared by research organizations worldwide. Approximately 100,000 *new* titles are added and indexed into the NTIS collection annually.

For more information about NTIS products and services, call NTIS at 1-800-553-NTIS (6847) or (703) 605-6000 and request the free *NTIS Products Catalog,* PR-827LPG, or visit the NTIS Web site **http://www.ntis.gov**.

NTIS
Your indispensable resource for government-sponsored information—U.S. and worldwide

U.S. DEPARTMENT OF COMMERCE
Technology Administration
National Technical Information Service
Springfield, VA 22161 (703) 605-6000